The Dissertation Committee for Cameron Bennett Faxon certifies that this is the approved version of the following dissertation:

Urban Atmospheric Chlorine Chemistry: Mechanism Development, Evaluation and Implications

Committee:

_____

David T. Allen, Supervisor

_____

Lea Hildebrandt Ruiz, Co-Supervisor

_____

Elena McDonald-Buller

_____

Richard L. Corsi

_____

Gary T. Rochelle

Urban Atmospheric Chlorine Chemistry: Mechanism Development, Evaluation and Implications

by

Cameron Bennett Faxon, B.S. Bio. E.

Dissertation

Presented to the Faculty of the Graduate School of

The University of Texas at Austin

in Partial Fulfillment

of the Requirements

for the Degree of

Doctor of Philosophy

The University of Texas at Austin

May 2014

Acknowledgements

I would like to acknowledge my advisors, Dr. David Allen and Lea Hildebrandt Ruiz who provided support and guidance throughout the course of my research. I would also like to acknowledge my current and former colleagues at the Center for Energy and Environmental Resources for their help during the completion of this work. In particular, I would like to thank Gookyoung Heo, Yosuke Kimura, Adam Pacsi, Daniel Zavala and Jeff Bean.

Urban Atmospheric Chlorine Chemistry: Mechanism Development, Evaluation and Implications

Cameron Bennett Faxon, Ph.D.

The University of Texas at Austin, 2014

Supervisor: David T. Allen

Co-Supervisor: Lea Hildebrandt Ruiz

Detailed photochemical modeling is used to guide air quality management activities around the world. These models use condensed chemical mechanisms to describe the multiphase processes that lead to chemical transformations in the atmosphere. Condensed mechanisms have generally not included the reactions of halogens, yet an expanding body of ambient observational evidence indicates that halogen chemistry, particularly chlorine chemistry, can be important in urban environments.

This thesis is focused on the development, implementation, and evaluation of condensed chemical mechanisms that incorporate chlorine chemistry pathways. Gas phase reactions involving molecular chlorine and nitryl chloride ($ClNO_2$), as well as heterogeneous reactions involving particulate chloride species are addressed. The predictions of the modeling work presented here are compared to environmental chamber experiments and field observations.

Table of Contents

List of Tables

List of Figures

Chapter 1: Introduction

Ozone, particulate matter and other photochemical air pollutants are formed in the atmosphere by reactions of volatile organic compounds (VOCs), oxides of nitrogen (NO_x), and sulfur dioxide, which are emitted by a variety of natural and man-made sources. Most air quality management plans focus primarily on reducing the emissions of SO_2, VOCs and NO_x, however, these emissions are not the only sources of ozone and other air pollutants in the atmosphere. Other sources of photochemical air pollutants can include halogens, especially chlorine. Chlorine-induced enhancement of ozone formation is due primarily to the photolysis of gas-phase chlorine containing compounds that leads to the production of chlorine radicals, which in turn react with gas-phase hydrocarbons. The resulting formation of alkylperoxy radicals fuels well-established chemical mechanisms leading of ozone formation. Though the entire mechanism includes a large set of reactions, the most important are listed in Reactions 1-1 to 1-4.

$$Cl_2 + h\nu \rightarrow 2Cl\bullet \qquad \text{(Reaction 1-1)}$$

$$HOCl + h\nu \rightarrow OH\bullet + Cl\bullet \qquad \text{(Reaction 1-2)}$$

$$Cl\bullet + RH \rightarrow R\bullet + HCl \qquad \text{(Reaction 1-3)}$$

$$R\bullet + O_2 \rightarrow RO_2\bullet \qquad \text{(Reaction 1-4)}$$

The first direct evidence of chlorine radical ($Cl^{\bullet}$) chemistry in urban atmospheres was observed in Houston, based on the quantification of two products unique to the $Cl^{\bullet}$ + isoprene reaction: 1-Chloro-3-methyl-3-butene-2-one (CMBO) and chloromethylbutenal (CMBA) (Nordmeyer et al., 1997; Ragains & Finlayson-Pitts, 1997; Riemer & Apel, 2002; Tanaka et al., 2003a). These measurements were made during the 2000 Texas Air Quality Study (TexAQS). Photochemical air quality modeling has suggested that the observed concentrations of these marker species, and other Cl reaction products, were consistent with a total emission rate of approximately 10 ton day^{-1} (Sunghye Chang & Allen, 2006a) during the

2000 TexAQS campaign. The magnitude and reactivity of these emissions have the potential to enhance 1-hour averaged ozone mixing ratios by tens of ppb in localized areas during morning hours. Over wider areas, and at times of day when peak ozone concentrations are observed, the impacts of chlorine emissions on ozone concentrations are typically predicted to be 5-10 ppb (Sunghye Chang & Allen, 2006a). Results from this previous modeling work are shown in Figure 1-1.

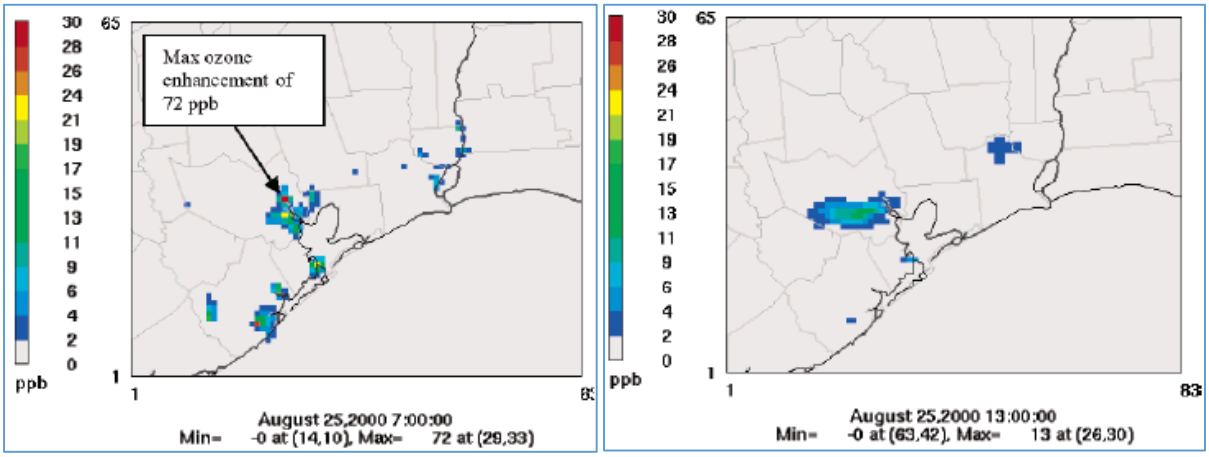

Figure 1-1: Predicted enhancements in ozone concentrations in southeast Texas due to the emissions of reactive gas phase chlorine species (Chang and Allen, 2006). Left: morning of August 25, 2000. Right: afternoon of August 25, 2000.

If these ozone enhancements due to chlorine were reduced, more flexibility could be achieved in the reductions in VOCs and NO_x that would be required to meet federal air quality standards. Chlorine emissions are more than twice as reactive as Highly Reactive Volatile Organic Compounds (HRVOCs) (William P L Carter, Luo, Malkina, & Pierce, 1995); the industrial HRVOC emissions in Harris County, TX, which are now subject to a cap, are limited to approximately 5 tons day^{-1}. This makes the 5-10 tons d^{-1} of chlorine emissions an important part of the overall reactivity of the atmosphere in Houston (Linlin Wang, Thompson, McDonald-Buller, & Allen, 2007).

The understanding of atmospheric chlorine chemistry in southeast Texas improved further during the second Texas Air Quality Study in 2006 (TexAQS II). During TexAQS II, the National Oceanic and Atmospheric Administration (NOAA), taking measurements aboard the Ronald H. Brown off the coast of southeast Texas, detected nitryl chloride ($ClNO_2$) concentrations at levels in excess of 1 ppbv

(Osthoff et al., 2008). These were the first detections of $ClNO_2$ in an urban environment. More recently, researchers have also detected $ClNO_2$ at concentrations ranging 0.25 – 0.5 ppb in mid-continental locations in Boulder, Colorado, as well as in the South Coast Air Basin in California (Mielke et al., 2011; J. A. Thornton et al., 2010). The detection of $ClNO_2$ at these levels in both coastal and continental regions has implications for atmospheric chlorine chemistry. First, nitryl chloride serves as a NO_x reservoir, preventing the conversion of NO_x into inert forms such as HNO_3 at night. Secondly, the daytime photolysis of nitryl chloride leads directly to the production of $Cl^{\bullet}$ as shown in reaction 1-5 (Atkinson et al., 2007). The combined effects of $ClNO_2$ on $Cl^{\bullet}$ availability and cycling as well as its role as a NO_x reservoir increase its impact on ozone formation (Osthoff et al., 2008; H. Simon et al., 2010).

$$ClNO_2 + h\nu \rightarrow Cl^{\bullet} + NO_2 \qquad \text{(Reaction 1-5)}$$

A heterogeneous chemical mechanism has been shown to produce $ClNO_2$. The mechanism involves the reactive uptake of dinitrogen pentoxide (N_2O_5) into chloride containing aerosols. When N_2O_5 reaches the surface of a particle, the heterogeneous reaction takes place through a sequence of events, including mass accommodation of the N_2O_5 onto the surface of the aerosol particle and subsequent diffusion of the accommodated N_2O_5 into the body of the aerosol. Laboratory studies have suggested that the next step is analogous to heterogeneous N_2O_5 hydrolysis (Wolfgang Behnke, George, Scheer, & Zetzsch, 1997; Schweitzer, Mirabel, & George, 1998; H. A. Simon, 2008a):

$$N_2O_5 + \textit{sea salt (aq)} \rightarrow NO_2^+ + NO_3^- \qquad \text{(Reaction 1-6)}$$

Once the N_2O_5 has become dissociated within the aqueous phase, dissolved chloride ions, as well as other competing ions, react with NO_2^+. The following reactions take place:

$$NO_3^-{}_{(aq)} + H^+{}_{(aq)} \rightarrow HNO_3{}_{(g)} \qquad \text{Reaction (1-7)}$$

$$NO_2^+{}_{(aq)} + Cl^-{}_{(aq)} \rightarrow ClNO_2{}_{(g)} \qquad \text{Reaction (1-8)}$$

NO_2^+ (aq) + $2H_2O$ (aq) → HNO_3 (g) + H_3O^+ (aq) Reaction (1-9)

It has been suggested by multiple studies that the uptake and dissociation of N_2O_5 is the rate limiting step of the mechanism (Wolfgang Behnke et al., 1997; Roberts et al., 2009; Schweitzer et al., 1998). The reaction of gas phase N_2O_5 with particles to produce nitric acid and gas phase $ClNO_2$ is assumed to be represented by a pseudo-first order rate expression (Jacob, 2000; Eladio M Knipping & Dabdub, 2003; Eladio M. Knipping, 2002; Thornton & Abbatt, 2005) as shown in Equations 1-1 and 1-2.

$$\frac{d[N_2O_5]}{dt} = k[N_2O_5] = \frac{\gamma\omega A}{4}[N_2O_5] \quad \text{Equation (1-1)}$$

$$\frac{d[ClNO_2]}{dt} = Yk[N_2O_5] = \frac{Y\gamma\omega A}{4}[N_2O_5] \quad \text{Equation (1-2)}$$

Here, k (s^{-1}) is the first order reaction rate constant, A ($cm^2\ cm^{-3}$) is the surface area density of chloride containing aerosols, γ (unit less) is the reactive uptake coefficient (i.e. the fraction of N_2O_5 molecules that will react upon impact with an appropriate aerosol particle), ω (m s^{-1}) is the average molecular speed of an N_2O_5 molecule, and Y represents the fractional amount of $ClNO_2$ produced per molecule of N_2O_5.

Previous work (H. Simon et al., 2009) incorporated this heterogeneous mechanism into regional photochemical models, and used the models to predict the magnitude of ozone formation in southeast Texas that could be due to these photochemical pathways. They found that the amount of $ClNO_2$ formation was limited by chloride availability. In order to explain the concentrations of $ClNO_2$ observed in southeast Texas, chlorine cycling is necessary (H. Simon et al., 2010). Specifically, in the chlorine cycling, chloride in the particle phase (for example, from sea salt) initially reacts with N_2O_5 to produce $ClNO_2$. $ClNO_2$ then photolyzes, producing chlorine radicals. The chlorine radicals react with hydrocarbons, generally producing HCl as a reaction product via the hydrogen abstraction pathway. The

HCl can then partition back into the particle phase, allowing the chlorine cycle to begin again. Even with this chlorine cycling, however, the magnitude of the impact of this heterogeneous chemistry on predicted ozone concentrations in southeast Texas was generally less than 1 ppb (H. Simon et al., 2009). The impact was distributed over a wide area, but the maximum changes in ozone concentration were relatively small (Figure 1-2)

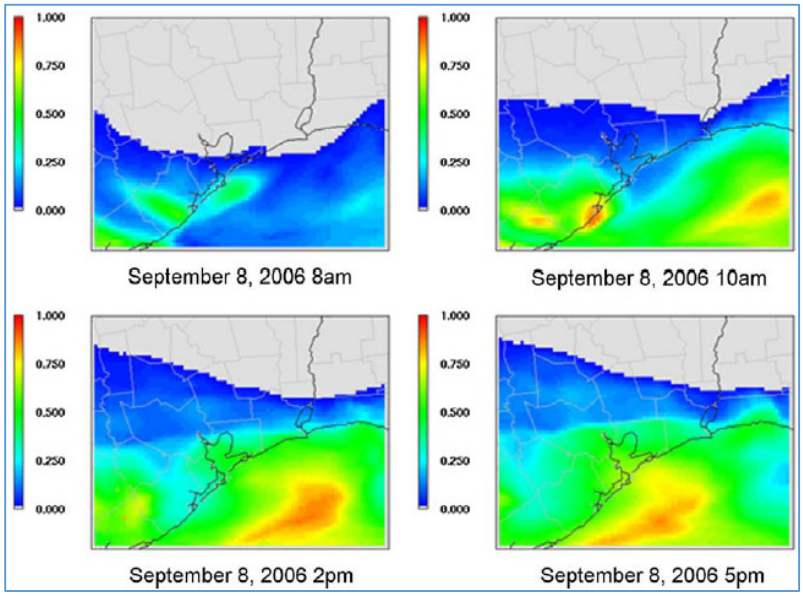

Figure 1-2: Time series of ozone increases caused by addition of ClNO chemistry (Simon, et al., 2009). Resulting ozone increases are relatively small, over a broad area.

By 2010, the role of chlorine chemistry in ozone formation in urban atmospheres was believed to be generally well established. Local hot spots of ozone formation could occur as the result of the emissions of reactive gas phase chlorine species. Regional ozone enhancements of a few ppb could occur through the activation and cycling of particle phase chlorine. This understanding was challenged, however, by measurements made in the Dallas Fort Worth area in the summer of 2011.

In 2011, at the Eagle Mountain Lake monitoring site northwest of Fort Worth, measurements were made of total gas and particle phase chloride. Total gas and particle chloride concentrations of roughly one ppb were measured regularly at the Eagle Mountain Lake site, as shown in Figure 1-3 (Griffin, Dibb, Lefer, & Steiner, 2011). The chloride is expected to be primarily gas phase species

(presumably HCl), since previous observations of particulate chloride in the region have been low. The magnitude of these chloride concentrations was unexpected given that (i) there are no sources of sea salt (believed to be the primary source of particulate chloride in most urban areas), and (ii) inventoried direct emissions of gas phase reactive chlorine in the region are small. In addition to the magnitude of the chloride observations being unexpected, the diurnal variation in the concentrations was also unexpected. The concentrations generally peaked in the mid-afternoon which is inconsistent with continuous direct gaseous releases of reactive chlorine (which tend to produce morning-time peaks in reaction product concentrations due to Cl_2 or HOCl concentrations that build at night) and the N_2O_5 heterogeneous reaction pathway (which also tends to produce morning peaks in reactive chlorine reaction products since N_2O_5 concentrations are highest at night).

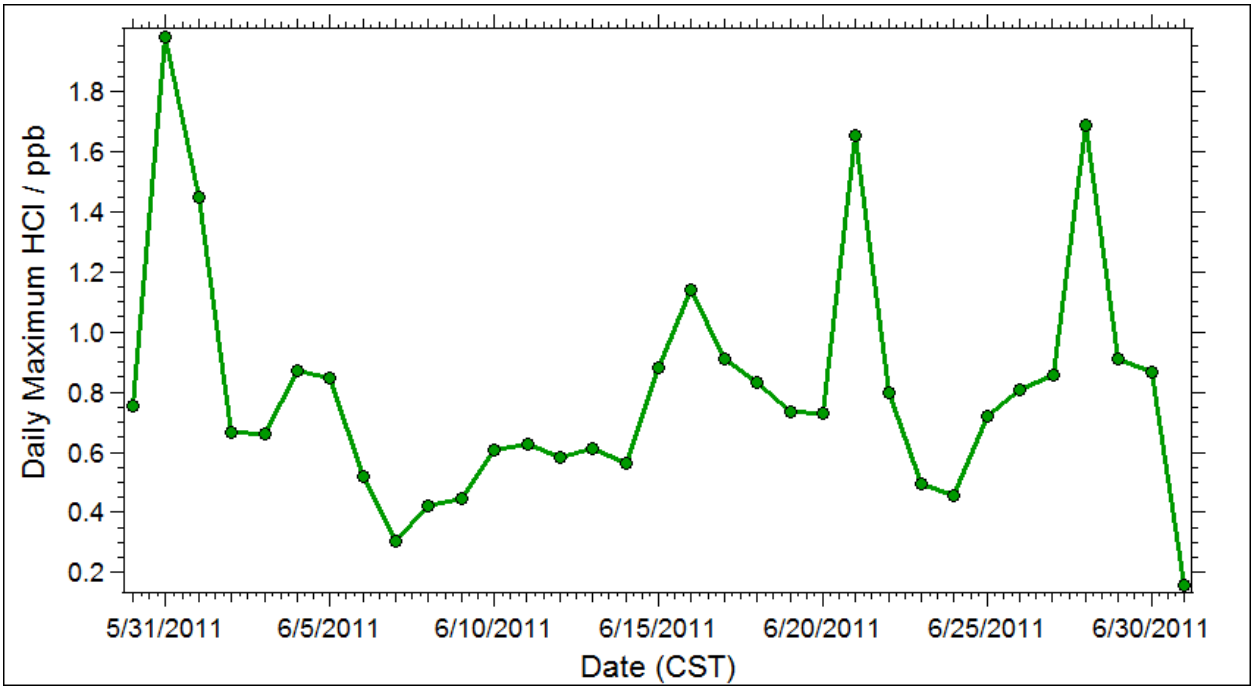

Figure 1-3: Daily maximum chloride concentrations observed during June 2011 at Eagle Mountain Lake (Griffin, et al., 2011)

Motivated by the need to explain this evidence, both gas phase and heterogeneous mechanisms can be proposed. One potential heterogeneous mechanism involves a surface reaction between hydroxyl radicals ($OH^{\bullet}$) in the gas phase and chloride ions in aerosol particles (E. M. Knipping, 2000a; Eladio M.

Knipping & Dabdub, 2002; Nissenson, Thomas, Finlayson-Pitts, & Dabdub, 2008). This mechanism is shown in Reactions 1-10 and 1-11, where $OH\bullet\bullet\bullet Cl^-$ represents the surface complex.

$$OH_{(g)} + Cl^{\bullet -}_{(aq,surface)} \rightarrow OH\bullet\bullet\bullet Cl^{\bullet -}_{(aq,surface)} \quad \text{(Reaction 1-10)}$$

$$2OH\bullet\bullet\bullet Cl^{\bullet -}_{(aq,surface)} \rightarrow Cl_{2,g} + 2OH^-_{(aq)} \quad \text{(Reaction 1-11)}$$

The chloride ions present in the aqueous phase of an NaCl solution have been shown to reside at the particle surface much more than sodium ions (11.9% and 0.2%, respectively), and it is suggested that the affinity of chloride ions for hydroxyl radicals in the gas phase is relatively high. Similar to the N_2O_5-particulate chloride mechanism, it is assumed that the initial formation of the $OH\bullet\bullet\bullet Cl^{\bullet -}$ complex is the rate limiting step (E. M. Knipping, 2000b; Eladio M. Knipping & Dabdub, 2002). While this is a feasible mechanism, the source of chlorine in inland regions such as Fort Worth and Boulder is still unclear.

Gas phase mechanisms could also account for the observations made at Eagle Mountain Lake if sufficient emissions of gas phase chlorinated species could be identified. As will be described later in this work, evidence of emissions of a variety of chlorinated organics suggests that homogeneous chemistry may also be important.

Objectives

The objectives of this thesis are to:

1. Quantify sources of gas and particulate phase chlorine emissions in inland regions, using Fort Worth as a case study; compare these chlorine inventories to observations of atmospheric chlorine in the same region.

2. Perform kinetic modeling to assess the importance of various homogeneous and heterogeneous mechanisms in chlorine cycling, at conditions relevant to both coastal and inland environments; assess the sensitivity of the reaction networks to key parameters.

3. Perform laboratory experiments to characterize the rates of the hydroxyl radical driven chlorine cycling.

4. Integrate proposed new chemistries into the carbon bond condensed chemical mechanism and assess the significance of the mechanisms on urban atmospheric reactions, particularly in inland environments.

The following chapters will provide details of the objectives. Chapter 2 contains a comprehensive literature review, covering previous research relevant to atmospheric chlorine chemistry. In particular, topics such as gas phase atmospheric chlorine chemistry, heterogeneous atmospheric chlorine chemistry, computational modeling of atmospheric processes and condensed chemical mechanisms will be covered. Chapter 3 consists of an emissions inventory of chlorine sources, both particulate and gas phase, within and surrounding the Dallas-Fort Worth, TX area. Sources considered include industrial point sources, cooling towers and drinking water, gas phase chlorocarbon emissions and wastewater treatment processes. Chapter 4 provides details regarding the parameters that control heterogeneous chlorine reactions in the atmosphere, particularly the interactions of $OH^{\bullet}$ and N_2O_5 with chloride containing aerosols. Sensitivity analyses of the relevant parameters governing these two reactions are presented and the results discussed. Chapter 5 describes environmental chamber studies which were carried out in order to characterize the rates and processes involved in hydroxyl radical driven atmospheric chlorine cycling. Chapter 6 contains details of the integration of homogeneous chlorocarbon reactions into the Carbon Bond condensed chemical mechanism and the results of modeling studies performed using the Comprehensive Air Quality Model with Extensions. Implications in relation to possible sources, source strengths, and previous observations in the region will also be included within this chapter. Chapter 7 will include a discussion and summary of conclusions that may be derived from this work.

Chapter 2: Chlorine Chemistry in Urban Atmospheres – A Review

C.B. Faxon and D.T. Allen. E*nvironmental Chemistry*, Vol. 10, No. 3, pp. 221-233, doi:10.1071/EN13026

2.1 Environmental Context

Atmospheric chlorine radicals can impact the chemical composition of the atmosphere through numerous reactions with trace species. In urban atmospheres, the reactions of chlorine radicals can lead to effects such as increases in ozone production, thus degrading local and regional air quality. This review summarizes the current understanding of atmospheric chlorine chemistry in urban environments and identifies key unresolved issues.

2.2 Abstract

Gas phase chlorine radicals ($Cl^{\bullet}$), when present in the atmosphere, react via mechanisms analogous to those of the hydroxyl radical ($OH^{\bullet}$). However, the rates of the $Cl^{\bullet}$-initiated reactions are often much faster than the corresponding $OH^{\bullet}$ reactions. The effects of the atmospheric reactions of $Cl^{\bullet}$ within urban environments include the oxidation of volatile organic compounds (VOCs) and increases in ozone production rates. Although concentrations of chlorine atoms are typically low compared to other atmospheric radicals, the relatively rapid rates of the reactions associated with this species lead to observable changes in air quality. This is particularly evident in the case of chlorine atom-induced localized increases in ozone concentrations. This review covers five aspects of atmospheric chlorine chemistry: (1) gas phase reactions; (2) heterogeneous and multi-phase reactions; (3) observational evidence of chlorine species in urban atmospheres; (4) regional modeling studies; and (5) areas of uncertainty in the current state of knowledge.

2.3 Introduction

Most management plans for the reduction of photochemical smog focus on reducing emissions of volatile organic compounds (VOCs) and nitrogen oxides (NO_x), leading to reduced formation of photochemical air pollutants, such as ozone, through various chemical pathways involving HO_x radicals.

A growing body of observations and modeling studies, however, indicates that halogen radicals, particularly the chlorine radical and related species, can play a significant role in urban atmospheric chemistry. This may occur through both emissions of chlorine radical precursors and through the involvement of chlorinated species in VOC-NO_x-HO_x pathways. This review will summarize current understanding of the role of chlorine radicals in urban photochemistry and will highlight key issues that are unresolved. The review is organized into five sections: gas phase chlorine chemistry in urban atmospheres, heterogeneous (gas-particle) and multi-phase chlorine chemistry in urban atmospheres, observations, regional modeling studies and critical gaps in current understanding.

2.4 Gas Phase Chlorine Chemistry in Urban Atmospheres

Various forms of chlorine (e.g., particulate chloride, inorganic gas species, and organohalogens) are present in the atmosphere. Analyses of natural emissions indicate an atmospheric loading of 23 Tg Cl, of which 8.4 Tg is comprised of reactive species. The two dominant reactive species are CH_3CCl_3 (29% of reactive species) and CH_3Cl (43%), with inorganic species accounting for 7% of reactive atmospheric chlorine (Khalil et al., 1999). Other common species include HCl, $CHClF_2$, Cl_2, HOCl, CCl_2=CCl_2, CH_2Cl_2, $COCl_2$ and $CHCl_3$. Photodissociation of chlorinated species, the sources of which may be natural or anthropogenic, is one of the most common routes to global tropospheric chlorine radical production. Other gas phase chemical pathways to the global formation of chlorine radicals include reactions of HCl and chlorocarbons (Graedel & Keene, 1995, 1996; H B Singh & Kasting, 1988). Gas phase species also participate in reactions involving particulate matter, which will be described in subsequent sections of this review (Graedel & Keene, 1995).

While important globally, photodissociation and oxidation of many of the most common chlorinated organic species occur at rates that are generally not fast enough to contribute significant concentrations of chlorine radicals in urban atmospheres. For example, the rate constant for chlorine radical generation via the oxidation of HCl by the hydroxyl radical at 298 K is reported to be 7.8×10^{-13}

cm^3 $molecule^{-1}$ s^{-1} (Atkinson et al., 2007; Sander et al., 2011). This rate constant is approximately two orders of magnitude lower than the rate of hydroxyl radical formation from the reactions of $O(^1D)$ and H_2O (1.63×10^{-10}) (Sander et al., 2011) Given that H_2O is also typically present in the urban atmosphere at concentrations far greater than those of HCl, the result is a smaller rate of generation for chlorine atoms compared to hydroxyl radicals. For chlorocarbon photolysis, rates of reaction are very low, approaching zero, in the urban atmosphere. For example, the photolysis of CH_3Cl has only been reported to occur during exposure to radiation at wavelengths below 216 nm (Atkinson et al., 2008). In the urban atmosphere, radiation of this wavelength is negligible.

Production of chlorine radicals through routes other than photolysis of chlorocarbon species and oxidation of common chlorinated species such as HCl can proceed at rates that are significant in urban atmospheres, however. The photolysis of Cl_2 is expected to proceed rapidly with a quantum yield of unity (Atkinson et al., 2007; Sunghye Chang & Allen, 2006a; Barbara J Finlayson-Pitts, 1993). One comparison of radical generation from 3 ppb HONO, a photolytic source of the hydroxyl radical, and 0.1 ppb Cl_2 in a polluted region estimates corresponding radical generation rates of 5×10^6 radicals cm^{-3} s^{-1} and 4×10^5 radicals cm^{-3} s^{-1} for hydroxyl radicals and chlorine radicals, respectively (Barbara J Finlayson-Pitts, 1993). So, if concentrations of species such as HOCl, $ClNO_2$ orCl_2 are sufficiently high, photolysis to produce chlorine radicals can be important in urban atmospheres. In some regions, direct anthropogenic emissions of these chlorine radical precursors can be significant. One estimate (Sunghye Chang & Allen, 2006a) suggests that anthropogenic HOCl and Cl_2 emissions in the Houston area are approximately 10^4 kg d^{-1}, coming from cooling towers, swimming pools, and industrial point sources (Sunghye Chang et al., 2002). In the vicinity of large anthropogenic sources of Cl_2 or HOCl, the reactions of Cl and related radicals can significantly impact photochemistry. Thus, while photolysis of many chlorocarbon species and oxidation of the most common gas phase chlorine species is not a significant contributor to radical production in urban atmospheres, there are situations where

anthropogenic emissions of chlorine radical precursors can make photolysis pathways significant. Table 2-1 shows a comparison of photolysis rates for some chlorine species and some other common atmospheric species involved in the photochemical cycle.

Table 2-1. Photolysis Rates (10^3 min^{-1})[A] of Gas Phase Atomic Chlorine Sources Compared to Other Common Photolysis Rates

Chemical Species	Zenith Angle		
	30	**50**	**70**
Cl_2	158.9	125.2	50.2
$ClNO_2$	24.0	17.3	5.5
HOCl	18.6	14.1	5.2
HONO	0.1057	0.0854	0.03547
NO_2	676.3	559.8	253.4
O_3[B]	2.2	1.1	0.1

[A] Photolysis rates from parameterizations developed for the SAPRC-07 condensed chemical mechanism (Carter et al., 2010)
[B] O_3 photolysis reaction producing $O(^1D)$

Chlorine radicals produced photolytically or through other mechanisms may react with and oxidize volatile organic compounds (VOCs). The examples below represent typical photolysis reactions and the initiating reaction for the oxidation of a generic VOC, denoted as RH (Atkinson et al., 2007; Sunghye Chang & Allen, 2006a; Barbara J Finlayson-Pitts, 1993; Sander et al., 2011; Jochen Stutz, Jobson, & Sumner, 2009; Watson, 1977).

$$Cl_2 + h\nu \rightarrow 2Cl^{\bullet} \qquad \text{(Reaction 2-1)}$$

$$HOCl + h\nu \rightarrow Cl^{\bullet} + OH^{\bullet} \qquad \text{(Reaction 2-2)}$$

$$Cl^{\bullet} + RH \rightarrow R^{\bullet} + HCl \qquad \text{(Reaction 2-4)}$$

The presence of reactive chlorine species can also modify HO_x levels and the $HO_2^{\bullet}/OH^{\bullet}$ ratio. This occurs from reactions resulting in the inter-conversion of $OH^{\bullet}$ and $HO_2^{\bullet}$. Examples of known reactions are shown below (Atkinson et al., 2007; Sander et al., 2011; Jochen Stutz et al., 2009; Watson, 1977).

$$Cl\bullet + O_3 \rightarrow ClO^{\bullet} + O_2 \qquad \text{(Reaction 2-4)}$$

$ClO^{\bullet} + HO_2^{\bullet} \rightarrow HOCl + O_2$ (Reaction 2-5)

$Cl^{\bullet} + HO_2^{\bullet} \rightarrow HCl + O_2$ (Reaction 2-6a)

$\rightarrow ClO^{\bullet} + HO^{\bullet}$ (Reaction 2-6b)

$ClO^{\bullet} + OH^{\bullet} \rightarrow Cl^{\bullet} + HO_2^{\bullet}$ (Reaction 2-7a)

$ClO^{\bullet} + OH^{\bullet} \rightarrow HCl + O_2$ (Reaction 2-7b)

$Cl_2 + OH^{\bullet} \rightarrow HOCl + Cl^{\bullet}$ (Reaction 2-8)

Unlike $OH^{\bullet}$, chlorine radicals are not regenerated within the oxidation cycle. However, chlorine atoms can be regenerated by heterogeneous cycling from chloride containing aerosols (discussed in the next section) or by the volatilization and oxidation of HCl shown below (Atkinson et al., 2007; Graedel & Keene, 1995; Sander et al., 2011; H B Singh & Kasting, 1988; Jochen Stutz et al., 2009; Watson, 1977).

$OH^{\bullet} + HCl \rightarrow Cl^{\bullet} + H_2O$ (Reaction 2-9)

Another important difference between the hydroxyl and chlorine radicals is the rates at which they oxidize hydrocarbons. The reactivity of chlorine with most VOCs is greater than that of the hydroxyl radical, such that even concentrations of chlorine atoms an order of magnitude or more lower than hydroxyl radicals can compete with normal atmospheric concentrations of hydroxyl radicals (Wingenter et al., 1999). The reaction rates of chlorine atoms with many alkanes, aromatics, alcohols and ethers typically range between one to two orders of magnitude greater than the identical reaction with the hydroxyl radical (Aschmann & Atkinson, 1995; Nelson, Rattigan, Neavyn, & Sidebottom, 1990; Jochen Stutz et al., 2009; Lin Wang, Arey, & Atkinson, 2005). This high reactivity causes the rates of such reactions to approach the collisional limit. For alkenes and alkynes, the difference is slightly smaller ($k_{Cl}/k_{OH} \approx$ 4-13). One exception to the increased reactivity of chlorine is the reaction

with benzene, for which the ratio k_{Cl}/k_{OH} is on the order of 10^{-4} (Sokolov et al., 1998; Jochen Stutz et al., 2009).

Reactions of biogenic VOCs (BVOCs) with chlorine also proceed more rapidly than corresponding reactions with $OH^{\bullet}$, with rate constants typically > 10^{-11} cm^3 $molecules^{-1}$ s^{-1} (Canosa-Mas et al., 1999). The oxidation of the common biogenic, isoprene, by chlorine atoms takes place primarily through chlorine addition, with approximately 10% of the reaction proceeding through the hydrogen abstraction pathway (Nordmeyer et al., 1997). Unique reaction products such as 1-chloro-3-methyl-3-butene-2-one (CMBO), and isomers of chloromethylbutenal (CMBA) result (Nordmeyer et al., 1997; Riemer & Apel, 2002). Though not a BVOC, the reaction of atomic chlorine and 1,3-butadiene also produces unique tracer species, 4-chlorocrotonaldehyde (CCA) and chloromethyl vinyl ketone, with yields varying depending on the presence or absence of NO (W. Wang & Finlayson-Pitts, 2001). Table 2-2 shows a comparison of the rate parameters of $OH^{\bullet}$ and $Cl^{\bullet}$ for some common alkanes, alkenes and BVOCs.

Table 2-2. Comparison of Rate Constants for OH and Cl for Common VOCs at 298K[A]

VOC	K_{OH}[B]	K_{Cl}[B]
Methane	6.3×10^{-15}	1.0×10^{-13}
Ethane	2.4×10^{-13}	5.7×10^{-11}
Propane	1.1×10^{-12}	1.4×10^{-10}
n-decane	1.25×10^{-11}	4.87×10^{-10}
Propene	3.01×10^{-11}	1.58×10^{-10}
Isoprene	8.92×10^{-11}	3.05×10^{-10}
α-pinene	7.15×10^{-11}	4.70×10^{-10}

[A] Rate constants were compiled from Sander et al., 2011, Aschmann and Atkinson, 1995, Finlayson-Pitts et al., 1999, Stutz et al., 1998, Gill et al., 2002, Atkinson et al., 1989, Aschmann et al., 2001).
[B] Rate Constants are given in units of cm^3 $molecule^{-1}$ s^{-1}.

These differences in reactivities contribute to the overall loss rates for each radical as well as the relative loss rates of different VOCs. Table 2-3 below shows a comparison of reaction rates for a VOC mixture (McCulloch et al., 1999) that was formulated to represent a typical urban mixture of reactive organic gases. More details on this mixture are available in Chapter 4 and Appendix A. The

comparisons shown in Table 2-3 indicate that relative rates of reaction with chlorine and hydroxyl radicals vary among hydrocarbon species. This difference in relative rates can be used, as will be described later in this review, to infer chlorine and hydroxyl radical concentrations, based on the relative rates of disappearance of selected hydrocarbons.

Table 2-3. Relative Radical Loss Rates for a Surrogate VOC Mixture Typical of Urban Atmospheres[A,B]

VOC	ppb ppmC^{-1}	R_{OH}[B] x 10^{23}	R_{Cl}[B] x 10^{23}	R_{Cl}/R_{OH}
n-Butane	70.7	-67.8	-61.4	0.9
n-Octane	22.3	-0.7	-34.6	47.1
Ethylene	13.4	-0.5	-5.4	11.6
Propene	10.4	-1.3	-6.7	5.2
t-2-Butene	10.4	-2.7	-16.9	6.3
Toluene	13.3	-0.3	-3.1	9.4
m-Xylene	16.3	-1.6	-9.3	5.7
Formaldehyde	7.9	-0.3	-2.3	7.8
Acetaldehyde	7.6	-0.5	-2.2	4.4
Inert/Lost Carbon	193.1	-	-	-
Total	365.4	-75.7	-141.9	10.9[D]

[A] Urban VOC mixture taken from Carter et al., 1995. More details are available in Chapter 4 and Appendix A.
[B] Rates are given in ppb s^{-1} at 298K and rate constants for calculations are from Manion et al., 2013.
[C] Cl and OH concentrations of 1 ppt were used for rate calculations
[D] Average ratio from mixture

2.5 Heterogeneous and Multiphase Chlorine Mechanisms

Chlorine in particulate matter is generally in the form of unreactive chloride, however, a variety of heterogeneous and multi-phase reaction processes can lead to the conversion of particulate chloride to gas phase, reactive chlorine species. Multiphase reactions include the reactions of dissolved gas phase species within aqueous droplets, while reactions taking place at the interface between two phases are considered heterogeneous (Eladio M Knipping & Dabdub, 2003; Ravishankara, 1997). These processes include acid displacement and reactions of N_2O_5, ozone and other species with chloride containing aerosol.

2.5.a Acid Displacement and Reactive Chlorine Cycling

Acid displacement involves the replacement of particulate chloride anions by anions associated with H_2SO_4, HNO_3, methane sulfonic acid (MSA) or other acids, and has been observed in particles of

marine origin (Brimblecombe & Clegg, 1988; Eriksson, 1959; Gard, 1998; Sturges & Barrie, 1988). In the case of HNO_3 or H_2SO_4, the process may be represented as the heterogeneous reaction of a gas phase acid with NaCl aerosols (De Haan & Finlayson-Pitts, 1997; Gard, 1998; Graedel & Keene, 1995; Saul, Tolocka, & Johnston, 2006). In the examples below, the subscripts (g) and (cd) denote gas phase and condensed phase species, respectively.

$$HNO_{3(g)} + NaCl_{(cd)} \rightarrow HCl_{(g)} + NaNO_{3(cd)} \qquad \text{(Reaction 2-10)}$$

$$H_2SO_{4(cd)} + 2NaCl_{(cd)} \rightarrow 2HCl_{(g)} + N_2SO_{4(cd)} \qquad \text{(Reaction 2-11)}$$

The uptake of HNO_3 is more effective when the particle is aqueous or in the presence of surface adsorbed water (SAW) (Saul et al., 2006). Reduction in aerosol pH can also enhance HCl production, which may increase by up to a factor of 20 between pH 5.5 and 3 (William C Keene et al., 1998). The presence of $MgCl_2$ in a particle increases SAW and thus increases reactive uptake at lower relative humidity. It is therefore expected that this reaction will proceed at normal conditions in the MBL and that sea salt chloride can be depleted within several hours of aerosol generation (De Haan & Finlayson-Pitts, 1997; Saul et al., 2006). HCl production via acid displacement is more efficient within the smaller size fractions of typical aerosol populations (Erickson, Suezaret, Keene, & Gong, 1999; Volpe, Wahlen, Pszenny, & Spivack, 1998).

The efficiency of chloride loss from aerosols is often quantified in terms of a particulate chloride deficit. This is defined as the amount of particulate chloride that is necessary to balance the observed concentrations of sea salt tracer cations, such as Na^+, that have no associated chloride.

2.5.b Reactive Uptake of Gases and Volatilization of Reactive Chlorine

Additional multi-phase and heterogeneous chlorine reactions include the reactive uptake of other, non-acid gases, leading to the accumulation of photoreactive chlorine species. Most known mechanisms require the presence of reactive nitrogen gases (Wingenter et al., 1996). Many of these reactions can

take place on dry, solid salt particles as well as aqueous droplets, though the reactions are typically slower in the absence of water (Raff et al., 2009). Some examples of these reactions, which can compete with the acid displacement reactions described above, are shown below (Wolfgang Behnke et al., 1997; De Haan & Finlayson-Pitts, 1997; B J Finlayson-Pitts, Ezell, & Pitts, 1989; B J Finlayson-Pitts, 2003; Eladio M Knipping & Dabdub, 2003; Livingston & Finlayson-Pitts, 1991; M J Rossi, 1996; Jochen Stutz et al., 2009).

$N_2O_{5(g)} + NaCl_{(cd)} \rightarrow ClNO_{2(g)} + NaNO_{3(cd)}$ (Reaction 2-12)

$O_{3(g)} + NaCl_{(cd)} \rightarrow Cl_{2(g)} + \text{products}$ (Reaction 2-13)

$OH_{(g)} + NaCl_{(cd)} \rightarrow \frac{1}{2} Cl_{2(g)} + NaOH_{(cd)}$ (Reaction 2-14)

$HOCl_{(g)} + NaCl_{(cd)} \rightarrow Cl_{2(g)} + NaOH_{(cd)}$ (Reaction 2-15)

$HO_{2(g)} + NaCl_{(cd)} \rightarrow \text{products}$ (Reaction 2-16)

$ClONO_{2(g)} + KBr_{(cd)} \rightarrow BrCl_{(g)} + KNO_{3(cd)}$ (Reaction 2-17)

$ClONO_{2(g)} + NaCl_{(cd)} \rightarrow Cl_{2(g)} + NaNO_{3(cd)}$ (Reaction 2-18)

$ClNO_{2(g)} + KBr_{(cd)} \rightarrow BrNO_{2(g)} + KCl_{(cd)}$ (Reaction 2-19)

A mechanism involving the formation of a surface complex between particulate chloride and $OH^{\bullet}$ ($OH\bullet\bullet\bullet Cl^{\bullet -}$) has been proposed to explain the processes involved in reaction 2-14 (E. M. Knipping, 2000a; Eladio M. Knipping, 2002).

$OH_{(g)} + Cl^{\bullet -}_{(aq)} \rightarrow OH\bullet\bullet\bullet Cl^{\bullet -}$ (Reaction 2-20)

$2OH\bullet\bullet\bullet Cl^{\bullet -} \rightarrow Cl_{2(g)} + 2OH^-_{(aq)}$ (Reaction 2-21)

Gas phase chlorine species have also been found to react in the presence of ice surfaces or particles to produce other chlorine species (Crowley et al., 2010; B J Finlayson-Pitts et al., 1989; Livingston & Finlayson-Pitts, 1991; M J Rossi, 1996).

$ClONO_{2(g)} + HCl_{(cd)} \xrightarrow[H_2O_{(s)}]{} Cl_{2(g)} + HNO_{3(cd)}$ (Reaction 2-22)

$ClONO_{2(g)} + H_2O_{(cd)} \xrightarrow[H_2O_{(s)}]{} HOCl + HNO_{3(cd)}$ (Reaction 2-23)

$N_2O_{5(g)} + HCl_{(cd)} \xrightarrow[H_2O_{(s)}]{} ClNO_2 + HNO_{3(cd)}$ (Reaction 2-24)

The direct uptake and scavenging of HCl by dust particles has also recently been observed, resulting in dust particles up to 9% HCl by mass (Sullivan et al., 2007). In general, the cycling of chlorine can be summarized in the steps listed below (Graedel & Keene, 1995; William C Keene et al., 1990).

1. Volatilization of Cl_2, HOCl, or other photolytic chlorine species from NaCl aerosols or other source
2. Photolysis of the volatilized species to produce $Cl^{\bullet}$
3. Hydrogen atom abstraction from non-methane hydrocarbons to produce HCl
4. Removal of HCl via reaction with $OH^{\bullet}$, wet/dry deposition or scavenging by aerosols.

2.5.c N_2O_5 and $ClNO_2$ Production

One heterogeneous mechanism that has been suggested and confirmed as a source of reactive chlorine (gas phase $ClNO_2$) is the reaction of N_2O_5 with chloride aerosols. It is known that heterogeneous uptake of N_2O_5 plays a critical role in overall NO_x chemistry, with up to 50% of NO_x removal being attributed to its heterogeneous mechanisms (Thornton, Kercher, Riedel, Wagner, Cozic, Holloway, Wolfe, et al., 2010). Reactions involved chloride activation include (Aldener et al., 2006; B J Finlayson-Pitts, 2003; Schweitzer et al., 1998):

$2NO_{2(g)} + NaCl_{(cd)} \rightarrow ClNO_{(g)} + NaNO_{3(cd)}$ (Reaction 2-25)

$N_2O_{5(g)} + NaCl_{(cd)} \rightarrow ClNO_{2(g)} + NaNO_{3(cd)}$ (Reaction 2-26)

$ClONO_{2(g)} + NaCl_{(cd)} \rightarrow Cl_{2(g)} + NaNO_{3(cd)}$ (Reaction 2-27)

Of these three, reaction 2-25 is not thought to be important (Schweitzer et al., 1998). However, reaction 2-26 plays an important role in the activation of chloride and $ClNO_2$ production (Brown et al., 2009; Roberts, Osthoff, Brown, & Ravishankara, 2008a), although the process may involve multiple steps, as outlined below. Acid displacement by HNO_3 is up to two orders of magnitude slower than the interaction with N_2O_5 (Laux, Hemminger, & Finlayson-Pitts, 1994). Atmospheric implications of this reaction are important, since tropospheric concentrations of N_2O_5 can range from 1 - 15 ppb (Laux et al., 1994; Livingston & Finlayson-Pitts, 1991). The reaction results in a buildup of $ClNO_2$ in the morning, limited by N_2O_5 uptake. N_2O_5 formation, which occurs from a reversible reaction between NO_3 and NO_2, is favored at night due to the photochemical instability of NO_3 (Laux et al., 1994). Although $ClNO_2$ can form via homogeneous gas phase chemistry, the reactions are extremely slow (Sander et al., 2011), preventing significant production of $ClNO_2$.

Hints that reaction 2-26 existed arose during studies of the rates of chlorine atom production from irradiated NaCl aerosols in the presence of NO_x. A smog chamber experiment using initial NO_2, O_3 and NaCl concentrations of 200 ppbv, 108 ppbv, and 1.5 mg m^{-3}, respectively, found a large chlorine atom source upon irradiation of the mixture after 100 minutes in the dark. The observed source, if occurring from the reaction between gas phase HCl and OH, would have required a 1.5 ppmv HCl mixing ratio at OH concentrations of 1.7×10^7 cm^{-3} (W Behnke & Zetzsch, 1990). Similar smog chamber studies following up these unexplained observations indicated that $ClNO_2$ was produced at a high yield when the relative humidity was in the range of 71-92% (Zetzsch & Behnke, 1992).

A mechanism was proposed to explain the characteristics of the reaction, including the dependence of $ClNO_2$ yields on particle chloride concentrations. Due to the fact that N_2O_5 does not react directly with chloride ions, there is no observable dependence of the uptake coefficient on chloride concentrations present in the aqueous solution. This is because aqueous chloride ions react not with aqueous N_2O_5 but with its dissociation products as shown below (Schweitzer et al., 1998). Direct

hydrolysis was found to account for approximately only 20% of the overall reaction, and dissociation of N_2O_5 has since been cited as the rate limiting step (Wolfgang Behnke et al., 1997; Roberts et al., 2009; Schweitzer et al., 1998).

$$N_2O_{5(aq)} \leftrightarrow NO_2^+{}_{(aq)} + NO_3^-{}_{(aq)} \quad \text{(Reaction 2-28)}$$

$$NO_2^+{}_{(aq)} + H_2O_{(l)} \rightarrow H^+_{(aq)} + HNO_{3(aq)} \quad \text{(Reaction 2-29)}$$

$$NO_2^+{}_{(aq)} + Cl^-_{(aq)} \rightarrow ClNO_{2(aq)} \quad \text{(Reaction 2-30)}$$

Taking this proposed mechanism a step further, Bertram and Thornton (Bertram & Thornton, 2009) proposed a reaction scheme involving the initial uptake of N_2O_5 into the aqueous phase and formation of a hypothetical protonated nitric acid intermediate as the initiating step in the production of $ClNO_2$ (Bertram & Thornton, 2009). $ClNO_2$ then partitions into the gas phase where it can undergo photolysis to produce chlorine radicals (Thornton & Abbatt, 2005; Thornton, Kercher, Riedel, Wagner, Cozic, Holloway, Dubé, et al., 2010).

$$N_2O_{5(g)} \leftrightarrow N_2O_{5(aq)} \quad \text{(Reaction 2-31)}$$

$$N_2O_{5(aq)} + H_2O \leftrightarrow H_2ONO_2^+{}_{(aq)} + NO_3^-{}_{(aq)} \quad \text{(Reaction 2-32)}$$

$$H_2ONO_2^+{}_{(aq)} + H_2O \rightarrow H_3O^+_{(aq)} + HNO_{3(aq)} \quad \text{(Reaction 2-33a)}$$

$$H_2ONO_2^+{}_{(aq)} + Cl^-_{(aq)} \rightarrow ClNO_{2(aq)} + H_2O_{(aq)} \quad \text{(Reaction 2-33b)}$$

$$ClNO_{2(aq)} \leftrightarrow ClNO_{2(g)} \quad \text{(Reaction 2-34)}$$

$$ClNO_{2(g)} + h\nu \rightarrow Cl^{\bullet}_{(g)} + NO_{2(g)} \quad \text{(Reaction 2-35)}$$

An experimental study to examine the kinetics of this mechanism concluded that either reaction 2-31 or 2-32 is the rate limiting step at 50% relative humidity, thus corroborating previous suggestions that mass accommodation and hydrolysis of N_2O_5 are the processes limiting the overall reaction rate. This same study showed that the decay of gas phase N_2O_5 concentrations in the presence of simulated

sea salt aerosols is log-linear, implying a first order loss mechanism (Thornton & Abbatt, 2005). A coexisting reaction pathway producing Cl_2, in which $ClNO_2$ is an intermediate, is observed below a pH of two (Roberts et al., 2009; Roberts, Osthoff, Brown, & Ravishankara, 2008b).

$ClNO_2$ can also undergo reactions within particles instead of being released into the gas phase. The uptake and solubility of $ClNO_2$ into aqueous particles is inhibited by the presence of chloride due to its dissociation reaction in the aqueous phase (Frenzel et al., 1998).

$$ClNO_2 \leftrightarrow Cl^- + NO_2^+ \qquad \text{(Reaction 2-36)}$$

2.6 Observations of Atmospheric Chlorine Radicals and Related Species

The preceding sections have summarized gas phase, heterogeneous and multi-phase reactions of chlorine radicals and related species, believed to important in urban atmospheres. The relative importance of these pathways has been examined in a variety of observational studies. In this section, observational evidence of the presence of various atmospheric chlorine species will be explored.

2.6.a Observations of Chloride Deficits and Volatilization

Overall, depending on region and aerosol size, particle chloride volatilization of 70-80% is possible (Erickson et al., 1999). A study of volatile chlorine over the North Atlantic Ocean determined that the concentrations of volatilized chlorine from aerosols, as determined from particulate chloride deficits, tended to be approximately equal to measured HCl concentrations, ranging from below detection limits up to 125 nmol m^{-3} (3 ppbv) (William C Keene et al., 1990). A separate study of chlorine chemistry in polluted air which had been advected offshore noted that the cycling of chlorine between particle and gas phases can lead to a Cl_2 increase of 90 parts per trillion by volume (pptv) and 125 pptv in no wind and high wind scenarios, respectively (Pechtl & von Glasow, 2007). Shown below are the dominant reactions responsible for this increase. The sequence is initiated by acid displacement (reactions 10-11) (Pechtl & von Glasow, 2007).

$HCl + OH^{\bullet} \rightarrow Cl^{\bullet} + H_2O$ (Reaction 2-37)

$Cl^{\bullet} + O_3 \rightarrow ClO^{\bullet} + O_2$ (Reaction 2-38)

$ClO^{\bullet} + HO_2^{\bullet} \rightarrow HOCl + O_2$ (Reaction 2-39)

$HOCl_{(g)} \leftrightarrow HOCl_{(aq)}$ (Reaction 2-40)

$Cl^-_{(aq)} + HOCl_{(aq)} + H^+_{(aq)} \rightarrow Cl_{2(aq)} + H_2O_{(l)}$ (Reaction 2-41)

$Cl_{2(aq)} \rightarrow Cl_{2(g)}$ (Reaction 2-42)

The correlation between particulate chloride deficits and HCl concentrations was observed to be much higher in air polluted with combustion products, nearing a [HCl]/[Cl^- deficit] ratio of 1 in polluted air masses compared to 4.5 in cleaner air masses (William C Keene et al., 1990).

Deficits vary regionally, and air in the southern hemisphere exhibits lower particulate chloride deficits while chloride deficits in the northern hemisphere have approached 100%. However, once particulate chloride is removed, HCl serves as a chloride reservoir and can be scavenged by aerosols to replenish particulate chloride concentrations (Thornton, Kercher, Riedel, Wagner, Cozic, Holloway, Wolfe, et al., 2010). It is predicted that HCl has a lifetime in the marine boundary layer of 10 minutes before it is scavenged by sea salt aerosols (Sullivan et al., 2007).

2.6.b Observations of Hydrogen Chloride (HCl) and Molecular Chlorine (Cl_2)

Surface concentrations of HCl in remote ocean regions range from 100-300 pptv, while peak concentrations in urban areas can be approximately 1500 pptv. Multiple studies note that peak HCl concentrations typically occur in the afternoon, coinciding with peak photochemical smog production and HNO_3 concentrations (Appel, Tokiwa, Povard, & Kothny, 1991; Griffin et al., 2011; Harrison & Allen, 1990; John, Wall, & Ondo, 1988; Matusca, Schwarz, & Bachmann, 1984). This is generally attributed to the volatilization of chloride from aerosol particles (Graedel & Keene, 1995; John et al., 1988; Matusca et al., 1984). HCl generally exhibits a trend of vertical distribution, decreasing with

altitude. Previous reviews of continental tropospheric HCl observations have reported peak concentrations of up to 1 – 3 ppbv in urban areas (Graedel & Keene, 1995). A marked drop off in concentration to 50-100 pptv typically occurs at altitudes above the boundary layer (Graedel & Keene, 1995; William C Keene et al., 1990).

In Virginia Key, FL, mist chamber techniques (Wllllam C Keene, Pszenny, Gallowayt, Division, & Causeway, 1993) were used to measure total HCl* (HCl and possibly $ClNO_x$ species), which ranged between 40-268 pptv Cl. The same technique was used to measure total Cl_2* (Cl_2 + some HOCl) and found concentrations ranging from below the detection limit of 26 pptv up to 254 pptv Cl. Cl_2* built up during the night and sharply decreased after sunrise corresponding with an HCl* increase. This suggests the photolysis of Cl_2 and/or HOCl at sunrise, followed by VOC oxidation via hydrogen atom abstraction by $Cl^{\bullet}$, producing HCl. Photochemical modeling performed in this study indicated that if the observed levels of Cl_2* were completely photolyzed, it would lead to a $Cl^{\bullet}$ concentrations of 10^4-10^5 cm^{-3} (Wllllam C Keene et al., 1993). It was observed that higher levels of Cl_2 and HOCl were present in winds coming from the Atlantic as opposed to those from the North, suggesting a marine origin (Wllllam C Keene et al., 1993).

Other authors have also noted that high concentrations of molecular chlorine in incoming marine air along the coasts of North America (Spicer et al., 1998). Using the mist chamber technique in the Hawaii boundary layer, HCl* and Cl_2* concentrations up to 250 and 38 pptv, respectively, were detected (A. A. P. Pszenny et al., 2004). Cl_2 concentrations in La Jolla, CA have been observed to average 2.3 pptv (Finley & Saltzman, 2008). In Irvine, CA, Cl_2 concentrations ranging from 2.5 to 20 pptv with a two month mean of 3.5 pptv have been reported. Modeling the photochemistry of this observed Cl_2 showed a 5-8 ppb increase in daily maximum O_3 concentrations (Finley & Saltzman, 2006). Earlier evidence of O_3 production increases from the presence of chlorine was observed in industrial plumes in Telemark, Norway (Hov, 1985). In Houston, Texas, the detection of the tracer species (CMBO) at peak

concentrations of 12 – 126 pptv (Tanaka et al., 2003a) provided evidence of chlorine radical concentrations estimated to be approximately < 5 x 10^3 – 3.3 x 10^5 atoms cm^{-3} (2 x 10^{-4} – 1.3 x 10^{-2} pptv) (Riemer & Apel, 2002). Associated enhanced ozone production rates of > 75 ppbv hr^{-1} were observed when small amounts of Cl_2 were injected into captive ambient air during chamber experiments (Tanaka, 2003a; Tanaka et al., 2003a).

Off the coast of Long Island, New York, a concentration up to 150 pptv Cl_2 was observed at night, with a rapid decline to less than 15 pptv after sunrise. Such amounts of Cl_2 would lead to chlorine atom concentrations of 1.3 x 10^5 atoms cm^{-3} (5.1 x 10^{-3} pptv) and require a daily source of approximately 330 pptv Cl_2. In this case, the air was again of marine origin (Spicer et al., 1998). The authors suggest that a mechanism aside from photolytically driven aqueous phase mechanisms (Wllllam C Keene et al., 1993; Oum, Lakin, DeHaan, Brauers, & Finlayson-Pitts, 1998) is needed to explain these observations. A study in the arctic coastal location of Alert, Northwest Territories utilized the photoreactive halogen detector method (Impey, Shepson, Hastie, Bartie, & Lafayette, 1997) to detect levels of photolyzable Cl, which ranged between < 9 – 100 pptv. Concentrations were reported as Cl_2, although they may have also included HOCl or other photolyzable species. A nocturnal buildup of photolytic chlorine species followed by a rapid decline after sunrise was once again observed. To explain the night time buildup of these species, the following nocturnal mechanism was proposed (Impey, Shepson, Hastie, & Barrie, 1997):

$$Cl^{\bullet} + O_3 \rightarrow ClO^{\bullet} + O_2 \qquad \text{(Reaction 2-43)}$$

$$ClO^{\bullet} + HO_2^{\bullet} \rightarrow HOCl + O_2 \qquad \text{(Reaction 2-44)}$$

$$HOCl_{(g)} + \text{acidic aerosol}_{(aq)} \rightarrow HOCl_{(aq)} \qquad \text{(Reaction 2-45)}$$

$$HOCl_{(aq)} + Cl^-_{(aq)} + H^+_{(aq)} \rightarrow Cl_{2(g)} + H_2O_{(l)} \qquad \text{(Reaction 2-46)}$$

In Charlottesville, Virginia, approximately 250 miles inland, researchers using the tandem mist chamber technique (Wllllam C Keene et al., 1993) found HCl* concentrations ranging from < 39 to 2800 pptv, with most measurements falling under 300 pptv. Most measurements of Cl_2 and HOCl in the same study were under the 26 pptv $Cl^{\bullet}$ detection limit, indicating that HCl (and possibly $ClNO_x$) was the dominant form of volatile chlorine (Maben, Keene, Pszenny, Galloway, & C, 1995). Because of results such as this, another proposed explanation of the marine origin of Cl_2 has been made by suggesting a heterogeneous reaction between particulate chloride and either ozone or the hydroxyl radical (Graedel & Keene, 1995; Impey, Shepson, Hastie, & Barrie, 1997; William C Keene et al., 1990; Wingenter et al., 1996). An alternate reaction explaining the mechanism described in reactions 20-21 was put forward as an explanation (W Behnke & Zetzsch, 1989; Wllllam C Keene et al., 1993):

$$2Cl^-_{(cd)} + O_{3(cd)} \xrightarrow{H_2O} \quad Cl_{2(g)} + 2OH^-_{(cd)} + O_{2(g)} \qquad \text{(Reaction 2-47)}$$

Assuming a steady state between Cl_2 volatilization by reaction 2-47 and reuptake of HCl into aerosols, this mechanism results in a Cl_2 source of approximately 1 ppbv hr^{-1} with corresponding net O_3 production rates of 1.4 ppbv hr^{-1} during the day (William C Keene et al., 1990). Table 2-4 contains a summary of observations from the studies discussed in this section.

Table 2-4. Summary of Ranges of HCl and Cl_2 Observations[A]

Environment	HCl[B]	Cl_2[B]
Marine	50-1200	-
Coastal/Island	40-268	2.3 – 254
Urban	39-8000	2.5 – 20
Arctic Coastal	-	9.0 – 100

[A] Concentrations are in pptv
[B] Data from studies reporting HCl* or Cl_2* are included

Reactions 2-43 – 2-47, or other pathways that also lead nocturnal buildup of photolytic chlorine species, can potentially lead to increases in VOC oxidation, NO-to-NO_2 conversion and O_3 production early in the day. The effects of the sudden introduction of a large source of chlorine radicals would be

analogous to the effect elicited by the nocturnal buildup and sunrise photolysis of a hydroxyl radical source such as HONO.

2.6.c Observations of Atomic Chlorine (Cl•) and Chlorine Monoxide (ClO•)

Analysis of Non-Methane Hydrocarbon (NMHC) decay rates has led to estimates of chlorine atom concentrations on the order of 10^5 molecules cm^{-3} (4 x 10^{-3} pptv) in the Pacific marine boundary layer (MBL). These concentrations were deduced from observed decay rates of VOCs such as ethane, propane and acetylene by back calculating necessary chlorine radical concentrations to compensate for a lack of sink strength from the $OH^{\bullet}$ reaction alone (H. B. Singh et al., 1996). At Appledore Island, Maine, observations of increased NMHC reactivity implied chlorine radical concentrations of 2.2 x 10^4 – 5.6 x 10^4 atoms cm^{-3} (8.6 x 10^{-4} – 2.2 x 10^{-3} pptv). These concentrations were deduced by measuring C_2-C_{10} NMHC compounds, calculating the back trajectories of sampled air parcels and then calculating the chlorine radical concentration necessary to explain observed NMHC decay rates that were too fast to be fully explained by $OH^{\bullet}$ concentrations (A. a. P. Pszenny, Fischer, Russo, Sive, & Varner, 2007). In the Southern Ocean, average $Cl^{\bullet}$ concentrations of 720 atoms cm^{-3} (2.8 x 10^{-5} pptv) have been reported (Wingenter et al., 1999). At Great Lake, Utah, 3.8 x 10^8 molecules $ClO^{\bullet}$ (15 pptv) was observed, suggesting mobilization of chloride from salt beds in the area (Jochen Stutz, Ackermann, Fast, & Barrie, 2002). This observation also implied a chlorine atom concentration on the order of 10^5 atoms cm^{-3} (4 x 10^{-3} pptv) , which would double the reactivity of the air in the area, increase OH concentrations by up to 50% through radical propagation and convert NO_x into halogenated nitrates (Jochen Stutz et al., 2002).

2.6.d Observations of Nitryl Chloride

Direct correlations between $ClNO_2$, N_2O_5, and aerosol surface area concentrations have been noted in field observations (Osthoff et al., 2008; Parrish et al., 2009). During the Texas Air Quality Study II (TEXAQS II), concentrations of $ClNO_2$ up to 1200 pptv were found in ship engine plumes, near NO_x sources in the Houston Ship Channel and in surrounding urban areas (Osthoff et al., 2008; Parrish

et al., 2009). Contemporaneously measured N_2O_5 concentrations and consumption rates suggest that anthropogenic pollutants contributed significantly to the observed $ClNO_2$ (Osthoff et al., 2008; Parrish et al., 2009).

Additionally, $ClNO_2$ concentrations up to 450 pptv have also been found as far inland as Kohler Mesa outside of Boulder, CO. The Kohler Mesa is 1400 km from any coastal area, but it is thought that the air masses during the measurement period were potentially influenced by long distance chlorine transport from coastal areas or inland salt beds and pollution from combustion in the Boulder, CO area (Thornton, Kercher, Riedel, Wagner, Cozic, Holloway, Wolfe, et al., 2010). More recent observations in Los Angeles, CA revealed concentrations of $ClNO_2$ up to 2100 pptv (Riedel et al., 2012). In 2011, observed $ClNO_2$ mixing ratios up to 250 pptv were observed in Calgary, Albert, Canada(Mielke et al., 2011). Arctic observations of N_2O_5 and $ClNO_2$ were made during the International Chemistry in the Arctic Lower Troposphere (ICEALOT) campaign. $ClNO_2$ and N_2O_5 were observed to range, on average, 150-250 and 150-200 pptv, respectively (Kercher, Riedel, & Thornton, 2009). Table 2-5 summarizes observations of $ClNO_2$ in several locations.

Table 2-5. Detection of $ClNO_2$ Chemistry in Continental North America.

Locale	N_2O_5 (ppbv)	$ClNO_2$ (pptv)	N_2O_5 loss rate, k_{het} (s^{-1})
Texas Gulf Coast	0-0.750	0-1200	(0.1-3) x 10^{-3}
Boulder	0-1.5	0-450	-
Los Angeles	0-25	0-2100	-
Calgary	1.9-60	0-250	-

Texas Gulf Coast data are from Osthoff et al., 1998. Boulder, Colorado data are from Thornton et al., 2010. Los Angeles, California data are from Riedel et al., 2012. Calgary, Ontario data are from Mielke et al., 2011. Only NO_y data for Los Angeles and Calgary were reported in this study.

2.6.e Observations of Chlorine Tracer Species

CMBO and CMBA are known tracer compounds of chlorine's oxidation of isoprene. Observations of these compounds were made during the Texas Air Quality Study (TEXAQS) in Houston, Texas (Tanaka et al., 2003b). Chlorine atom concentrations were deduced from CMBO and CMBA concentrations and were determined to range between 5 x 10^3 – 3.3 x 10^5 atoms cm^{-3} (2 x 10^{-4} –

1.3 x 10^{-2} pptv) (Riemer & Apel, 2002). In comparison, Maben et al (1995) approximated chlorine atom concentrations to be less than 10^4 atoms cm^{-3} (4 x 10^{-4} pptv) in continental air over eastern North America, at the lower end of the range of the Houston observations. During the Atlantic Stratospheric Transition Experiment/Marine Aerosol and Gas Exchange (ASTEX/MAGE), observed hydrocarbon concentrations were used to determine average chlorine atom concentrations between 6:00-11:00 LT, which were approximated at (3.3 ± 1.1) x 10^4 molecules cm^3 (1.2 (± 0.4) x 10^{-3} pptv). Noontime concentrations were calculated to be (6.5 ± 1.4) x 10^4 molecules cm^{-3} (2.6 (± 0.6) x 10^{-3} pptv), and the authors suggest a nocturnal buildup of photolyzable chlorine as the source (Wingenter et al., 1996).

2.6.f Summary of Observations

Observational evidence suggests that chlorine chemistry is occurring over both oceanic and continental areas, with observed chlorine radical concentrations on the order of 10^3 – 10^5 molecules cm^{-3} (4 x 10^{-5} – 4 x 10^{-3} pptv) not being uncommon (Graedel & Keene, 1995; Jobson, Niki, Bottenheim, Hopper, & Leaitch, 1994; Maben et al., 1995; A A P Pszenny et al., 1993; Riemer & Apel, 2002; Wingenter et al., 1996). While observations have generally supported known gas phase chemical pathways, observational evidence (Osthoff et al., 2008; A A P Pszenny et al., 1993; Spicer et al., 1998; Thornton, Kercher, Riedel, Wagner, Cozic, Holloway, Dubé, et al., 2010) hinting at a more complex role for chlorine illuminated gaps in the understanding of reactive gas phase chlorine sources in the atmosphere. Such observations have led to the proposal and investigation of heterogeneous mechanisms to explain the volatilization of chloride from aerosol particles (E. M. Knipping, 2000b; Eladio M Knipping & Dabdub, 2003; Eladio M. Knipping & Dabdub, 2002; Oum et al., 1998; Roberts et al., 2009, 2008b; Thornton & Abbatt, 2005). More recently, daytime concentrations of chlorine species such as HCl and $ClNO_2$ on the order of 1-2 ppbv have been reported inland in regions such as Dallas-Ft. Worth (Griffin et al., 2011) and Boulder Colorado (Thornton, Kercher, Riedel, Wagner, Cozic,

Holloway, Wolfe, et al., 2010). These observations may suggest sources other than sea salt for atmospheric chlorine.

2.7 Modeling Studies

As the importance of chlorine as an atmospheric oxidant has become increasingly apparent, atmospheric chemistry models have been supplemented with basic gas phase chlorine chemistry mechanisms. This section describes condensed chlorine mechanisms, and their use in regional photochemical modeling studies.

2.7.a Condensed Chlorine Mechanism Development

A critical component of regional models is a condensed photochemical mechanism that is computationally efficient while retaining enough accuracy be used in the study of atmospheric chemical processes. The Carbon Bond mechanism (G Z Whitten, Hogo, & Killus, 1980; Yarwood & Rao, 2005) is one of the most commonly used condensed chemical mechanisms; reactions representing chlorine chemistry in urban atmospheres were devised and added to a modified version of the Carbon Bond mechanism (Tanaka, 2003b) for use in the Comprehensive Air quality Model with extensions (CAMx). The mechanism included the reaction of chlorine with ozone and VOCs through condensed reactions for olefins and paraffins. Reactions with ethene, methane, 1,3-butadiene and isoprene were explicitly represented in order to account for the unique products of these reactions while also enabling comparisons between observations and predictions of the concentrations of these molecular tracers. Photolysis reactions for Cl_2 and HOCl were included, and the rates of photolysis for these species were scaled to the photolysis rates of NO_2 and isoprene oxidation products, respectively (Tanaka, 2003b). Since the creation of this initial mechanism, chlorine reaction sets have been implemented as adjunct mechanisms in both the Carbon Bond 05 (CB05) and the SAPRC-07 mechanisms (William P L Carter, 2010b; Yarwood & Rao, 2005), and these mechanisms have been used in both box (Heo et al., 2010)

and regional (Sunghye Chang & Allen, 2006a; Faraji, Kimura, McDonald-Buller, & Allen, 2008; G. Sarwar, Simon, Bhave, & Yarwood, 2012; H. Simon et al., 2009, 2010; Tanaka et al., 2003b) modeling.

Recent chlorine mechanism development has involved the addition of heterogeneous pathways, including $ClNO_2$ production chemistry (G. Sarwar et al., 2012; H. Simon et al., 2009, 2010) and the $OH^{\bullet}$-mediated formation of gas phase Cl_2 (E. M. Knipping, 2000b; Eladio M Knipping & Dabdub, 2003; Eladio M. Knipping & Dabdub, 2002). One study (H. Simon et al., 2009) implemented a surrogate gas phase reaction for investigating $ClNO_2$ chemistry (reactions 2-28 – 2-30); Simon et al. (2010) improved upon the scheme by using a heterogeneous parameterization (Jacob, 2000; Ravishankara, 1997; Thornton & Abbatt, 2005). Parameter values cited from the literature were used and varied by region based on proximity to the Gulf Coast (H. Simon et al., 2010). Further work on $ClNO_2$ chemistry included dependencies (Bertram & Thornton, 2009) on particle liquid water, particle nitrate and particle chloride in the parameterization of $ClNO_2$ chemistry for modeling within the continental United States (G. Sarwar et al., 2012). A parameterized (Jacob, 2000; Ravishankara, 1997) version of reactions 20-21 was implemented to study the impact of sea salt and related chlorine emissions on coastal urban ozone in the South Coast Air Basin, CA (Eladio M Knipping & Dabdub, 2003).

2.7.b Regional Modeling of Atmospheric Chlorine Chemistry

Photochemical models are used to probe the impacts of atmospheric chlorine chemistry on continental to global scale. The focus in this section will be on regional models since the reduced computational intensity of these models, relative to global models, has allowed more detailed treatments of chlorine chemistry.

In Houston, TX, the inclusion of anthropogenic chlorine emissions in regional modeling revealed a maximum localized ozone increase of 16 ppb and moderate increases over a larger spatial area. The maximum modeled O_3 increase coincided with a maximum CMBO mixing ratio of 59 ppt (Tanaka et al., 2003b). Another study found that chlorine increased 1 hour and 8 hour ozone during peak ozone hours

by 8 ppb and 9 ppb, respectively. This same study also found a maximum increase during morning hours, at the times of maximum rates of Cl_2 and HOCl photolysis, of 45 ppbv (Linlin Wang, Thompson, McDonald-Buller, et al., 2007; Linlin Wang, Thompson, Mcdonald-buller, Webb, & Allen, 2007). Since some of the peak enhancements of ozone concentrations predicted in these models are highly localized near chlorine radical precursor sources, the maximum predictions of the models are very sensitive to the grid cell dimensions used in the work. Wang, et al. (2007a, 2007b) used a nested grid with horizontal spatial resolutions as small as 4 km. In similar work, but with horizontal grid cell dimensions of 12-36 km, another study (Golam Sarwar & Bhave, 2007) modeled the effect of chlorine chemistry on ozone levels over the eastern half of the United States. The study found major impacts only in the Houston, TX and New York-New Jersey areas, where 1-hour O_3 averages increased by 12 and 6 ppbv, respectively. 8-hour increases were 8 and 4 ppbv, respectively. Similarly, a study of a photochemical pollution episode in September, 2000 in Southeast Texas, using a 4-km horizontal spatial resolution found highly localized non-peak O_3 concentration increases up to 70 ppbv, with peak hour concentration increases typically below 10 ppbv (Sunghye Chang & Allen, 2006a). Yet another study in Texas found a 1 hour average O_3 increase of 1.5 ppb from inclusion of $ClNO_2$ production and photolysis (H. Simon et al., 2009).

Modeled $ClNO_2$ concentrations in southeast Texas have ranged from 256-1210 pptv, compared to previous field measurements in the region of 1300 pptv. A limiting factor in the modeling was the modeled availability of chloride. Scenarios assuming excess particulate chloride resulted in peak ground-level $ClNO_2$ concentration increases of up to 3200 pptv compared to a base case scenario without excess particulate chloride (H. Simon et al., 2010). More recently, modeling of $ClNO_2$ chemistry across the continental U.S. revealed monthly mean 8-hr O_3 increases of 1-2 ppbv (3-4%), with maximum daily 8-hr maximum increases of up to 13 ppbv in the northeastern United States. Resulting reductions in total nitrate ranged from 11-21%. This study used a single domain of 12 km grid cells (G.

Sarwar et al., 2012). Regional modeling of the South Coast Air Basin (SOCAB) suggests that sea salt-derived chlorine chemistry reduces weekend ozone levels while increasing average weekday peaks, thus reducing the difference between the two (Cohan, Chang, Carrerassospedra, & Dabdub, 2008). A separate study in the SOCAB (Eladio M Knipping & Dabdub, 2003) included several chlorine reaction mechanisms (reactions 2-10, 2-11, 2-20, 2-22, 2- 28, 2-29, 2-30) and found a maximum 1-hour ozone enhancement of 12.7 ppbv with a corresponding peak in Cl_2 concentrations of 12 pptv. In both of these cases, 5 km grid cells were used (Cohan et al., 2008; Eladio M Knipping & Dabdub, 2003). A summary of results from the studies discussed above is shown in Table 2-6.

Table 2-6. Summary of Grid Cell Sizes used in Regional Photochemical Modeling

Reference	Region[A]	Nested	Grid Size (km)	Maximum 1-hr O_3 Enhancement (ppbv)	Chlorine Species Reported	Maximum Predicted Cl Species Concentration (pptv)
Knipping and Dabdub, 2003	SOCAB, CA	No	5	12.7	Cl_2	12
Tanaka et al., 2003a	Houston, TX	Yes	36, 12, 4	16	CMBO	59
Chang and Allen, 2006	Houston, TX	Yes	36, 12, 4	72	CMBO	100
Wang et al., 2007 a,b	Houston, TX	Yes	36, 12, 4	48	-	-
Heo et al., 2010	Eastern U.S.	Yes	36, 12	12	-	-
Cohan et al., 2008	SOCAB, CA	No	5	80	Cl_2	1000
Simon et al., 2009	Houston, TX	Yes	36, 12, 4	-C	$ClNO_2$	> 3200
Simon et al., 2010	Houston, TX	Yes	36, 12, 4	1.5	$ClNO_2$	719
Sarwar et al., 2012	Continental U.S.	No	12	13.3[B]	$ClNO_2$	4500

[A] Indicates region of focus for the highest resolution grid. For simplicity, the largest urban metropolitan area within the finest mesh grid is cited where appropriate.
[B] 8-hr average O_3 increases were reported in this study
[C] – indicates that no value was explicitly reported in this study

The concentrations predicted from these modeling studies correspond well with documented observations of reactive chlorine. However, in order to model chlorine radical concentrations at magnitudes that are consistent with observed concentrations, modelers must assume rates for the most likely heterogeneous mechanisms. Along with uncertainties in anthropogenic and natural source strength approximations, the values of these rate parameters in heterogeneous reactions remain a gap in current understanding of urban atmospheric chlorine chemistry.

2.8 Critical Gaps in Current Understanding

This section addresses two primary areas of uncertainty in the understanding of atmospheric chlorine chemistry. The first area of uncertainty is accurate estimation of the parameters used to model heterogeneous chlorine chemistry. The parameters involved in the heterogeneous $ClNO_2$ mechanism that was described in previous sections is included as a case study of the range of predictions that can result from application of models, employing reaction rate parameters within accepted ranges. The second area of uncertainty is the issue of the chlorine emissions sources driving the chemistry.

2.8.a Sensitivity Analysis of Heterogeneous $ClNO_2$ Production

The parameters that must be known to model heterogeneous reactions include (Ravishankara, 1997):

1. Particle surface area.
2. The phase(s) in or on which the reaction is taking place.
3. Chemical composition of the phases.
4. Concentrations of species involved in the reaction.
5. A reactive uptake coefficient for the gas species involved.

These physical parameters can be lumped into a single rate constant (Jacob, 2000; Ravishankara, 1997):

$$k = \frac{\gamma_{obs}\omega A}{4} \qquad \text{(Reaction 2-48)}$$

Here, γ_{obs} is the observed reactive uptake coefficient, ω is the average molecular velocity of the reactant, and A is the surface area density of particles ($cm^2\ cm^{-3}$). The reactive uptake coefficient is the number of molecules lost through the surface relative to the number of molecules hitting the surface and is a unit-less parameter (Frenzel et al., 1998). In addition to these parameters, fractional yield of the product can be included on the right hand side of equation 48 when competitive reaction pathways are present within the condensed phase.

A wide variety of yield and reactive uptake values for reactions producing $ClNO_2$ have been reported in the literature (Aldener et al., 2006; W Behnke, Krüger, Scheer, & Zetzsch, 1991; De Haan & Finlayson-Pitts, 1997; C. George et al., 1994; J. H. Hu & Abbatt, 1997; Jacob, 2000; Laux et al., 1994; Livingston & Finlayson-Pitts, 1991; Osthoff et al., 2008; Schütze & Herrmann, 2002; Schweitzer et al., 1998; Thornton & Abbatt, 2005; Thornton, Kercher, Riedel, Wagner, Cozic, Holloway, Wolfe, et al., 2010). The range of heterogeneous reaction rate parameters reported in the literature was used to develop a range for the values of the reactive uptake coefficient (γ) and the $ClNO_2$ yield (Y_{ClNO2}) for the reaction of N_2O_5 with particulate chloride. Previous regional modeling studies of this mechanism used limited, and typically fixed, parameter values (H. Simon et al., 2009, 2010). One recent study (G. Sarwar et al., 2012) has implemented parameterizations (Bertram & Thornton, 2009; Roberts et al., 2009; Thornton, Kercher, Riedel, Wagner, Cozic, Holloway, Wolfe, et al., 2010) which account for influences from particulate species such as H_2O and NO_3^- for continental-scale modeling within the U.S. These parameterizations are shown below, where *f* and *r* subscripts indicate directionality of the reversible reactions that are referenced (Bertram & Thornton, 2009; Roberts et al., 2009).

$$Y_{ClNO_2} = \frac{\Delta ClNO_2}{\Delta N_2O_5} = \left(\frac{k_{33a}[H_2O]}{k_{33b}[Cl^-]} + 1\right)^{-1} \qquad \text{(Reaction 2-49)}$$

$$\gamma_{N_2O_5} = Ak'_{32f}\left(1 - \frac{1}{\left(\frac{k_{33a}[H_2O(l)]}{k_{32r}[NO_3^-]}\right)+1+\left(\frac{k_{33b}[Cl^-]}{k_{32r}[NO_3^-]}\right)}\right) \qquad \text{(Reaction 2-50)}$$

$$k'_{32f} = \beta - \beta e^{(-\delta[H_2O(l)])} \qquad \text{(Reaction 2-51)}$$

The ratio of k_{33b}/k_{33a} has been determined by several studies to range between (450 $\pm$ 100) – (836 $\pm$32) (Aldener et al., 2006; Wolfgang Behnke et al., 1997; Bertram & Thornton, 2009; Brown et al., 2009; Roberts et al., 2009). For the other parameters involved, A is 3.2 x 10^{-8} s, $\beta$is (1.15 $\pm$0.3) x 10^5 s^{-1}, and δ is (1.3 $\pm$0.5) x 10^{-1} (Bertram & Thornton, 2009). While the introduction of

parameterizations such as in equations 48-50 is an important advance over fixed parameter values, the parameterization still assumes that heterogeneous rates parameters can be quantified with precision.

The objective of the sensitivity analysis described here is to quantify upper and lower limits to the impacts of this mechanism with respect to O_3 formation chemistry. Effects of varying VOC concentrations and composition as well as NO_x availability were tested. Changes in peak O_3 and $ClNO_2$ concentrations between simulations were quantified and compared to a base case scenario lacking heterogeneous chemistry. Methods used in the sensitivity analyses are summarized in Chapter 4 and Appendix A.

Using well established parameter ranges, the heterogeneous reaction of N_2O_5 with aerosol chloride is able to reproduce $ClNO_2$ concentrations at levels that have been observed. Depending on the combination of heterogeneous parameters, VOCs, and NO_x, the mechanism contributed to both peak ozone reduction as well as peak ozone increases. The range of impact was a -10.5% to 27% change in peak O_3 concentrations relative to a base case scenario with no heterogeneous reactions. The decreases in ozone typically resulted from low values of $ClNO_2$ yield (0-15%, depending on the amount and types of VOCs present). Relative decreases in O_3 occurred in simulations including the heterogeneous chemistry due to the fact that the mechanism served as a NO_x sink, particularly in cases with low $ClNO_2$ yields. This NO_x sink was not present in the simulations without heterogeneous chemistry. Combinations of yields above 25% and reactive uptake coefficients greater than zero resulted in increases in peak ozone levels.

The effect of changing base VOC concentrations was also examined. Four scenarios with differing initial VOC concentrations were used: (1) 0 ppbC VOCs; (2) 300 ppbC VOCs; (3) 1000 ppbC VOCs; (4) 300 ppbC t-2-butene. The reason for isolating the impacts of t-2-butene within a single scenario is that it rapidly reacts with $NO_3^{\bullet}$, thus producing HNO_3 instead of N_2O_5 through the reaction of $NO_3^{\bullet}$ with NO_2. For all values of γ examined, the effect of increasing the value of the yield parameter

from 0 – 100% at a fixed γ was a linear increase in peak ozone concentrations. These results are summarized in Appendix A. Increasing the reactive uptake at a fixed yield value resulted in an intensification of the effect on peak ozone concentrations elicited by the value of the yield parameter. These, and additional, results are also discussed in Chapter 4 and Appendix A.

The range of impact that heterogeneous $ClNO_2$ production has on peak ozone levels in the scenarios described above reflects the potential significance of this chemistry to ozone formation. However, the broad range of reported parameter values and the potential for both increases and decreases in ozone production from this mechanism highlight the importance of accurate parameter estimation. Maximum changes in peak O_3 concentrations ranged from -10.5% to 27%. $ClNO_2$ formation via this mechanism resulted in concentrations up to 4.0 ppb at the highest combination of parameter values, with peak concentrations of 1.0-2.0 ppb being typical of more moderate parameter value combinations (e.g. 20-50% yield and a reactive uptake of 0.03). It should be noted that this analysis excluded the consideration of impacts from meteorology, mass transport and dilution. However, it serves in identifying an upper boundary of impacts for the chemistry alone.

2.8.b Uncertainty in Emissions Estimates

Traditionally, sources of molecular chlorine, and other inorganic sources of chlorine atoms, have not been included in photochemical modeling. Studies covered in the section on regional modeling (Sunghye Chang & Allen, 2006a; Cohan et al., 2008; G. Sarwar et al., 2012; Golam Sarwar & Bhave, 2007; H. Simon et al., 2009, 2010; Tanaka et al., 2003b; Linlin Wang, Thompson, McDonald-Buller, et al., 2007; Linlin Wang, Thompson, Mcdonald-buller, et al., 2007) highlighted the effects of including chlorine emissions into the modeling of photochemical episodes. Inventories have been developed for both anthropogenic (S Chang, Tanaka, Mcdonald-buller, & Allen, 2001; McCulloch et al., 1999) and natural (Erickson et al., 1999; C. Keene et al., 1999; Lobert, Keene, Logan, & Yevich, 1999; Reff et al., 2009) sources. However, uncertainties exist within these inventories. Uncertainty in inventory

development can stem from uncertainty in observations used to deduce source strengths and the methods or assumptions associated with extrapolating these measurements to larger scales (Khalil et al., 1999). Assumptions in emissions factors as well as approximations in their implementation into models are two additional sources of uncertainty (Lobert et al., 1999). In general, any uncertainty in the understanding of the biogeochemical processes involved in the natural chlorine cycle can lead to a corresponding uncertainty within inventories (C. Keene et al., 1999).

Chang et al. (2001) developed a comprehensive inventory for Houston, TX that evaluated industrial point sources, cooling tower use, water and wastewater treatment, swimming pool chlorination, tap water use, sea salt chloride and chlorinated organics as potential chlorine radical precursor sources in the region. The authors cite particularly high uncertainty in the emission rates of chlorinated organics and sea salt aerosols. Uncertainty in the form of volatile reactive chlorine species (HOCl and Cl_2) produced by anthropogenic sources such as cooling tower operation has also been noted (S Chang et al., 2001). The contribution of inorganic chlorine from biomass burning, and particularly the anthropogenic contribution via this mechanism, is inherently uncertain due to the problem of accurately estimating the natural rate of fires in a scenario in which humans are not present. One study noted that while biomass burning could potentially contribute up to 25 % of total HCl emissions, the source strength is highly uncertain and not likely to be a significant source of particulate chloride, globally (Lobert et al., 1999). Sinks and removal processes for chlorine species can also be a source of uncertainty (C. Keene et al., 1999). Emissions estimates from coal combustion also suffer from uncertainty in the amount of chloride present in the coal (McCulloch et al., 1999). Sinks and removal processes for chlorine species are also a source of uncertainty (C. Keene et al., 1999).

2.9 Summary

Most of the studies cited in this review have presumed that sea salt is the dominant source of atmospheric chlorine, however, markers of chlorine chemistry such as HCl and $ClNO_2$, observed at

inland locations such as Dallas-Ft. Worth and may suggest sources other than sea salt for atmospheric chlorine. An important step in improving the understanding of chlorine's role in urban atmospheres would be to more accurately model the processes underlying emissions of the various chlorine radical precursors that have been observed. Improved emissions inventories could be coupled with the increasing knowledge of heterogeneous processes in order produce more meaningful computational predictions of the impact that chlorine species have in urban environments. As seen from the evidence related to enhanced ozone production from the presence of chlorine, this would prove extremely useful to researchers addressing issues in urban air quality.

The literature review described in this chapter indicates that the knowledge of chlorine's role in tropospheric chemistry is a steadily evolving field of study. In addition to ambient measurements and experimental studies, the use of computational modeling will play an integral part in completely illuminating the nature of the interactions between tropospheric chlorine chemistry and air quality. The concentrations predicted from the aforementioned modeling studies typically fall within the same order of magnitude of concentrations reported from ambient observations of reactive chlorine. Modeling studies on the effects of chlorine chemistry on ozone formation in the lower atmosphere provide insights into the extent of chlorine's potential impact on this NAAQS criteria pollutant. In many instances, modeling studies predict concentrations of reactive chlorine species by using assumed rates of chlorine generation from indefinite mechanisms.

As the understanding of these mechanisms increases so will confidence in explanations of the results of field observations and the predictions of modeling studies. As mentioned previously, one source of inorganic chlorine in the lower atmosphere involves the interaction of gas phase compounds with chloride containing aerosol particles, particularly those that are deliquesced. Within the following chapters (Chapters 4, 5 and 6), experimental and modeling investigations into two of the mechanisms involved in these types of interactions will be discussed. Chapter 4 will expand upon the sensitivity

analysis covered in this chapter. Chapter 3 details the development and testing of a chlorine emissions inventory for the Dallas-Ft. Worth region in central Texas.

Additional review of the literature relevant to urban tropospheric chlorine chemistry can be found in Appendix B.

Chapter 3: Development of a Reactive Chlorine Emissions Inventory for the Dallas-Ft. Worth Region

3.1 Introduction

Previous work has shown that the presence of gas phase atomic chlorine radical ($Cl^{\bullet}$) precursors, such as Cl_2, can have impacts on ozone formation (Tanaka, 2003a; Tanaka et al., 2003a). In addition to the influences that reactive gas phase chlorine species may exert on the photochemical cycle, chloride aerosol in the form of NaCl from sea salt (B J Finlayson-Pitts, 2003), and NH_4Cl (Sunghye Chang & Allen, 2006b) can also play a role. Multiple studies have examined mechanisms by which chloride from sea salt can volatilize in reactive forms from chloride aerosol (Oum et al., 1998; H. Simon et al., 2009, 2010; Spicer et al., 1998; Thornton & Abbatt, 2005; Thornton, Kercher, Riedel, Wagner, Cozic, Holloway, Dubé, et al., 2010). The mechanism involving the reactive uptake of N_2O_5 has been of particular interest, and recent studies continue to reveal its potential impacts on both ozone and nitrate chemistry (G. Sarwar et al., 2012).

Traditionally, sources of precursors for reactive chlorine have not been included in photochemical modeling of urban atmospheres. However, studies over the past decade have begun to indicate the importance of including emissions of reactive chlorine and its precursors in the modeling of photochemical episodes (Chang and Allen, 2006a, 2006b; Chang et al., 2002; Cohan et al., 2008; Sarwar and Bhave, 2007; Sarwar et al., 2012; Tanaka, 2003b; Wang et al., 2007a, 2007b; Tanaka et al., 2003). Other studies have also suggested that heterogeneous chemistry may play an important role in tropospheric chemistry, especially in the presence of significant sources of particulate chloride, such as sea salt aerosols (Eladio M Knipping & Dabdub, 2003; H. Simon et al., 2009, 2010; Spicer et al., 1998; Thornton & Abbatt, 2005; Thornton, Kercher, Riedel, Wagner, Cozic, Holloway, Dubé, et al., 2010).

A first step in photochemical modeling of reactive chlorine chemistry in urban atmospheres is to develop an inventory of the emissions of reactive chlorine and its precursors. Several chlorine emissions

inventories have previously been developed, focusing on both anthropogenic (S Chang et al., 2001; McCulloch et al., 1999) and natural sources (Erickson et al., 1999; C. Keene et al., 1999; Khalil et al., 1999; Lobert et al., 1999; Reff et al., 2009). While these inventories serve as working approximations, the extrapolation of source strengths to large scales, assumptions made in developing emissions factors, and approximations made during model implementation are factors that can lead to uncertainty (Khalil et al., 1999; Lobert et al., 1999). In urban regions, the primary anthropogenic sources of the precursors of gas phase reactive chlorine include industrial point sources, water and wastewater treatment, swimming pool chlorination and biocide use in cooling towers (S Chang et al., 2001). For a case study of Houston, Texas, which has a large petrochemical industry, as well as a large urban population, the primary sources of reactive chlorine in the urban environment were hypochlorous acid (HOCl) and molecular chlorine (Cl_2).

Photochemical modeling of chlorine emissions in Houston, TX indicated highly localized increases in O_3 concentrations up to 70 ppb for 1-hour averages in the morning hours and on the order of 1-10 ppb during peak O_3 hours (Sunghye Chang & Allen, 2006a). Another modeling study in Houston, TX (Tanaka et al., 2003b) noted a maximum localized O_3 increase of 16 ppb. In the same region, another study found that reactive chlorine chemistry increased peak 1- and 8-hour O_3 concentrations by 8 and 9 ppb, respectively (Linlin Wang, Thompson, McDonald-Buller, et al., 2007; Linlin Wang, Thompson, Mcdonald-buller, et al., 2007). Inventories have been developed and tested for other regions as well. Regional modeling done for the eastern portion of the United States found that the major enhancements of O_3 were centered in urban areas such as Houston, TX and New York-New Jersey. Resulting predicted 1-hour O_3 increases were 12 ppb and 6 ppb for Houston and New York-New Jersey, respectively. Corresponding 8-hour O_3 increases were 8 and 4 ppb (Golam Sarwar & Bhave, 2007). Additionally, the impacts of heterogeneous $ClNO_2$ production have been estimated in several modeling studies. Modeling of $ClNO_2$ chemistry across the continental United States indicated monthly average

8-hour O_3 increases 1 – 2 ppb (3 – 4%) and a maximum daily h-hour O_3 increase of 13 ppb. Additionally, total nitrate concentrations were reduced by 11 – 21% (G. Sarwar et al., 2012). $ClNO_2$ production resulted in 1-hour average O_3 increases of 1.5 ppb in a separate modeling study focusing on Houston, TX (H. Simon et al., 2009). Modeled $ClNO_2$ concentrations in this region ranged from 256 – 1210 ppt (H. Simon et al., 2010), which corresponds well with observations (Osthoff et al., 2008). Modeling of reactive chlorine emissions in the South Coast Air Basin (SOCAB) near Los Angeles, CA indicated that weekend O_3 concentrations were reduced while weekday concentrations increased (Cohan et al., 2008). Further modeling of chlorine chemistry in this same region indicated 1-hour O_3 increases of 12.7 ppb which were accompanied by maximum Cl_2 concentrations of 12.7 ppt (Eladio M Knipping & Dabdub, 2003).

In the development of the chlorine emissions inventories used in all of these studies, several challenges and sources of uncertainty are present. One source is uncertainty in available observations that are sometimes used to deduce source strengths in a given region. Additionally, the methods used for extrapolating a given set of observations often require assumptions that may introduce further uncertainty (Khalil et al., 1999). Assumptions used when estimating emissions factors and approximations of their temporal and spatial profiles are additional sources of uncertainty (Lobert et al., 1999). Any uncertainty or lack of data with respect to any biogeochemical process within the chlorine cycle could also add to uncertainty in emissions estimates. For instance, sea salt and organochloride emissions rates have been cited as having high uncertainty (S Chang et al., 2001). Uncertainty in the removal processes and sinks of chlorine can cause over-predictions in atmospheric chlorine (C. Keene et al., 1999), and sources such as coal combustion can vary widely and are dependent on the chloride content of the coal being used in a particular situation (McCulloch et al., 1999). Significant sources of chlorine in inland environments, where there is a lack of a significant sea salt source, can be difficult to

identify and characterize. Such circumstances may make the identification of a source and explanation of observations of chlorine species challenging.

This work develops an emission inventory of reactive chlorine emissions and emissions of reactive chlorine precursors for an inland region in a natural gas production region: the Dallas Fort Worth metropolitan area and the nearby Barnett Shale natural gas field. Predictions of ambient concentrations made using this emissions inventory will be compared to ambient observations made in a recent field measurement campaign conducted in the Barnett Shale. The primary measurement used in the evaluation of the inventory are concentrations of hydrogen chloride (HCl), made at Eagle Mountain Lake (EML) near Ft. Worth during the summer of 2011 (Griffin et al., 2011). Measurements were made using Mist chamber-Ion Chromatography (MC-IC) techniques. Daily peak concentrations were on the order of 1-2 ppb and exhibited a pronounced diurnal cycle that peaked in late afternoon (3 – 6 PM). Figure 3-1 shows the time series for this data, and Figure 3-2 shows the average diurnal pattern during the month of June, 2011. These measurements, and particularly their diurnal variation, suggest a significant level of photochemical activity involving chlorine.

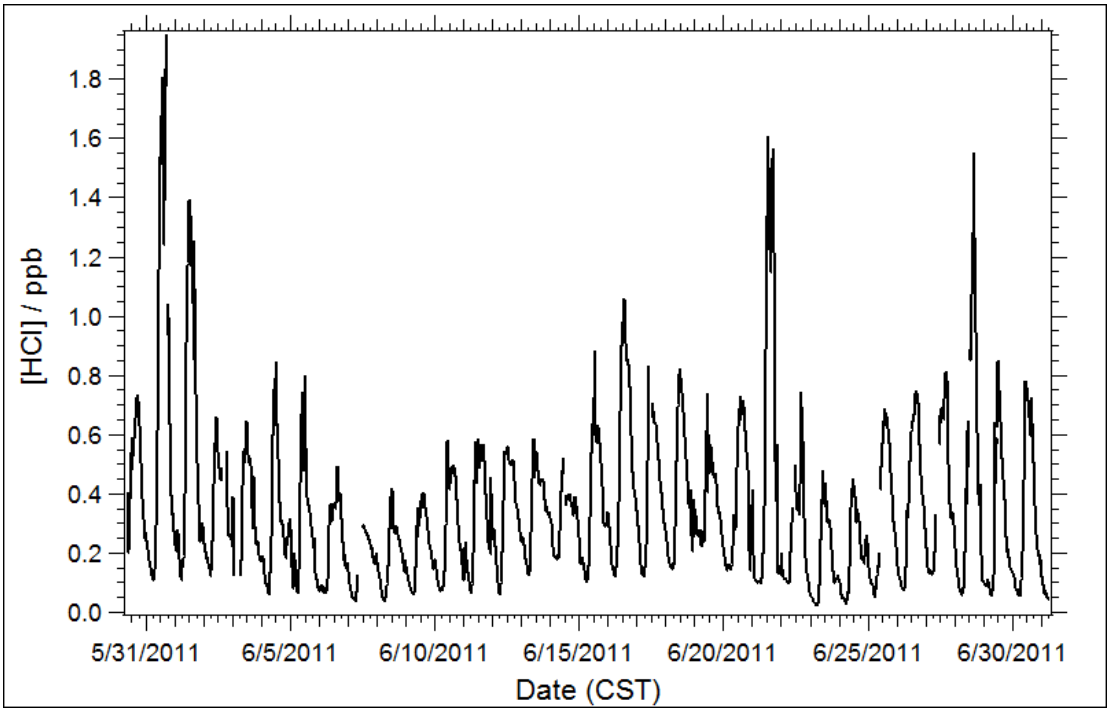

Figure 3-1: Gas phase HCl time series from Eagle Mountain Lake, observed during June, 2011.

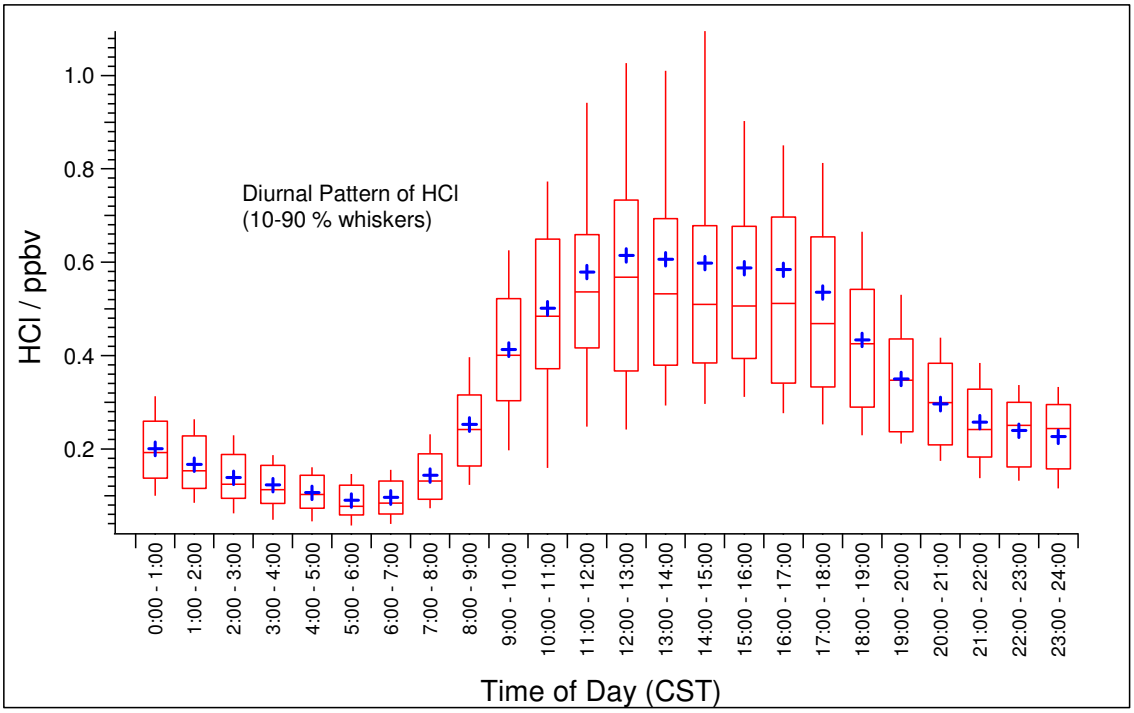

Figure 3-2: Diurnal pattern of HCl at Eagle Mountain Lake in June, 2011

3.2 Materials and Methods

3.2.1 Inventory Development Methods

Sources of atomic chlorine precursors and particulate chloride in the Dallas-Ft. Worth area were initially estimated from 8 sources:

1. Point source emissions of Cl_2 reported through the EPA Toxic Release Inventory and TCEQ's Point Source Database (PSDB)
2. Point source releases of atomic chlorine precursors from the use of chlorine as a biocide in cooling towers.
3. Point source releases of atomic chlorine precursors associated with water and wastewater treatment.
4. Area sources of atomic chlorine associated with chlorine use as a disinfectant in swimming pools.
5. Area sources of atomic chlorine precursors associated with sea salt or other aerosols.

6. Area sources of atomic chlorine precursors associated with tap water usage.

7. Area sources of atomic chlorine precursors associated with reactions of chlorinated organics.

8. Area sources of atomic chlorine precursors associated with wildfire events.

A. Point Source Emissions

Using the Environmental Protection Agency's Toxic Release Inventory (www.epa.gov/tri) and the TCEQ Point Source Database (PSDB), point sources of Cl_2 were identified within the 19 county region comprising the Dallas-Fort Worth metroplex. These counties included Collin, Cooke, Dallas, Delta, Denton, Ellis, Fannin, Grayson, Henderson, Hood, Hunt, Johnson, Kaufman, Palo Pinto, Parker, Rockwall, Somervell, Tarrant and Wise. The data were collected from 2010 (TRI), 2012 (TRI) and 2010 (PDSB), the most recent years on record in both inventories. For the TRI inventory, values from the 2010 were used as they were the most recently available data at the time this work was completed.

Of the 19 counties, only two contained point sources with significant (> 0.5 tons per year (tpy)) emissions of Cl_2. These counties were Dallas and Johnson counties. The highest emissions were reported in Johnson County, totaling 0.927 tpy. Reported emissions in Dallas County were 0.619 tpy. Hunt and Tarrant counties had molecular chlorine emissions of less than 0.5 tpy. The remaining counties in the region had no reported emissions Cl_2. A list of significant sources in Dallas and Johnson County is compiled in Tables 3-1 and 3-2.

There are some differences in emission estimates between the two databases (TRI and PSDB), as shown in Tables 3-1 and 3-2. For cases where both databases report emissions for the same facility, the values to be used in this work are taken from the larger of the values from the two databases. In summary, total emissions in the 19-county region are equivalent to 0.0046 tons Cl_2 d^{-1}. The recommended temporal distribution for point sources is a constant emissions rate, 7 days wk^{-1}, 365 days yr^{-1}. Where stack parameters are available in the PSDB, they should be used. Otherwise, default

parameters of height = 3 m, diameter = 0.2 m, T = 294 K, and stack gas velocity = 0.5 m s^{-1} should be used.

Table 3-1: Point source releases of molecular chlorine in Dallas County.

Facility	Latitude	Longitude	2010 reported releases[i]	2012 reported releases[i]	2010 TNRCC PSDB[i]	Emission Rate for this work[ii]
Petra Chemical Co. - Dallas Plant	32.9	-96.9	(0.114) 83	(0.186) 136	-	0.114
DRS RSTA Inc.	32.9	-96.8	-	-	(0.023) 16.8	0.023
Littelfuse LP	32.9	-97.0	-	-	(0.0008) 0.6	0.0008
Texas Instruments	32.9	96.9	-	-	(1.56) 1140	1.56
Total	-	-	83	136	1160	1.70

[i] Units for emissions are reported in (tons d^{-1} x 10^{-3}) and lb yr^{-1}.
[ii] Units for emissions rates used in this work are in tons d^{-1} x 10^{-3}.

Table 3-2: Point source releases of molecular chlorine in Johnson County.

Facility	Latitude	Longitude	2010 reported releases[i]	2012 reported releases[i]	TNRCC PSDB[i]	Emissions Rate for this work[ii]
DPC Industries Inc.	32.4	-97.4	(0.240) 175	(0.240) 175	-	0.240
Sachem Inc.	32.4	-97.4	(2.29) 1670	(2.29) 1670	-	2.29
Total			(2.53) 1850	(2.53) 1850	-	2.53

[i] Units for emissions are reported in (tons d^{-1} x 10^{-3}) and lb yr^{-1}.
[ii] Units for emissions rates used in this work are in tons d^{-1} x 10^{-3}.

B. Point Source Releases of Atomic Chlorine Precursors Associated with Biocide Use in Cooling Towers

In order to prevent biofouling in cooling towers, HOCl or Cl_2 may be added to the water being used. However, this technique can lead to the release of atomic chlorine precursors. Previous research has identified three primary fates for chlorine in cooling towers (Holzwarth, Balmer, & Soni, 1984a, 1984b).

1. *Chlorine Demand:* The portion of chlorine that reacts with other substances (organic and inorganic) in the cooling tower water.
2. *Blowdown:* The blowdown stream flows away from the tower during operation and can carry any residual chlorine compounds with it.

3. *Flash-off:* Loss of volatile compounds in cooling tower water is caused by volatilization into the air flowing through the cooling tower.

With respect to potential atmospheric release of atomic chlorine precursors, flash-off is the most important of these three to consider. Estimates of flash-off rates have been made based on both a theoretical mass transfer approach, as well as field measurements (Holzwarth et al., 1984a, 1984b). Field measurement studies were based on measurements of chlorine demand rate and free active chlorine (FAC) concentrations in the water of a 1,200,000 gallon transverse flow, forced draft cooling tower at a U.S. refinery. The observations were made before and after shock chlorine treatment. The program of shock treatment consisted of 28,000 g Cl_2 hr^{-1} for three hours, followed by 17,000 g Cl_2 hr^{-1} for 1.5 hours and 3,750 g Cl_2 hr^{-1} for the rest of the 24 hour period. The recirculation rate of the tower was 60,000 gallons min^{-1}, and the makeup rate was 1,000 gallon min^{-1}(1.44 mgd).

Analysis of the field and laboratory data revealed that chlorine flash-off fraction is dependent on both temperature and pH. Higher temperatures lead to higher flash-off fractions, while higher pH levels result in lower flash-off fractions. To estimate chlorine release from cooling towers, a flash-off fraction of 0.1 (10%) will be used, which is in in agreement with observed values(Holzwarth et al., 1984a, 1984b).

Another factor to consider is the form of chlorine being released. Potential species include Cl_2, HOCl, and possibly chloramines if ammonia is present. The rates of photolysis for each of these species vary, with Cl_2 expected to photolyze within 10-20 minutes while HOCl would take up to 10 times longer (S Chang et al., 2001). For the calculation of a straightforward emissions estimate, the emitted chlorine will be assumed to be in the form of Cl_2. However, modeling comparisons between flash-off emissions of Cl_2 and HOCl are recommended.

Using a flash-off fraction of 0.1 and assuming emissions are in the form of Cl_2, the emissions estimate for a cooling tower with a makeup rate of 1.44 mgd following the shock treatment program described above can be determined:

$(28\ kg\ hr^{-1} * 3\ hr\ day^{-1} + 17\ kg\ hr^{-1} * 1.5\ hr\ day^{-1} + 3.75\ kg\ hr^{-1} * (24\text{-}4.5)\ hr\ day^{-1})*0.1$

$= 18\ kg\ chlorine\ emission\ day^{-1}$

Previous estimates and measurements of chlorine use in cooling towers agree with this result. These measurements were performed during a study by Science Applications International (SAI) to ascertain chloroform emissions in the South Coast Air Basin (Rogozen et al., 1988). During a survey of refineries in the South Coast Air Basin, it was determined that the use of chlorine in cooling towers (primarily in the form of gaseous Cl_2) was on the order of 500,000 lbs yr^{-1} for seven refineries. This is equivalent to approximately 1,400 lbs day^{-1} collectively, or 200 lbs day^{-1} per refinery. With the assumed flash-off fraction of 0.1 used above, this corresponds to 20 lbs day^{-1} atmospheric chlorine emissions per refinery. An effort to extend these results to the Dallas-Ft. Worth area requires estimation of the number of cooling towers in the region using chlorine as a biocide, which includes both industrial and commercial cooling towers.

Commercial cooling towers include those in schools, hospitals, hotels, universities and most other large buildings. A previous chlorine inventory approximated average water usage at 500,000 gallons per month for commercial cooling towers (S Chang et al., 2001). However, the actual usage can range widely from 50,000 gallons per month for smaller towers up to 4,000,000 gallons per month for larger towers, such as those at large airports. Additionally, commercial towers can use up to twice as much water during the summer and less in the winter, varying with the demand for air conditioning.

Although the number of commercial cooling towers in the region could be substantial, data from a previous study (Rogozen et al., 1988) suggested that very few smaller sized commercial cooling towers use chlorine as a biocide. It can therefore be assumed for the purposes of emissions estimates that all chlorine used as biocide is used only at industrial, manufacturing and refining facilities. Publicly available data on biocide use and treatment procedures at individual facilities is not available, and is beyond the scope of this inventory. An order of magnitude estimate could be calculated by

approximating the number of cooling towers in the Dallas-Ft. Worth region by assuming that the number of refinery cooling tower emissions are negligible and scaling the per capita tower density from a survey taken in the SoCAB (Rogozen et al., 1988) to the population of Dallas-Ft. Worth. However, results from this survey noted that the vast majority (> 98 %) of chlorine use in industrial cooling towers came from industries categorized under SIC codes 2033, 2813, 2822 and 2911. Data from the State of Texas Air Reporting System (STARS) indicates that there are no major industries of this type within the Dallas-Ft. Worth region. Therefore, emissions from these industrial sectors would also be nonexistent. For this reason, emissions from cooling towers are not expected to be a major source of atomic chlorine precursor in the region and are not included in the inventory.

C. Point Source Releases of Atomic chlorine Precursors from Water and Wastewater Treatment

Previous work (Ayres & Ayres, 1997) suggest that 5% of the United States' chlorine consumption is used in water and wastewater treatment. These uses could be potential sources of Cl_2 or HOCl, and should be included in an inventory. In the following sections, water and wastewater treatment are considered separately.

Chlorination in Water Treatment

Both Fort Worth and Dallas obtain their drinking water supply from surface water sources. In Fort Worth, typical dosages of chloramines range between 4.5 – 5.5 mg L^{-1}, and typical residual chlorine concentrations range from 2.5 – 3.5 mg L^{-1} (Pior, 2012). Chlorine demand is the difference between the amount of chlorine added for treatment and the residual chlorine after treatment, and it can be written as:

Chlorine demand = Chlorine dose – Chlorine residual

Chlorine demand can result from a combination of factors including reactions between the added chlorine and organic or inorganic compounds, reaction with ammonia, reactions due to sunlight and volatilization. Referencing interviews with water treatment experts, previous chlorine emissions

inventories for metropolitan areas in Texas have assumed that approximately 20% of chlorine demand can be attributed to volatilization (S Chang et al., 2001).

Along with volatilization rate, the volume of water processed on a daily basis needs to be taken into account. Dallas water treatment plants supply 1.2 million people while Fort Worth's supply around 0.9 million (http://www.dallascityhall.com; http://fortworthtexas.gov/water/info/). Combined, the Dallas-Ft. Worth area supplies a total of 222.91 billion gallons per year (bgy). This is equivalent to 610 million gallons per day (mgd). Using a chlorine dosage of five mg L^{-1} and a residual chlorine concentration of 3.5 mg L^{-1} (Pior, 2012), the following estimated emissions rate results. Note that although the chlorination process involves chloramines, the concentrations used for the calculations are mg L^{-1} Cl_2.

$$0.2 * (5 - 3.5)\ 10^{-6}\ kg\ L^{-1} * 610\ mgd * 1.0 * 3.7854\ L\ gal^{-1} \approx 700\ kg\ d^{-1}$$

(chloramine treatment of surface water)

Chlorination in Wastewater Treatment

In total, Dallas and Fort Worth have three wastewater treatment plants. Listed in Table 3.3 are the names, address and phone numbers of the treatment plants. It is assumed that the amount of chlorine used is close to the amount used during water treatment. The average rate of wastewater treatment for the Dallas plants in 2010-2011 was 144.66 mgd (http://www.dallascityhall.com). The daily average treatment rate for Fort Worth in 2008 (the most recently available data) was 108.77 mgd (http://fortworthtexas.gov/water/info/). Together, this results in 253.43 mgd for the Dallas-Ft. Worth region. The wastewater treatment rates are therefore approximately two fifths of the magnitude of water treatment rates. Although wastewater may have a higher chlorine demand than water treated to be used as drinking water, the absence of specific data necessitates the assumption that chlorine emissions from wastewater treatment are similar to those from water treatment; that is, on the order of several hundred kg per day.

In order to avoid harm to environments and ecosystems into which treated wastewater is discharged, residual chlorine must be removed prior to discharge. To accomplish this, sulfur dioxide is added to facilitate removal of residual chlorine to levels below 0.01 mg L^{-1}. The mechanism of removal is the conversion of free chlorine to chloride, and it is assumed that a major fraction of the chlorine will be scavenged. The volatilization of residual chlorine in the wastewater is assumed to be negligible (S Chang et al., 2001). Taking into account these factors, an estimate of atomic chlorine precursors from chlorination during wastewater treatment is shown below:

Wastewater treatment releases = (2/5) * (emissions from water treatment)

$= 470 \text{ kg day}^{-1}$

Table 3-3: Wastewater treatment facilities in Dallas-Ft. Worth

Facility Name	Address	Phone Number
Village Creek Water Reclamation Facility	4500 Wilma Lane Arlington, TX 76012	(817)-392-4960
City of Dallas Southside Wastewater Treatment Plant	1011 Log Cabin Rd. Dallas, TX 75253	(214)-948-4517
City of Dallas Central Wastewater Treatment Plant	1020 Sargent Rd Dallas, TX 75203	(214)-670-7406

D. Atomic Chlorine Precursor Emissions from Swimming Pools

Swimming pools may also serve as a source of atomic chlorine precursors due to the use of chlorine for sanitation procedures. As of 2007, the total number of swimming pools within the United States is estimated at 8.6 million (SBI, 2007). Therefore, the total number of swimming pools within the Dallas-Ft. Worth region can be estimated by the following calculation, where P_{DFW} and P_{US} are the total populations of DFW and the U.S., respectively (Hall, 2012; U.S. Dept. of Commerce: U.S. Census Bureau, 2013).

$$N_{pools\_DFW} = N_{pools\_US} * (P_{DFW}/P_{US})$$

$$= 8{,}600{,}000*(6{,}908{,}767/313{,}914{,}040) = 189{,}273 \text{ pools}$$

Due to average summer temperatures being higher in Dallas-Ft. Worth than the majority of the U.S., it is assumed that there are approximately 1.5 times more swimming pools than average:

N_{pools_DFW} = 178,489 * 1.5 = 283,909 swimming pools.

This ratio of swimming pools to population is in line with estimates from a study in the South Coast Air Basin which cites the presence of approximately 250,000 swimming pools in Los Angeles for a population of 11 million. The same study suggests that chlorine is added to swimming pools during the summer at a rate of 2 gallons (as NaOCl; 10-12.5% solution by weight) per week per pool (Rogozen et al., 1988). Using these values, the estimate of total hypochlorous acid use during the summer time can be approximated (where R_{Cl} is the rate of hypochlorous acid use, R_s is the rate of addition of NaOCl solution and F_{NaOCl} is the fraction, by weight, of NaOCl in the solution used):

$R_{Cl} = F_{NaOCl} * R_s * 3.7854$ kg $gal^{-1} * 283{,}909$ pools

$= 0.1 * 0.286$ gal $day^{-1} * 3.7854 * 283{,}909$ pools = 30,700 kg day^{-1}

By assuming that approximately half of the chlorine in pools volatilizes, then daily emissions of precursors from swimming pools would be approximately 15,400 kg day^{-1}. However, one can also estimate emissions via a mass transfer approach. This includes considering an overall mass transfer coefficient for volatilization coupled with pool surface area from which chlorine may volatilize.

A previous study in southern California (Rogozen et al., 1988) determined the average surface area of residential pools to be approximately 40 m^2. The same study determined an overall mass transfer for chloroform, taking into consideration turbulent and placid pool surface conditions, of 22 μg m^{-2} min^{-1}. Relating this to hypochlorous acid by taking into account differences in Henry's law coefficients and molecular weights, the corresponding mass transfer coefficient for hypochlorous acid is in the range of approximately 10-100 μg m^{-2} min^{-1}. Using these values, one may approximate the mass rate of hypochlorous acid volatilization from swimming pool surfaces:

$A_{total} = 283{,}909$ pools * 40 m^2 $pool^{-1} = 1.14 \times 10^7$ m^2

$R_{volatilization}$ = 10-100 μg m^{-2} min^{-1} * 1.071 x 10^7 m^2 * 1440 min day^{-1}

= 163,532 - 1,635,316 g day^{-1} = 163 - 1,645 kg day^{-1}

This calculation assumes a constant concentration of hypochlorous acid on the order of one ppm for the entire volatilization period. However, the high rate of volatilization shows that the chlorine would evaporate in less than a day, making it difficult to maintain a chlorine concentration at the magnitude in the absence of continuous addition. Assuming that the average pool size is 5m x 5m x 2m (50,000 L), that chlorine is added twice a week and that the required chlorine mixing ratio is between 1-3 ppm (NSPF, 2012), another estimate of residual chlorine available for volatilization can be made:

$R_{volatilization}$ = 283,909 pools * 50,000 L $pool^{-1}$ * 2 ppm * 10^{-6} kg L^{-1} ppm^{-1} * (2/7)

= 8110 kg/day

The residual chlorine is assumed to completely volatilize into the atmosphere. Therefore, if it is assumed that the average pool is chlorinated twice a week to a concentration of 2 ppm of chlorine, then the daily emissions rate in the Dallas-Ft. Worth area is approximately 8.11 metric tons day^{-1}. A summary of emissions from swimming pools is given below.

Total emissions from swimming pools in the Dallas-Ft. Worth region was 8.11 metric tons Cl_2 day^{-1} or 12.00 metric tons day^{-1} as HOCl. To appropriately distribute swimming pool emissions, population densities must be taken into account. Relative population fractions for each county were used to calculate the county-level emissions from the region-wide swimming pool emissions total. Each source can be modeled either as a point source located in the middle of each grid cell or as an area source for the entire grid cell. If the point source approach is taken, default stack parameters could be used and emissions should be placed into the ground layer with no plume-in-grid calculations included so that essentially it is identical to the area source method. Assuming that chlorination is performed

around midday and that emissions are constant throughout the afternoon, a constant emissions rate should be applied from the hours of 12-8 PM.

E. Atomic Chlorine Precursor Emissions from Sea Salt and Other Aerosols

In order to investigate whether particulate chloride is expected to be present in concentrations large enough to serve as a heterogeneous source of atomic chlorine precursors, CAMx simulations were performed with a base case particulate matter emissions inventory. During this modeling, the hypothesis of long-range sea salt transport into Dallas-Ft. Worth from the Gulf of Mexico as a significant source of particulate chloride was investigated. The gas phase inventory used was from the Texas Commission on Environmental Quality (TCEQ) Dallas-Fort Worth Eight-Hour Ozone SIP Modeling Episode. This modeling episode includes meteorological and photochemical inputs and was developed for the purposes of aiding the development of a State Implementation Plan (SIP) in Dallas-Fort Worth ozone non-attainment area. For particulate emissions, a model-ready primary particulate inventory was used (Heather Simon, 2006). PM emissions were categorized into fine (< 2.5 μm) and coarse (2.5 – 10 μm) mode size bins. The PM inventory included area sources, road dust, fugitive dust, on-road mobile sources and wild fires and offshore emissions (H. A. Simon, 2008b) Sea salt emissions in particular were developed using a custom program (Environ Inc.) using MM5 meteorological output files in combination with land cover data to identify grid cells covered by salt water. The meteorology on September 1st, 2006 was used as a representative day for the episode. Daily variability in wind conditions was not included due to uncertainty in inventory performance due to wind speed (H. A. Simon, 2008b). Modeling in CAMx was performed with a domain consisting of three nested grid cells with resolutions of 36 km, 12 km and 4 km, respectively. The finest mesh was centered on the Dallas-Fort Worth region, and the largest domain was centered on the Eastern half of the continental United States.

F. Atomic Chlorine Precursor Emissions from Tap Water Use

According to the U.S. EPA, the average family of four people uses approximately 400 gallons of water per day. This is equivalent to 100 gallons per person per day and (100 gpd), and this usage is broken down by application in Table 3-4 (U. S. E. P. A. USEPA, 2012).

Table 3-4. Water Usage per Capita (U.S.)

Use	% (of 100 gpd)
Shower	16.8
Toilet	26.7
Faucet	15.7
Clothes Washer	21.7
Leaks	13.7
Other	5.3

Leaks serve as potential sources of outdoor emissions. Assuming that 'other' uses include outdoor watering, car washing and other outdoor uses and that approximately 50% of leaks are exposed to the atmosphere, the daily amount of tap water that serves as a potential atomic chlorine precursor source in the Dallas-Ft.Worth area can be calculated:

R_{tap} = (0.053 + 0.137/2) * 100 gpd person^{-1} * 6,908,767 people

= 83,941,519 gpd

Using a residual chlorine concentration of 3.5 ppm for treated drinking water, and estimate of chlorine precursor emissions can be made:

3.50 ppm * 77,417,042 gpd * 3.7854 L gal^{-1} * 10^{-6} kg L^{-1} ppm^{-1}

= 1080 kg day^{-1}

Therefore, total emissions from tap water in the region are 1.08 metric tons d^{-1} as Cl_2 or 1.60 metric tons d^{-1} as HOCl (assuming equal amounts emitted as either species). Tap water usage and emissions should be spatially modeled as low-level area sources and allocated proportionally to each county in the region in an amount determined by the fraction of the regional population that resides

within that county. Temporal distribution of emissions: Emissions from tap water usage should be modeled at a constant rate, 24 hrs d^{-1}.

G. Area Sources of Atomic Precursors from Chlorinated Organics

Organic compounds containing chlorine may also serve as atomic chlorine precursors. These chlorinated organics are typically used as industrial solvents or pesticides (Ayres & Ayres, 1997). For example, the organic solvent, trichloroethylene (TCE), can react with hydroxyl radicals, producing species that can then undergo photolysis and lead to the release of atomic chlorine. This can lead to approximately a 60% yield of chlorine atoms relative to initial TCE concentrations (W P L Carter, Dongmin, & Malkina, 1997). On the other hand, the highly toxic chloropicrin, which was first used as a chemical warfare agent and is now used primarily as a nematicide, can photolyze within the troposphere at quantum yields up to 1.0, resulting in production of chlorine atoms. One study found that emission of chloropicrin into urban atmospheres can have up to 1.5 times the impact on ozone formation than other typical VOCs (W P L Carter, Luo, & Malkina, 1997).

Typically, organochlorides are slower to react in the troposphere than other volatile organic compounds. Yet there are many known chlorocarbon reactions that can lead to release of either chlorine precursors or hydrochloric acid. Some examples of such reactions are listed in reactions 3-1 through 3-5 (Atkinson et al., 2008).

$OH + CCl_4 \rightarrow HOCl + CCl_3^{\bullet}$ (Reaction 3-1)

$OH + CF_2Cl_2 \rightarrow HOCl + CF_2Cl_2$ (Reaction 3-2)

$OH + CFCl_3 \rightarrow HOCl + CCl_3$ (Reaction 3-3)

$O(^1D) + CCl_4 \rightarrow ClO + CCl_3$ (Reaction 3-4a)

$\rightarrow O(^3P) + CCl_4$ (Reaction 3-4b

$Cl + CH_3OCl \rightarrow Cl_2 + CH_3O$ (Reaction 3-5a)

$\rightarrow HCl + CH_2OCl$ (Reaction 3-5b)

In order to test the hypothesis that the HCl concentrations observed at the EML site (Griffin et al., 2011) are due to volatile chlorine species emissions from natural gas production activities, a chlorocarbon emissions inventory was created. The investigation of hydraulic fracturing activities as a possible chlorine source is justified by the fact that hydrochloric acid is the major component of hydraulic fracturing fluid (FracFocus, 2013; GWPC & ALL, 2009; O. of R. and D. USEPA, 2011a, 2011b) aside from water and silica sand (used as a proppant). The mixing ratios of hydrochloric acid in hydraulic fracturing fluid has been cited as comprising up to 0.123 % of the fluid by volume (GWPC & ALL, 2009; O. of R. and D. USEPA, 2011a, 2011b). This corresponds to an average mixing ratio of 0.122 % by mass as reported for wells in Tarrant County, TX in the Barnett Shale (FracFocus, 2013). The total amount of water used per well during the drilling and hydraulic fracturing process can vary between 2 – 4 million gallons, and usage of approximately 3 million gallons is commonplace (GWPC & ALL, 2009).

Various salts, such as NaCl, $CaCl_2$ or KCl, are typically used to make the fracturing fluid a brine solution. If these salts are taken into account, hydraulic fracturing fluid can be composed of 0.183 % chlorine containing species by volume (O. of R. and D. USEPA, 2011a). Figure 3.3 shows the total chlorine used in the hydraulic fracturing process that can be deduced from such concentrations. Data used for calculations in the scenarios where only HCl and KCl were considered is taken from US EPA data (O. of R. and D. USEPA, 2011a). Data for the calculation in the case where HCl and $CaCl_2$ were considered together comes from the Frac Focus website (FracFocus, 2013).

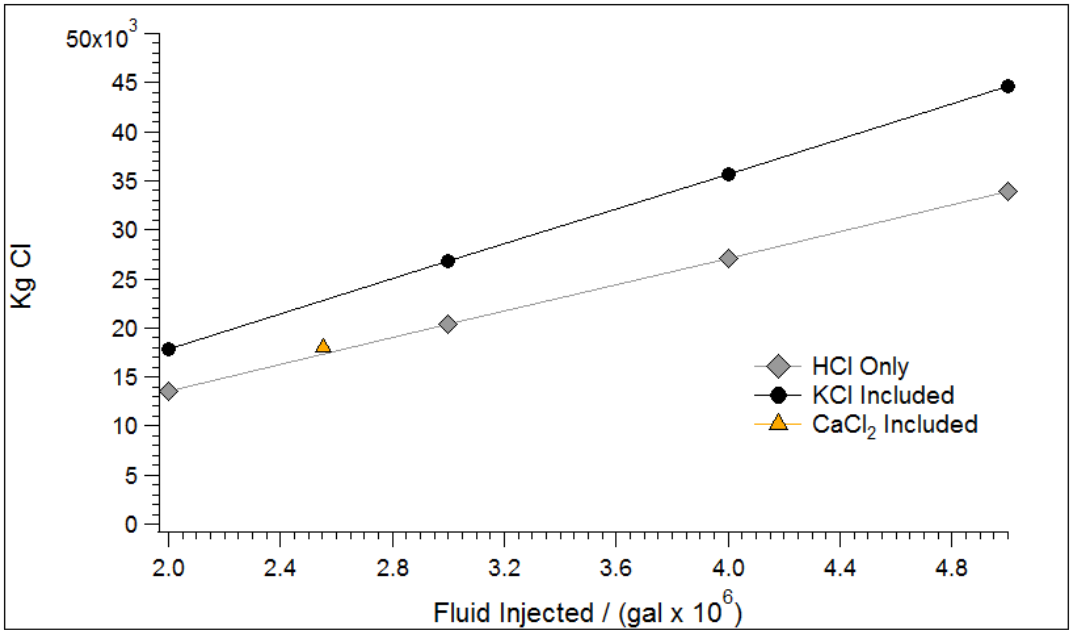

Figure 3-3: Total chlorine injected underground as a function of the amount of hydraulic fracturing fluid used.

Salts such as KCl or $CaCl_2$ typically comprise a much smaller fraction of the overall mixture than HCl. However, the difference in Figure 3-3 between magnitudes of chlorine injected for the scenarios including and excluding KCl demonstrates that it adds a significant amount of chlorine. This chlorine must be released into the atmosphere before it can begin to account for observed ambient HCl concentrations. Hypotheses concerning the exact mechanism of reaction and transformation of aqueous chloride into a volatile species are beyond the scope of this work. However, by assuming that a mechanism does exist and that an approximately constant rate of release occurs over a period of years, an emissions estimate of the maximum amount of chlorine that could potentially be released can be made. Table 3-5 shows estimated per well emissions rates of chlorine given a constant rate of release and assuming a viable mechanism for the production of volatile chlorine species.

Table 3-5: Estimated upper limit emissions assuming a constant rate of volatilization over 1, 5 and 10 years.

Fluid Used (10^6 gal.)	Cl Injected (10^3 kg)	Emissions Rate (kg d^{-1})		
		Over 10 years	Over 5 years	Over 1 year
2	18	5	10	49
3	27	7	15	73
4	36	10	20	98
5	45	12	24	122

Another estimate can be made through consideration of chloride found in flowback waters (also referred to as "produced waters") that are generated during the hydraulic fracturing process. Specifically, flowback refers to the hydraulic fracturing fluid that returns to the surface after the fracturing process but before the well is placed into production. Produced water refers to that which is produced during operation of the well (O. of R. and D. USEPA, 2011a, 2011b). Flowback water has very high chloride levels, due to both initial fluid composition as well as the mobilization of salts from the shale formation during the fracturing process. This wastewater is typically stored in tanks or open pits at the well site (O. of R. and D. USEPA, 2011a). Produced water samples in the Barnett Shale have shown mixing ratios of total chlorides up to 50,000 ppm (Allen, 2013). Additionally, chlorinated species such as chloromethane, chlorobenzene, tetrachloroethene and trichloroisocyanuric acid have been detected in flowback waters. Using the figure of 50,000 ppm, a conservative order of magnitude estimate of the total chlorine present from chloride at the surface can be made by assuming that 20 % of the fluid that is used returns to the surface as flowback water. This fraction is within the lower end of the 25 – 75 % range that has been observed (O. of R. and D. USEPA, 2011a). Table 3-6 shows estimates of the total chlorine that results at the surface for various volumes of fluid used.

Table 3-6: Total chlorine produced as chlorides in flowback water (from 20% return of injected fluid).

Fluid (10^6 gal.)	Flowback (10^6 gal.)	Flowback (10^3 kg)*	Cl-total (10^3 kg)**
2	0.4	1514	76
3	0.6	2271	114
4	0.8	3028	151
5	1	3785	189

* Calculation assumes a fluid density of 1 g cm^{-3}

** For a total chloride loading of 50,000 ppm by mass

Comparing the total amount of chlorine injected as HCl and KCl in the hydraulic fracturing fluid to the total chlorine present in flowback water, a considerable increase is observed. This equates to a four-fold increase in the mass of chloride. This suggests that chloride concentrations in the fluid are drastically increased due to the mobilization of chlorides present in the formation. Considering that this calculation only assumes a 20 % return of the initial fluid volume injected as flowback, higher rates of return could introduce even larger amounts of chlorine at the surface. Whether or not any of this chlorine subsequently volatilizes and in what form it does so is still an open question. However, the detection of chlorinated organic compounds in flowback water (O. of R. and D. USEPA, 2011a) suggests that this is a possibility. For the purposes of inventory development in this work, a chlorinated organic emissions inventory was developed.

Emissions estimates of potential chlorinated organic volatilization from hydraulic fracturing activities were created to test the hypothesis that this route is a source of significant atomic chlorine precursors in the region. In order to determine the magnitude of emissions as related to natural gas production, total county-level VOC emissions were referenced from the Texas Commission on Environmental Quality's Barnett Shale Area Special Inventory. Chlorinated hydrocarbon emissions were scaled on a county by county basis by assuming that a given amount (ratio by weight) of the chlorinated organic was emitted for each amount of total VOC (per day basis).

Emissions rates of chlorocarbons were calculated for an 18 county area in the Barnett Shale region using chlorocarbon to VOC ratios of 0.7-11.2. The included counties were: Bosque, Clay,

Cooke, Dallas, Denton, Eastland, Ellis, Erath, Hill, Hood, Jack, Johnson, Montague, Palo Pinto, Parker, Somervell, Tarrant, and Wise. In order to gauge the characteristics of the temporal and spatial distribution of these emissions with respect to the location of the EML site, a scenario involving a non-reactive tracer species was included.

Reactive chlorinated organic inventories were developed for two different temporal emissions patterns for all of the organochloride-to-VOC scaling factors examined (0.7, 1.4, 2.8, 5.6, 11.2). The first temporal pattern consisted of a steady rate of emission 24 hours a day, seven days a week. The second temporal pattern was created such that the emissions started between 5-6 AM, peaking at 11-12 PM, and returned to zero by 8 PM. This emissions pattern was intended to simulate condensate breathing losses from storage tanks. Emissions of this pattern were then combined with the constant 24 hour hourly emissions to create the emissions pattern for the second inventory. The emissions were combined such that 50 % of the total emissions were from each temporal pattern. This inventory and the inventory using constant hourly emissions were tested in CAMx simulations using a reaction mechanism that was modified to include the reactions of chlorinated organics and hydroxyl radicals.

H. Area Sources of Atomic Chlorine Precursors from Wildfire Events

Wildfires have been estimated to emit 6350 Gg Cl yr^{-1} total chlorine in the form of volatile inorganic and particulate chloride (Lobert et al., 1999). Additionally, over 702 Gg Cl yr^{-1} is expected to be emitted from this source in the form of chlorinated organic species. In order to ascertain whether or not natural wildfire events are a possible source of significant amounts of atomic chlorine precursors in the Dallas-Ft. Worth region, data from the Fire Inventory from NCAR (FINN) (Wiedinmyer et al., 2011) was analyzed. Wildfire events from May 28, 2011 – June 30, 2011 were downloaded, and the locations of wildfires within Texas during this time period were mapped.

Out of these events, only those that occurred to the south-southeast of Dallas-Ft. Worth were included in the full analysis. This choice is justified by the fact that prevailing winds during this period

were overwhelmingly from this direction. This is verified through back-trajectories calculated by the HYSPLIT (R R Draxler, 1999; Roland R Draxler & Hess, 2010, 1998; Rolph, 2014) software. Figures 3-4, 3-5 and 3-6 show these back-trajectories for altitudes of 5 m, 20 m, and 500m, respectively. Each line represents a 48 hour back-trajectory for each day during the period of June 1 – July 2, 2011. The endpoint chosen was the EML monitoring site, where HCl observations were made. The coordinates for the EML monitoring site are 32°59'16.47"N, 97°28'37.30"W.

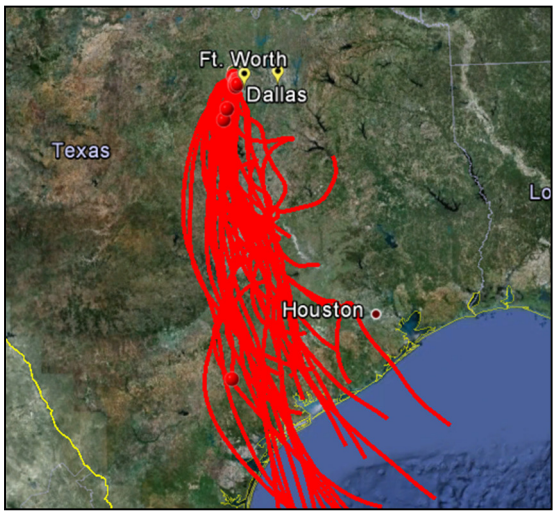

Figure 3-4: HYSPLIT Back-trajectories at an altitude of 5 meters for the period of June 1st – July 2nd, 2011.

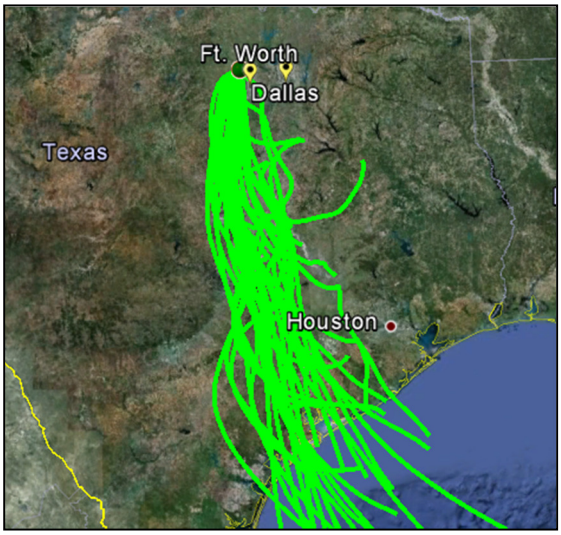

Figure 3-5: HYSPLIT Back-trajectories at an altitude of 20 meters for the period of June 1st – July 2nd, 2011.

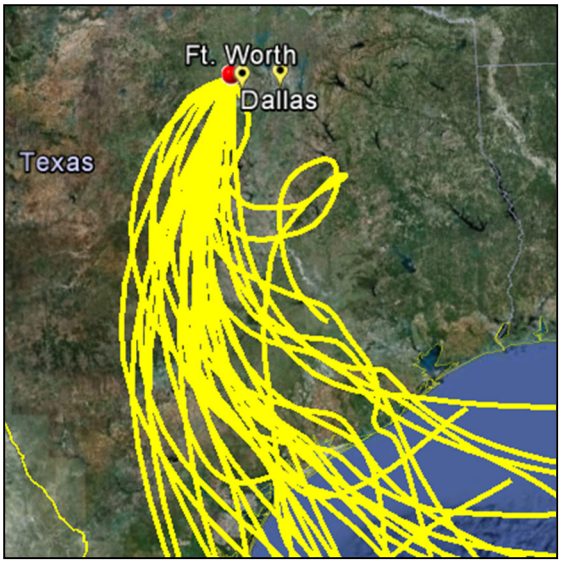

Figure 3-6: HYSPLIT Back-trajectories at an altitude of 500 meters for the period of June 1st – July 2nd, 2011.

The back-trajectories in Figures 3-4, 3-5 and 3-6 can be compared to the locations of the wildfire events to the south and southeast of Dallas-Ft. Worth in June 2011 shown in Figure 3-7.

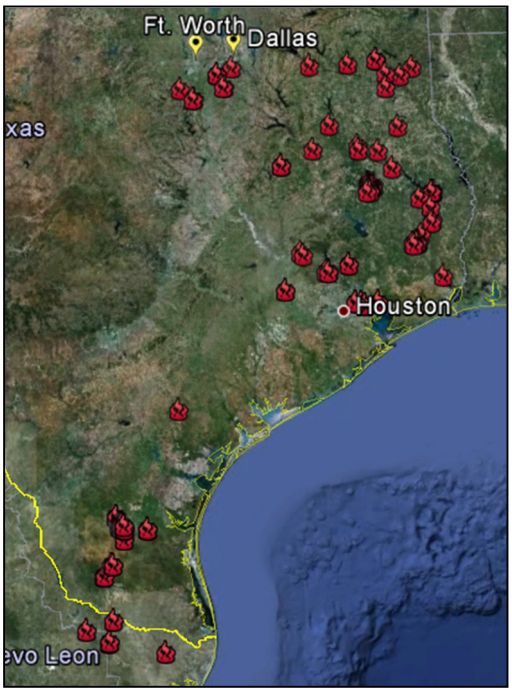

Figure 3-7: Locations of wildfire events in June 2011, generated by the FINN software

In addition to the locations of the wildfires, data on total emissions of combustion products and dates were examined. For each day in the period of May 28th – June 30th, total CO_2 emissions from every fire event occurring on that specific date were summed. CO_2 emissions were chosen as a marker

of biomass combustion for comparison with daily maximum hourly average HCl concentrations at Eagle Mountain Lake. Figure 3-8 shows a scatter plot comparing total daily CO_2 emissions from wildfires for the entire region shown in Figure 3-4 and daily maximum HCl concentrations detected at the EML monitoring on those same days. The reader should note that wildfires events generated by the FINN software occurred only on 17 days out of the 33 day period for which HCl observational data is available. Note also that both CO_2 emissions and daily HCl concentrations are scaled to the episode maximum emissions and concentrations respectively.

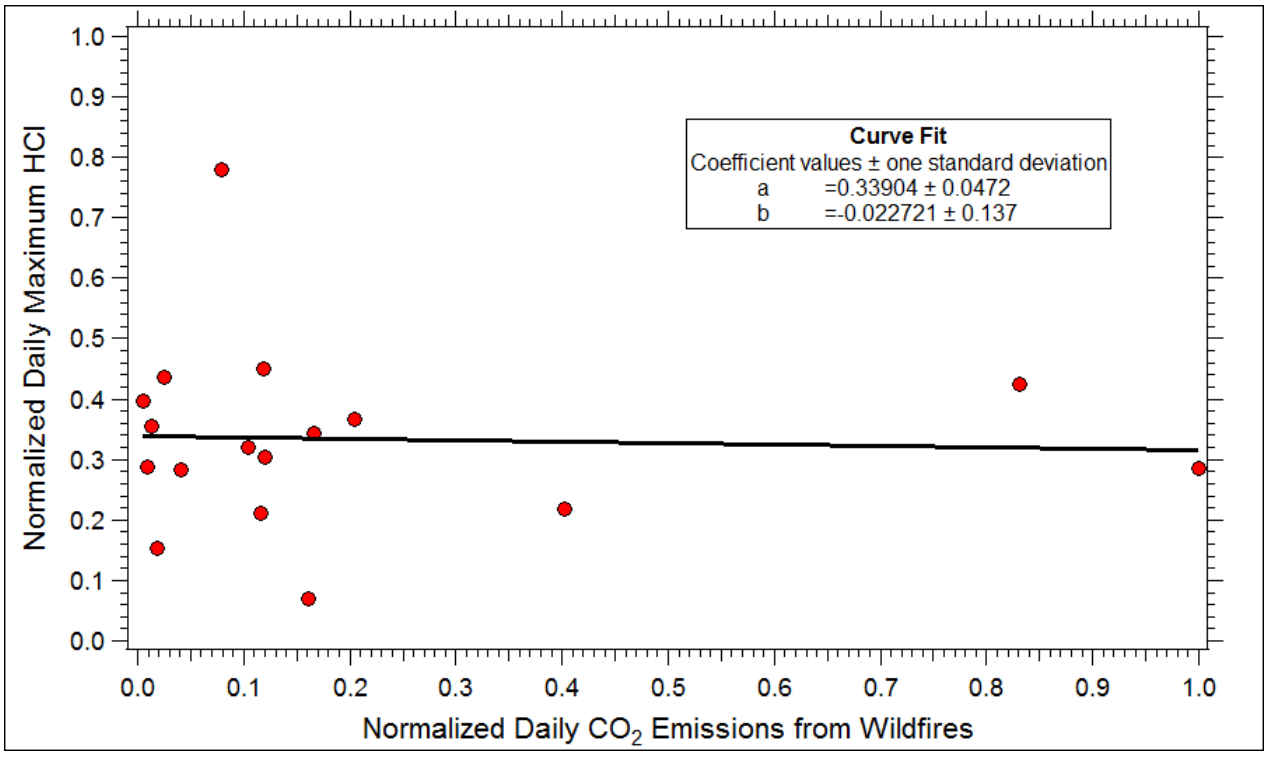

Figure 3-8: A comparison of daily maximum hourly average HCl concentrations and total CO_2 emissions from all wildfires occurring in the region shown in Figure 3.7. Data shown includes every day during May 28th – June 30, 2011 on which there was a wildfire event.

As can be seen in Figure 3-8, there appears to be no direct correlation between biomass combustion emissions from wildfire events and fluctuations in the maximum HCl concentrations at the measurement site. However, considering that over 66% of the wildfire events take place at a distance greater than 200 km from the measurement site, it would be reasonable to expect a lag between any particulate or gas phase chlorine emissions from the fires and the detection of HCl concentrations at

Eagle Mountain Lake due to the long range transport necessary. A considerable portion of the events take place at a distance ≥ 600 km, and this would increase the time necessary for transport to take place. Therefore, a comparison of the data shown in Figure 3-8 was modified to compare HCl concentrations two days after the reported timing of the wildfire events. This comparison is shown in Figure 3-9.

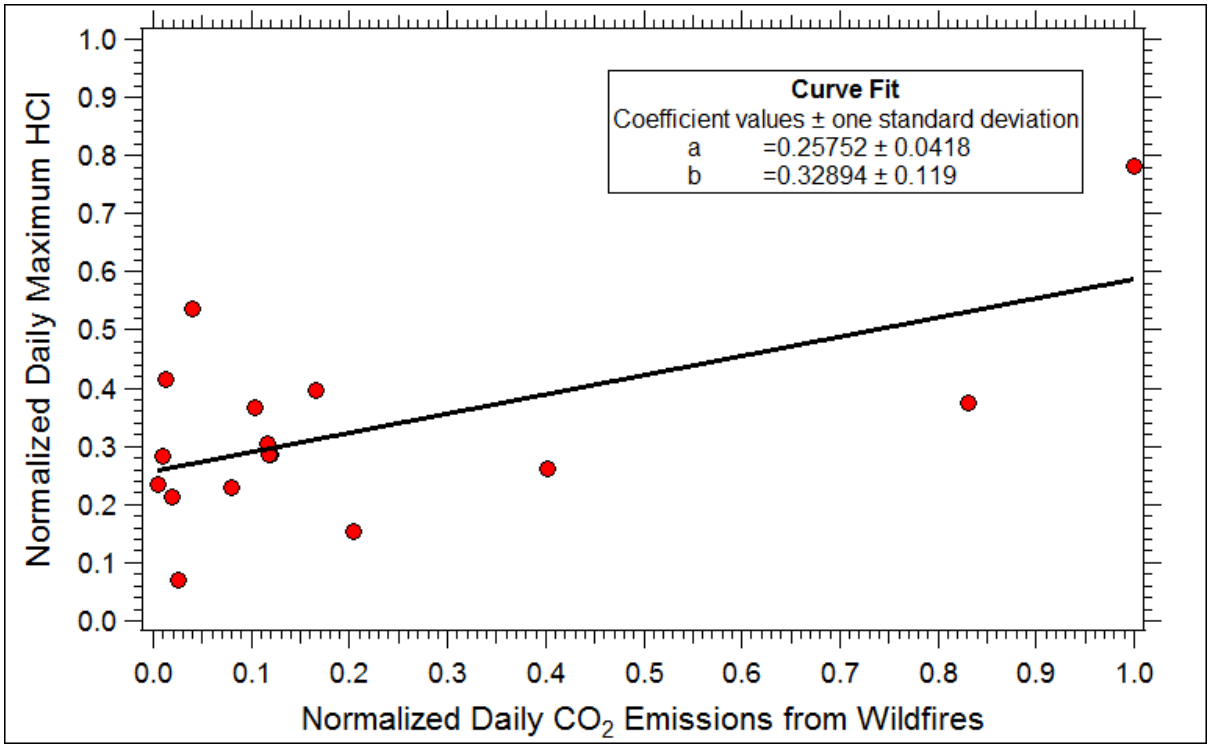

Figure 3-9: A comparison of daily maximum hourly average HCl concentrations and total CO_2 emissions from all wildfires occurring in the region shown in Figure 3-7. Data represented here is modified from that shown in Figure 3-8 to include an offset of 2 days for HCl concentrations.

From Figure 3-9, it can be seen that a two day offset for HCl concentrations improves the correlation between the two datasets. However, there are still several days where HCl concentrations are at the high end of the distribution while wildfire CO_2 concentrations are low. Additionally, as is shown in Figure 3-10, there are several periods during which wildfire emissions are low, but maximum HCl concentrations over the next few days increase. One example of this is the period from June 9th to June 15th. Conversely, there are also period where wildfire emissions are the highest during the episode, and peak chlorine concentrations trend downwards or do not significantly change. This takes place in the time period from June 18th to June 24th.

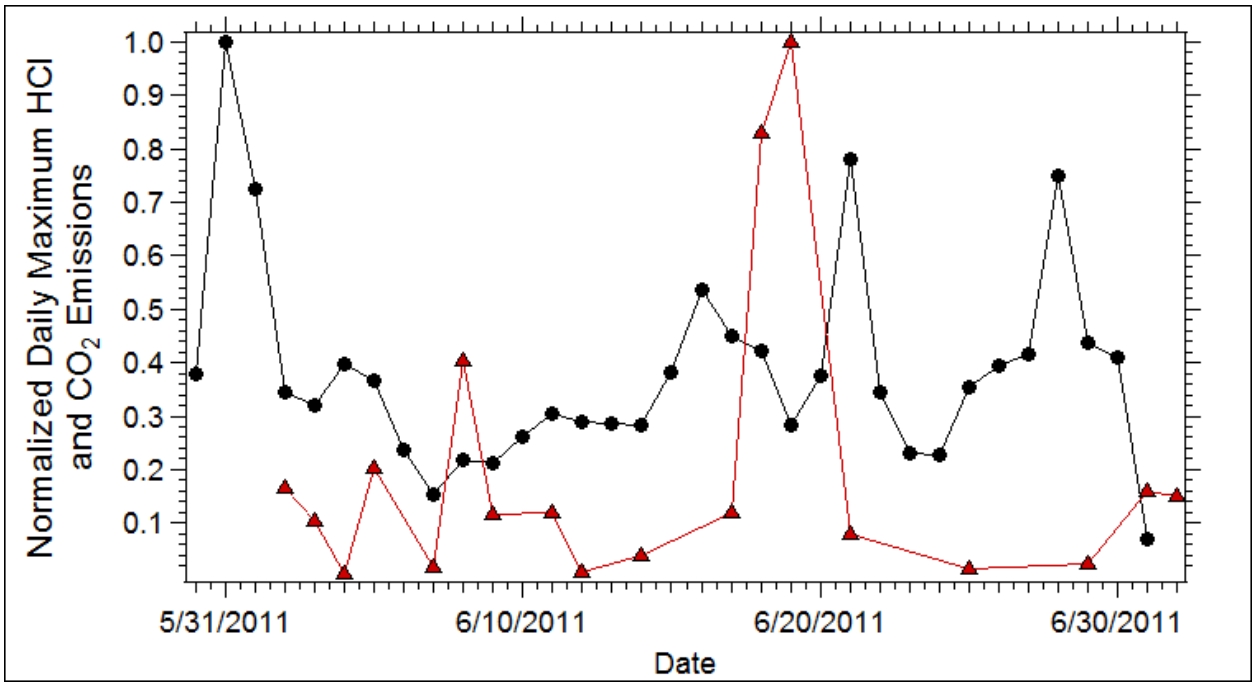

Figure 3-10: Time series of maximum daily hourly average HCl concentrations at the Eagle Mountain Lake monitoring site and combined daily CO_2 emissions from all wildfires events that occurred during June 2011 in the region shown in Figure 3-7.

Due to these inconsistencies and the lack of any strong correlation between wildfire emissions and maximum daily hourly average HCl concentrations, wildfires are not expected to be a consistent major source of particulate or gas phase atomic chlorine precursors during the time period being examined. While single wildfire events could possibly cause elevated concentrations of atmospheric chlorine species in the region, the lack of consistency between wildfire emissions and the HCl dataset examined here suggest that it is not a persistent source in the Dallas-Ft. Worth region. A more detailed study of the exact temporal and spatial distribution of particulate and gas phase chlorine species from the emissions of these wildfire events and the resulting impacts on regional air quality is beyond the scope of this work.

3.2.2 Modeling Procedures

The Comprehensive Air Quality Model with Extensions (CAMx) was used to assess the impacts of the various source inventories on ambient concentrations. The scenario used for meteorological inputs and base inventory emissions was the dfw8h2 modeling episode

(http://www.tceq.texas.gov/airquality/airmod/data/dfw8h2) from the Texas Commission on Environmental Quality's (TCEQ). This episode was initially developed to support the development of a State Implementation Plan (SIP) for 8-hour ozone standard attainment in the DFW region. The geographical domain of the model is comprised of a nested grid structure which includes 36, 12 and 4 km gridded domains. The 4 km domain is a centered on the DFW area, as is shown in Figure 3-11.

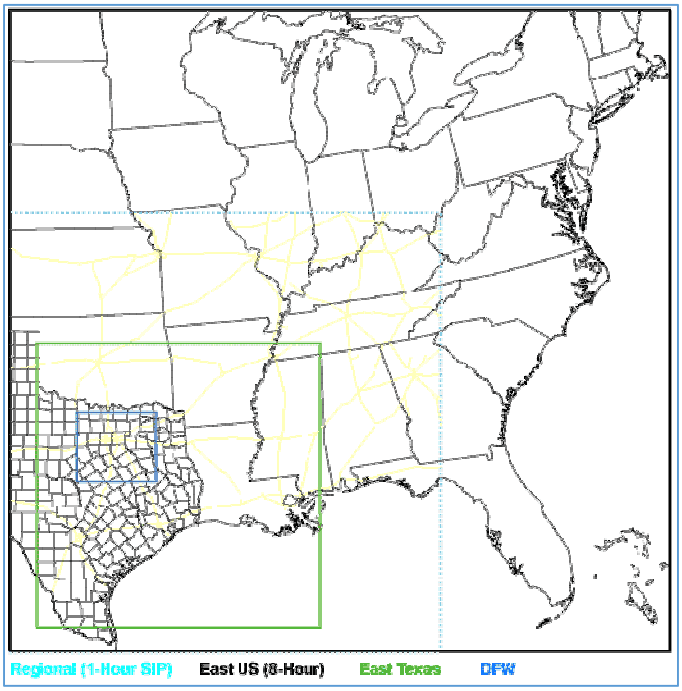

Figure 3-11: CAMx modeling domain used in this work

Aside from grid location, the dfw8h2 modeling domain was chosen for its time period (May 31 – July, 2006), which coincides with the time of year during which HCl measurements at the EML monitoring site were made (Griffin et al., 2011). Although the modeling and observations are from different time years, the same large scale meteorological and climactic patterns are expected to be consistent between the two years for the month of June. For comparison to observations, average hourly modeled concentrations in the 4 km grid cell containing the coordinates of the EML monitoring site (32.987891° N, -97.477175 W) were used. Additionally, diurnal patterns of concentrations were compared.

The base inventories in the model include inland and oceanic sources of particulate chloride. However, no significant sources of gas phase chlorine exist in the base inventory for the DFW area. A series of sensitivity analyses were performed, investigating the potential impact of various chloride and reactive chlorine emission sources, beyond those in the base case inventory.

3.3 Results

3.3.1 Modeling Results: Anthropogenic Emissions

To quantify the impact of the anthropogenic emissions that were inventoried in previous sections, the CAMx predictions of HCl concentrations were compared to observed values at Eagle Mountain Lake. The average concentration of HCl in the 4 km grid cell surrounding Eagle Mountain Lake was used for comparison. Figure 3-12 and 3-13 show the resulting HCl time series and diurnal pattern, respectively. Observed concentrations are included for comparison.

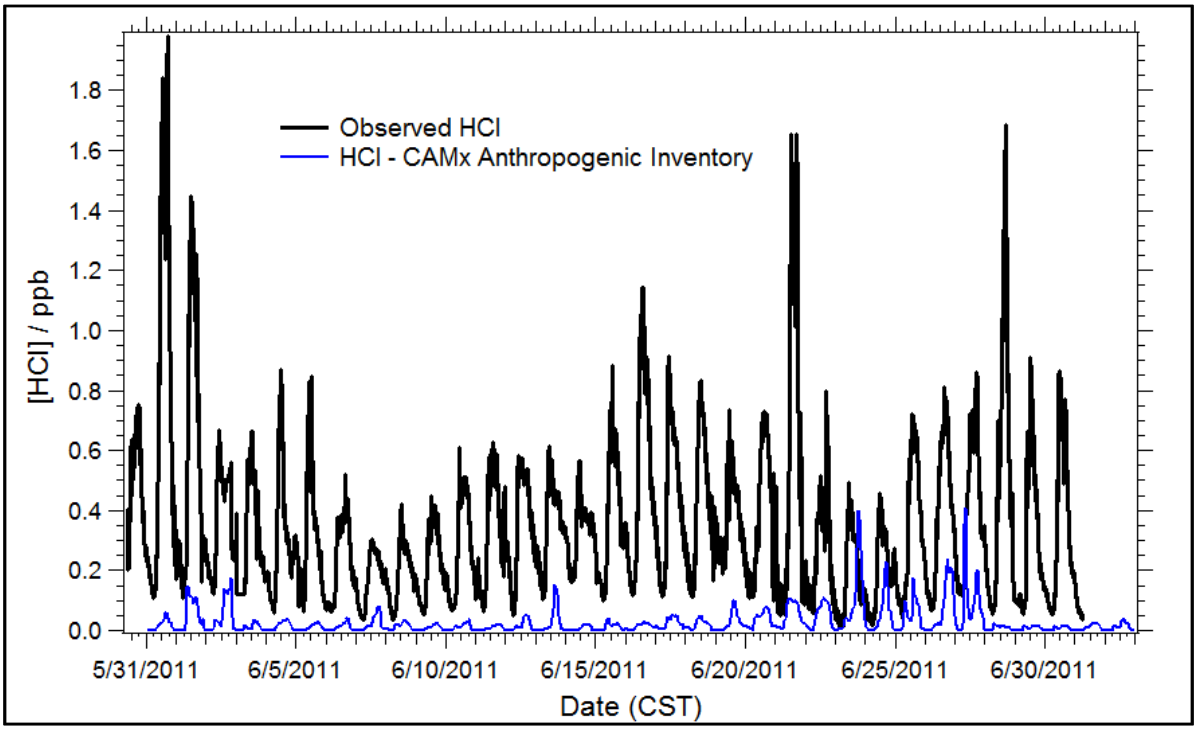

Figure 3-12: Time series of observed HCl concentrations at Eagle Mountain Lake compared to modeled concentrations from the modeling of the anthropogenic emissions inventory in CAMx.

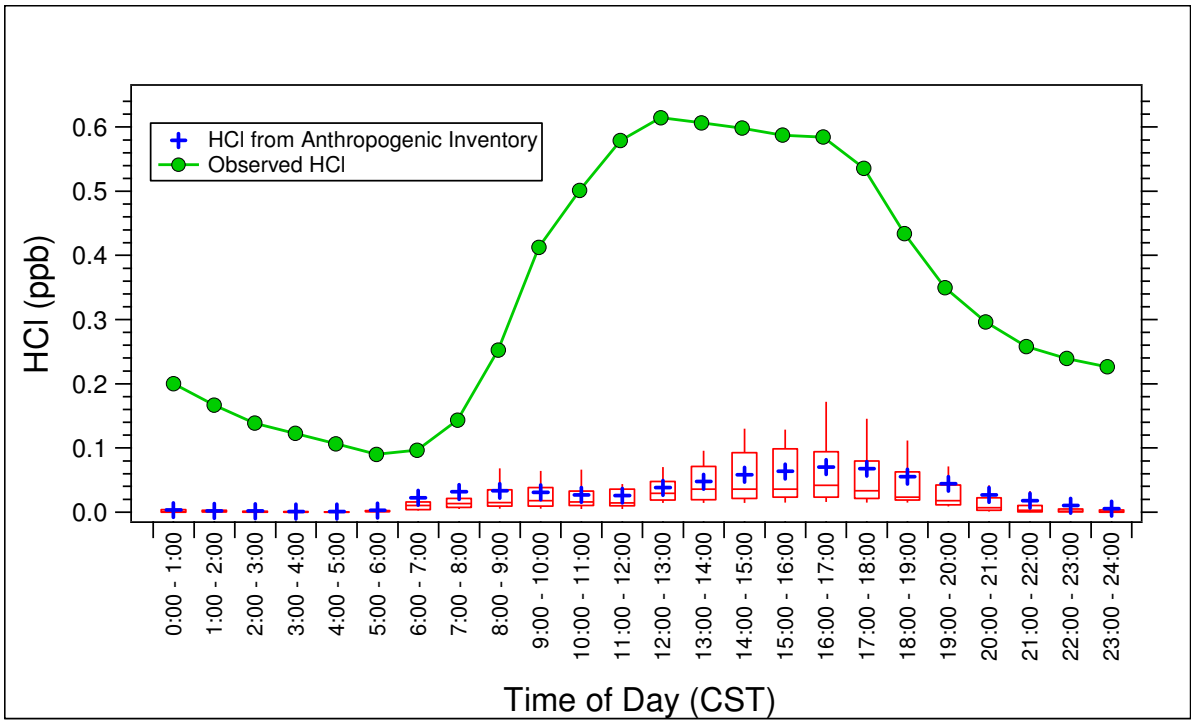

Figure 3-13: Diurnal Patterns with hourly averages for observed HCl values compared to resultant modeled concentrations using the anthropogenic inventory.

From Figure 3-12, it is evident that the base case anthropogenic emissions alone are unable to account for the observed concentrations of HCl. During some periods, when observed values are at the low end of the range and predicted values are at the high end of their range, there is modest agreement. However, for most of the time period, concentrations appear to be underestimated by approximately an order of magnitude. The peak in the diurnal pattern of both modeled and observed concentrations occurs during the mid to late afternoon, suggesting a photochemical source. These results suggest that additional sources of reactive chlorine that actively participate in photochemistry are likely contributing to the elevated HCl concentrations.

3.3.2 Modeling Results: Chlorinated VOC Emissions

Non-reactive Tracer vs Reactive Emissions

To evaluate the hypothesis that photochemically produced HCl, rather than primary HCl emissions, was driving observations at Eagle Mountain Lake CAMx simulations were performed with

emissions of a non-reactive tracer species. In these simulations, concentrations of the tracer species peaked in the early morning, between 5 – 6 AM. This is expected, but also inconsistent with the observed peak of HCl concentrations in the late afternoon. Based on these results, remaining simulations focused on emissions of reactive chlorinated organic precursors. The subsequent modeling results (Faxon & Allen, 2014a) including emissions of a reactive chlorinated organic suggested that regional emissions on the order of at least 10^2 metric tons organochloride day^{-1} (modeled as dichlorobenzene) are required to explain the average hourly HCl concentrations observed at Eagle Mountain Lake. Additionally, the value of the rate constant for the reaction between the organochloride and $OH^{\bullet}$ must be on the order of 3.4×10^{-12} – 3.4×10^{-10}, making it a relatively fast reaction for $OH^{\bullet}$ and a hydrocarbon (Atkinson et al., 2007; Sander et al., 2011).

For the purposes of modeling chlorinated organics within the CAMx mode, dichlorobenzene was chosen as a surrogate species for chlorinated organics, which are may originate from natural gas production activities within the Barnett Shale. This compound was chosen because it had previously been detected in the region (Eastern Research Group & Sage Environmental Consulting, 2011) and has a known rate constant for its reaction with $OH^{\bullet}$ (Wahner & Zetzsch, 1983). A reaction with $OH^{\bullet}$ was hypothesized due to the apparent photochemical nature of the diurnal patterns of observed HCl concentrations (Figure 3-4). Additionally, previous work suggests the production of $Cl^{\bullet}$ results from this reaction, and secondary products (e.g., chlorophenol) have been shown to produce $Cl^{\bullet}$ as well (Kılıç & Çınar, 2008; Kiliç, Koçtürk, San, & Cinar, 2007; Xu et al., 2010).

The emissions estimate of 10^2 metric tons d^{-1} is the mass emitted of the reactive VOC, not tons chlorine, and the surrogate chlorinated organic used in the calculations had a molecular weight equivalent to dichlorobenzene. If each molecule of the model organic is assumed to produce one chlorine atom upon reacting, then these emissions are equivalent to chlorine emissions ranging on the

order of 10-10^2 metric tons Cl d^{-1}, depending on the rate of reaction. The emissions rate is doubled if the model compound is assumed to produce two chlorine atoms per molecule.

A comparison of the observed hourly averages to the diurnal patterns obtained from two chlorocarbon emissions scenarios are shown in Figure 3-14. The diurnal HCl patterns at Eagle Mountain Lake resulting from emissions rates ranging 80 – 600 metric tons Cl d^{-1} and reaction rates ranging 10^{-12} – 10^{-11} cm^3 $molecules^{-1}$ s^{-1} are shown. Further details on modeling of the chlorinated organic reaction mechanism, as well as additional scenarios involving direct emission of inorganic $Cl^{\bullet}$ precursors, can be found in chapter 6 of this thesis (Faxon & Allen, 2014a).

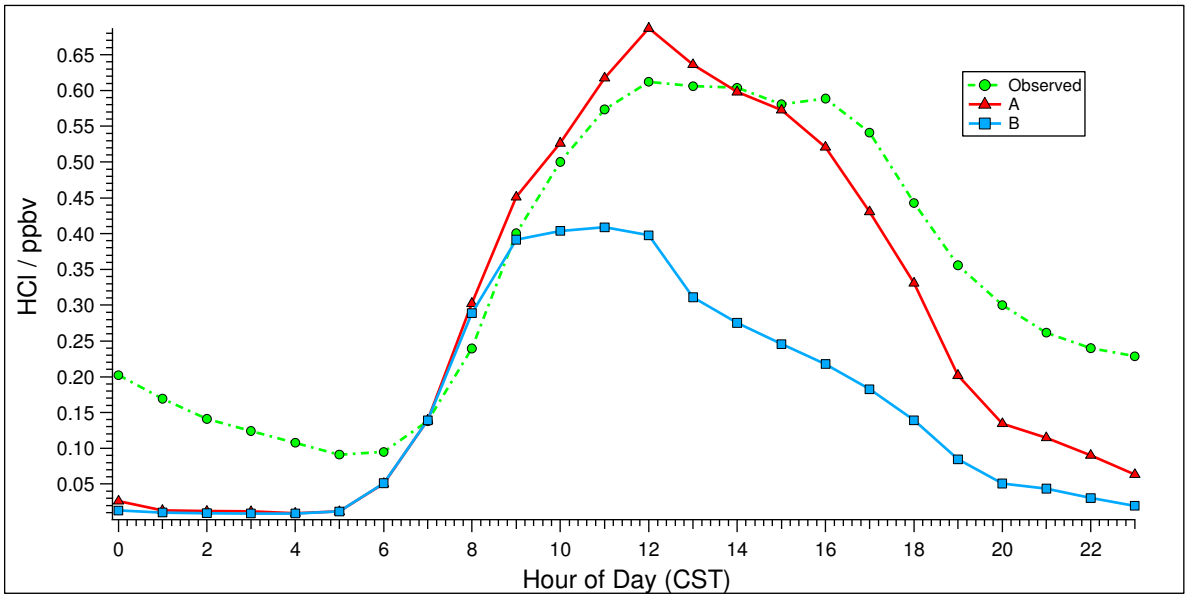

Figure 3-14: Comparison of HCl hourly averages observed at Eagle Mountain Lake during June 2011 and modeled hourly average HCl two chlorocarbon emissions scenarios. Scenario A included chlorocarbon emissions (modeled as dichlorobenzene) and a chlorocarbon + $OH^{\bullet}$ reaction rate 600 metric ton Cl d^{-1} and 3.4 x 10^{-12} cm^3 $molecule^{-1}$ s^{-1}. The emissions and reaction rate for scenario B were 80 metric ton Cl d^{-1} and 3.4 x 10^{-11} cm^3 $molecule^{-1}$ s^{-1}, respectively. Though the concentrations in scenario B are not high enough to fully explain the observed values, it demonstrates how significantly less organochloride emissions are needed if an increase of an order of magnitude in the rate constant is included.

By comparing the observed and modeled diurnal HCl concentration patterns from Figure 3.14, several conclusions can be deduced. First, the modeled diurnal pattern in scenario A matches the EML observations very well. However, the required emissions rate (600 metric ton Cl d^{-1}) is very large in comparison to other regional sources. In comparison, the diurnal pattern in scenario B peaks at the

same order of magnitude and at approximately the same time of day as the observations while requiring a much lower emissions rate (600 metric ton Cl d^{-1}). The higher amount of HCl produced to chlorocarbon emitted in scenario A compared to scenario B results from a rate constant for the chlorocarbon + $OH^{\bullet}$ reaction that is an order of magnitude larger than that used in scenario A. This result underscores the decrease in emissions necessary to explain the observations for a more reactive species. A further reduction in the chlorocarbon emissions necessary to explain observed HCl concentrations results from the use of the alternative emissions scenario described in section 3.2.1. The results of these scenarios are discussed further in Chapter 6.

3.3.3 Results: Sea Salt Emissions and Transport

Another possible explanation for elevated HCl concentrations observed at Eagle Mountain Lake is the volatilization of particulate chloride through acid displacement by gas phase HNO_3 or H_2SO_4, as shown in reactions 1 and 2, where (cd) represents condensed phase species (De Haan & Finlayson-Pitts, 1997; Gard, 1998; Graedel & Keene, 1996; Saul et al., 2006).

$$HNO_{3(g)} + NaCl_{(cd)} \rightarrow HCl_{(g)} + NaNO_{3(cd)} \qquad \text{(Reaction 3-1)}$$

$$H_2SO_{4(g)} + NaCl_{(cd)} \rightarrow HCl_{(g)} + NaNO_{3(cd)} \qquad \text{(Reaction 3-2)}$$

Figure 3.15 compares concentrations of gas phase HNO_3 and HCl during the month of June 2011. During some time periods, such as the periods around 6/5 and 6/25, there is a direct correlation between increasing HNO_3 and HCl. However, the days during which the highest concentrations of HCl are observed occur during periods where HNO_3 concentrations are at the low end of their detected range. HNO_3 concentrations were observed to peak during the same time periods as HCl on most days (Figure 3-16), which results in the correlations shown in Figure 3-15.

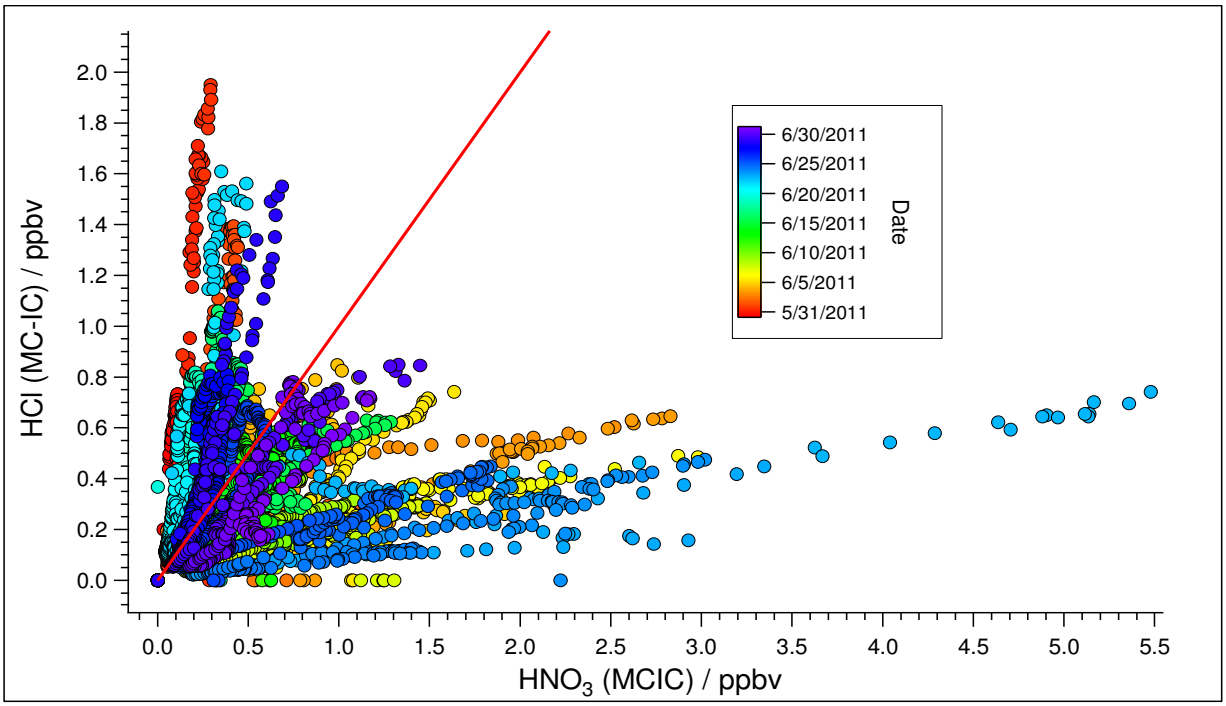

Figure 3-15: Comparison of HCl and HNO_3 concentrations detected in June, 2011 using MC-IC techniques. A 1:1 line is added for reference.

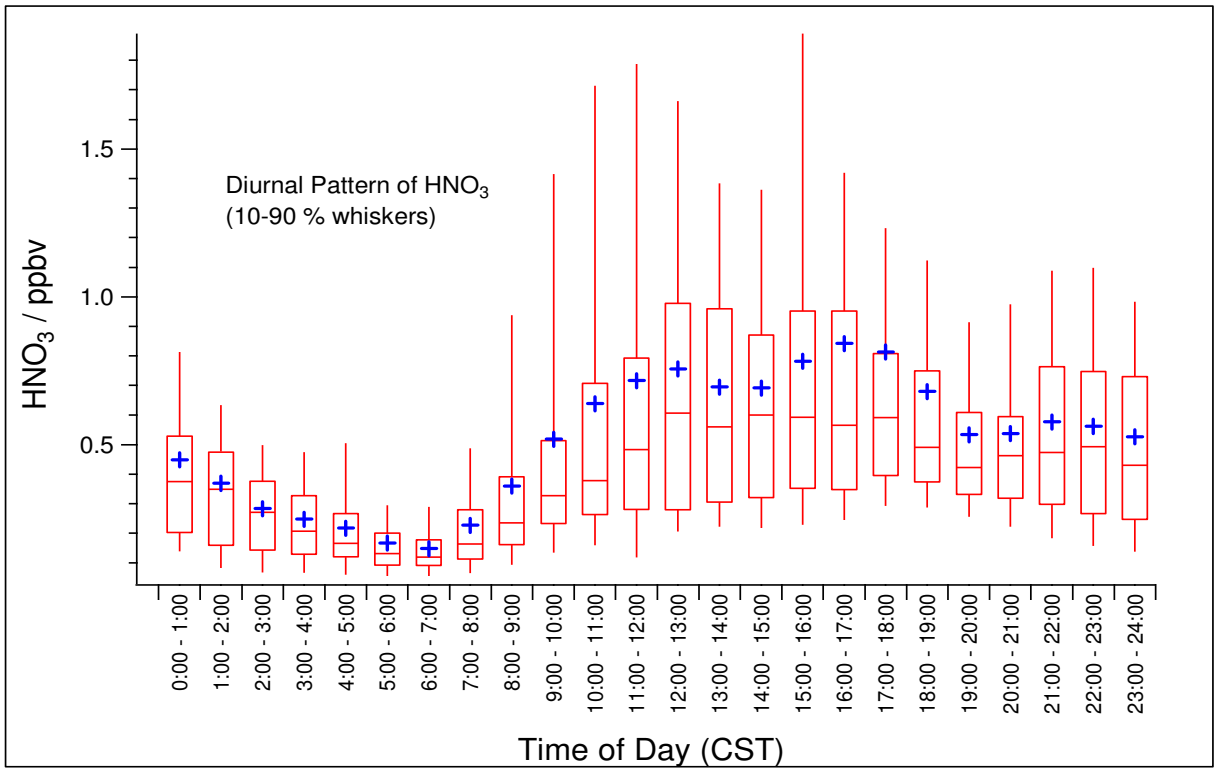

Figure 3-16: Diurnal pattern of HNO_3 at Eagle Mountain Lake as observed by MC-IC.

While both HCl and HNO_3 show diurnal patterns consistent with photochemical production, particle nitrate data are not consistent with a chloride displacement by nitric acid source for the observed

HCl. When comparing detected HCl concentrations to AMS nitrate (Figure 3-17), there is no discernable correlation. A similar absence of correlation between HCl and particulate sulfate observed during the same period can be seen in Figure 3-18. Additionally, there are no distinct peaks in the afternoon for the diurnal profiles of particulate sulfate and nitrate concentrations (Figures 3-19 and 3-20). In addition to the lack of correlation between gas phase HCl and particulate nitrate or sulfate, contemporaneous observations of particulate chloride were below the detection limit of Particle in Liquid Sampler (PILS) instrumentation at the site for the duration of the campaign.

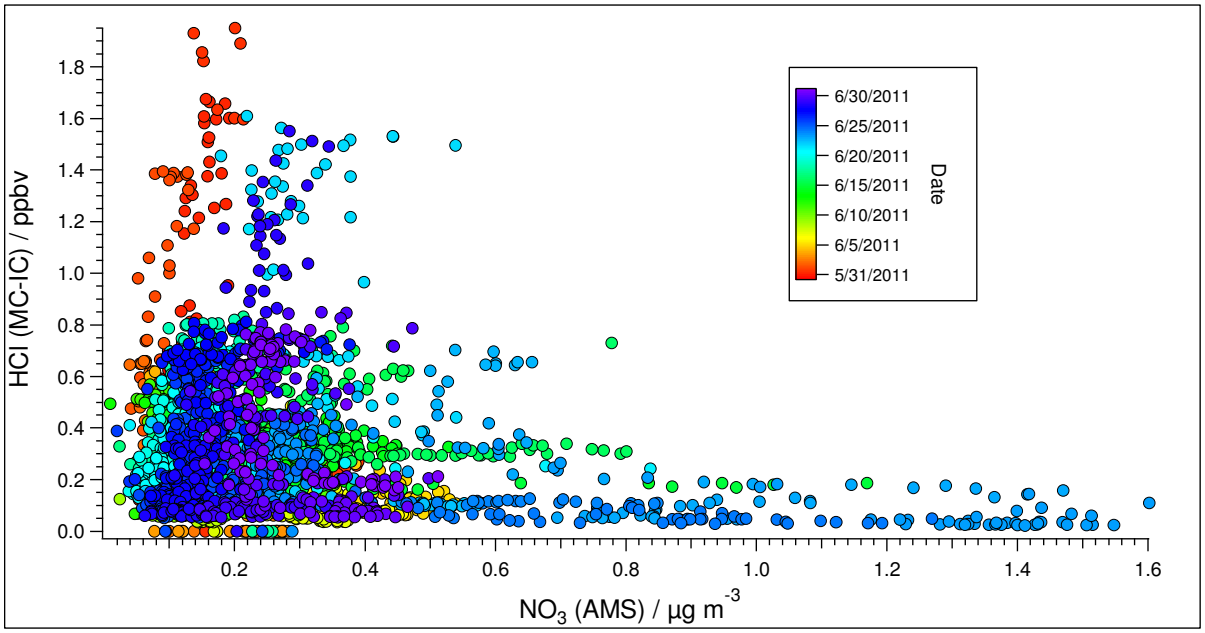

Figure 3-17: Comparison of HCl from MC-IC and particle NO_3 concentrations measured by AMS.

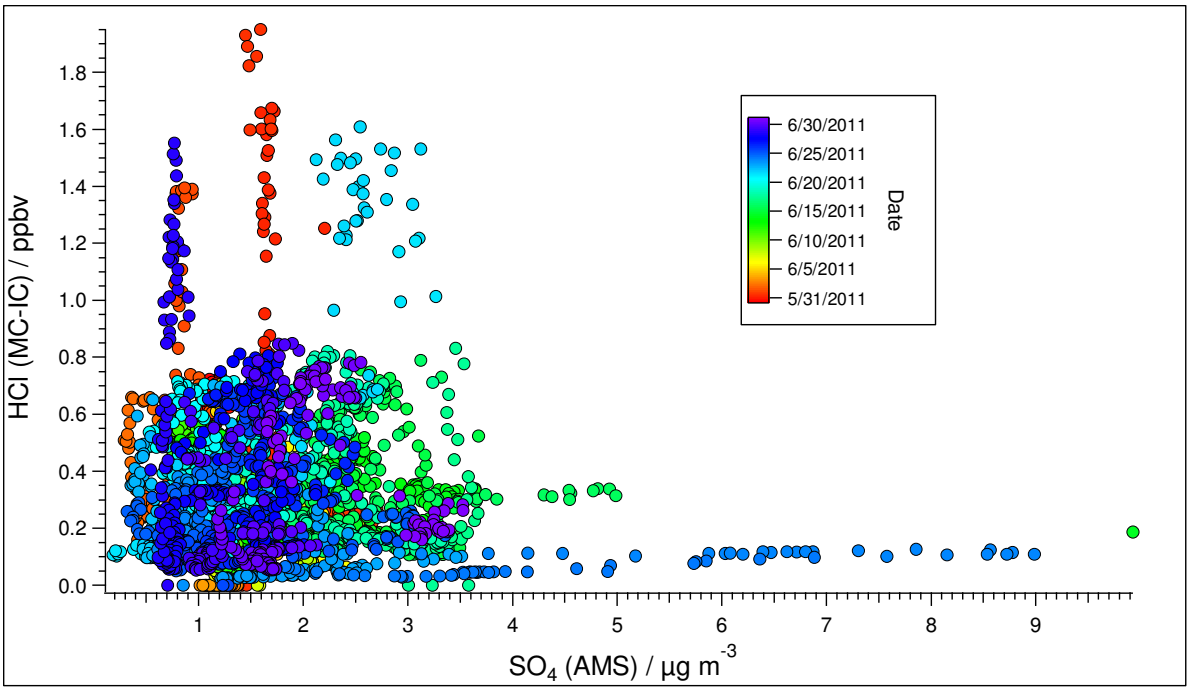

Figure 3-18: Comparison of HCl concentrations from MCIC concentrations and particle SO_4 concentrations from AMS measurements.

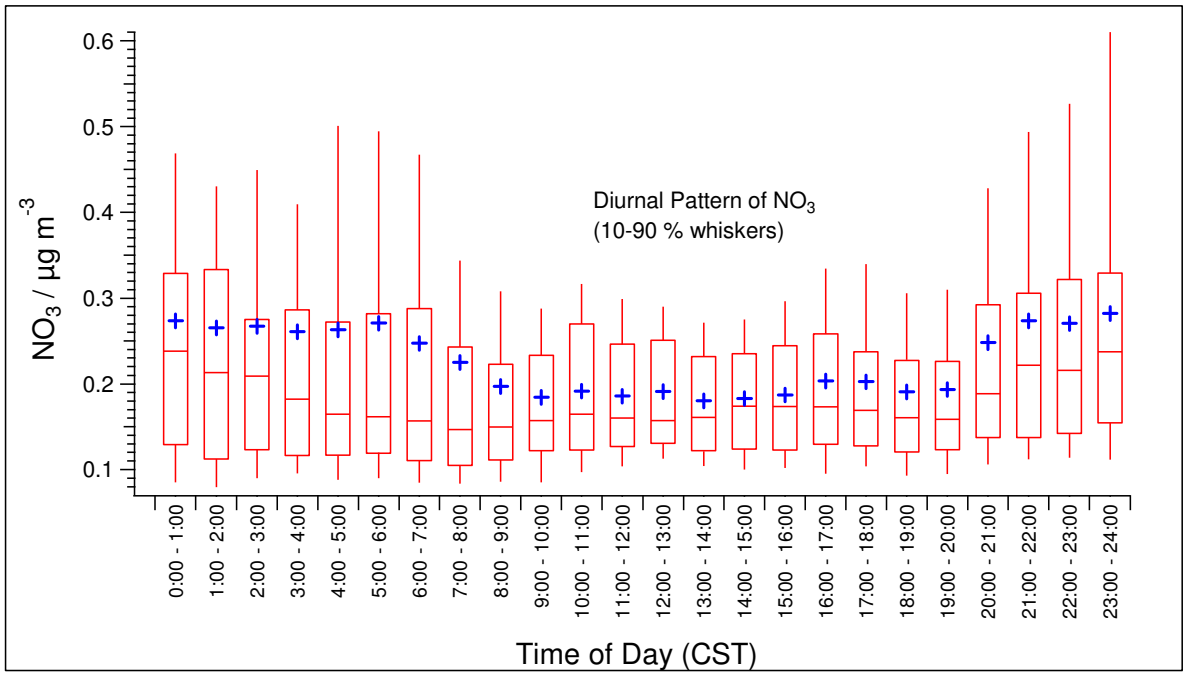

3-19: Diurnal pattern of particulate nitrate from AMS measurements taken during June 2011.

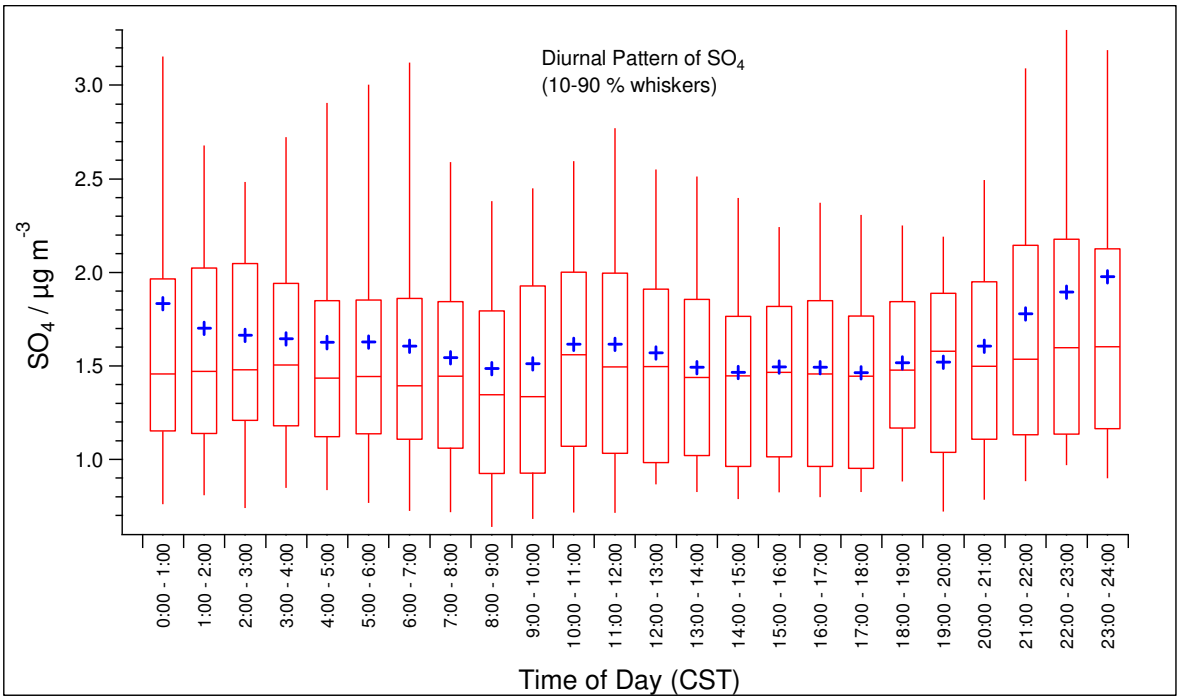

Figure 3-20: Diurnal pattern of particulate sulfate from AMS measurements taken during June 2011.

Furthermore results of the sea salt transport modeling episode (described 6 of this thesis) indicate two major conclusions: 1) particulate chloride is not typically present at the location of the Eagle Mountain Lake monitoring site at concentrations larger than 8 x 10^{-3} ppb, and 2) under the meteorological conditions used, sea salt transport into the region accounts for a small fraction (< 20% on most days) of ground level particulate chloride concentrations at Eagle Mountain Lake.

The lack of correlation resulting from comparisons of gas phase HCl to particulate sulfate and nitrate concentrations suggests that acid displacement by either nitrate or sulfate is not a primary source. Additionally, the fact that particulate chloride concentrations from PILS measurements were usually under the detection limit(Griffin et al., 2011), suggest that particulate chloride does not make a significant contribution as a source towards the observed HCl concentrations at Eagle Mountain Lake. These observations are supported by the lack of significant sea salt transport in the modeling results. This conclusion leaves an unknown source of reactive chlorine, for which chlorine from natural gas production activities is suggested by this work. HCl concentrations resulting from this hypothesized source were briefly discussed in section 3.3.2 and are discussed in further detail in Chapter 6 of this

work. Though the amount of chloride emissions necessary to explain the observed HCl in these scenarios is high compared to other emissions sources inventoried in this work, calculations in section 3.2.1 demonstrate that enough chlorine is present from natural gas production activities to account for such a source.

3.4 Conclusions

The data from the EML site qualifies as an interesting case study for a chlorine emissions inventory development. Inventoried direct emissions of gas phase reactive chlorine within the region are small. Additionally, the fact that concentrations peaked in the mid to late afternoon is inconsistent with what would be expected from continuous gas phase emissions. Even in the event that sufficient particulate chloride was present, known N_2O_5 driven heterogeneous $ClNO_2$ production would produce $Cl^{\bullet}$ concentration peaks in the early morning hours. Therefore, the observations are in need of an explanation outside of the most well documented sources of reactive chlorine. The observations serve as a top down approach to quantifying the amount of gas phase chlorine present in the region, which can be combined with the modeling results presented here to quantify the relative contribution of known chlorine sources in the region. Comparison of average observed and modeled concentrations from known anthropogenic contributions (Figure 3-13) indicate that an additional source that contributes at least 0.5 ppb HCl, on average, during the afternoon (3- 6 PM) is necessary to explain observed concentration patterns.

Table 3-7 summarizes the daily emissions from the sources discussed in this work. The largest source of molecular chlorine emissions in the region is swimming pool chlorination at 8110 kg d^{-1}. Water and wastewater treatment and tap water usage both contribute approximately 1000 kg d^{-1}. Though highly localized, emission of molecular chlorine from industrial point sources, reported in the EPA TRI and the TCEQ PSDB, is the lowest category of emissions. The contribution to chlorine concentrations in DFW from extra-regional sea salt transport is negligible. Additionally, wildfires are

not expected to be a major source of atomic chlorine precursors in the region. Estimated emissions of chlorinated organics from natural gas production that are required to explain the Eagle Mountain Lake observations are the largest source in terms of magnitude. However, the calculated usage of chloride in hydraulic fracturing activities suggests that a sufficient reservoir of potentially reactive chlorine could be present in the region. A specific mechanism for formation of volatile species and a route to the production of atomic chlorine are required to further investigate the potential of this reservoir. Investigation into possible pathways to volatile chlorine production and the development of mechanisms for photochemical modeling are recommended for future work.

Table 3-7: Comparison of Inventoried Emissions of Atomic Chlorine Precursors in the DFW Region

Source	**Average Source Magnitude (kg Cl_2 d^{-1})**
Industrial Point Sources	4
Non-refinery Cooling Towers	-
Water and Wastewater Treatment	1170
Swimming Pool Chlorination	8110
Tap Water Usage	1080
Chlorinated VOC Emissions[i]	10^4-10^5
Long-Range Sea Salt Transport	-
Wildfires	-
Total[ii]	10364

[i] Emissions rate reported as kg Cl d^{-1} emitted as chlorinated VOCs

[ii] Emissions of chlorinated organics are not included in the total

Chapter 4: Impacts of the Heterogeneous Reactions Involving Chlorine on Ozone Formation

4.1 Introduction

Development of plans for attaining National Ambient Air Quality Standards (NAAQS) for ozone is typically performed using gridded photochemical models that incorporate condensed photochemical mechanisms. These mechanisms account for the oxidation of volatile organic compounds (VOCs) in the presence of nitrogen oxides (NO_x). However, field studies performed in Houston, TX, and subsequent photochemical modeling have shown that anthropogenic emissions of gas phase chlorine species can accelerate the rate of ozone production, potentially leading to localized increases in ozone concentrations (Tanaka, 2003a; Tanaka et al., 2003a). To take this phenomenon into account, a chlorine chemistry mechanism was integrated into the Carbon Bond condensed chemical mechanism, which included photolysis of two primary anthropogenic chlorine sources, Cl_2 and HOCl, and the ensuing reactions of the chlorine radicals (Tanaka, 2003b).

More recently the National Oceanic and Atmospheric Administration (NOAA) reported the first detection of ambient concentrations of nitryl chloride ($ClNO_2$) (Osthoff et al., 2008). The reported observations, made along the Gulf Coast in 2006, indicated the presence of $ClNO_2$ at concentrations exceeding 1 ppbv. Similar observations have since been made during studies in California and Colorado (Mielke et al., 2011; Thornton, Kercher, Riedel, Wagner, Cozic, Holloway, Wolfe, et al., 2010). Investigation of the Gulf Coast results suggested that heterogeneous chlorine chemistry was responsible for the presence of $ClNO_2$. The mechanism of this heterogeneous chemistry was determined to be the uptake of dinitrogen pentoxide (N_2O_5) into chloride containing aerosols followed by the reaction of N_2O_5 with otherwise unreactive chloride, such as sea salt, to produce $ClNO_2$, which then partitions back into the gas phase (H. Simon et al., 2009). The implications to ozone formation chemistry result from

the provision, through $ClNO_2$, of a pathway for the release of reactive chlorine into the gas phase, while also releasing NO_2 upon photolysis (Osthoff et al., 2008; H. Simon et al., 2009, 2010).

In addition to the heterogeneous production of $ClNO_2$ as a reaction important to chlorine cycling in the environment, recent measurements showing gas phase HCl concentrations on the order of one ppb that peak in the mid-afternoon suggest that other routes might also be important to chlorine cycling under some circumstances (Griffin et al., 2011). One proposed mechanism that might account for this phenomenon involves a surface reaction between hydroxyl radicals ($OH^{\bullet}$) in the gas phase and chloride ions in aerosol particles (E. M. Knipping, 2000a; Eladio M. Knipping & Dabdub, 2002; Nissenson et al., 2008).

This Chapter explores the implications of variations in the parameters describing these two heterogeneous mechanisms involving Cl chemistry in and on aerosol particles. Reactions involving N_2O_5 uptake and $ClNO_2$ production as well as those involving the OH-chloride ion surface reaction are explored. Depending on the combination of heterogeneous parameters, the production of $ClNO_2$ from N_2O_5 can lead to both increases and decreases in ozone production. Previous regional studies of this chemistry have used parameter values that were varied over a small range (H. Simon et al., 2009, 2010). This work is intended to explore the full range of sensitivity of ozone formation to variations in reactive uptake parameters, gas phase chemistry parameters, and atmospheric conditions (e.g., available aerosol surface area, particle nitrate content, particle water content, VOC/NO_x ratios).

4.2 N_2O_5 Uptake and $ClNO_2$ Production

The heterogeneous reactions of oxides of nitrogen with halide salts in solid or aqueous particles are thought to play an important role in halogen activation. It is known that heterogeneous uptake of N_2O_5 plays a critical role in overall NO_x chemistry, with up to 50% of global NO_x emissions being removed via heterogeneous mechanisms. The reactions involved in halogen activation can be written in

terms of a generic halogen, X, and the particulate phase can be either aqueous or solid (denoted by (cd)) (Aldener et al., 2006; B J Finlayson-Pitts, 2003; Schweitzer et al., 1998):

$$2NO_{2(g)} + NaX_{(cd)} \rightarrow XNO_{(g)} + NaNO_{3(cd)} \qquad \text{(Reaction 4-1)}$$

$$N_2O_{5(g)} + NaX_{(cd)} \rightarrow XNO_{2(g)} + NaNO_{3(cd)} \qquad \text{(Reaction 4-2)}$$

$$ClONO_{2(g)} + NaCl_{(cd)} \rightarrow Cl_{2(g)} + NaNO_{3(cd)} \qquad \text{(Reaction 4-3)}$$

Reaction 4-1 is not thought to be very important for atmospheric halogen activation (Schweitzer et al., 1998). However, the reaction of N_2O_5 appears to play an important role in the activation of chloride, and provides an efficient method of $ClNO_2$ production (Brown et al., 2009; Roberts et al., 2008a). The standard acid displacement reaction involving the interaction of NaCl particles with HNO_3 is up to two orders of magnitude slower than the interaction with N_2O_5 (Laux et al., 1994). Atmospheric implications of this reaction are important since tropospheric concentrations of N_2O_5 can reach levels of up to 15 ppb, although concentrations are more regularly around 1 ppb (Laux et al., 1994; Livingston & Finlayson-Pitts, 1991).

An early study of the production of chlorine radicals from irradiated NaCl aerosols in the presence of ozone and NO_x confirmed $ClNO_2$ production as a major pathway for chloride activation by comparing the rates of chlorine atom production to the photolysis rates of $ClNO_2$. The rate of production in this study was observed to be almost 400 times stronger than could be explained by the reaction of HCl with OH, which is a relatively slow reaction (W Behnke & Zetzsch, 1990; Eladio M Knipping & Dabdub, 2003). One study observed a direct correlation between $ClNO_2$ concentrations and the product of N_2O_5 concentrations and aerosol surface area, especially at night (Osthoff et al., 2008). However, the exact mechanism is still a subject of debate.

A mechanism that was hypothesized early on involved competition between the reactions of absorbed N_2O_5 with chloride ions or water (W Behnke et al., 1991; Wolfgang Behnke et al., 1997):

$$N_2O_{5(aq)} + H_2O \rightarrow 2HNO_3 \qquad \text{(Reaction 4-4)}$$

$N_2O_{5(aq)} + Cl^- \rightarrow ClNO_2 + NO_3^-$ (Reaction 4-5)

$ClNO_2 + H_2O \rightarrow 2H^+ + Cl^- + NO_3^-$ (Reaction 4-6)

However, analysis of the rates of N_2O_5 reactions with water and the chloride ion found these reactions unable to take the dependence of $ClNO_2$ yield on chloride concentrations into account. In fact, direct hydrolysis was found to account for approximately only 20% of the overall reaction, and dissociation of N_2O_5 has been proposed as the initial rate limiting step (Wolfgang Behnke et al., 1997; Roberts et al., 2009; Schweitzer et al., 1998):

$N_2O_{5(aq)} \leftrightarrow NO_2^+ + NO_3^-$ (Reaction 4-7)

$NO_2^+ + H_2O \rightarrow H^+ + HNO_3^-$ (Reaction 4-8)

$NO_2^+ + Cl^- \rightarrow ClNO_2$ (Reaction 4-9)

Since N_2O_5 does not react directly with chloride ions, there is no observable dependence of the uptake coefficient on chloride concentrations (Schweitzer et al., 1998). An alternate mechanism has been proposed that involves the initial uptake of N_2O_5 into the aqueous phase and formation of a protonated nitric acid intermediate as the initiating step of chloride activation in the form of $ClNO_2$ (Bertram & Thornton, 2009):

$N_2O_{5(g)} \leftrightarrow N_2O_{5(aq)}$ (Reaction 4-10)

$N_2O_{5(aq)} + H_2O \leftrightarrow H_2ONO_2^+{}_{(aq)} + NO_3^-{}_{(aq)}$ (Reaction 4-11)

$H_2ONO_2^+{}_{(aq)} + H_2O \rightarrow H_3O^+{}_{(aq)} + HNO_{3(aq)}$ (Reaction 4-12)

$H_2ONO_2^+{}_{(aq)} + Cl^-{}_{(aq)} \rightarrow ClNO_{2(aq)} + H_2O_{(aq)}$ (Reaction 4-13)

For the above mechanism, reaction 4-12 was determined to be the limiting step when the relative humidity is below 40%, while the initial mass accommodation and hydrolysis step are the limiting steps above 50% (Thornton & Abbatt, 2005). It should be noted that $H_2ONO_2^+{}_{(aq)}$ has not been directly observed but serves as a tool for conceptualizing competing pathways (Bertram & Thornton, 2009). A

coexisting reaction pathway in which $ClNO_2$ is an intermediate leading to the production of Cl_2 has been observed in conditions where the pH drops below two (Roberts et al., 2009, 2008a).

$ClNO_2$ can also undergo reactions within the particles to produce alternate forms of volatile chlorine instead of being released into the gas phase. The uptake and solubility of $ClNO_2$ into aqueous particles is inhibited by the presence of chloride, primarily due to its dissociation reaction in the aqueous phase (Frenzel et al., 1998):

$$ClNO_2 \leftrightarrow Cl^- + NO_2^+ \qquad \text{(Reaction 4-14)}$$

The uptake rate is very low with an uptake coefficient ranging from $(4.84 \pm 0.13) \times 10^{-6}$ on pure water to $(0.27 \pm 0.02) \times 10^{-6}$ on 4.6 M NaCl (W Behnke, Elend, Krüger, & Zetzsch, 1999). Once absorbed into the aqueous phase, however, $ClNO_2$ as well as other halogen species can undergo reactions such as those in reactions 4-15 to 4-18, where X represents a halogen (Schweitzer et al., 1998).

$$ClNO_2 + NaX \rightarrow XCl + NaNO_2 \qquad \text{(Reaction 4-15)}$$

$$ClNO_2 + NaX \rightarrow XNO_2 + NaCl \qquad \text{(Reaction 4-16)}$$

$$XCl + NaX \rightarrow X_2 + NaCl \qquad \text{(Reaction 4-17)}$$

$$XNO_2 + NaX \rightarrow X_2 + NaNO_2 \qquad \text{(Reaction 4-18)}$$

Regardless of the details of what happens once N_2O_5 is absorbed into the aqueous phase, all proposed mechanisms agree that uptake of N_2O_5 from the gas phase into the aqueous phase is an initial step and one that is important to the rate of the overall mechanism. Experiments have shown that the decay of gas phase N_2O_5 concentrations in the presence of simulated sea salt aerosols is log-linear, implying a first order loss mechanism (Thornton & Abbatt, 2005).

The parameters that must be known to properly model such heterogeneous reactions include (Ravishankara, 1997):

1. Particle surface area.

2. The phase(s) in or on which the reaction is taking place.
3. Chemical composition of the phases.
4. Concentrations of species involved in the reaction.
5. A reactive uptake coefficient for the gas species involved.

Important physical parameters, including the surface area and the reactive uptake coefficient, can be related to the observed rate of N_2O_5 loss (Jacob, 2000; Ravishankara, 1997; Thornton & Abbatt, 2005):

$$k = \frac{\gamma_{obs}\omega A}{4} \qquad \text{(Equation 4-1)}$$

Here, γ_{obs} is the observed reactive uptake coefficient, ω is the average molecular velocity of N_2O_5, and A is the surface area density of particles. The reactive uptake coefficient has been defined as the number of molecules lost through the surface relative to the number of molecules hitting the surface (Frenzel et al., 1998). In contrast, the mass accommodation coefficient can be defined as the probability that a molecule is absorbed upon impacting a surface. It is strictly a mass transfer parameter, whereas the reactive uptake coefficient takes into account diffusion, uptake and reaction (Ravishankara, 1997). Reactive uptake can be more explicitly modeled from the following parameters (Wolfgang Behnke et al., 1997; Frenzel et al., 1998; Schweitzer et al., 1998):

$$\frac{1}{\gamma} = \frac{1}{\alpha} + \frac{\langle c \rangle}{4HRT\left(k\, D_{aq}\right)^{1/2}} \qquad \text{(Equation 4-2)}$$

In this equation, γ is the uptake coefficient, α is the mass accommodation coefficient, ⟨c⟩ is the aqueous phase concentration of the species in question, H is the Henry's law coefficient, D_{aq} is the aqueous phase diffusion coefficient and k is the first order rate constant for reaction of the species in question within the aqueous phase. This equation was derived from the assumption of infinite film thickness, and the 1/α term can be ignored for species with large mass accommodation coefficient values (Wolfgang Behnke et al., 1997).

For situations where reaction is limited by gas phase diffusion and an observed uptake coefficient on aqueous particles has been measured, the following equations, which are nearly identical to one another, have been used by researchers to calculate the uptake coefficient, where P is the pressure and d is the particle diameter (C. George et al., 1994; Schweitzer et al., 1998):

$$\gamma = \frac{1}{\frac{1}{\gamma_{obs}} - \frac{\langle c \rangle d}{8 D_g / P}} \quad \text{(Equation 4-3)}$$

$$\gamma = \frac{1}{\frac{1}{\gamma_{obs}} - \frac{\langle c \rangle d}{8 D_g} - \frac{1}{2}} \quad \text{(Equation 4-4)}$$

A detailed parameterization specifically suited for the competing reactions involved in heterogeneous nitryl chloride production is given by equation 4-5 (Bertram & Thornton, 2009).

$$\gamma_{N_2O_5} = A k'_{4-11} \left(1 - \frac{1}{\left(\frac{k_{4-12}[H_2O(l)]}{k_{-(4-11)}[NO_3^-]} \right) + 1 + \left(\frac{k_{4-13}[Cl^-]}{k_{-(4-11)}[NO_3^-]} \right)} \right) \quad \text{(Equation 4-5)}$$

$$k'_{4-11} = \beta - \beta e^{(-\delta[H_2O(l)])} \quad \text{(Equation 4-6)}$$

The parameters within these equations have been determined as $\beta = 1.15 \times 10^6 \pm 3 \times 10^5 s^{-1}$, $\delta = 1.3 \times 10^{-1} \pm 5 \times 10^{-2} M^{-1}$ and $A = 3.2 \times 10^{-8}$ s. This parameterization is valid only for aqueous particles. The determination of parameters in equations 4-5 and 4-6 has been the focus of many experimental and modeling studies. Accurate values of the parameters must be used if the N_2O_5-sea salt interaction mechanism to yield accurate predictions when implemented in current models.

In one study the value of the reactive uptake coefficient was reported to exhibit negative temperature dependence in the range of 262-278K (C. George et al., 1994). However, another study found no temperature dependence over the range of 262-278K (Schweitzer et al., 1998). Organic compounds, when present at the surface of aqueous particles, can seriously inhibit the uptake of N_2O_5. One study showed that when mM level concentrations of hexanoic acid were present at the surface of

particles the reactive uptake coefficient decreased by three to four times (Thornton & Abbatt, 2005). The presence of water has been found to be crucial for this reaction mechanism (Roberts et al., 2009). The molar ratio of water to NO_3^- is also important to the overall chemistry, with suppression of the reactive uptake coefficient at molar ratios of $[H_2O]/[NO_3^-]$ below 20. However, this suppression is negated by even trace amounts of $Cl^-_{(aq)}$, allowing N_2O_5 uptake to take place at normal rates (Bertram & Thornton, 2009). Since only small concentrations of $Cl^-_{(aq)}$ are needed for $ClNO_2$ production, these factors carry implications for heterogeneous chlorine chemistry in non-coastal areas (Roberts et al., 2009). Table 4-1 summarizes some of the values that have been found for the reactive uptake coefficient.

Table 4-1: Reported Values of the Reactive uptake Coefficient of N_2O_5

Reactive Uptake Value (γ)	Medium	Reference
0.024 - 0.05	NaCl aerosol	Behnke et al., 1991
0.03 - 0.013 **0.032 ± 0.003**	Water 5.8-1.8 M NaCl aerosol	George et al., 1994
0.018 ± 0.003	Varied aerosol compositions	Schweitzer et al., 1998
0.023 ± 0.004	H_2SO_4 (17% by wt.) aerosol	Hu and Abbatt, 1997
0.005 ± 0.004 **0.03 ± 0.008**	Partially crystalline artificial sea salt aerosol Aqueous sea salt aerosol	Thornton and Abbatt, 2005
0.03	Aerosol at > 0.5M Cl-	Osthoff et al., 2006
0.0037 - 0.0091	Water droplets	Schutze and Herrmann, 2001
0.03 ± 0.02		Aldener et al., 2006
0.0025 (lower limit)	Dry NaCl	Livingston and Finlayson-Pitts, 1991
0.0025 (lower limit)	Dry NaCl	Laux et al., 1994
0.005 - 0.03		Thornton et al., 2010
0.01 – 1		Jacob, 2000
0.0006 - 0.019	Neutralized ammonium sulfate aerosols (≈54% organic matter)	Brown et al., 2009

Another important parameter in this reaction is the yield of $ClNO_2$. An estimate for the upper limit of $ClNO_2$ production can be calculated as follows, by taking into account the rates of the reaction

between NO_2^+ and either H_2O or Cl^- (Bertram & Thornton, 2009; Brown et al., 2009; Roberts et al., 2009; H. Simon et al., 2010; Thornton, Kercher, Riedel, Wagner, Cozic, Holloway, Wolfe, et al., 2010):

$$Y_{ClNO_2} = \frac{\Delta ClNO_2}{\Delta N_2O_5} = \left(\frac{k_{4-12}[H_2O]}{k_{4-13}[Cl^-]} + 1\right)^{-1} \qquad \text{(Equation 4-7)}$$

The ratio of rates for the reaction with chloride over the rate of reaction with water has been experimentally determined to be 836 ± 32 (Wolfgang Behnke et al., 1997). A separate study found the ratio to be 450 ± 100 (Brown et al., 2009; Roberts et al., 2009). Yet another experimental study found the ratio to be between the two at 483 ± 175 (Bertram & Thornton, 2009). The yield has been found to vary non-linearly below 1 M NaCl, with $ClNO_2$ being the main product at 0.5 M and almost the only product at 1 M. Aside from concentrations of NaCl, high sea salt levels, high concentrations of NO_2 and high ratios of $[N_2O_5]/([NO_2][NO_3])$ all enhance $ClNO_2$ yield (Wolfgang Behnke et al., 1997). Table 4-2 summarizes some of the values determined from the literature.

Table 4-2: Reported Values of $ClNO_2$ Yield

Yield Value (Y)	Medium	Reference
0.61 - 0.30		Behnke et al., 1991
0.65 (average)		Behnke et al., 1997
0.50	Sea salt aerosol	Thornton and Abbatt, 2005
1	Aerosol at > 0.5M Cl^-	Osthoff et al., 2006
0.30 - 0.90	Aerosol at $[Cl^-] \leq$0.05-1M	Brown et al., 2009
1		Livingston and Finlayson-Pitts, 1991
0.25	Aerosol at $[Cl^-]$ = 0.1M	Osthoff et al., 2008
0.07 - 0.36		Thornton et al., 2010
0.25 - 0.40 **0.95-0.97**	Sub-µm aerosol at $[Cl^-]$ = 0.04-1.0M Super-µm aerosol at $[Cl^-]$ = 2.5-10M	Simon et al., 2010
0.2-0.8	$[Cl^-]$ = 0.02-0.5M	Roberts et al., 2009

The overall rate of the reaction derived from observations has been found to range from 0 to 4 x 10^4 molecules cm^3 s^{-1}. Rates in this range lead to a calculated upper limit of $ClNO_2$ production of 3 x 10^4 molecules cm^{-3} s^{-1} (Aldener et al., 2006). Another study calculated a $ClNO_2$ production rate of 1.4 x 10^6 molecules cm^{-3} molecules cm^{-3} s^{-1} by assuming a reactive uptake coefficient of 2.5 x 10^{-3}, an average

aerosol radius of 1 μm, and an average sea salt aerosol concentration of 30 cm^{-3} (Livingston & Finlayson-Pitts, 1991).

4.3 $OH-Cl^-$ Surface Reaction Mechanism

Some authors have suggested the presence of a photochemical reaction involving ozone and salt particles to account for chloride deficits as well as molecular chlorine concentrations reaching up to 100 ppb when sea salt particles are irradiated in the presence of ozone (Oum et al., 1998). Initial investigations into such a chlorine generating mechanism involving ozone and deliquesced NaCl particles included smog chamber studies that irradiated mixtures of the two and observed the production of molecular chlorine. Chlorine atom production rates that were determined to be on the order of 10^6 times faster than one would expect to be initiated from the aqueous phase reaction of O_3 with Cl^- resulted in chlorine atom concentrations up to 3.4×10^3 cm^{-3}. It was concluded that Cl_2 was the source of the chlorine atoms since the rate of production most closely matched the rate of photolysis for Cl_2. Upon observation of these results, the aqueous phase mechanism in reactions 4-19 to 4-22 was proposed (Zetzsch, Pfahler, & Behnke, 1988).

$$OH + Cl^- \leftrightarrow HOCl^- \qquad \text{(Reaction 4-19)}$$

$$HOCl^- + H^+ \leftrightarrow Cl + H_2O \qquad \text{(Reaction 4-20)}$$

$$Cl + Cl^- \leftrightarrow Cl_2^- \qquad \text{(Reaction 4-21)}$$

$$2Cl_2^- \rightarrow Cl_2 + 2Cl^- \qquad \text{(Reaction 4-22)}$$

A later experimental study of this same system emphasized that no Cl_2 was produced until the system was exposed to light (E. M. Knipping, 2000b). A mechanism involving reaction between aqueous phase chloride ions with gas phase hydroxyl radicals at the particle interface was eventually proposed to explain the observed rates of Cl_2 production. After the initial, rate limiting formation of a surface complex species, the primary reaction pathway is hypothesized to be a reaction of the complex

with itself, leading to the production of gas phase chlorine and aqueous phase hydroxide ions (I. J. George & Abbatt, 2010; Hunt et al., 2004; Eladio M. Knipping & Dabdub, 2002).

$$OH_{(g)} + Cl^-_{(interface)} \rightarrow [OH\bullet\bullet\bullet Cl^-]_{interface} \quad \text{(Reaction 4-23)}$$

$$2[OH\bullet\bullet\bullet Cl^-]_{(interface)} \rightarrow Cl_{2(g)} + 2OH^-_{(aq)} \quad \text{(Reaction 4-24)}$$

The self-reaction rate has been approximated at the same rate as the self-reaction of Cl_2- in some studies. The rate for the initial complex formation has been approximated as equaling the product of the number of collisions by hydroxyl radicals, the [Cl-]:[H_2O] ratio and a factor of 1.6 to account for the relative availability of chloride ion surface area compared to water molecules (E. M. Knipping, 2000a).

It has been proposed that the complex formed at the surface is likely distinct from HOCl-. The Cl•••OH complex may react with Cl- at the interface, and the rate of this reaction can be approximated to take place at the same rate as the reaction between HOCl- and Cl- (E. M. Knipping, 2000a; Eladio M. Knipping & Dabdub, 2002):

$$OH\bullet\bullet\bullet Cl^{\bullet-}_{surface} + Cl^-_{(aq),surface} \rightarrow Cl_2^{\bullet-}{}_{(aq)} + OH^-_{(aq)} \quad \text{(Reaction 4-25)}$$

The viability of this mechanism is reinforced by residence of chloride ions on the surface of deliquesced NaCl particles (I. J. George & Abbatt, 2010; Hunt et al., 2004; E. M. Knipping, 2000a; Eladio M. Knipping & Dabdub, 2002; Jochen Stutz et al., 2009). Molecular dynamics simulations revealed 11.9% chloride ion surface coverage, while sodium ions were found to cover less than 0.2%. An extrapolation of this percentage surface coverage, assuming an NaCl:H_2O ratio of 1:9, implies that the average chloride ion will have more surface area exposed than the average H_2O molecule. The prevalence of these ions near the surface results in a partial negative charge at the surface of the particles (E. M. Knipping, 2000a).

In addition to the presence of chloride at the particle surface, when the particle is impacted by an OH molecule the contact time is estimated at 1-30 ps and is sufficiently long to facilitate a reaction between the two species (B J Finlayson-Pitts, 2003; Hunt et al., 2004). Furthermore, quantum

calculations have revealed that these chloride ions that are present at the surface should be strongly inclined to attack gas phase hydroxyl radicals and initiate reaction. It is expected that this mechanism will be most effective and important at pH levels above 4 (E. M. Knipping, 2000a). This is important since the production of two OH- molecules from reaction 4-24 above leads to an increase in pH, which also increase the rate of S(IV) oxidation by ozone drastically (Hunt et al., 2004). However, gas phase Cl_2 production by this mechanism only takes place if the particles are deliquesced (Eladio M. Knipping & Dabdub, 2002).

The reactions above can be combined and rewritten with the assumption that the complex formation is the rate limiting step, and the overall rate can be parameterized as shown in equations 4-8 and 4-9 (Eladio M Knipping & Dabdub, 2003; Eladio M. Knipping & Dabdub, 2002).

$OH^{\bullet}_{(g)} + Cl^{-}_{(aq)} \rightarrow 1/2Cl_{2(g)} + OH^{-}_{(aq)}$ (Reaction 4-26)

$$R_{4-27} = \frac{1}{2}\frac{d[Cl_2]}{dt} = \gamma_s \frac{\omega}{4} A[OH] \quad \text{(Equation 4-8)}$$

$$\gamma_s = 0.04[Cl^-] \quad \text{(Equation 4-9)}$$

The reactive uptake (γ_s) is in units of M^{-1} and represents the damping or enhancing of the reaction rate as chloride ion concentrations decrease or increase, respectively. An alternative parameterization is given in equation 4-10 (Nissenson et al., 2008), where the first term in parenthesis is equivalent to a mass transfer rate coefficient (E. M. Knipping, 2000a; Eladio M. Knipping & Dabdub, 2002):

$$R_{int} = \left(\frac{r^2}{3D_g} + \frac{4r}{3\omega\gamma}\right)^{-1} \left[OH_g^{\bullet}\right] \quad \text{(Equation 4-10)}$$

A few modeling studies have been performed to assess the impact of this reaction mechanism. One study compared the resulting modeled noontime chlorine atom concentrations to observations from the North Atlantic during the same time period and found that the modeled concentration was within

50% at 3.7 x 10^4 atoms cm^{-3} of what was observed at 6.5 x 10^4 atoms cm^{-3} (E. M. Knipping, 2000a). This comparison led to the conclusion that this mechanism involving an OH-Cl surface complex was able to account for observed Cl_2 levels. It was estimated that the interfacial mechanism was responsible for 40% and 20% of chlorine atom production in remote marine and polluted coastal scenarios, respectively (Eladio M. Knipping & Dabdub, 2002). Modeling has also shown that including such sea salt chloride related chemistry can increase ozone predictions by up to 12 ppb along coastal regions, where chlorine atom concentrations can reach high enough levels to dominate oxidation by OH (Eladio M Knipping & Dabdub, 2003).

The mechanisms described above both result in the release of otherwise nonreactive chloride into the gas phase. However, they produce different species of gas phase chlorine, which photolyze at different rates. Additionally, the timing of the release is distinctly different in each case. The N_2O_5 to $ClNO_2$ mechanism takes place at significant rates only in the dark due to the high photolysis rate of N_2O_5. This results in a night time build up and morning time photolysis of $ClNO_2$, causing a spike in atomic chlorine fairly early in the day. On the other hand, the hydroxyl-chloride surface reaction coincides with peak photochemical activity during the day, resulting in a release of chlorine atoms towards the midafternoon.

4.4 Simulation Methods

4.4a Sensitivity Analyses

Motivated by the wide range of values reported in the literature for the rates of heterogeneous N_2O_5 chemistry, a sensitivity analysis of the relevant physical parameters involved in the mechanism was undertaken. The analysis was performed using reactive uptake coefficient (γ) and the overall $ClNO_2$ yield (Y_{ClNO2}) as the uncertain variables. Previous regional modeling studies of this mechanism used limited, and typically fixed, parameter values (H. Simon et al., 2009, 2010). More recent work has implemented the parameterizations represented in equations 4-5 through 4-7 into regional modeling

within the U.S (G. Sarwar et al., 2012). The objective of the sensitivity analysis described in this chapter is to quantify upper and lower limits to the impacts of heterogeneous N_2O_5 chemistry on peak O_3 and $ClNO_2$ production. Aside from the effects of varying parameter value combinations, the effects of varying VOC concentrations and composition as well as NO_x availability were tested. To evaluate the effects of these variations, changes in peak ozone and $ClNO_2$ concentrations between simulations were quantified and compared to a base case scenario in which the heterogeneous reaction was not present.

A preliminary sensitivity analysis was also performed for the proposed surface mechanism between gas phase hydroxyl radicals and particulate chloride (E. M. Knipping, 2000b; Eladio M Knipping & Dabdub, 2003; Eladio M. Knipping & Dabdub, 2002). Of particular interest were the effects of this mechanism on ozone production and the extent of HCl production due to the release of molecular chlorine. In the modeled representation of this mechanism, no explicit yield parameter exists, and thus variation of the reactive uptake parameter was the primary focus. The ranges of variation for physical parameters involved in both the N_2O_5 and $OH^{\bullet}$ mechanisms are discussed in section 4.3c.

The software used for the box model simulations was the SAPRC software developed by Dr. William Carter at UC Riverside. For a base photochemical mechanism, the CB05 condensed mechanism (Yarwood & Rao, 2005) was used and modified to include the parameterizations of the heterogeneous mechanism. Simulations for the N_2O_5 chemistry were run from sunset on the initial day until approximately sunset the next day. This allowed for a night time buildup and morning time photolysis of $ClNO_2$. Initial conditions included ozone and NO_x concentrations of 50 and 20 ppb, respectively. Additionally, a scenario with emissions of 50 ppb hr^{-1} NO_x (75/25 NO/NO_2 ratio) for two hours in the morning was used to simulate morning emissions from mobile and industrial sources in an urban region. While a 90/10 NO/NO_2 ratio is standard for mobile sources, the 75/25 ratio takes into account the sum of other non-mobile sources within an urban area as well as changes in diesel engine control measures that have been shown to increase NO_2/NO ratios. Simulations with varied parameters

and emissions were compared to a base case with no heterogeneous chemistry. The parameterizations of the heterogeneous reactions were modeled as a pseudo first order reaction by expressions of the following form:

$$-\frac{d[N_2O_5]}{dt} = \frac{1}{4}\gamma\omega A_a[N_2O_5] \quad \text{(Equation 4-11)}$$

$$\frac{d[ClNO_2]}{dt} = \frac{1}{4}\gamma\omega Y A_a[N_2O_5] \quad \text{(Equation 4-12)}$$

$$-\frac{d[OH]}{dt} = \frac{1}{4}\gamma\omega A_a[OH] \quad \text{(Equation 4-13)}$$

$$\frac{d[Cl_2]}{dt} = \frac{1}{8}\gamma\omega A_a[OH] \quad \text{(Equation 4-14)}$$

4.4b VOC Mixture

The mixture of VOCs used in the simulations was a surrogate mixture formulated to represent an average urban VOC mixture. The formulation of the surrogate mixture was based on EPA data collected from 1985 to1988 in 66 U.S. cities and has been used extensively since then in both measurement and modeling studies. The 182 species represented in this dataset were condensed down to the nine representative reactive species present in the surrogate mixture. These condensed species are considered to represent the same overall reactivity, per ppmC, as the original mixture. An "Inert/Lost Carbon" category is included to represent the compounds that were removed due to low reactivities or condensed into smaller representative species. Table 4-3 shows the constituents of the reactive organic gas (ROG) mixture that was used in simulations during the sensitivity analysis (William P L Carter et al., 1995).

Table 4-3: Surrogate VOC Mixture Composition Used in SAPRC Simulation

Species	CB05 Species	ppb $ppmC^{-1}$
n-Butane	4 PAR	70.7
n-Octane	7 PAR, 1 NR	22.3
Ethylene	ETH	13.4
Propene	1 PAR, 1 OLE	10.4
t-2-Butene	IOLE	10.4
Toluene	TOL	13.3
m-Xylene	XYL	16.3
Formaldehyde	FORM	7.9
Acetaldehyde	ALD2	7.6
Inert/Lost Carbon	NR	193.1

4.4c: Parameter Ranges

As is shown in Table 4-4, the reactive uptake for the N_2O_5 heterogeneous reaction was varied along 11 values between 0 and 0.038, a reasonable upper limit determined from values reported in the literature (W Behnke et al., 1991; Schweitzer et al., 1998; Thornton & Abbatt, 2005; Thornton, Kercher, Riedel, Wagner, Cozic, Holloway, Wolfe, et al., 2010).

Table 4-4: Values used for Reactive Uptake in Sensitivity Simulations

Simulation Number	Value (10^{-2})
1	0.1
2	0.47
3	0.84
4	1.21
5	2.58
6	1.95
7	2.32
8	2.69
9	3.06
10	3.43
11	3.8

The particle surface area was approximated by assuming a three mode particle distribution, with 30%, 50%, and 20% (by mass) having average diameters of 0.1, 0.5 and 1.0 μm, respectively. In this way, typical values of aerosol population mass were chosen, and the surface area was calculated

accordingly. In most simulations, an aerosol concentration of 15 μg m^{-3} was assumed while 50 μg m^{-3} was used to represent a high concentration of particulate matter in some simulations.

$ClNO_2$ yield was varied between zero and one (at intervals of 0.05) to represent up to a 100% yield. Such a wide range of yield values has previously been reported in the literature from multiple sources (W Behnke et al., 1991; Wolfgang Behnke et al., 1997; Osthoff et al., 2008; Roberts et al., 2009; H. Simon et al., 2010; Thornton & Abbatt, 2005; Thornton, Kercher, Riedel, Wagner, Cozic, Holloway, Wolfe, et al., 2010). VOC levels were varied between 0-1000 ppbC (i.e., 0, 300, 1000, 1000 t-2butene only) with a value of 300 ppbC considered to be a level representing a moderate urban concentration of VOCs.

For preliminary modeling of the heterogeneous OH reaction, the reactive uptake was varied between 4 x 10^{-4} – 4 x 10^{-1} (i.e., 4 x 10^{-4}, 2 x 10^{-3}, 4 x 10^{-3}, 1 x 10^{-2}, 2 x 10^{-2}, 4 x 10^{-2}, 1 x 10^{-1}, 2 x 10^{-1}, 3 x 10^{-1}, 4 x 10^{-1}), and it was calculated using particle chloride concentrations ranging from 0.01-10 M (Eladio M Knipping & Dabdub, 2003). Surface areas and VOC concentrations were similar to those used for the N_2O_5 reaction.

4.5 Results and Discussion

4.5a *$N_2O_5 \rightarrow ClNO_2$ Mechanism Parameter Variation*

The heterogeneous N_2O_5 to $ClNO_2$ conversion mechanism is able to reproduce $ClNO_2$ concentrations that have been observed in the environment within parameter ranges used in this study. Depending on the combination of heterogeneous parameters, VOCs, and NO_x, the mechanism contributed to both peak ozone reduction as well as peak ozone increases. The range was a -10.5% to 27% change in peak O_3 concentrations relative to the base case scenario containing no heterogeneous chemistry. The decreases in ozone typically resulted from low values of $ClNO_2$ yield (0-15% depending on the amount and types of VOCs present). This was likely due to a higher conversion rate of NO_x into nitric acid at lower $ClNO_2$ yield values, which simultaneously reduced the amount of $ClNO_2$ produced.

Combinations of yields above 25% and reactive uptake coefficients greater than zero resulted in increases in peak ozone levels.

In Figure 4-1 below, ranges of ozone peak ozone concentrations obtained from box modeling simulations are shown for a $ClNO_2$ yield variation from 0-100%. Three scenarios are shown, including one scenario with no VOCs present, one with 300 ppbC VOC, and one with 300 ppbC VOC and NO_x emissions of 50 ppb hr^{-1} for two hours in the morning.

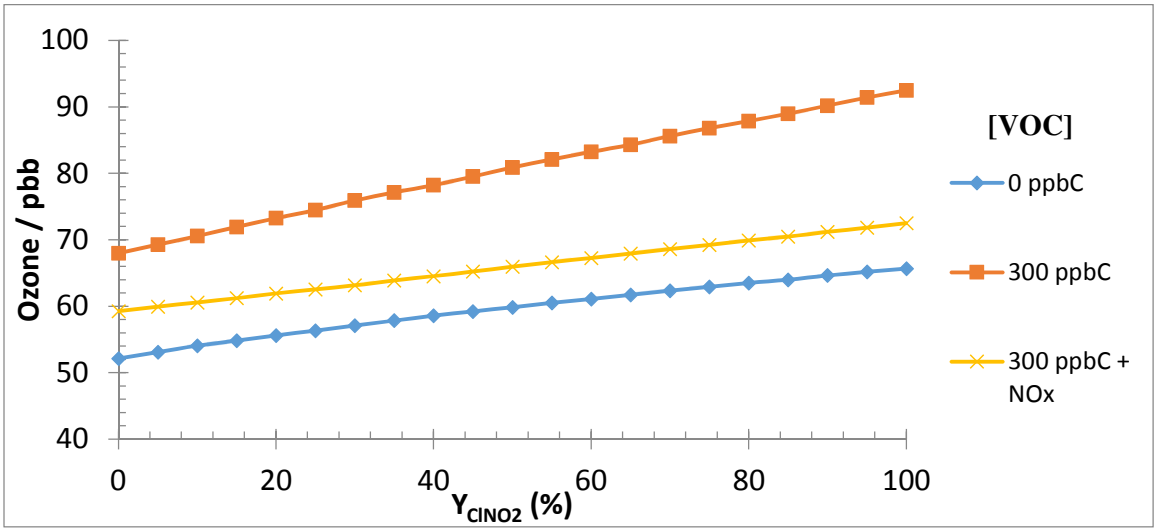

Figure 4-1: Peak O_3 concentrations during box modeling simulations. The scenario including NO_x had emissions of +50 ppb NOx hr^{-1} for two hours at sunrise during the simulation. Surface area was equivalent to PM = 15 µg m^{-3}.

Figure 4-2 below shows the same data on a percentage basis as percentage decrease or increase in peak O_3 concentrations compared to corresponding base case scenarios (the base case assumes no heterogeneous reaction). Two additional scenarios are also included. One of the additional scenarios is a high VOC case (1000 ppbC) and the other is a case where 300 ppbC of the previously discussed ROG mixture were substituted with 300 ppbC of t-2-butene. The reason for choosing t-2-butene as the highly reactive species is that it rapidly reacts with the NO_3 radical, converting it into HNO_3 instead of allowing it to react with NO_2 and form N_2O_5. The implications of this can be seen in Figure 4-2 by the relatively unchanging impact of yield variation on peak ozone concentrations in the t-2-butene only scenario.

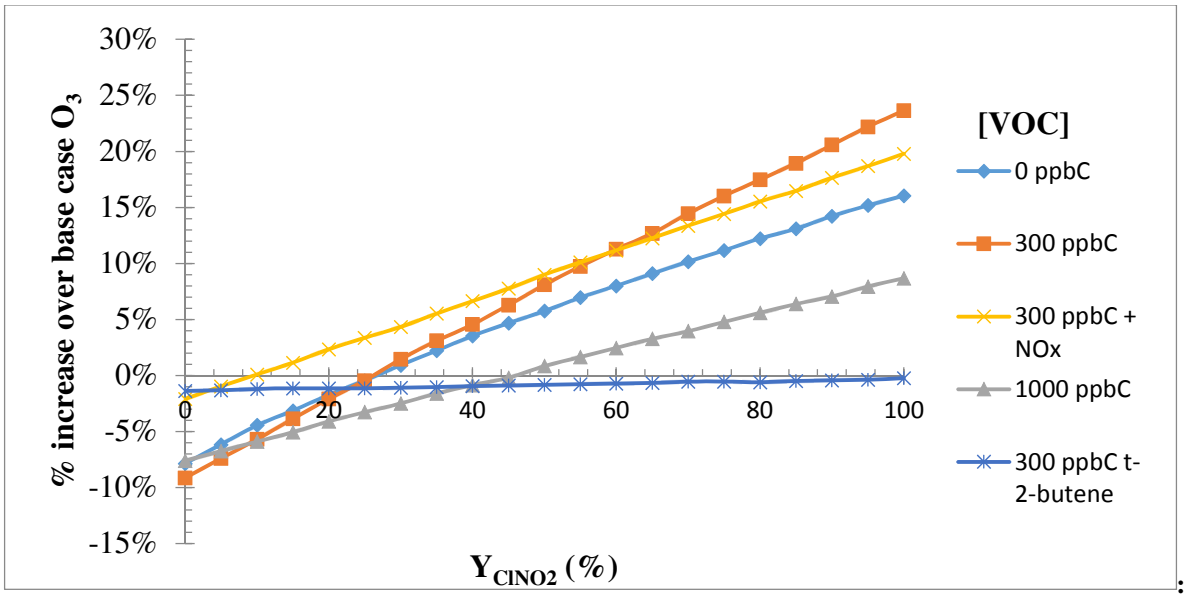

Figure 4-2: Differences in peak O_3 concentrations (as %) compared to base case scenarios. Particulate surface area was equivalent to PM = 15 µg m^{-3}.

Figure 4-3 shows the corresponding peak $ClNO_2$ concentrations during the yield variation scenarios.

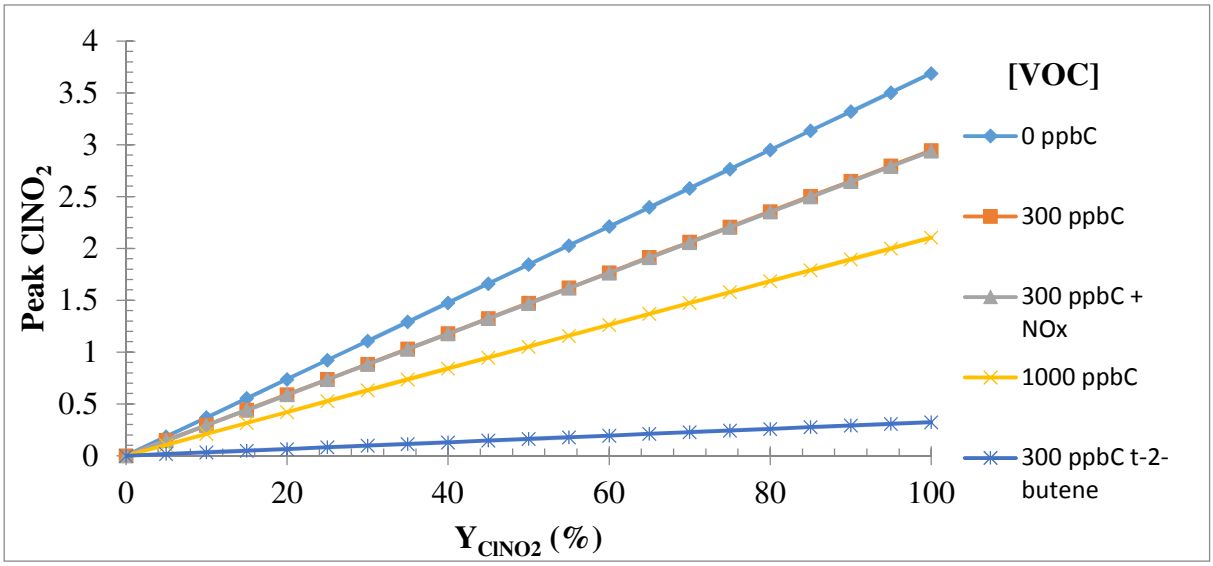

Figure 4-3: Figure 4-3: Peak $ClNO_2$ concentrations from box modeling simulations.

For variations in the reactive uptake coefficient, $ClNO_2$ yield values were held constant at values ranging between 0 and 100 percent. Figure 4-4 summarizes the impacts of these variations on peak ozone formation in simulations where surface area was held at the equivalent of PM = 15µg m^{-3} and [VOC] = 300 ppbC. Figure 4-5 shows the peak $ClNO_2$ production from the same set of simulations.

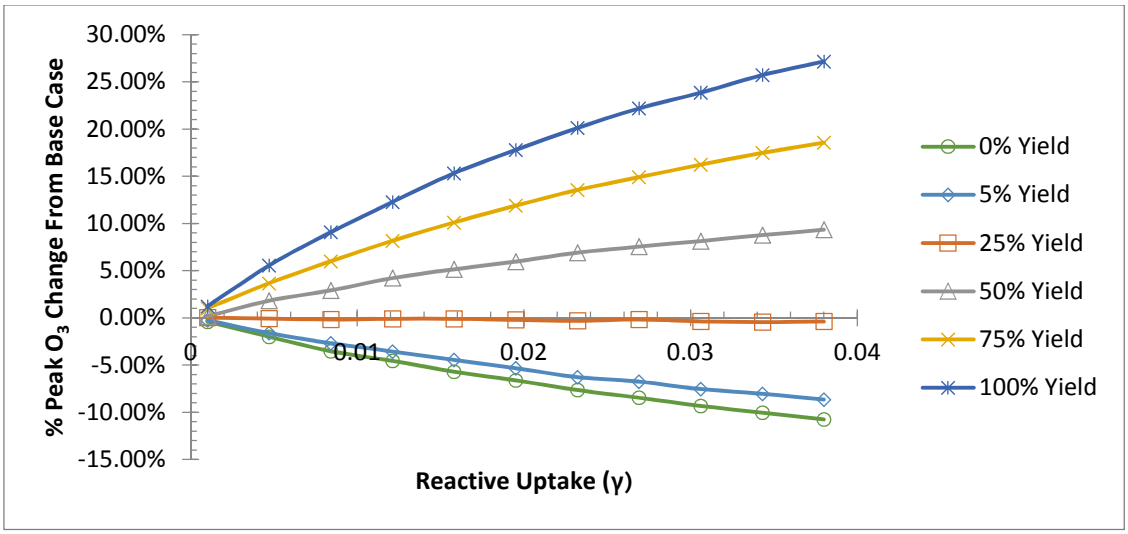

Figure 4-4: Resulting peak O_3 increases over base case scenario from reactive uptake variation.

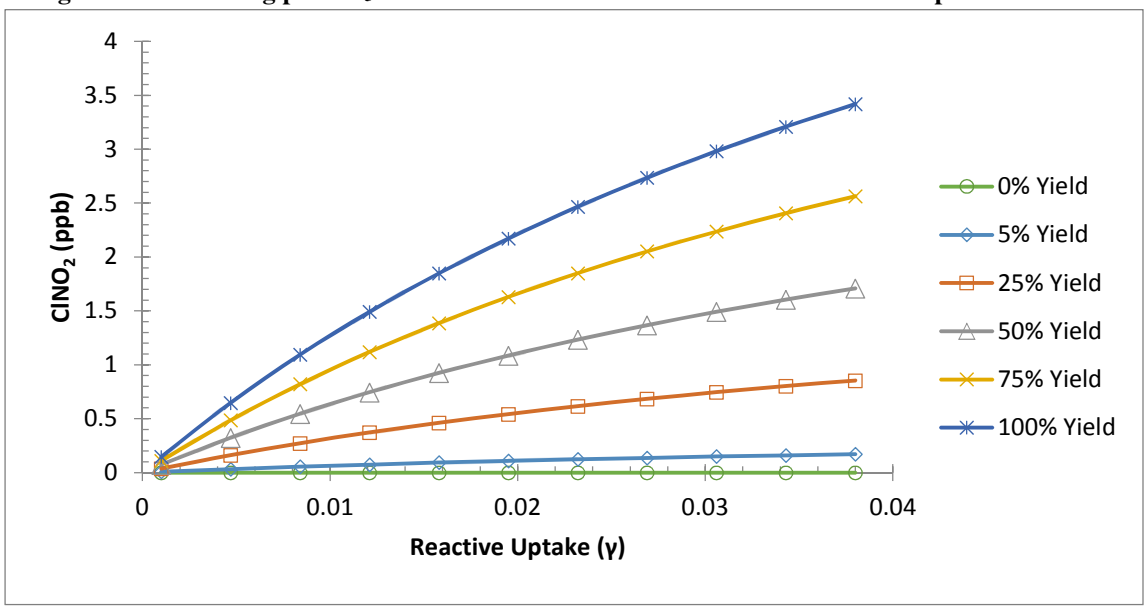

Figure 4-5: Resulting peak $ClNO_2$ concentrations from reactive uptake variation.

The combined effects of the variation of multiple parameters can also be examined. As the contour plots in Figures 4-6 and 4-7 below show, higher combinations of parameter values lead to higher peak concentrations of $ClNO_2$ in the morning as well as larger increases in peak O_3 concentrations over the base case simulation in which no heterogeneous chlorine chemistry was included. However, the variation of different parameters results in different effects. For example, a 16% ozone increase over the base case results for a scenario with 300 ppbC, a reactive uptake coefficient of 0.03 and a yield value of 0.75. By fixing reactive uptake at a value of 0.03 and increase

yield from 0 to 0.75, the resulting increase in peak ozone concentration is 18.82 ppb_v, which is 22.5% of the peak ozone value in the base case. However, by fixing the yield parameter at a value of 0.75 and increasing the reactive uptake from 0 to 0.03 results in a peak ozone increase of 12.14 ppb_v, which is 15.2% of the base case peak concentration.

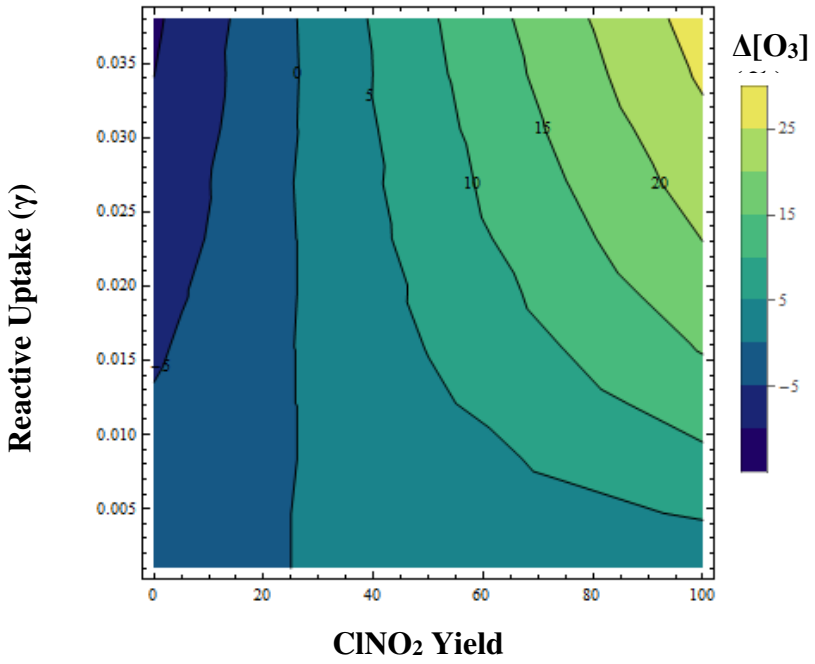

Figure 4-6: Percentage peak O_3 increases over the base case scenario for various combinations of the $ClNO_2$ yield and reactive uptake parameter values.

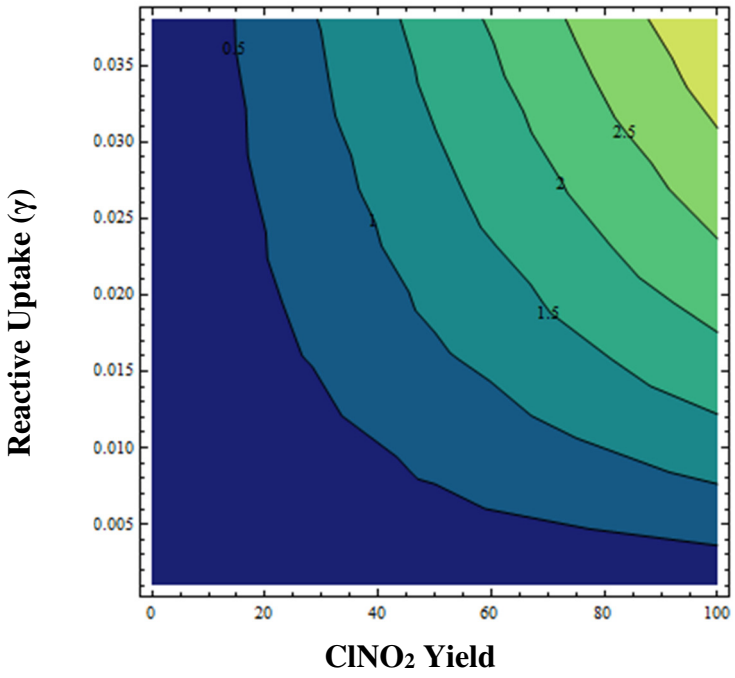

Figure 4-7: Peak $ClNO_2$ concentrations (ppb) for various combinations of the $ClNO_2$ yield and reactive uptake parameter values.

4.5b *OH→ Cl_2 Mechanism Parameter Variation*

With respect to gas phase chlorine production, preliminary modeling of heterogeneous OH chemistry shows HCl peaks in the mid to late afternoon approximately from 5-7 PM as a result of Cl_2 and chlorine radical peaks around noontime. However, in this modeling, neither HCl deposition nor repartitioning of HCl back into the particle phase was taken into account. Thus, the HCl peak may occur slightly earlier under the influence of these factors. Typical peak HCl concentrations obtained from the simulations were on the order of several hundred ppt. At the highest combination of concentrations of both chloride and particulate matter, HCl production of almost 0.6 ppb was obtained. However, this resulted from the presence of 10 M of Cl^- in the particle phase and a particle concentration of 50 μg m^{-3}. This combination of parameters is unlikely to occur for the amount of time necessary for this mechanism to be able to produce the resulting HCl concentrations on the order of half a ppb. A more probable upper limit of HCl production from this mechanism is likely on the order of 0.2 ppb.

The effects of this mechanism on O_3 production compared to scenarios without the heterogeneous chemistry were modest, since the gain in gas phase reactivity of the system through the introduction of Cl_2 is balanced by the loss of OH into the particle phase. Increases in O_3 were on the order of 1 ppb with VOCs and NO_x at 300 ppbC and 20 ppb, respectively. Figure 4-8 shows the total HCl produced by the heterogeneous OH mechanism under a variety of circumstances. Figure 4-9 shows the time series of HCl concentrations from a subset of the simulation results presented in Figure 4-8. The rate of reaction in these scenarios was modeled after the parameterization shown in Equation 4-9.

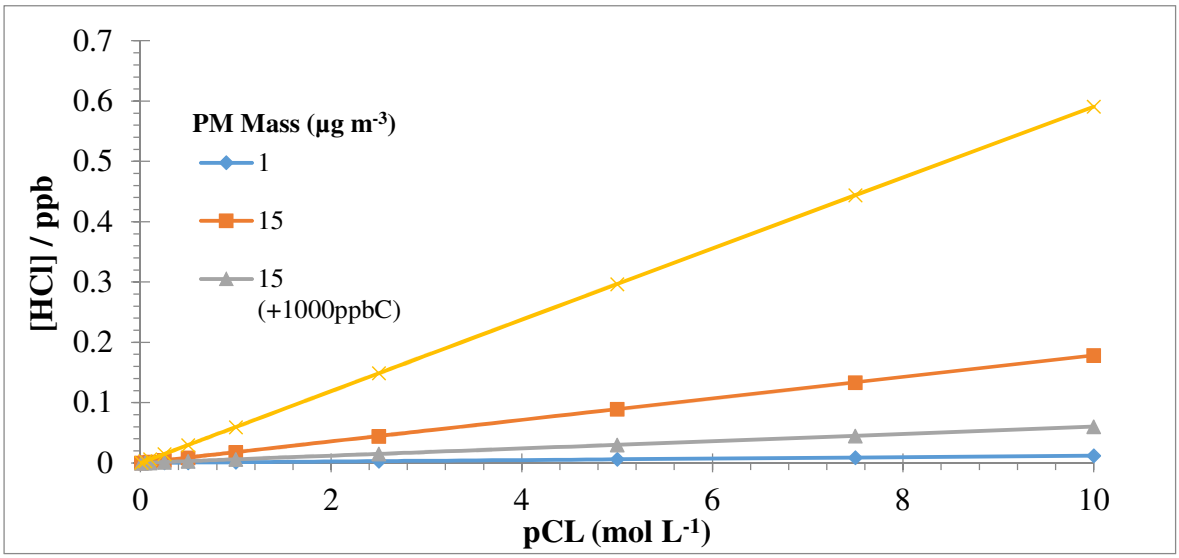

Figure 4-8: Total HCl produced by the heterogeneous reaction of OH and Cl^- containing particles. Shown are scenarios with various combinations of $[Cl^-]$ and particulate matter concentrations.

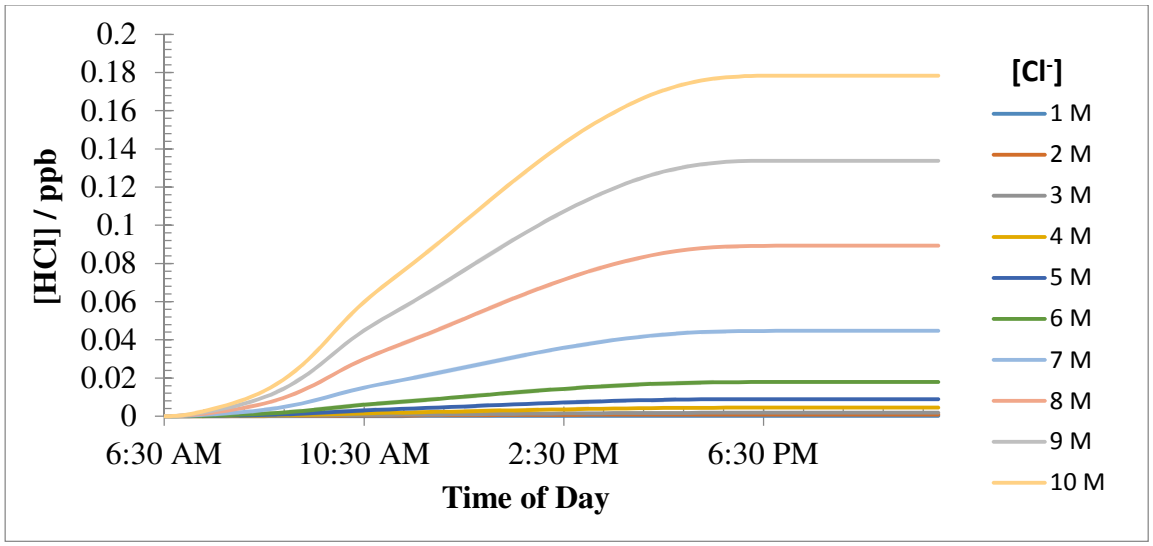

Figure 4-9: The time series of HCl concentrations produced from the heterogeneous OH mechanism during box modeling simulations. For the simulations shown here, the particle concentration was held at 15 µg m^{3-3}, $[Cl^-]$ ranged from 0 to 10 M and deposition of HCl was not included.

4.6: Summary

The range of impact that heterogeneous $ClNO_2$ production has on peak ozone levels in the scenarios described in this Chapter reflects the potential significance of this chemistry to ozone formation. However, the broad range of parameter combinations and their subsequent effects on ozone chemistry highlight the importance of correctly estimating or calculating the parameters involved. Maximum changes in peak O_3 formation caused by the inclusion of the heterogeneous mechanism ranged from -10.5% to 27%. $ClNO_2$ formation via this mechanism resulted in concentrations up to 4.0 ppb at the highest combination of parameter values, with peak concentrations of 1.0-2.0 ppb being typical of more moderate parameter value combinations (e.g. 20-50% yield and a reactive uptake of 0.03).

With respect to the OH heterogeneous mechanism, impacts on O_3 production are expected to be small under most circumstances. However, if particle and chloride concentrations are high enough, it may have an impact on HCl production that is on the order of 0.05-0.1 ppb.

Chapter 5: Environmental Chamber Studies of the Heterogeneous Reaction of Hydroxyl Radicals with Chloride Aerosols

5.1. Introduction

Previous studies have demonstrated that the presence of gas phase atomic chlorine radicals ($Cl^{\bullet}$) can impact the chemistry of the troposphere in ways that can influence atmospheric composition through the oxidation of mercury compounds (Lin and Pehkonen, 1999), enhancing or reducing O_3 production (Chang and Allen, 2006a; Tanaka, 2003; Tanaka et al., 2003) and inorganic particle formation (Chang and Allen, 2006b). Additionally, the reaction of $Cl^{\bullet}$ with volatile organic compounds (VOCs) has been found to result in secondary organic aerosol (SOA) formation (Cai et al., 2008; Karlsson et al., 2001), which has implications for human health (Davidson et al., 2005), visibility (Mazurek et al., 1997) and climate (Charlson et al., 1992; Kanakidou et al., 2005). The photolysis of Cl_2 and HOCl leads to $Cl^{\bullet}$ production, which in turn can lead to the production of alkyl radicals (denoted by $R^{\bullet}$) as shown in reactions (Reaction 5-1 through 5-3) (Atkinson et al., 2007; Chang and Allen, 2006a; Finlayson-Pitts, 1993; Sander et al., 2011; Stutz et al., 2009; Watson, 1977).

$$Cl_2 + h\nu \rightarrow 2Cl^{\bullet} \qquad \text{(Reaction 5-1)}$$

$$HOCl + h\nu \rightarrow Cl^{\bullet} + OH^{\bullet} \qquad \text{(Reaction 5-2)}$$

$$Cl^{\bullet} + RH \rightarrow R^{\bullet} + HCl \qquad \text{(Reaction 5-3)}$$

Anthropogenic sources of these gas phase $Cl^{\bullet}$ precursors include industrial point sources, biocide use in cooling towers and swimming pools (Chang and Allen, 2006a; Chang et al., 2002; Faxon and Allen, 2013). Photodissociation of chlorinated organic species can also produce $Cl^{\bullet}$, but the reactions of most common organochlorides are generally too slow in the troposphere to contribute as a significant source (Faxon and Allen, 2013).

Another class of sources is comprised of the reactions leading to the volatilization of gas phase $Cl^{\bullet}$ precursors from particulate chloride. For example, reactions resulting in the volatilization of

hydrogen chloride (HCl) through the displacement of condensed phase particulate chloride by other gas phase acids are well documented. Reactions such as these can be termed acid displacement reactions and examples are shown in reactions 5-4 and 5-5, where (cd) and (g) denote condensed and gas phase species (Gard, 1998; Graedel and Keene, 1995; De Haan and Finlayson-Pitts, 1997; Saul et al., 2006).

$$HNO_{3(g)} + NaCl_{(cd)} \rightarrow HCl_{(g)} + NaNO_{3(cd)} \qquad \text{(Reaction 5-4)}$$

$$H_2SO_{4(cd)} + 2NaCl_{(cd)} \rightarrow 2HCl_{(g)} + Na_2SO_{4(cd)} \qquad \text{(Reaction 5-5)}$$

Heterogeneous reactions, which involve the uptake and reaction of gas phase species into a particle to produce volatile chlorine species, fall under this same category. One of the more well-understood mechanisms is the production of nitryl chloride ($ClNO_2$) from the reactive uptake of dinitrogen pentoxide (N_2O_5) on particles containing chloride, wherein the uptake and dissociation of N_2O_5 is the rate limiting step (Behnke et al., 1997; Roberts et al., 2009; Schweitzer et al., 1998). Subsequent studies further elucidated the mechanism and there is general agreement on the overall mechanism shown in reactions (Reactions 5-6 through 5-10) (Bertram & Thornton, 2009; Thornton & Abbatt, 2005; Thornton, et al., 2010).

$$N_2O_{5(g)} \leftrightarrow N_2O_{5(aq)} \qquad \text{(Reaction 5-6)}$$

$$N_2O_{5(aq)} + H_2O_{(l)} \leftrightarrow H_2ONO_2^+{}_{(aq)} + NO_3^-{}_{(aq)} \qquad \text{(Reaction 5-7)}$$

$$H_2ONO_2^+{}_{(aq)} + H_2O_{(l)} \rightarrow H_3O^+{}_{(aq)} + HNO_{3(aq)} \qquad \text{(Reaction 5-8a)}$$

$$H_2ONO_2^+{}_{(aq)} + Cl^-{}_{(aq)} \rightarrow ClNO_{2(aq)} + H_2O_{(l)} \qquad \text{(Reaction 5-8b)}$$

$$ClNO_{2(aq)} \leftrightarrow ClNO_{2(g)} \qquad \text{(Reaction 5-9)}$$

$$ClNO_{2(g)} + h\nu \rightarrow Cl^{\bullet}{}_{(g)} + NO_{2(g)} \qquad \text{(Reaction 5-10)}$$

$ClNO_2$ has been detected in a variety of regions including Boulder, CO (Thornton et al., 2010), Los Angeles, CA (Riedel et al., 2012), Calgary, Alberta, Canada (Mielke et al., 2011), Conroe, TX (Faxon et al., unpublished), the arctic lower troposphere (Kercher et al., 2009), rural Germany (Phillips

et al., 2012) and Houston, TX (Osthoff et al., 2008; Parrish et al., 2009). Photochemical modeling of the chemistry across the continental United States revealed resulting increases of monthly mean 8-h O_3 of 1 – 2 ppb and decreases in total nitrate of 11 – 21% (Sarwar et al., 2012). Furthermore, a sensitivity analysis of parameters involved in $ClNO_2$ production indicates that resulting impacts on O_3 production range from -10.5 to 27% (Faxon and Allen, 2013).

In addition to $ClNO_2$, Cl_2 has been detected in various regions, including Virginia Key, FL (Pszenny et al., 1993), Hawaii, (Pszenny et al., 2004), La Jolla, CA (Finley and Saltzman, 2008), Irvine, CA (Finley and Saltzman, 2006), Conroe, TX (Faxon et al., unpublished), Alert, NW Territories (Impey et al., 1997) and off the coast of Los Angeles, CA (Riedel et al., 2012). Cl_2 concentrations up to 150 ppt_v have been detected in marine air at night, suggesting a nocturnal 330 ppt_v day^{-1} Cl_2 source (Spicer et al., 1998). Additionally, two other studies (Finley and Saltzman, 2006, 2008) reported detection of Cl_2 in both coastal marine and coastal urban air. Aside from instances of evidence of industrial Cl_2 emissions, many of these studies attributed the Cl_2 source to natural processes involving particulate chloride.

A mechanism involving the reaction between gas phase hydroxyl radicals and particulate chloride has been proposed as one possible mechanism for the heterogeneous production of Cl_2 (Knipping and Dabdub, 2002, 2003; Knipping, 2000a; Nissenson et al., 2008). This mechanism was initially proposed to account for the observation that Cl_2 is produced when aqueous NaCl aerosols and O_3 are irradiated (W Behnke & Zetzsch, 1989; Keene et al., 1990; Knipping and Dabdub, 2003; Knipping and Dabdub, 2002; Oum, Lakin, DeHaan, Brauers, & Finlayson-Pitts, 1998). The production of Cl_2 has been reported to occur in the presence of light (Behnke and Zetzsch, 1989; Knipping, 2000a; Oum et al., 1998; Zetzsch et al., 1988), but observations of production in the dark have also been reported (Keene et al., 1990; Sadanaga et al., 2001; Spicer et al., 1998; Zetzsch et al., 1988). Proposed mechanisms are varied and include direct heterogeneous reaction of O_3 at the particle surface (Behnke

and Zetzsch, 1989; Keene et al., 1990), aqueous phase mechanisms (Herrmann et al., 2003; Oum et al., 1998) and heterogeneous reaction of $OH^{\bullet}$ at the particle surface (Knipping and Dabdub, 2002; Knipping, 2000a). It has been suggested that the extent of observed Cl_2 production cannot be explained by known aqueous phase mechanisms (Knipping, 2000a), and that the heterogeneous surface reaction serves as the best explanation. The formation and reaction of a surface complex from the reaction of chloride ions and gas phase $OH^{\bullet}$ has been proposed (George and Abbatt, 2010; Knipping and Dabdub, 2002; Knipping, 2000b), with the formation of the surface complex being the rate-limiting step (Knipping and Dabdub, 2002) of the overall mechanism of Cl_2 production. Reactions 5-11 – 5-12 represent the formation and reaction of the hypothetical surface complex, and reaction 5-13 represents the overall mechanism (Knipping and Dabdub, 2002).

$$OH_{(g)} + Cl^{\bullet -}_{(aq)} \rightarrow OH\bullet\bullet Cl^{\bullet -} \qquad \text{(Reaction 5-11)}$$

$$2OH\bullet\bullet Cl^{\bullet -} \rightarrow Cl_{2(g)} + 2OH^-_{(aq)} \qquad \text{(Reaction 5-12)}$$

$$OH_{(g)} + Cl^-_{(aq)} \rightarrow \tfrac{1}{2}\, Cl_{2(g)} + OH^-_{(aq)} \qquad \text{(Reaction 5-13)}$$

$$2\left.\frac{d[Cl_2]}{dt}\right|_{R13} = \gamma_s \frac{\omega}{4} A[OH] \qquad \text{(Equation 5-1)}$$

$$\gamma = 0.04[Cl^-] \qquad \text{(Equation 5-2)}$$

The most important factors involved in the reaction are believed to be the presence of particulate chloride, O_3 and relative humidity (RH) above the deliquescence RH of the aerosol (Knipping and Dabdub, 2002; Knipping, 2000a; Oum et al., 1998; Zetzsch et al., 1988). Regional modeling of this mechanism alongside gas phase Cl_2 chemistry in the South coast Air Basin of California indicated that predicted ozone concentrations were increased by up to 12 ppb and 4 ppb in the morning and afternoon, respectively. Aerosol nitrate formation and the rate of hydrochloric acid displacement were unaffected (Knipping and Dabdub, 2003).

Areas where further investigation has been suggested (Knipping, 2002) include the impacts of chlorine decomposition in alkaline solutions (e.g. reaction with H_2O_2, CO_3^{2-} and OH^-) on the effectiveness of the mechanism, and determination of typical rates under conditions similar to the remote marine boundary layer (MBL), polluted coastal regions and the polar troposphere (Knipping and Dabdub, 2002). Previous experimental work on this mechanism was performed at conditions that were not typical of ambient conditions and utilized high initial concentrations of O_3 ranging from several hundred to several thousand ppb (Behnke and Zetzsch, 1989; Knipping and Dabdub, 2002). Therefore, one of the primary motivations for this present work is the observation of the mechanism of Cl_2 production under conditions comparable to the troposphere. Additionally, several experimental scenarios are investigated to pursue the following objectives.

1. Determination of the efficacy (i.e., extent of Cl_2 production) for the mechanism under realistic atmospheric conditions
2. Investigation of the dependence of the mechanism on particle surface area
3. Determination of a range of values for the reactive uptake coefficient corresponding to the efficiency of the mechanism under the conditions studied
4. Observation of the impacts of relative humidity levels and RH dependency of mechanism
5. Observing the impact of mixed organic-inorganic particle composition on mechanism efficacy
6. Determination of the efficacy of Cl_2 production in the presence of non-chloride particles and gas phase HCl

5.2. Methods and Materials

5.2.1 Experimental Setup

A series of environmental chamber experiments were undertaken at the University of Texas' Center for Energy and Environmental Resources (CEER). The chamber is similar to Teflon chambers

used in previous studies (Hildebrandt et al., 2009, 2011). It consists of a 12 m^3 Teflon bag (Welch Fluorocarbon) suspended inside a temperature controlled environment. The walls of the temperature controlled enclosure are equipped with UV lights (204 GE T12 Blacklights; peak emission at 368 nm), which were used for inducing photolysis and photo-oxidation reactions. The UV source in the chamber was characterized by measuring the NO_2 photolysis rate, which was determined to be 7 x 10^{-3} s^{-1}. The chamber was prepared for experiments by overnight venting and cleaning using zero air generated by an AADCO 737-11 Pure Air Generator, which generates air consisting of less than 5 ppb CO_2, VOCs, O_3, SO_2, H_2S, NH_4 and NO_x. The air is dried after generation, and is free of particulates. Between experiments, the chamber was vented continuously with zero air for a period of at least 10 hours. Additionally, 'blank' experiments were performed in order to insure that no residual chlorine species or VOCs were present at the start of the next experiment. A blank experiment consisted of the injection of O_3 to oxidize any potential contaminants and $(NH_4)_2SO_4$ seed particles to facilitate the condensation of oxidized VOCs.

For the base case reactant mixture, gas phase hydrogen peroxide (H_2O_2) was used as a photolytic hydroxyl radical ($OH^{\bullet}$) source and was injected into the chamber by bubbling zero air through a 30% (wt.) solution (Fisher Scientific). Ammonium chloride (NH_4Cl, Sigma Aldrich, 99.99%) was used as the primary particulate chloride source and was added to the chamber via an aerosol generation system (Brechtel Manufacturing Incorporated, Model 9200) using a 0.05 M NH_4Cl feedstock solution. Prior to injection, the generated aerosol particles were passed through a drier. Relative humidity was elevated above the deliquescence relative humidity (DRH) of NH_4Cl (Hu et al., 2011; Seinfeld and Pandis, 2006) (78%) for several scenarios. For all other experiments, relative humidity was maintained below 5%. Oxides of nitrogen (NO_x) were added as pure nitric oxide (NO) sourced from a gas canister at a concentration of 9.94 ppm NO in N_2 (Airgas). Due to the presence of O_3 in the reactant mixture at concentrations typically 2 – 3 times higher than NO_x, the NO was converted to nitrogen dioxide (NO_2)

via the NO + O_3 reaction prior to the initiation of photochemistry. For the duration of the experiment, the photolysis of NO_2 to produce NO was counteracted by the oxidation of NO to NO_2 and NO remained close to zero. O_3 was added to the chamber with an ozone generator (Ozone Solutions, TG-10) using a 10.01 ppm O_2 feedstock sourced from a gas cylinder of UHP O_2 (Airgas). Once all components were injected into the chamber, additional zero air was added to fill the chamber to its full volume, and several minutes were allowed for mixing. Once it was observed that the components were well-mixed, as determined by stable concentration readings from the instrumentation, the UV lights were turned on to initiate photochemistry.

Concentrations of additional gas phase species were measured using a High Resolution Time-of-Flight Chemical Ionization Mass Spectrometer (HR-ToF-CIMS, Aerodyne Research Inc.). The HR-ToF-CIMS (Bertram et al., 2011a, 2011b; Yatavelli et al., 2012) is capable of operating in both negative and positive ion detection modes and can accommodate a variety of reagent ion sources for this purpose. For the experiments presented here the instrument was operated in single reflection (V) mode, which provides higher sensitivity but lower resolution than the double reflection (W) mode. Data for the spectrum from *m/z* 2 – 500 was recorded at a frequency of 0.5 Hz. The detection of chlorine species was accomplished through the use of the iodide (I^-) regent ion, and the HR-ToF-CIMS was operated in negative mode. Additional information and a full analysis of possible reagent ions used with the HR-ToF-CIMS can be found in other work (Bertram et al., 2011b; Yatavelli et al., 2012). I^- reagent ions were generated by passing a 2 LPM N_2 flow over a permeation tube containing methyl iodide (CH_3I, Sigma Aldrich, 99%). The permeation tube used is 90 mm long and is constructed of a 5 mm OD PFA Teflon tubing and housed within a 9.5 mm OD stainless steel housing. Upstream of the permeation tube, a reservoir containing Milli-Q (model Advantage A10) purified water. The N_2 stream is first bubbled through the water reservoir to create the humidification necessary to produce $I(H_2O)_n^-$ clusters

which facilitate the ionization reaction involved for the detection of certain gas phase species, including H_2O_2, Cl_2, $ClNO_2$ and N_2O_5 (Aljawhary et al., 2013):

$$I(H_2O)_n^- + M \rightarrow n(H_2O) + I(M)^- \qquad \text{(Reaction 5-14)}$$

A 2 LPM sample flow was pulled into the instrument inlet from the chamber during the experiments. Data analysis was performed using the data analysis software Tofware provided by the manufacturer and written in Igor Pro (WaveMetrics). Calibration for primary species of interest was performed on a normalized basis, where a relationship was determined between the ratio of the signal for the measured species (S_i) and the signal for the sum of I^- and $I(H_2O)_n^-$ ($S_{clusters}$). For all species discussed, the relationship was found to be linear for the concentration ranges observed during the experiments.

Cl_2 and HCl concentrations were quantified using the HR-ToF-CIMS through the detection of the ions $(Cl_2)I^-$ (*m/z* 197, 199, and 201) and $(HCl)I^-$ (*m/z* 163 and 165), respectively. The detection limit was determined from equation 5-3 (Kercher et al., 2009). In this equation, S/N is the signal to noise ratio, which was fixed at a value of 2 to fit the statistical definition of a detection limit (Kercher et al., 2009). C_f (Hz ppt^{-1}) is the calibration coefficient for a given species, B (Hz) is the underlying background count rate, [X] is the detection limit for the species, and t (s) is the length of the integration period. The detection limit for Cl_2 with the HR-ToF-CIMS was determined to be 0.06 ppt for an integration period of 60 s. For HCl over the same integration period, the detection limit was 33.4 ppt.

$$\frac{S}{N} = \frac{C_f[X]t}{\sqrt{C_f[X]t+2Bt}} \qquad \text{(Equation 5-3)}$$

The number and size distribution of the aerosol population in the chamber during each experiment was measured using a Scanning Electrical Mobility System (SEMS, model 2002, Brechtel Manufacturing Inc.), which consists of a differential mobility analyzer (DMA) coupled to a turbulent-mixing-based condensation particle counter (MCPC, model 1710). From these measurements, total

particle mass, volume and surface area could be calculated. Particle mass was simultaneously measured by an Aerosol Chemical Speciation Monitor (ACSM, Aerodyne Research Inc.). The ACSM consists of a quadrupole mass spectrometer that uses electron impact for ionization of samples. The ACSM has the capability to speciate sampled particulate matter components and differentiate between organics, NO_3, SO_4, NH_4, and Cl. More details on the standard operation of the ACSM can be found in elsewhere (Ng et al., 2011). Standard sample averaging time was 140 seconds in a cycle which consisted of one sample from the chamber combined with one background filter sample. The vaporizer temperature was set at 600°C in order to correspond to standard operating procedures followed by other ACSM users (Ng et al., 2011).

Testing prior to the experiments revealed an issue regarding the measurement of chloride salts with the ACSM. Detection of chloride present in sodium chloride (NaCl) particles was not possible due to a high background concentration of chloride resulting from a slow rate of vaporization. During a given sample period, the slow rate of vaporization of NaCl resulted in sample and background signals for Cl^- (*m/z* 35 and 37) that were approximately equivalent. The resulting concentration calculation was thus under predicted, typically reading approximately zero. This issue persisted regardless of the actual NaCl particle loading present within the chamber. Additionally, Na was undetectable due to a boiling point that is significantly higher (883°C) than the standard vaporizer operating temperature. Due to this problem, NH_4Cl was used as an alternative. Although high background signals for Cl^- persisted, they were not as pronounced as with NaCl and often resulted in net positive, though likely under predicted, concentrations for chlorine. Additionally, NH_4 is detectable with the ACSM at a vaporizer temperature of 600°C, making it a useful tracer for NH_4Cl particles in the chamber. Comparison of ACSM NH_4 and Cl concentrations to SEMS data revealed that the ACSM was still under predicting mass concentrations significantly. The cause of this is likely that the NH_4-Cl bond does not readily flash vaporize at 600 C° similar to NaCl. In the same system, NH_4NO_3 and $(NH_4)_2SO_4$ particles regularly exhibit a collection

efficiency (CE) of 0.4 – 0.5 (higher if secondary organic aerosol is present in the particles). However, NH_4Cl particles were always significantly under predicted

H_2O_2 concentrations were quantified using the HR-ToF-CIMS signal at *m/z* 161 ($I(H_2O_2)^-$). The detection of O_3 and NO_x was accomplished through the use of trace gas monitors (Teledyne, models 400E and 200E). Relative humidity in the chamber was measured using a Vaisala temperature and humidity probe (model HMP60). Chamber temperature was monitored using thermocouples (Omega Engineering, Inc.). All environmental parameters as well as NO_x and O_3 concentrations were recorded using a custom program written in LabView (National Instruments).

Two separate experiments utilized α-pinene as a VOC precursor to facilitate the addition of secondary organic aerosol (SOA). For these experiments, liquid α-pinene (Sigma Aldrich, ≥ 99%) was injected into a glass injection bulb through a septum using a 10 µl syringe (Hamilton). To induce SOA formation, NH_4Cl seed particles, O_3 and α-pinene were injected prior to any other reactant, and ozonolysis was allowed to proceed in the dark. Monitoring of the organic aerosol component using the ACSM was used to deduce when an adequate amount of SOA had been produced. The amount produced depended heavily on the initial concentration of α-pinene injected, and therefore both high (21 ppb) and low (6 ppb) concentration scenarios were investigated. Particle size distribution data from the SEMS was used to verify that minimal homogeneous organic nucleation took place during this time period, suggesting that the resulting particles were of a mixed inorganic-organic composition.

The base case mixture was comprised of the components described up to this point, including initial concentrations of O_3, NH_4Cl, H_2O_2, and NO_x. In total, 12 scenarios involving variations on the base case reactant mixture were examined. These are listed in Table 5-1.

Table 5-1: A Description of the Scenarios Investigated in the Environmental Chamber Experiments

Scenario #	Description
0	H_2O_2 + NH_4Cl only
1	Base Case: O_3, H_2O_2, NO_x[i], NH_4Cl
2	Base Case + high RH (>79%), SOA[ii]
3	Base Case + high RH (>79%)
4	Base Case + 21.4 ppb α-pinene
5	Base Case + 6.1 ppb α-pinene
6	Base Case + Double NH_4Cl
7	O_3 and NH_4Cl only
8	$(NH_4)_2SO_4$, O_3, H_2O_2, NO_x, O_3, HCl
9	$(NH_4)_2SO_4$, O_3, H_2O_2, HCl, low NO_x

[i] NO_x was added as NO and was converted to NO_2 via the O_3 + NO reaction
[ii] The source of SOA in scenario 2 was organic contamination in the chamber.

5.2.2 Quantifying the Rate of Heterogeneous Reaction

5.2.2.1 *Parameterizing the Heterogeneous Reaction Rate*

Heterogeneous reactions can be defined as the reaction taking place at the interface of two phases, such as a particle surface (Knipping and Dabdub, 2003; Ravishankara, 1997). To quantify the rate of such a reaction, several parameters must be known and defined including total particle surface area density, identity of the reactant species and the reactive uptake coefficient of the gas phase reactant species. Once these are known, a pseudo first order heterogeneous reaction rate constant for reaction on a spherical particle can be deduced (Jacob, 2000; Ravishankara, 1997):

$$k = \frac{(\gamma_{obs})\omega A}{4} \qquad \text{(Equation 5-4)}$$

Here, k is the overall first order rate constant (s^{-1}), γ_{obs} is the observed reactive uptake coefficient, ω is the average molecular speed of gas phase reactant and A is the particle surface area density present in the system ($cm^2\,cm^{-3}$). The reactive uptake coefficient is the fraction of gas phase reactant molecules lost through reaction at the surface or uptake at the surface and reaction in the bulk aerosol relative to the total number of molecules reaching the surface of the particle. It is a unit-less parameter (Frenzel et al., 1998). This rate parameterization was used to quantify the rate of Cl_2 production in the present study. In the absence of gas phase chlorine concentrations or a known homogeneous route to significant Cl_2 production, it was assumed that a heterogeneous reaction represented by reaction (Reaction 5-11)

was the primary source of Cl_2 during the experiments. This assumption is backed by previous work suggesting that the rate of heterogeneous Cl_2 production in similar systems significantly outpaces any aqueous routes that may be active in the aerosol (Knipping, 2000a).

5.2.2.2 *Calculating Reactive uptake*

Using the observed rates of Cl_2 production from HR-ToF-CIMS data, the rate parameterization in equation 5-4 was used to deduce a reactive uptake coefficient for the proposed heterogeneous reaction of OH (13). The heterogeneous reaction was assumed to be the primary source, and photolysis was considered the primary sink for Cl_2 (Atkinson et al., 2007; Sander et al., 2011):

$$Cl_2 + h\nu \rightarrow 2\ Cl^{\bullet} \qquad \text{(Reaction 5-15)}$$

The following rate expression is derived from equation 5-13 for production of Cl_2 from reaction 13:

$$\frac{d[Cl_2]}{dt} = \gamma_s \frac{\omega}{8} A[OH] \qquad \text{(Equation 5-5)}$$

The rate of Cl_2 photolysis can be combined with equation 5-5, and the resulting observed reactive uptake coefficient is defined as:

$$\gamma_{obs} = \frac{\left(\frac{d[Cl_2]}{dt} + j_{Cl_2}[Cl_2]\right) * 8}{\omega * A_S * [OH]} \qquad \text{(Equation 5-6)}$$

For this calculation, the rate of Cl_2 photolysis (j_{Cl2}) and an estimated OH concentration were determined using the SAPRC chamber modeling software (Carter, 2010). Using the NO_2 photolysis rate that was determined for the chamber as input into the model, it was determined that the Cl_2 photolysis rate in the chamber is $2.30 \times 10^{-3}\ s^{-1}$. OH concentrations were determined by running simulations with the initial measured H_2O_2, O_3 and NO_x concentrations present in the chamber. The resulting modeled OH concentration over the first four hours of photochemistry was used during the calculation of a reactive uptake coefficient in each scenario. Since the concentrations of these species varied slightly between experiments, a unique simulation was run for each scenario. Additionally, water content in the

model was adjusted for the high RH scenarios by modifying the H_2O input concentration in the SAPRC model. An average reactive uptake coefficient was calculated from the period during which the lights were on for each experiment. These results are discussed further in the results section.

5.2.3 Quantifying Particulate Matter

As can be seen from the heterogeneous parameterization (equation 5-5), total particle surface area is a crucial parameter for calculating the reactive uptake coefficients. To this end, particle population sizing data from the SEMS was used to determine the surface area present during the experiment. One issue that introduces uncertainty into the use of this measurement as a metric for available particulate surface area is the loss of particles to the wall, including losses due to turbulent mixing, particle charge in an electric field and coagulation-evaporation (Crump and Seinfeld, 1981; Liu and Agarwal, 1974; McMurry and Rader, 1985; Pierce et al., 2008). In the scenarios where α-pinene SOA is introduced into the reactant mixture, it was assumed that the wall deposition rate of organic and inorganic particles were the same (e.g., the particles were of mixed composition). Data supporting the assumption of mixed particles are discussed in the results section in addition to reasoning for using the SEMS data as a proxy for NH_4Cl concentrations in the chamber. In lieu of accurate chloride salt speciation data from the ACSM, the SEMS data was used as a measure of the number concentration, size distribution and surface area of the suspended particulate NH_4Cl population, during the experiments. For reactive uptake coefficient calculations, suspended particulate surface area was used in equation 5-5.

5.3. Results

5.3.1 Cl_2 and HCl Production

During the experiments, Cl_2 production was observed to commence immediately upon irradiation of the mixture in all scenarios tested. In several scenarios, elevation in the Cl_2 concentration was observed upon the addition of O_3 before the UV lights were turned on. The quantity produced in the

dark was less than the concentrations resulting when the mixture was exposed to light. In cases where dark a-pinene ozonolysis occurred, enhanced Cl_2 production was observed in the dark. This is possibly due to the production of additional $OH^{\bullet}$ as a product of the reaction between O_3 and α-pinene at yields of up to 70% (Paulson et al., 1998). A representative time series of Cl_2 production is shown in Figure 5-1. The trend of a steady increase in Cl_2 concentrations after the lights were turned on followed by a leveling off in production after several hours was common to all experiments. The reader should note an increase in Cl_2 production from the presence of additional surface area, as well as a decrease in the rate of production from the addition of SOA in scenario 4. Cl_2 production was seen in most scenarios when O_3 was injected, and this phenomenon was most pronounced in those scenarios with high RH or α-pinene.

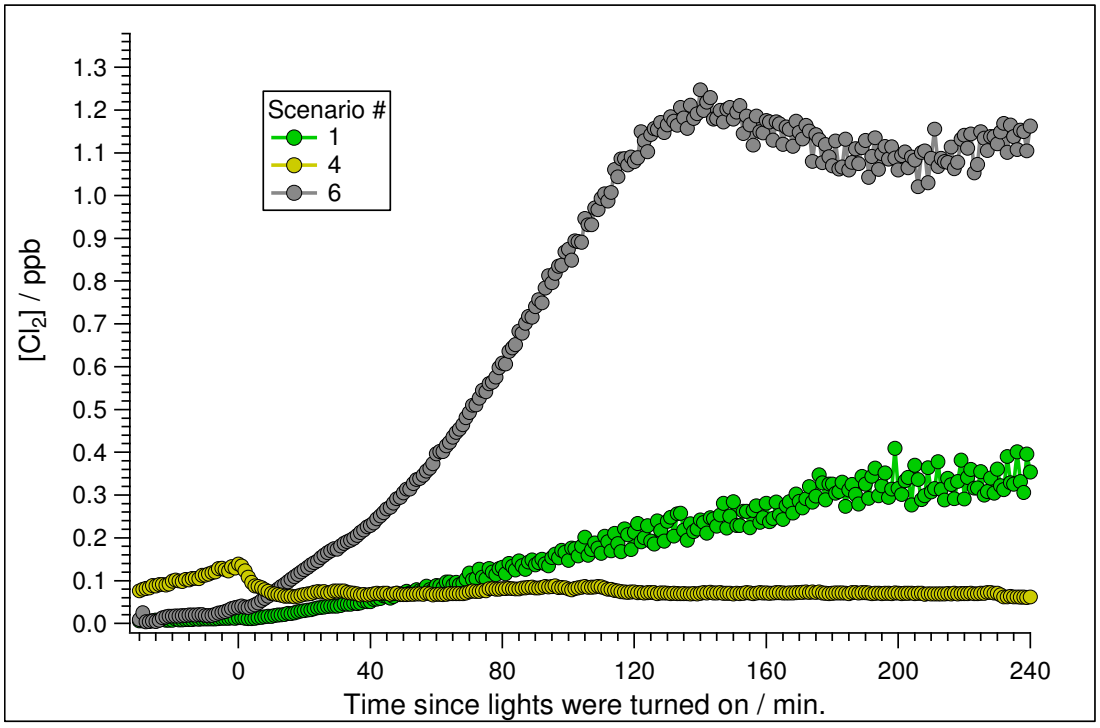

Figure 5-1: Time Series of Cl_2 in scenarios 1, 4 and 6. Data is averaged over one minute intervals. The drop in Cl_2 concentrations in scenario 6 is due to the lights being shut off.

HCl concentrations were also found to increase during the same time period that Cl_2 production was observed. Likely sources of the HCl are the reaction of $Cl^{\bullet}$ atoms produced from the photolysis of Cl_2. In the presence of organics, $Cl^{\bullet}$ can react via hydrogen abstraction path ways, yielding HCl as a

product (Sander et al., 2011). However, inorganic routes to HCl production also exist in the presence of HO_x (Atkinson et al., 2007; Faxon and Allen, 2013; Sander et al., 2011; Stutz et al., 2009; Watson, 1977).

$$Cl^{\bullet} + O_3 \rightarrow ClO^{\bullet} + O_2 \quad \text{(Reaction 5-16)}$$

$$ClO^{\bullet} + HO_2^{\bullet} \rightarrow HOCl + O_2 \quad \text{(Reaction 5-17)}$$

$$Cl^{\bullet} + HO_2^{\bullet} \rightarrow HCl + O_2 \quad \text{(Reaction 5-18)}$$

$$\rightarrow ClO^{\bullet} + OH^{\bullet} \quad \text{(Reaction 5-19)}$$

$$ClO^{\bullet} + OH^{\bullet} \rightarrow Cl^{\bullet} + HO_2^{\bullet} \quad \text{(Reaction 5-20)}$$

$$\rightarrow HCl + O_2 \quad \text{(Reaction 5-21)}$$

Another source that must also be considered is the displacement of HCl from particles by nitric acid (reaction 5-4), as has been observed for NaCl particles (Gard, 1998; Graedel and Keene, 1995; De Haan and Finlayson-Pitts, 1997; Saul et al., 2006). A representative plot of several HCl time series is shown in Figure 5-2. The same scenarios as were shown in Figure 5-1 are represented here.

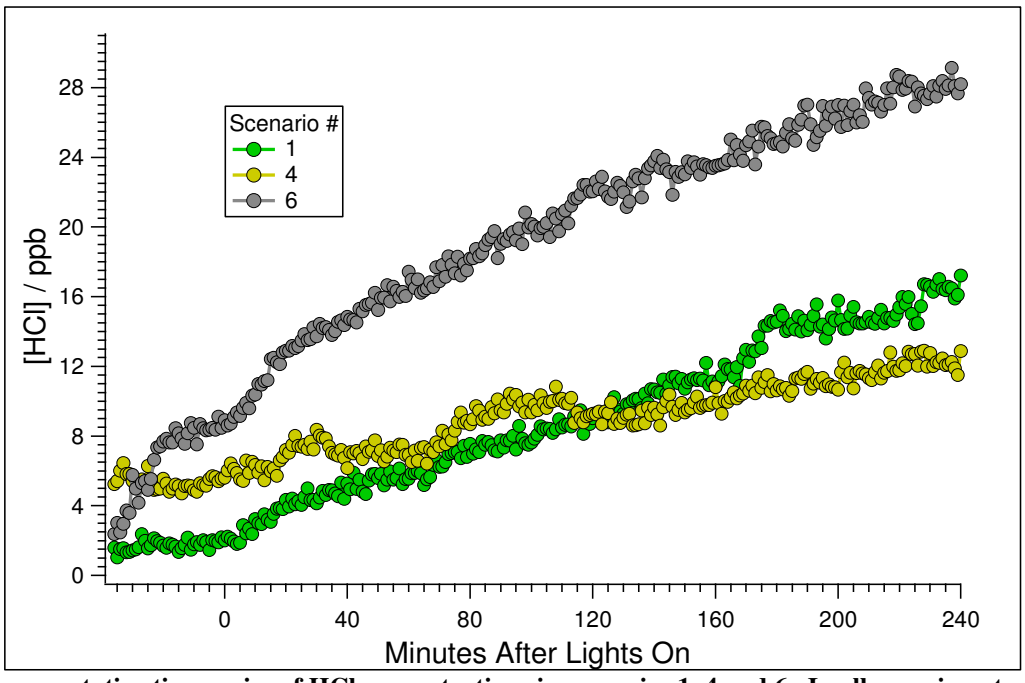

Figure 5-2: Representative time series of HCl concentrations in scenarios 1, 4 and 6. In all experiments, an increase in HCl was observed when O_3 was injected before lights were turned on.

5.3.2 Observed Values of the Reactive Uptake Coefficient

Utilizing equation 5-6, the reactive uptake for each scenario was calculated assuming that reaction 5-13 was the dominant heterogeneous route to Cl_2 production. However, when γ_{obs} was calculated assuming this OH-driven heterogeneous mechanism as the primary source of Cl_2 the resulting calculated values of γ_{obs} were greater than unity. Since the reactive uptake coefficient as formulated by equation 5-5 (Jacob, 2000; Ravishankara, 1997) represents the fraction of gas phase reactant molecules that are lost through heterogeneous reaction, calculated γ_{obs} values > 1 indicate rate of Cl_2 production that is too large to be accounted for by the direct heterogeneous reaction of OH, at least as parameterized by equation 5-5. One source of uncertainty that exists in this calculation comes from the estimation of $OH^{\bullet}$ concentrations by the SAPRC software. Estimated $[OH^{\bullet}]$ ranged from (7 – 8) x 10^6 molecules cm^{-3} for all scenarios discussed in this work. The possibility of an under prediction of OH concentrations by the software was considered. However, the assumption of an under estimation of $[OH^{\bullet}]$ by a factor of 10^3 molecules cm^{-3} is required to bring the average calculated value of γ_{obs} below 1. Considering that $OH^{\bullet}$ concentrations on the order of 10^6 are typical in atmospheric conditions similar to the conditions tested here (Prinn et al., 1987, 1992; Singh, 1977) and that several other scenarios (e.g., 3, 6 and 7) resulted in higher values of γ_{obs} relative to the base case, it is unlikely that such a large under prediction by the modeling software is the source of the error.

However, since the only source of chlorine in each experiment is particulate chloride (aside from scenarios 8 and 9), a heterogeneous reaction is most likely the primary source of the observed Cl_2 production. Due to the fact that observed Cl_2 production exceeded that which can be explained by the reactive uptake of OH alone, it is proposed that the heterogeneous mechanism is better parameterized by the reactive uptake of O_3. Although relative humidity was elevated about the DRH of NH_4Cl in scenario 3, fully aqueous particles were likely not present in the other scenarios in which Cl_2 production was observed. Although some liquid water likely stays absorbed on the surface of the particles as noted in

previous studies (Oum et al., 1998; Saul et al., 2006), it is unlikely that enough water is present such that the primary route of Cl_2 production in these scenarios results from purely aqueous routes, as has been proposed for deliquesced chloride aerosols (Oum et al., 1998). Assuming a direct reaction of O_3 (shown in reaction 5-21) similar to that which has been proposed previously (Behnke and Zetzsch, 1989; Keene et al., 1990; Sadanaga et al., 2001) allows for the calculation of reactive uptake coefficient values by the formula in equation 5-7 through the use of a pseudo first-order heterogeneous rate approximation (Jacob, 2000; Ravishankara, 1997). Further discussion of the exact mechanism modeled by this parameterization and it's relation to the proposed interfacial $OH^{\bullet}$ mechanism (Knipping and Dabdub, 2002; Knipping, 2000b) can be found in Section 5-4.

$$2\ Cl^-_{(cd)} + O_{3(g)} \xrightarrow{H_2O} Cl_{2(g)} + 2\ OH^-_{(cd)} + O_{2(g)} \qquad \text{(Reaction 5-21)}$$

$$\gamma_{obs} = \frac{\left(\frac{d[Cl_2]}{dt} + j_{Cl_2}[Cl_2]\right) * 4}{\omega * A_S * [O_3]} \qquad \text{(Equation 5-7)}$$

Resulting reactive uptake coefficient values calculated from equation 5-7 are shown in Table 5-2. For comparison, the concentrations of Cl_2 and HCl measured after four hours of exposure to UV lighting are also provided. Initial particulate matter concentrations are reported in μg m^{-3} (ρ_{NH4Cl} = 1.53 g cm^{-3}) and γ_{obs} values are unitless. Unless otherwise specified, all other concentrations are in ppb and indicate values observed at the initiation of photochemistry.

Table 5-2: Summary of Experimental Conditions and Resulting Chlorine Production

Scenario		Initial Conditions[i]					Chlorine Production[ii]		
#	Seed Type	$[PM]_0$ ($\mu g\ m^{-3}$)	$[O_3]_0$ (ppb)	$[NO_x]_0$[iii] (ppb)	$[H_2O_2]_0$ (ppb)	$[\alpha\text{-pinene}]_0$ (ppb)	$[Cl_2]_f$ (ppb)	$[HCl]_f$ (ppb)	γ_{obs} x (10^{-3})
0	NH_4Cl	47.3	-	-	655	-	2463	20.9	0.24
1	NH_4Cl	16.3	39	19.5	690	-	362	17.4	0.15
2	NH_4Cl	17.8	66	18.4	150	-[iv]	41	14.2	0.01
3	NH_4Cl	12.9	37	19.7	213	-	223	31.2	0.95
4	NH_4Cl	24.6	30	19.8	1300	21.4	72	12.9	0.01
5	NH_4Cl	24.0	38	20.0	1210	6.1	261	13.6	0.05
6	NH_4Cl	43.8	76	22.4	1105	-	1132	28.2	0.37
7	NH_4Cl	26.4	86	-	157	-	742	30.9	0.58
8	$(NH_4)_2SO_4$	45.5	68	16.9	521	-	1480	18.1	1.30
9	$(NH_4)_2SO_4$	30.7	66.4	-	485	-	1690	23.4	2.67

[i] All experiments were done at a temperature of 298 K. Initial concentrations cited are those present when the UV lights were turned on.
[ii] Cl_2 and HCl concentrations reported here are the concentrations observed after 4 hours of photochemistry.
[iii] NO_x was added as NO, but was oxidized to NO_2 via the O_3 + NO reaction by the time the UV lights were turned on.
[iv] Significant organic contamination of an unknown type/origin was present and led to SOA formation in this scenario.

The reactive uptake values reported in Table 5-2 were calculated assuming that the total suspended particle surface area as measured by the SEMS data was the actual amount of available surface area on which the heterogeneous reaction could take place. Though the available surface area in each scenario varied due to slight differences in initial particle loadings, this is not thought to have differentially influenced the deduced rates of reactive uptake since surface area is accounted for in the heterogeneous parameterization. A visual comparison of γ_{obs} values are shown in Figure 5-3.

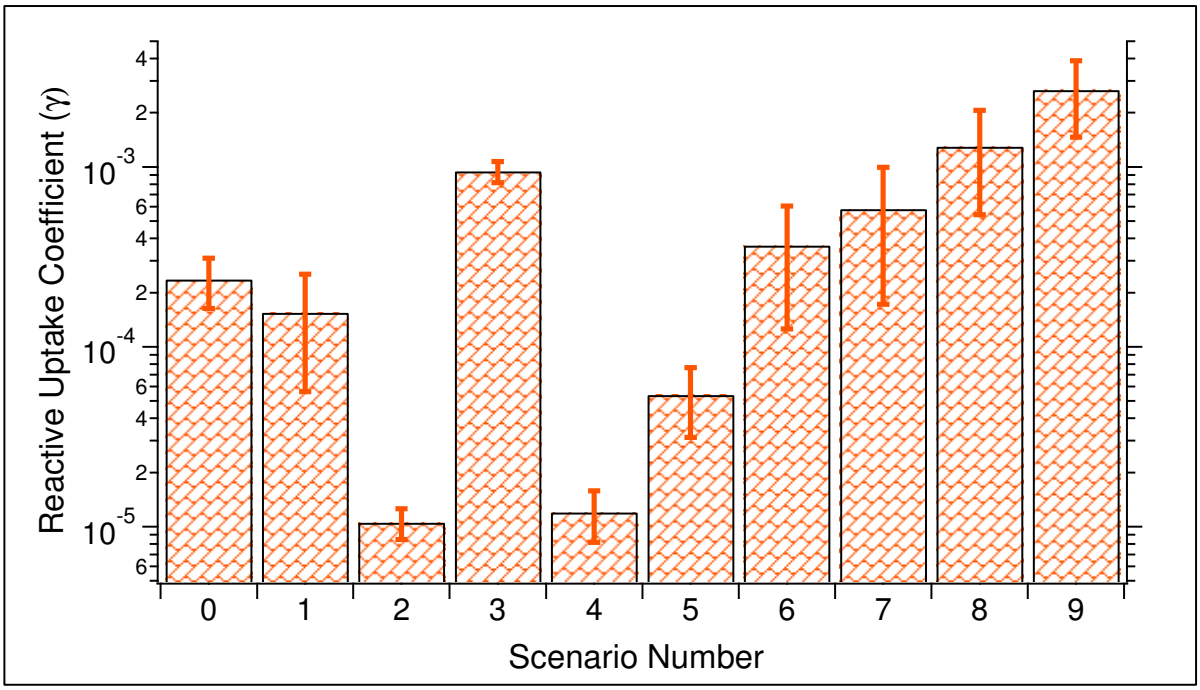

Figure 5-3: Plot of γ_{obs} values for comparison between experimental scenarios.

5.3.3 α-Pinene SOA Production and Particle Mixing

A total of three scenarios included an organic component to the aerosol mixture. Two of these (scenarios 4 and 5) introduced SOA to the particle population via ozonolysis of α-pinene prior to the initiation of photochemistry. The third, scenario 2, involved the unintentional introduction of SOA through an unknown source of organic contamination. It is possible that water source used to humidify the chamber during this experiment was contaminated or that a loose seal allowed the introduction of air from the laboratory external to the chamber. Regardless of the source of contamination, and despite a lack of data characterizing the organic components present, scenario 2 provides a unique set of circumstances relative to the other scenarios presented. That is, scenario 2 included a particle population of mixed composition in the presence of elevated RH, whereas other experiments involving SOA were performed under dry conditions.

Figure 5-4 shows the time series of the concentration of organic species in the particle phase as determined from ACSM data. Note that in Scenarios 4 and 5, a steady concentration of SOA is produced form α-pinene ozonolysis, but this concentration increases further once the lights are turned on. This effect is more pronounced in Scenario 4. In scenario 2, SOA production coincides with the initiation of photochemistry.

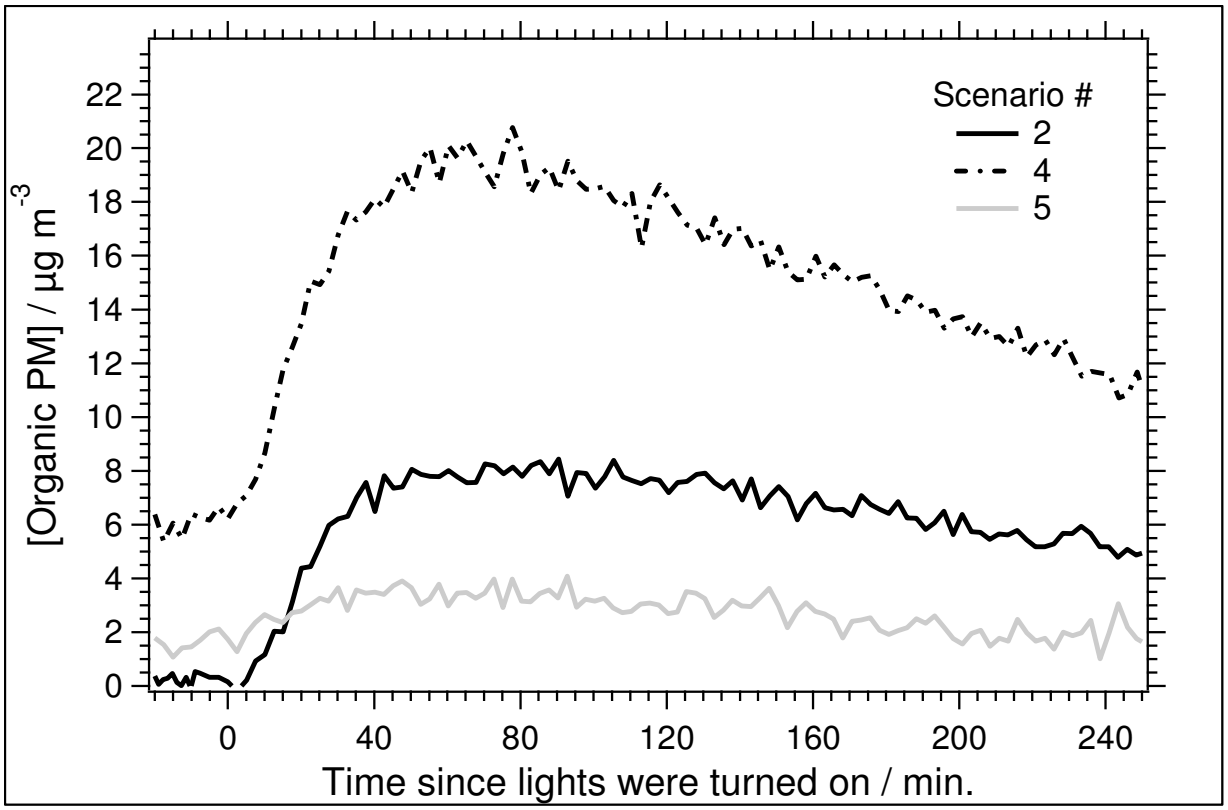

Figure 5-4: SOA production from scenarios 2, 4 and 5 as measured by the ACSM.

In the experiments that include SOA, one issue that can arise is the homogeneous nucleation oxidized organic species. This can result in a population that is not of mixed composition but that is comprised of two coexisting populations, one of organic composition and one inorganic. Figure 5-5 shows a plot of particle growth as a function of time for scenario 4. The absence of nucleation in the presence of particle diameter increase indicates that the resulting particle population is of mixed composition. For comparison, Figure 5-6 shows the same type of plot for scenario 5, which had a 71% lower gas phase organic precursor concentration than scenario 4.

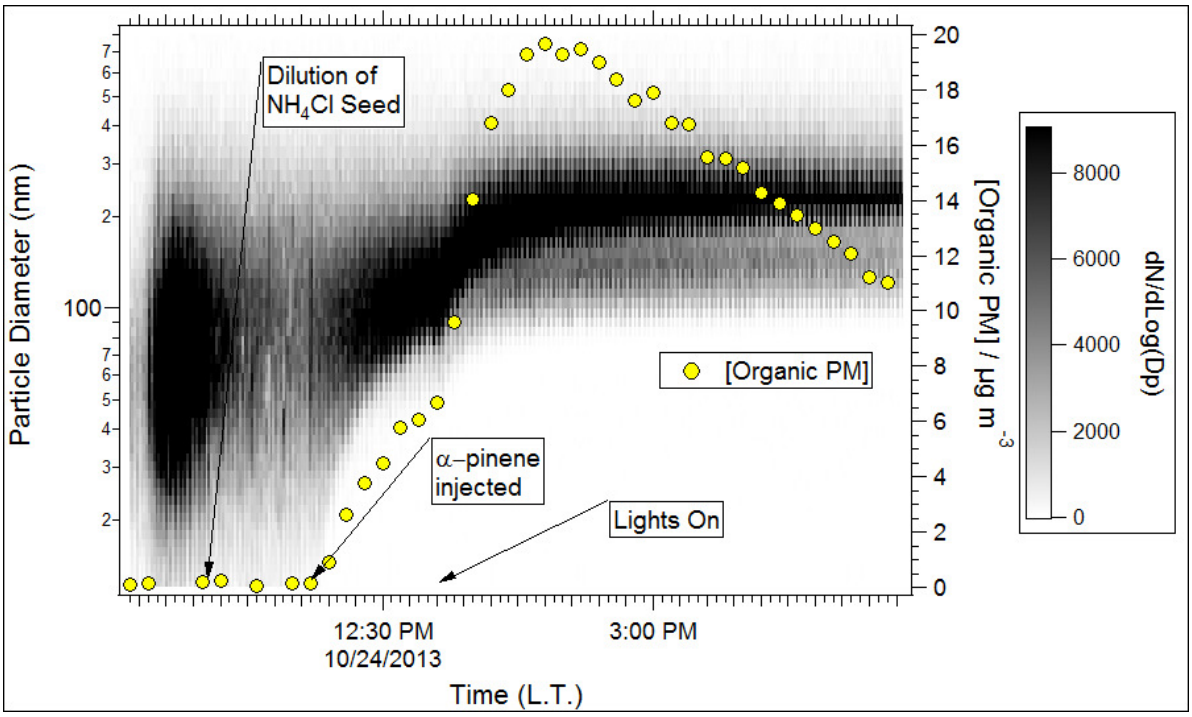

Figure 5-5: Plot of particle population growth from scenario 4. The absence of a nucleation event and the increase in median diameter of the population indicates growth of the aerosol through condensation of organic vapors.

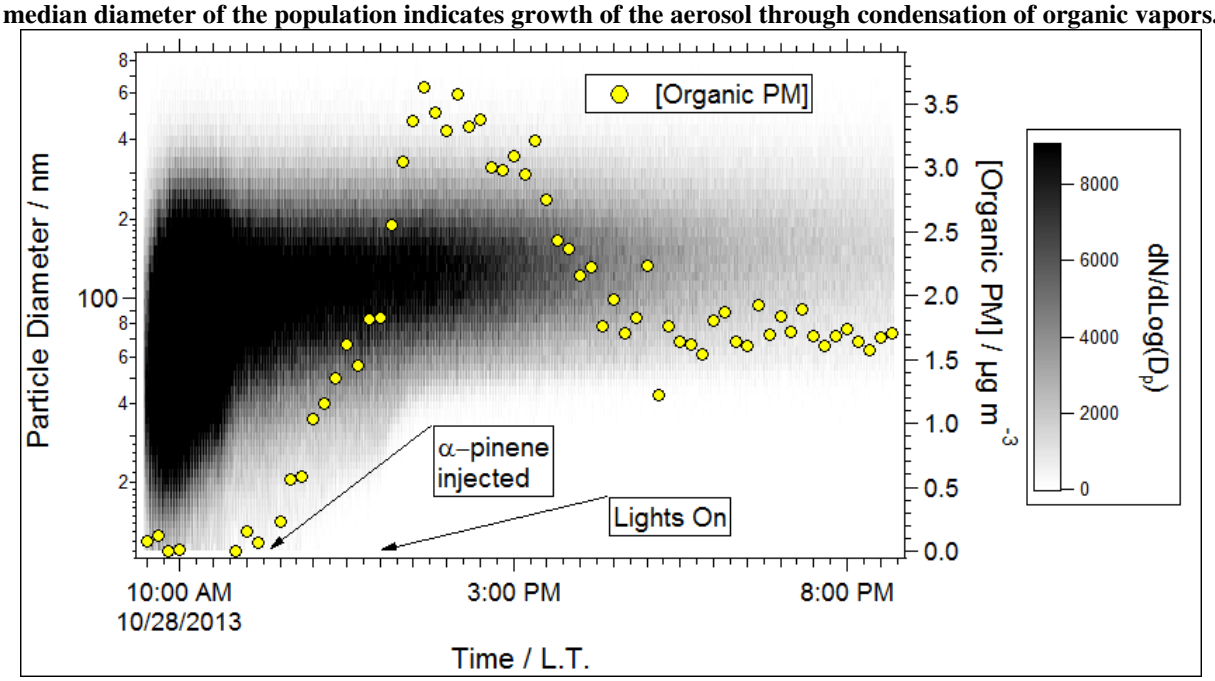

Figure 5-6: Plot of particle population growth from scenario 5 alongside the concentration of organic PM. Lack of a nucleation event as organic PM concentrations increase suggests that the resulting particle population is of a mixed composition.

In the absence of speciation data for NH_4 and Cl from the ACSM, SEMS data could be used to predict concentrations throughout the course of the experiments. However, total mass is not a parameter of extreme importance in these experiments, and total particle surface area plays a much large role. The

formation of SOA during scenarios such as those shown in Figures 5-4 - 5-6 increased surface area. However, despite this increase in surface area in those scenarios, the heterogeneous mechanism was suppressed and observed reactive uptake coefficient values were low. For comparison, Figure 5-7 shows the time series of total particulate surface area in the system for all of the scenarios tested.

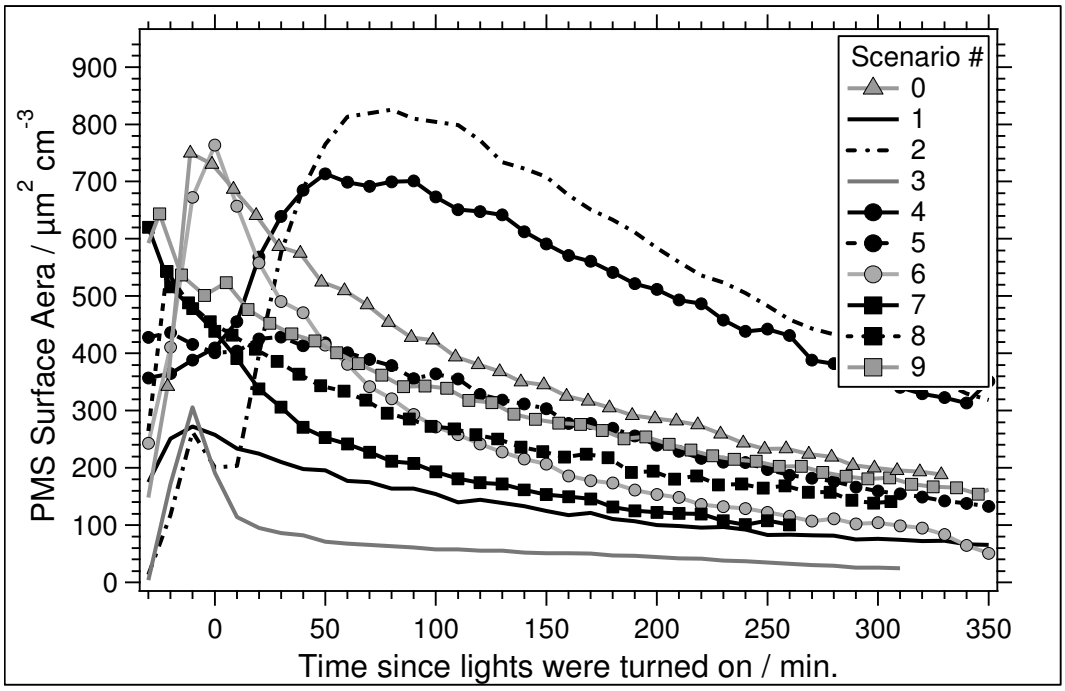

Figure 5-7: Total PM surface area for all experimental scenarios. All scenarios contained NH_4Cl seed particles with the exception of scenarios, which contained $(NH_4)_2SO_4$.

5.4. Discussion

5.4.1 Production of Cl_2 at Low Relative Humidity

One result that stands out is the production of Cl_2 in scenarios with less than 5% RH. Blank experiments, as described in Section 5.2.1, did not demonstrate production of Cl_2, suggesting that the Cl_2 was not from chlorine contamination on the chamber walls. Previous studies (Knipping and Dabdub, 2002; Knipping, 2000a; Oum et al., 1998) have indicated that Cl_2 production from the presence of O_3 from chloride aerosol requires an aqueous chloride aerosol for the reaction to proceed efficiently. As opposed to the results here being contradictory to these previous studies, it is more likely that a small yet significant amount of surface absorbed water (SAW) was present on the particles generated in this study as has been noted to occur in previous work (Knipping and Dabdub, 2002; Oum et al., 1998; Saul et al.,

2006). However it is also worth noting that previous studies of this mechanism have often used light sources below 290 nm , which may result in slight differences in the characteristics of the observed reactions compared to the black light UV source used here and in other studies (Behnke and Zetzsch, 1989; Sadanaga et al., 2001). At a minimum, it requires that the photolysis of Cl_2 be accounted for as a major sink.

Additionally, as seen in Table 5-2, the concentrations of Cl_2 produced in scenarios with dry conditions were comparable to those from the high RH scenarios. In some cases (e.g., scenarios 0, 1, 6 and), gas phase Cl_2 production exceeded that in the high RH base case (scenario 3). This result suggest that the total Cl_2 production may depend more on total particulate chloride available in the system than on the liquid water content of the aerosol. However, other explanations for this difference exist. The presence of SAW would result in a highly concentration salt solution to be present at the particle surface, which would then allow for the reaction to proceed at rates comparable to those seen on deliquesced aerosol (scenario 3). Any further uptake of water from higher RH in scenario 3 would lead to a more dilute solution, which could possibly lower the rate of the reaction if the overall heterogeneous rate is indeed modulated by the molarity of the solution (Knipping and Dabdub, 2002; Thomas et al., 2006). However, when taking into account the lower available particulate surface area during the course of the experiment in scenario 3, the observed value of the reactive uptake coefficient (γ_{obs}) in high RH conditions was the largest out of all scenarios involving NH_4Cl seed aerosol.

A second explanation for the lack of enhanced gas phase Cl_2 concentrations in the high RH experiment is the partitioning of heterogeneously produced Cl_2 back into the aqueous phase during the course of the experiment. This would also introduce the issue of the decomposition of aqueous phase Cl_2 in an alkaline solution through reaction with species such as $H_2O_{2(aq)}$. A previous sensitivity study of the mechanism indicates that increasing liquid water content in the particle can lead to a large sink for Cl_2 processes if the solution is alkaline (Knipping and Dabdub, 2002). In an aqueous solution, H_2O_2 can

directly decompose Cl_2 (via reaction 5-31). The presence of HO_x species in a solution can also degrade Cl_2 (reaction 27). Several source reactions for the aqueous HO_x species $HO_2^{\bullet}$ and $OH^{\bullet}$ are shown in reactions 5-21 to 5-26 (Bielski, 1978; Buxton et al., 1988; Elliot and Buxtont, 1992; Neta et al., 1988; Sauer et al., 1984).

$$H_2O_2 \leftrightarrow H^+ + HO_2^- \qquad \text{(Reaction 5-21)}$$

$$H_2O_2 + h\nu \rightarrow 2\ OH^{\bullet} \qquad \text{(Reaction 5-22)}$$

$$OH^{\bullet} + H_2O_2 \rightarrow HO_2^{\bullet} + H_2O \qquad \text{(Reaction 5-23)}$$

$$OH^{\bullet} + O_3 \rightarrow HO_2^{\bullet} + O_2 \qquad \text{(Reaction 5-24)}$$

$$HO_2^{\bullet} + O_2^{\bullet -} \rightarrow HO_2^- + O_2 \qquad \text{(Reaction 5-25)}$$

$$OH^{\bullet} + O_2^{\bullet -} \rightarrow OH^- + O_2 \qquad \text{(Reaction 5-26)}$$

Examples of reactions by which the HO_x species lead to aqueous phase degradation of Cl_2 are shown in reactions 5-27 – 5-32 (Bjergbakke et al., 1981; Connick, 1947; Davis et al., 1992; Held et al., 1978; Knipping and Dabdub, 2002; Makower and Bray, 1933; Ruiz-ibanez and Sandall, 1991).

$$Cl_2 + HO_2^{\bullet} \rightarrow Cl_2^{\bullet -} + H^+ + O_2 \qquad \text{(Reaction 5-27)}$$

$$Cl_2 + OH^- \rightarrow HOCl + Cl^- \qquad \text{(Reaction 5-28)}$$

$$Cl_2 + HO_2^- \rightarrow 2\ Cl^- + H^+ + O_2 \qquad \text{(Reaction 5-29)}$$

$$Cl_2 + CO_3^{2-} + H_2O \rightarrow HOCl + Cl^- + HCO_3^- \qquad \text{(Reaction 5-30)}$$

$$Cl_2 + H_2O_2 \rightarrow 2\ Cl^- + 2\ H^+ + O_2 \qquad \text{(Reaction 5-31)}$$

$$Cl_2 + h\nu \rightarrow 2\ Cl^{\bullet} \qquad \text{(Reaction 5-32)}$$

Of these, 5-28 – 5-30 are the primary alkaline routes for the degradation of Cl_2, but there remains significant uncertainty in the rates of these reactions (Knipping and Dabdub, 2002). The presence of these reactions as a chlorine sink is a likely possibility that is consistent with the results of scenario 3

since high concentrations of H_2O_2 were used as a hydroxyl source, and the argument can be made that significant concentrations of aqueous H_2O_2 and $HO_2^{\bullet}$ were present in the aerosol due to the solubility of these species. Relative to other gas phase species present in the system (e.g., Cl_2, O_3, O_2), both H_2O_2 and $HO_2^{\bullet}$ have high Henry's coefficients. Table 5-3 shows a comparison of these coefficients at 298 K (Kosak-Channing and Helz, 1983; Lind et al., 1994; Marsh and McElroy, 1985; Schwartz, 1984; Wilhelm et al., 1977).

Table 5-3: Comparison of Henry's constants at 298 K (H_{298}) for species present in the experiments.

Species	Henry's Constant (H_{298} / M atm^{-1})
O_2	1.3×10^{-3}
Cl_2	0.091
O_3	0.011
HCl	1.1
H_2O_2	1.0×10^{5}
$HO_2^{\bullet}$	1.2×10^{3}

5.4.2 Production of Cl_2 from Non-Chloride Particles

In addition to the production of Cl_2 at low RH, the production of Cl_2 was observed in scenarios 8 – 9 where $(NH_4)_2SO_4$ seed aerosol was used in place of NH_4Cl. This was an unexpected result since the few previous studies on this mechanism (Knipping and Dabdub, 2002; Knipping, 2000a) used NaCl and suggested that an aqueous chloride aerosol was necessary for the reaction to proceed at a significant rate. However, other previous studies have documented the production of Cl_2 from HCl in the presence of TiO_3 (Behnke and Zetzsch, 1989), although the mechanism in this case was not necessarily driven by O_3. The primary source of the chloride in scenarios 8 and 9 is gas phase HCl, which was injected prior to turning on the UV lights. In spite of lack of initial particulate chloride, these scenarios had some of the highest final Cl_2 concentrations and exhibited the highest reactive uptake coefficients. However, the exact mechanism of conversion likely differ significantly from the production of Cl_2 from chloride aerosol, and calculated γ values from these scenarios should be considered carefully when comparing to the values calculated for chloride aerosol.

One possibility that can likely be ruled out is the homogeneous production of Cl_2 from the reactant mixture present in these scenarios. Ostensibly, there is no known homogeneous route for the production of Cl_2 from HCl that proceeds at a rate high enough to produce the Cl_2 concentrations observed in these scenarios. HCl can react with $OH^{\bullet}$ to form $Cl^{\bullet}$, which could lead to $ClO^{\bullet}$ production. $ClO^{\bullet}$ can then lead to homogeneous Cl_2 production (Sander et al., 2011), but the reactions involved in this mechanism (31 –33) are relatively slow and should not lead to significant concentrations of Cl_2 in the conditions investigated in this work.

$OH^{\bullet} + HCl \rightarrow H_2O + Cl^{\bullet}$ (Reaction 5-31)

$Cl^{\bullet} + O_3 \rightarrow ClO^{\bullet} + O_2$ (Reaction 5-32)

$ClO^{\bullet} + ClO^{\bullet} \rightarrow Cl_2 + O_2$ (Reaction 5-33a)

$\rightarrow ClOO^{\bullet} + Cl^{\bullet}$ (Reaction 5-33b)

$\rightarrow OClO^{\bullet} + Cl^{\bullet}$ (Reaction 5-33c)

In the absence of significant homogenous routes for the production of Cl_2 from HCl, these results suggest that the heterogeneous production of Cl_2 can take place on non-chloride particles. If the observed production of Cl_2 is driven through the surface reactions between chloride and $OH^{\bullet}$ or O_3, the results also suggest that the source of the chlorine involved in the previously proposed surface mechanism (George and Abbatt, 2010; Knipping and Dabdub, 2002; Knipping, 2000a) need not be particulate chloride. However, it is a possibility that the conversion takes place through a surface reaction that does not necessarily require the uptake of HCl as particle phase chloride, such as has been observed on TiO_3 particles (Behnke and Zetzsch, 1989).

5.4.4 Reactive Uptake Coefficient Values

The observed value of γ for reaction 5-21 in this work ranged from $(0.01 – 2.67) \times 10^{-3}$, as parameterized for by the reactive uptake of O_3 (equation 5-7). The magnitude of the coefficient for this reaction is slightly smaller than that observed for other heterogeneous chlorine reactions. For example,

the $ClNO_2$ production mechanism shown in reactions 5-6 – 5-10 has been reported to exhibit a reactive uptake coefficient value for N_2O_5 of up to 0.03 (Bertram and Thornton, 2009; George et al., 1994). However, the concentrations of chlorine produced by the two mechanisms are not directly comparable due to multiple factors, such as particle composition and acidity, which may differentially affect the production of Cl_2 vs $ClNO_2$, as has been noted in previous studies (Roberts et al., 2008). It is plausible that in the atmosphere both mechanism could take place simultaneously under certain circumstances (e.g., in the presence of elevated N_2O_5 and a significant dark hydroxyl radical source). Additionally, $ClNO_2$ is only produced in significant quantities in the dark due to the rapid photolysis of N_2O_5, and it photolyzes rapidly after sunrise. In the experiments discussed in this paper, ppb-level concentrations of Cl_2 were generated under UV exposure. In the ambient environment, factors such as dilution by clean air, reduced particle surface area due to lower PM concentrations or larger average particle sizes, or the presence of precipitation could temper the impact of this mechanism with respect to gas phase Cl_2 production. Additionally, the production of several hundred ppt of Cl_2 has also been observed to take place nocturnally (Pszenny et al., 1993), and experimental work (Sadanaga et al., 2001) has observed the production of Cl_2 in the presence of O_3 in dark conditions.

Several trends regarding the effects of certain conditions on the value of the γ_{obs} were discerned. Elevated RH conditions (scenario 3) resulted in a 510% increase in the reactive uptake coefficient relative to the base case in scenario 1. This was equivalent to an increase in γ_{obs} of approximately 300% in scenario 3 over scenario 0, which had similar conditions to scenario 1 but with less O_3 and no NO_x present. These results are consistent with previous studies that cite an aqueous chloride particle will facilitate faster rates of the heterogeneous reaction (Knipping and Dabdub, 2002; Knipping, 2000a). However, if the relative value of the γ_{obs} and $[Cl_2]_{max}$ are considered for low and high RH base case scenarios (scenarios 1 and 3, respectively), it is notable that higher concentrations of Cl_2 resulted from the conditions in scenario 1. As noted previously, this could be due to the existence of additional sinks

for Cl_2 in the presence of an alkaline aqueous phase. It should also be noted that competing reaction pathways for intermediates in the reaction process may be present, resulting in a process that would be better modeled by the inclusion of a separate yield parameter (Kercher et al., 2009; Simon et al., 2010; Thornton and Abbatt, 2005) similar to other heterogeneous chlorine mechanisms. In the present study however, variations in rate due to these processes have been included into an overall reactive uptake value.

A reduction in the value of γ_{obs} was observed for scenarios in which organic components were incorporated into the aerosol phase. This phenomenon has previously been documented for heterogeneous $ClNO_2$ production chemistry (Thornton and Abbatt, 2005). Researchers have hypothesized that this reduction in reactive uptake is due to the partitioning of the organic components to the aerosol-gas interface (Thornton and Abbatt, 2005). The largest reduction in γ_{obs} was seen in scenario 2 where both high RH and an organic aerosol component were present. In this case, the suppressing effect of the organic components was greater than the enhancing effect of elevated RH. This occurred in spite of the fact that scenario 2 had less SOA present than scenario 4, which exhibited less of a reduction in γ_{obs} relative to the base case. This could possibly be due to differences in the structure and composition of the SOA components in each scenario. However, a more detailed analysis into the cause of this is not available due to the fact that the SOA in scenario 2 was the result of an unknown gas phase organic contaminant in the system.

5.5. Conclusions and Recommendations for Future Work

Parameterization of the mechanism of heterogeneous Cl_2 production assuming the direct reactive uptake of $OH^{\bullet}$ as the primary mechanism resulted in γ_{obs} values larger than unity. Previous modeling studies suggesting that the primary mechanism is the reactive uptake of OH have utilized additional factors in their parameterizations to insure that the reactive uptake does not exceed one. Though $OH^{\bullet}$ may play a direct or indirect role in the exact reaction mechanism occurring on the surface of the

particle, the findings in this chapter suggest that the heterogeneous reaction is better parameterized by the reactive uptake of ozone (equation 5-7). The overall range of values for the reactive uptake of O_3 (γ_{obs}) in the mechanism represented by reaction 5-21 was found to be (0.01 – 2.67) x 10^{-3}. High RH conditions (>79%) increased γ_{obs} by 510% over the base case. Relative to scenario 1, the reduction of γ_{obs}, due to the addition of SOA to the seed aerosol via α-pinene ozonolysis was equivalent to 92% and 65% in scenarios 4 and 5, respectively. The suppressing effect of SOA was found to be in effect even at high RH (scenario 2), though no direct comparison can be made to scenarios 4 and 5 since the nature of the SOA in that experiment was from an unknown source. In addition to the heterogeneous production of Cl_2 in dry conditions, significant Cl_2 production was observed from non-chloride particles in the presence of gas phase HCl. This was an unexpected result and, along with the suppression of Cl_2 production by the addition of SOA to the particle phase, supports the hypothesis that a surface-mediated heterogeneous reaction is leading to Cl_2 production. Extrapolations of the γ values reported here to the rate of the reaction on NaCl aerosol should be made with care as the mechanism in that scenario may differ slightly.

Chapter 6: Analysis of Reactive Chlorine Sources in the Dallas-Ft. Worth Region Using a Revised Chlorine Chemistry Mechanism in the Comprehensive Air Quality Model with Extensions (CAMx)

6.1. Introduction

The addition of chlorine chemistry into chemical mechanisms for use in photochemical modeling has allowed for more accurate modeling in regions impacted by chlorine emissions (G. Sarwar et al., 2012; Golam Sarwar & Bhave, 2007; Tanaka, 2003b; Tanaka et al., 2003b), and can help provide a more accurate reactivity estimate for chlorinated VOCs (William P L Carter, 2010a). This is partially due to differences in reactivity between reactive chlorine species and common atmospheric oxidants, such as $OH^{\bullet}$ and O_3. Within the urban atmosphere, the reactions of chlorine radicals ($Cl^{\bullet}$) with VOCs typically take place at a much faster rate than its reaction with hydroxyl radical (Tanaka, 2003b). The rate constants for the reaction of many alkanes, aromatics, alcohols and ethers with $Cl^{\bullet}$ are 1 – 2 orders of magnitude faster than the corresponding rate constants for their reactions with hydroxyl radicals ($OH^{\bullet}$) (Aschmann & Atkinson, 1995; Nelson et al., 1990; Spicer et al., 1998; J. Stutz, Ezell, Ezell, & Finlayson-Pitts, 1998; Jochen Stutz et al., 2009; Lin Wang et al., 2005). Unique products(Nordmeyer et al., 1997; Ragains & Finlayson-Pitts, 1997; Riemer & Apel, 2002; Tanaka et al., 2003b; W. Wang & Finlayson-Pitts, 2001) resulting from the reactions of $Cl^{\bullet}$ with VOCs can be used as tracers of reactive chlorine chemistry. One example is the production of 1-chloro-3-methyl-3-butene-2-one (CMBO) and chloromethylbutenal (CMBA)(Nordmeyer et al., 1997) from the reaction of isoprene and $Cl^{\bullet}$, which have both been observed in ambient measurements (Riemer & Apel, 2002; Tanaka et al., 2003b).

The reaction between $Cl^{\bullet}$ and VOCs, when resulting in hydrogen abstraction, produces both HCl as well as alkyl radicals. The alkyl radicals can then undergo further reactions to produce alkylperoxy radicals ($RO_2^{\bullet}$) (Seinfeld & Pandis, 2006). Thus, the production of $Cl^{\bullet}$ leads to a sequence of reactions that can enhance ozone formation rates (Sunghye Chang & Allen, 2006a; Sunghye Chang et al., 2002;

Golam Sarwar & Bhave, 2007; Seinfeld & Pandis, 2006; Tanaka et al., 2003a). The oxidation of VOCs by $Cl^{\bullet}$ can lead to both inorganic (Sunghye Chang & Allen, 2006b) aerosol and secondary organic aerosol (SOA) formation (Cai & Griffin, 2006; Cai et al., 2008; Karlsson et al., 2001). Due to the numerous aforementioned impacts on atmospheric composition and air quality, chlorine emissions and reactions are important to take into account when modeling the photochemical activity of any region where significant sources of reactive chlorine are present.

Initial efforts to incorporate chlorine chemistry into condensed chemical mechanisms included the development of a 13-reaction mechanism (Tanaka, 2003b) for use within the Carbon Bond IV (CBIV) mechanism (Adelman, Zachariah, 1999; G Z Whitten et al., 1980) and the addition of chlorine chemistry into the SAPRC-07 mechanism (William P L Carter, 2010a). The CBIV mechanism included photolysis reactions for two atomic chlorine ($Cl^{\bullet}$) precursors, Cl_2 and HOCl. Reactions of $Cl^{\bullet}$ with ozone and volatile organic compounds (VOCs) were also included. The SAPRC-7 mechanism includes additional representation of nitryl chloride ($ClNO_2$), chlorinated peroxy radicals and chlorinated organic product species (William P L Carter, 2010a).

The original CBIV gas phase chlorine mechanism (Tanaka, 2003b) was expanded during the development of the Carbon Bond 5 (CB05) mechanism to include reaction rate and product updates as well as explicit reactions with species such as methane (Yarwood & Rao, 2005). More recent updates to the Carbon Bond mechanism (CB6) (Yarwood et al., 2010) include the addition of $ClNO_2$ chemistry and gas phase parameterizations for HCl displacement from particulate matter by HNO_3. Heterogeneous N_2O_5 chemistry has been investigated on a regional scale (H. Simon et al., 2009, 2010) using the CB05 mechanism within the Community Air Quality Model with Extensions (CAMx). This chemistry was later incorporated into the CMAQ regional model, (G. Sarwar et al., 2012) and used to study the predicted effects of $ClNO_2$ chemistry across the U.S. This particular implementation included full parameterization of the heterogeneous reaction rate as a function of particle chloride, nitrate and water

content (Bertram & Thornton, 2009; Roberts et al., 2009). Results from this study indicate that $ClNO_2$ can significantly increase daily 8-hour maximum O_3, and account for up to 34% of total NO_y in some instances (G. Sarwar et al., 2012). A sensitivity analysis of the heterogeneous $ClNO_2$ production mechanism has suggested upper limits for the impact of heterogeneous N_2O_5 chemistry on $ClNO_2$ and O_3 production (Faxon & Allen, 2013). Additionally, several modeling studies exist concerning the mechanism of a heterogeneous surface reaction of $OH^{\bullet}$ on chloride aerosols (E. M. Knipping, 2000b; Eladio M Knipping & Dabdub, 2003; Eladio M. Knipping & Dabdub, 2002; Nissenson et al., 2008; Thomas, Jimenez-Aranda, Finlayson-Pitts, & Dabdub, 2006), and there is evidence that the mechanism is a significant for Cl_2 volatilization from aerosol particles (Thomas et al., 2006).

Recently, a measurement campaign in Ft. Worth, TX revealed the daily presence of gas phase chlorine (assumed to be HCl) at the Eagle Mountain Lake (EML) measurement site during the time period of May 31st – June 30th, 2011. The measurements detected HCl concentrations reaching concentrations of up to 1 – 2 ppb using a Mist Chamber-Ion Chromatography (MC-IC) method. Observations of particulate chloride using a Particle in Liquid Sampler (PILS) were under the detection limit for the majority of this time period (Griffin et al., 2011). Peak HCl concentrations occurred towards the mid to late afternoon, the timing of which deviates from expected temporal patterns of chlorine from heterogeneous $ClNO_2$ conversion. A time series and diurnal pattern of the HCl observations are shown in Figures 6-1 and 6-2.

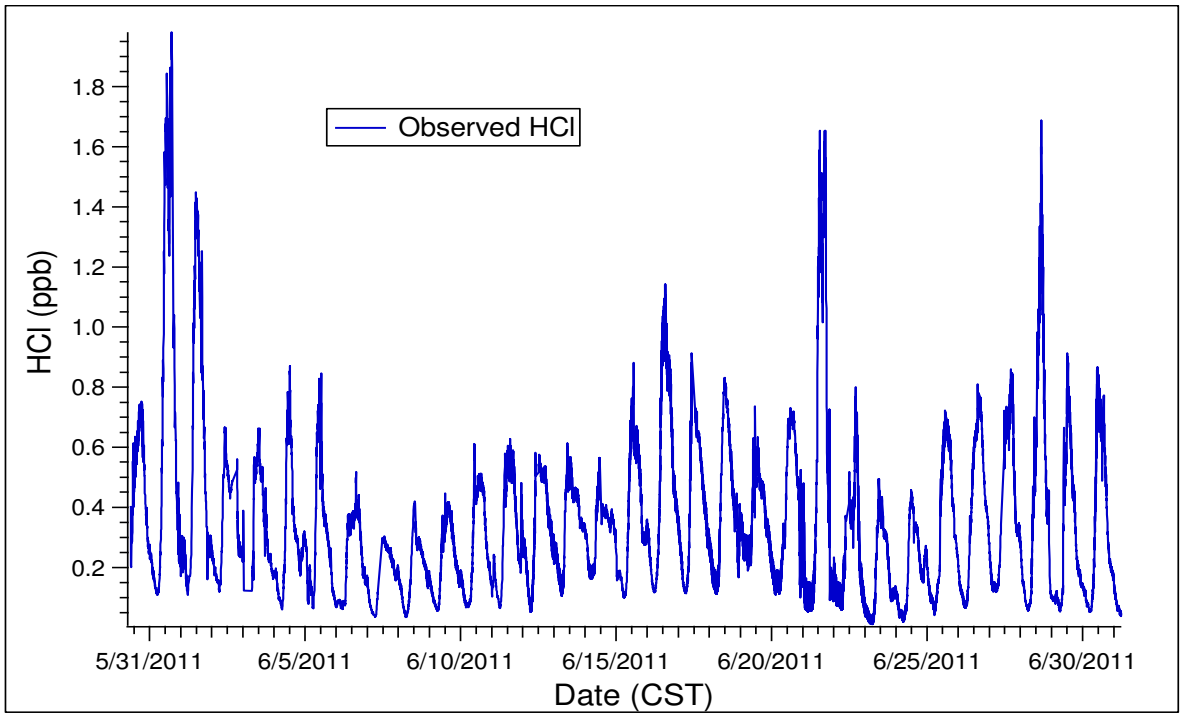

Figure 6-1: HCl Concentration time series from Eagle Mountain Lake, observed during June, 2011.

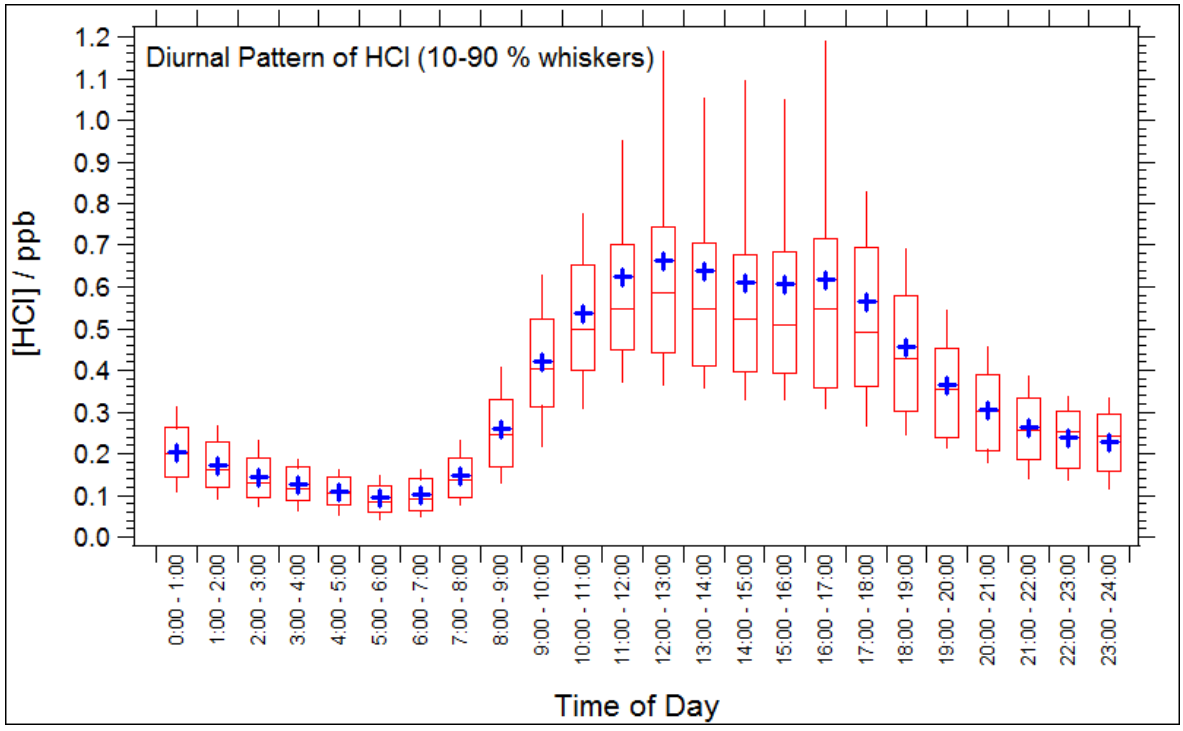

Figure 6-2: Diurnal pattern of HCl at the Eagle Mountain Lake monitoring site in June, 2011

Previously inventoried emissions of particulate chloride and gas phase chlorine species in the region are small. Therefore, in an effort to explain the source of these elevated HCl, several classes of sources are investigated in this work using a chlorine emissions inventory that was developed for the

Dallas-Fort Worth Region (Faxon & Allen, 2014b). Photochemical modeling using the CAMx software is used to assess the impacts of the emissions sources. Emissions categories that are investigated include:

1. Standard anthropogenic emissions (swimming pool chlorination, cooling tower biocide use, tap water usage, and industrial emissions)
2. Anthropogenic emissions related to natural gas production
3. Particulate chloride from sea salt transport into the region

6.2. Methods and Materials

6.2.1 Development of a Reaction Mechanism for Chlorinated Hydrocarbons

In order to test a chlorinated hydrocarbon emissions inventory that was developed in previous work (Faxon & Allen, 2014b), a chlorine reaction mechanism that includes basic inorganic chlorine reactions (Tanaka, 2003b; Gary Z. Whitten et al., 2010) and the reaction between the hydroxyl radical and a generic chlorinated hydrocarbon (CLV1) was developed. A non-reactive chlorinated organic (CLTR) was also included as a tracer species to facilitate analysis of the temporal and spatial distribution of emissions patterns. The addition of the surrogate chlorinated hydrocarbon, CLV1, was implemented in order to test the hypothesis that the observations of gas phase HCl at the EML site may have been the result of chlorinated hydrocarbon emissions from natural gas production activities in the region. To test this hypothesis, the reaction of a surrogate chlorocarbon species (CLV1) with $OH^{\bullet}$ is included. Dichlorbenzene was chosen as a model for the surrogate chlorinated VOC because it was previously observed in ambient measurements taken in the region (Eastern Research Group & Sage Environmental Consulting, 2011), and its reaction with $OH^{\bullet}$ has been shown to produce $Cl^{\bullet}$ (Mulder & Louw, 1986). Reaction of CLV1 with $OH^{\bullet}$ serves as the primary loss mechanism for ClV1 and is modeled after an ipso substitution reaction between $OH^{\bullet}$ and dichlorobenzene (Mulder & Louw, 1986). The mechanism is shown in Figure 6-3 for the case of p-dichlorobenzene. Step 2 (loss of $Cl^{\bullet}$) is

thermodynamically favorable to the reversal of step 1 and is expected to proceed at least 10^8 times more quickly (Mulder & Louw, 1986). In addition to the mechanism and rate of reaction, CLV1 solubility and deposition-related parameters were modeled after those of dichlorobenzene.

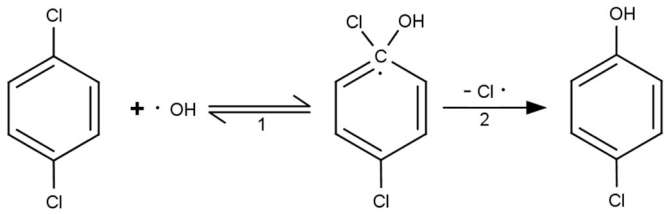

Figure 6-3: Ipso substitution mechanism for the reaction between OH• and p-dichlorobenzene.

A secondary reaction of the resulting organic product (CLP1) from this reaction was also included. Since CLV1 is modeled after dichlorobenzene, CLP1 corresponds to chlorophenol. Although the rate and product distribution for the reaction between chlorophenol and OH• reaction are uncertain (Kılıç & Çınar, 2008; Kiliç et al., 2007; Xu et al., 2010), the secondary reaction, which is assumed to produce an additional chlorine atom, was included as a hypothetical upper limit to atomic chlorine production from the emissions of a dichlorinated hydrocarbon. All reactions that were integrated into the CB05 are shown in Table 6-1.

Table 6-1: List of reactions involving chlorine in the CB05 mechanism. Species are written in terms of their model names.

Reaction #	Reactants	Products
1	CL2 + *hv*	2 CL
2	HOCl + *hv*	OH + CL
3	CL + O3	CLO
4	CLO + CLO	0.3 C2 + 1.4 CL
5	CLO + NO	CL + NO2
6	CLO + HO2	HOCL
7	CLO + NO2	N3CL
8	N3CL + *hv*	CLO + NO2
9	N3CL + *hv*	CL + NO3
10	CL + N3CL	CL2 + NO3
11	OH + HCL	CL
12	OH + FMCL	CL + CO
13	FMCL + *hv*	CL + CO + HO2
14	CL + H2	HCL + HO2
15	CL + CH4	HCL + MEO2
16	CL + PAR	HCL + 0.87 XO2 + 0.13 XO2N + 0.11 HO2 + 0.06 ALD2 – 0.11 PAR + 0.76 ROR + 0.05 ALDX
17	CL + ETHA	HCL + 0.991 ALD2 + 0.991 XO2 + 0.009 XO2N + HO2
18	CL + ETH	FMCL + 2 XO2 + HO2 + FORM
19	CL + OLE	0.13 HCL + 0.87 FMCL + 0.58 ALD2 + 0.29 ALDX + 0.13 OLE + 0.13 FORM + 1.87 XO2 + HO2 - PAR
20	CL + IOLE	0.2 HCL + 0.8 FMCL + 0.27 ALD2 + 0.53 ALDX + 0.2 OLE + 0.2 FORM + 0.2 PAR + 1.8 XO2 + HO2
21	CL + ISOP	0.15 HCL + 0.85 FMCL + 0.92 ISPD + 1.7 XO2 + 0.08 XO2N + 0.92 HO2
22	CL + TERP	0.4 HCL + 0.6 FMCL + 0.45 ALDX + 1.8 PAR + 1.2 XO2 + 0.25 XO2N + 0.75 HO2
23	CL + TOL	HCL + 0.88 XO2 + 0.12 XO2N + 0.84 +HO2
24	CL + XYL	HCL + 0.84 XO2 + 0.16 XO2N + 0.84 HO2
25	CL + FORM	HCL + HO2 + CO
26	CL + ALD2	HCL + C2O3
27	CL + ALDX	HCL + CXO3
28	CL + MEOH	HCL + HO2 + FORM
29	CL + ETOH	HCL + HO2 + ALD2
30	N2O5 + HCL	NTCL + HNO3
31	NTCL + *hv*	CL + NO2
32	SS + HNO3	NTR + HCL
33[i]	CLV1 + OH	CL + CLP1
34[i]	CLP1 + OH	CL + CLS1
35	CLTR	CLTR

[i] This reaction not included in the standard distribution and was added for the purpose of this work.

Table 6-2 contains definitions of these CB05 modeled species, in terms of real species. For more details on the condensed chemical mechanisms involved, the reader is referenced to the Carbon Bond

mechanism documentation (Adelman, Zachariah, 1999; Tanaka, 2003b; G Z Whitten et al., 1980; Gary Z. Whitten et al., 2010; Yarwood & Rao, 2005; Yarwood et al., 2010).

Table 6-2: CB05 Mechanism Species Definitions

CB05 Species Name	Corresponding Species
CL2	Molecular chlorine
CL	Atomic chlorine radical
HOCl	Hypochlorous acid
CLO	Chlorine monoxide
N3CL	Chlorine nitrate
HCL	Hydrogen chloride
FMCL	Formyl chloride
MEO2	Methylperoxy radical
MEOH	Methanol
ETOH	Ethanol
PAR	Paraffin carbon bond (C-C)
OLE	Terminal olefin carbon bond (R-C=C)
IOLE	Internal olefin carbon bond (R-C=C-R)
XO2	NO to NO2 conversion from alkylperoxy radical
XO2N	NO to organic nitrate conversion from alkylperoxy radical
ALD2	Acetaldehyde
ALDX	Propionaldehyde and higher aldehydes
ROR	Secondary alkoxy radical
ETH	Ethene
ETHA	Ethane
FORM	Formaldehyde
ISOP	Isoprene
ISPD	Isoprene product (lumped methacrolein, methyl vinyl ketone, etc.)
TERP	Terpene
TOL	Toluene
XYL	Xylene
C2O3	Acetylperoxy radical
SS	Sea salt aerosol
NTCL	Nitryl chloride
NTR	Aerosol nitrate
CLTR	Non-reactive chlorinated hydrocarbon tracer
CLV1	Chlorinated volatile organic
CLP2	Primary product of the reaction of CLV1
CLS1	Product of secondary chlorinated organic reaction (non-reactive)

6.2.2 Model Configuration

Version 5.40 of the CAMx software was used to model chlorine emissions sources and analyze the resulting impacts on atmospheric composition and air quality. As a base case scenario, the TCEQ's Dallas-Fort Worth Eight-Hour Ozone SIP Modeling 2006 episode (dfw8h2) was utilized. The episode included the necessary meteorological and photochemical inputs. The time period modeled spanned from May 31 – June 02, 2006. Modeling was performed over a domain consisting of three nested grids with resolutions of 36km, 12km and 4 km, respectively. The largest grid was centered on the Eastern U.S. and the finest mesh grid (4km) was centered on the DFW region. A representation of the nested grid structure used is shown in Figure 6-4. When comparing the Eagle Mountain Lake observations to modeled concentrations, 1-hour average concentrations from the 4 km grid cell that contains the EML measurement site's coordinates (32.987891° N, -97.477175 W) were used.

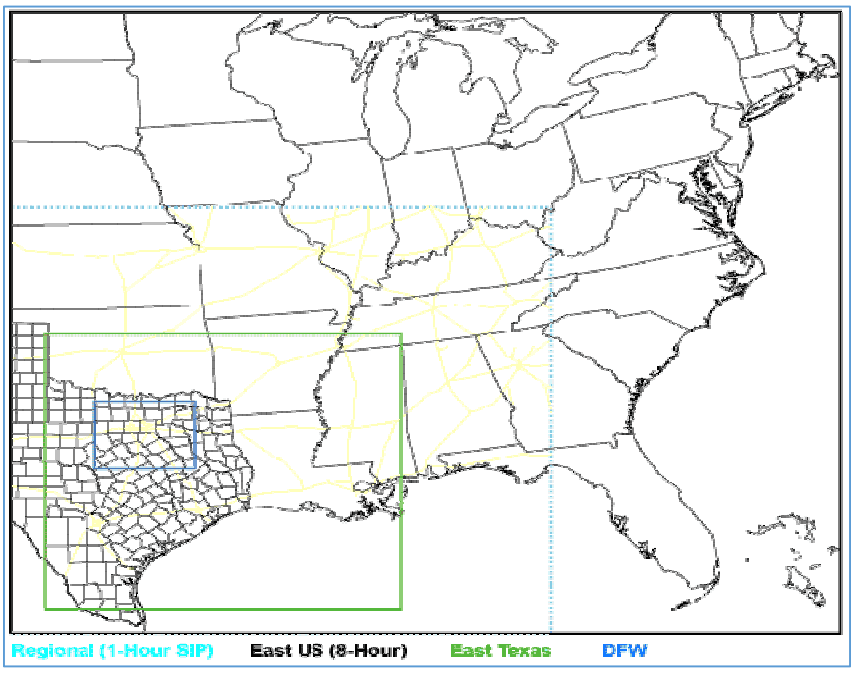

Figure 6-4: A depiction of the nested grid structure used in the CAMx modeling.

In addition to coinciding with the geographical domain wherein the HCl observations were made, the dfw8h2 episode spans a time period (May 28th – June 2nd, 2006) during the same months in which the measurement campaign took place. Though the observations and modeling episode occur in

different years, major climactic and meteorological patterns are expected to be consistent enough for comparison.

For anthropogenic emissions test cases, CAMx inputs included the modified CB05 chemical mechanism described above (gas phase chemistry only) and a gas phase emissions inventory that included VOC and NOx emissions from shale gas production operations in the Barnett Shale (TCEQ Barnet Shale Area Special Inventory) in addition to emissions from all other regional sources. For the long range sea salt transport scenario, a particulate inventory was used which included marine and inland sources of particulate chloride. Anthropogenic reactive chlorine inventories(Faxon & Allen, 2014b) were added to the base inventory. In one instance, a sensitivity analysis of sea salt aerosol source strength transport was performed by enhancing source strengths for comparison to the base case scenario. However, the spatial distribution of emissions was left unchanged.

6.2.3 Emissions Patterns and Scenarios

The preparation of chlorinated VOC (CLV1) emissions was carried out by scaling emissions of CLV1 to total VOC emissions from shale gas production operations (taken from the Barnett Shale Special Inventory) in an 18 county area within the DFW region. Scaling of the emissions was performed on a percentage by weight basis using a molecular mass equivalent to that of dichlorobenzene (147.00 g mol^{-1}) for the chlorinated hydrocarbon surrogate, CLV1. Scaling ratios of 0.5-44.8 were investigated. Figure 6-5 shows the locations of natural gas production sites that were included for calculating county-by-county emissions, and the spatial distribution of the emissions is shown in Figure 6-6.

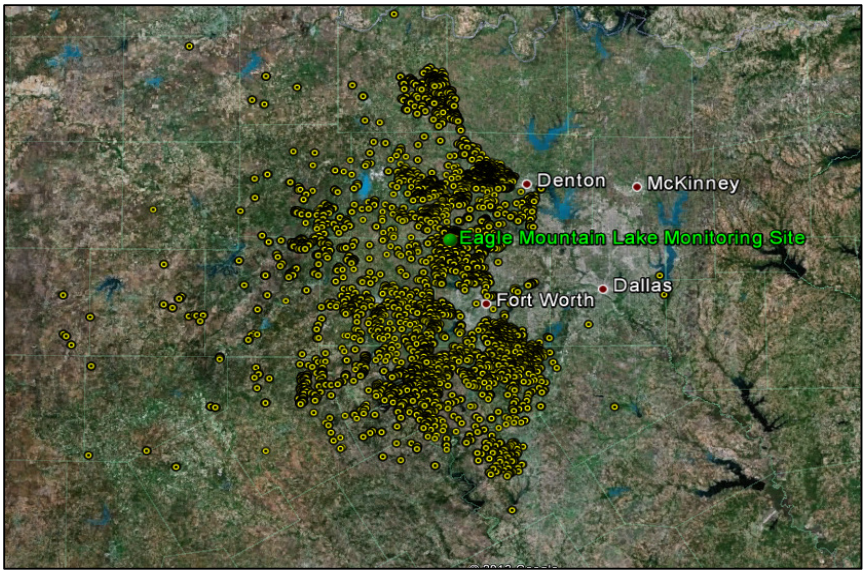

Figure 6-5: Locations of natural gas production sites (indicated as yellow circles) in the Barnett Shale that were used for this study

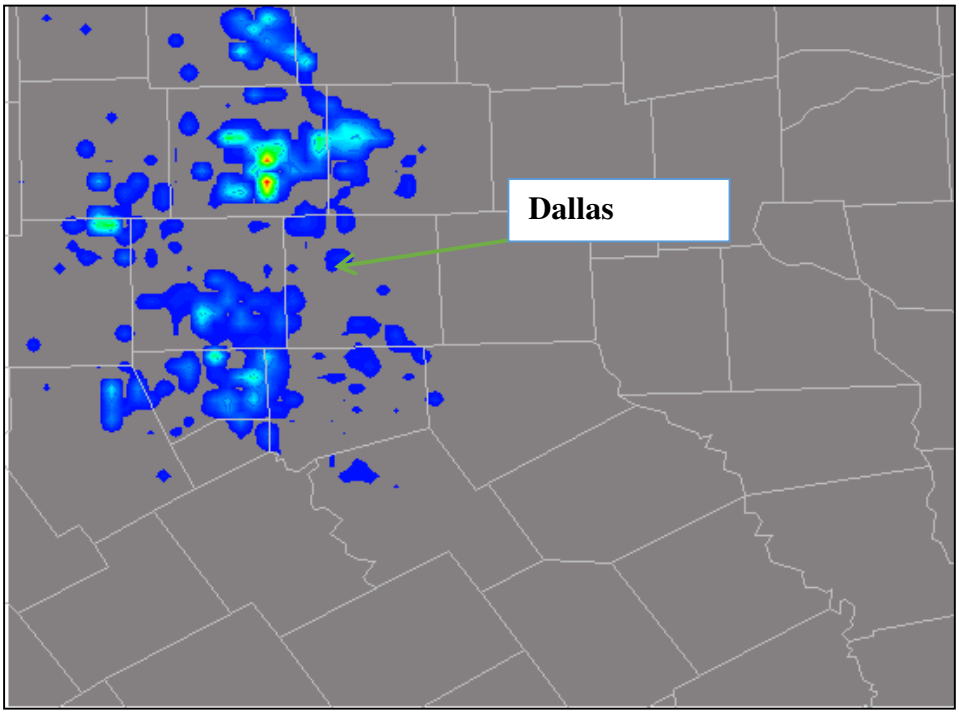

Figure 6-6: Spatial distribution of chlorinated VOC (CLTR or CLV1) emissions scaled from VOC emissions from the Barnett Shale Area Special Inventory

For scenarios involving CLV1 emission, a sensitivity analysis was performed by increasing the rate of reaction 33. The base case reaction rate was set at $k_{33} = 3.39 \times 10^{-13}$ cm^3 $molecules^{-1}$ s^{-1}. This rate was calculated from experimentally determined rate constants (Wahner & Zetzsch, 1983) which were weighted by the frequency of detection for each isomer (o-,m- and p-dichlorobenzene) found

during a previous study in the region (Eastern Research Group & Sage Environmental Consulting, 2011). Three additional scenarios involving perturbations of the reaction rate are included where k_{33} was multiplied by 10, 10^2 and 10^3 (k_{33}^{S1}, k_{33}^{S2}, k_{33}^{S3}). This was done in order to test the difference in the spatial and temporal patterns of HCl production resulting from various values of reaction rate. Therefore, four variations of the rate (k_{33}^{base}, k_{33}^{S1}, k_{33}^{S2}, k_{33}^{S3}) of the reaction were carried out for each emissions scaling ratio. This resulted in varying patterns of concentrations for markers of reactive chlorine chemistry (e.g., HCl). Both the magnitude and temporal pattern were affected. These results are discussed further in Section 6.3.

In addition to the constant, 24-hour day^{-1}, 7 day $week^{-1}$ emission pattern used as a base case, a more dynamic pattern was tested. A temporal pattern was created such that the emissions started between 5-6 AM, peaking at 11-12 PM, and returned to zero by 8 PM. This emissions pattern was intended to simulate condensate breathing losses from storage tanks or losses from other storage methods. Emissions of this pattern were then combined with the constant 24 hour hourly emissions to create the emissions pattern for the second chlorocarbon inventory. The emissions were combined such that 50 % of the total emissions were from each temporal pattern. That is, 50% constant, 24-hour emissions and 50% from emissions that peaked at noon. Results of modeling scenarios from both the base case and alternate emissions patterns are compared in Section 6-3.

To get a baseline for the prevalence of reactive atmospheric chlorine chemistry in the region, a base case anthropogenic chlorine emissions inventory for the DFW region was used (Faxon & Allen, 2014b). This included inorganic chlorine emissions from swimming pools, tap water usage, water and wastewater treatment and industrial point sources in the region (Faxon & Allen, 2014b), similar to a previously developed chlorine emissions inventory for Houston, TX (S Chang et al., 2001).

Additionally, a modeling scenario involving no anthropogenic chlorine emissions was performed in order to assess the possibility of long range sea salt transport into the DFW region. For this scenario,

a PM inventory that included sea salt emissions from the Gulf of Mexico was used (H. A. Simon, 2008a). This also includes particulate chloride sources that are inland, but which are orders of magnitude smaller than the sea salt source in the Gulf of Mexico. A test case was included as a sensitivity analysis wherein sea salt emissions from the Gulf were doubled in order to investigate whether chlorine and chloride concentrations in the region were sensitive to the strengths of marine sea salt sources. Modeling of these base case anthropogenic and natural inventories was used to create a baseline against which the results of the chlorinated hydrocarbon emissions scenarios could be tested.

6.3. Results

6.3.1 Modeling Results for Chlorinated Hydrocarbon Emissions Scenarios: CLTR

When chlorinated organic emissions were simulated as a non-reactive tracer (CLTR), average modeled concentrations in the Eagle Mountain Lake grid cell peaked early in the day and did not correspond to observed diurnal patterns of HCl. Figures 6-7 and 6-8 show a 5-day time series of CLTR concentrations compared to observed HCl concentrations (Griffin et al., 2011) and a comparison of hourly average concentrations for the entire modeling episode, respectively.

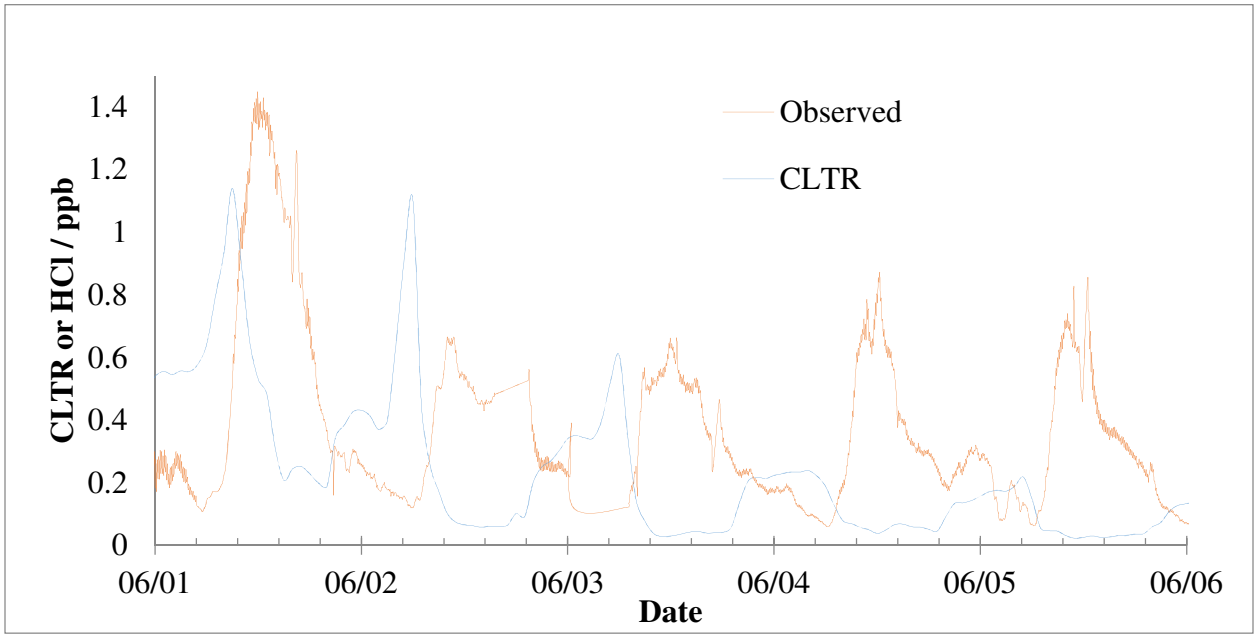

Figure 6-7: A time series from June 1 – June 6 comparing modeled average CLTR concentrations in the EML grid cell and observed HCl concentrations from the EML measurement site.

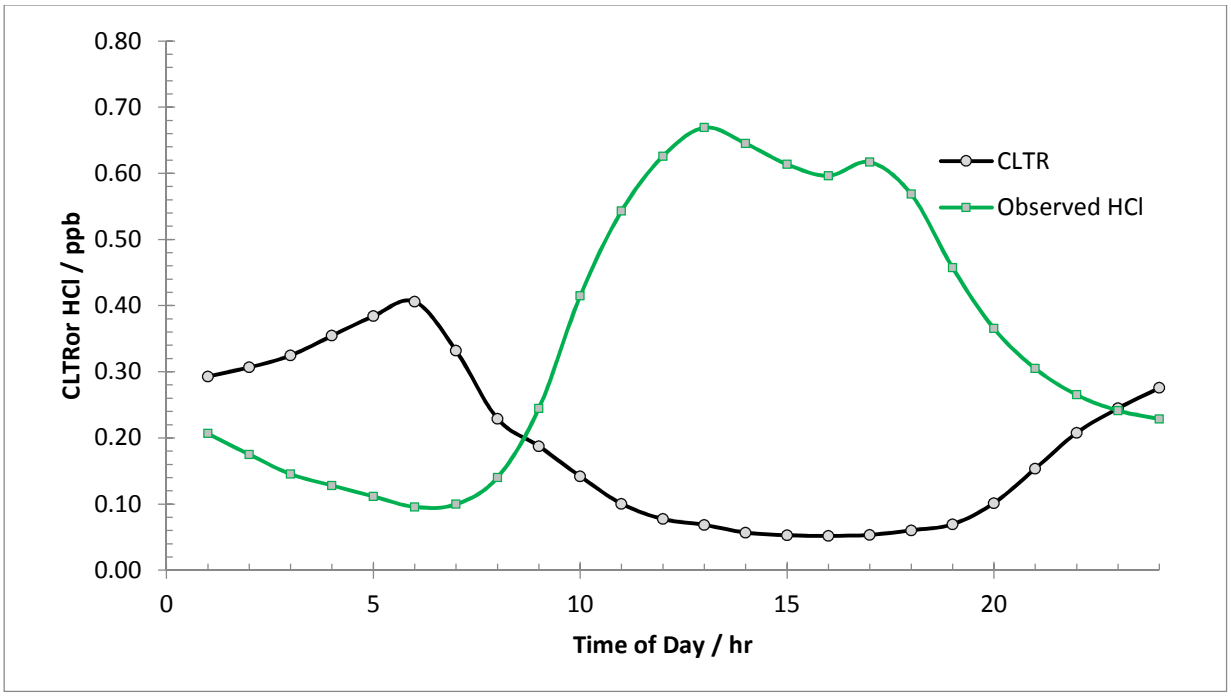

Figure 6-8: Comparison between hourly average concentrations for observed HCl concentrations and modeled CLTR concentrations for the entire modeling period.

Figure 6-7 demonstrates a consistent pattern of peak concentrations in the early morning which precede the timing of the observed concentrations. This pattern is apparent over the entire course of the month, as evidenced by comparing the hourly averages for the entire episode (Figure 6-8). Due to this inconsistency in timing, direct emission of HCl, as modeled by the non-reactive tracer is ruled out as a possibility.

6.3.2. Modeling Results for Direct Cl_2 and HOCl Emissions Scenarios

In addition to the non-reactive tracer emissions test case, scenarios involving the direct emissions of photolyzable inorganic species (Cl_2 and HOCl) from natural gas production activities were tested. These two test cases were devised in order examine HCl concentrations from direct emission and photochemical reaction of these species and to determine whether or not their direct emission was a viable hypothesis for explaining observations at Eagle Mountain Lake. Emissions inventories were created in a manner analogous to the methods used for the chlorinated hydrocarbon species, CLV1 and the tracer species, CLTR. Since both HOCl and Cl_2 photolyze rapidly after sunrise, either scenario

would likely produce similar results with respect to HCl production. Figure 6-9 shows an 8-day time series of HCl concentrations at the Eagle Mountain Lake grid cell from the modeling episode compared to observations (Griffin et al., 2011).

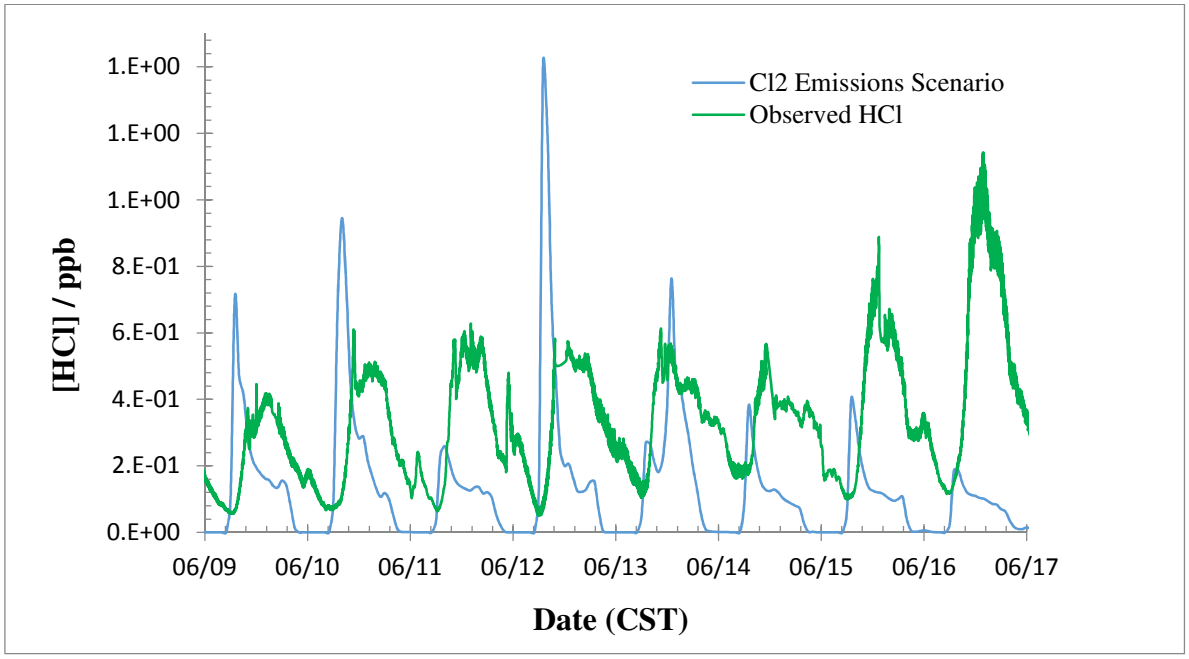

Figure 6-9: Comparison of observed HCl concentrations to modeled concentrations when using an emissions inventory including direct emissions of Cl_2 from natural gas production at a Cl_2 to VOC scaling ratio of 2.0.

It can be seen from the time series In Figure 6-9 that HCl concentrations resulting from direct Cl_2 emissions peak earlier than those that were observed. This same difference can also clearly be seen in the diurnal concentration patterns in Figure 6-10.

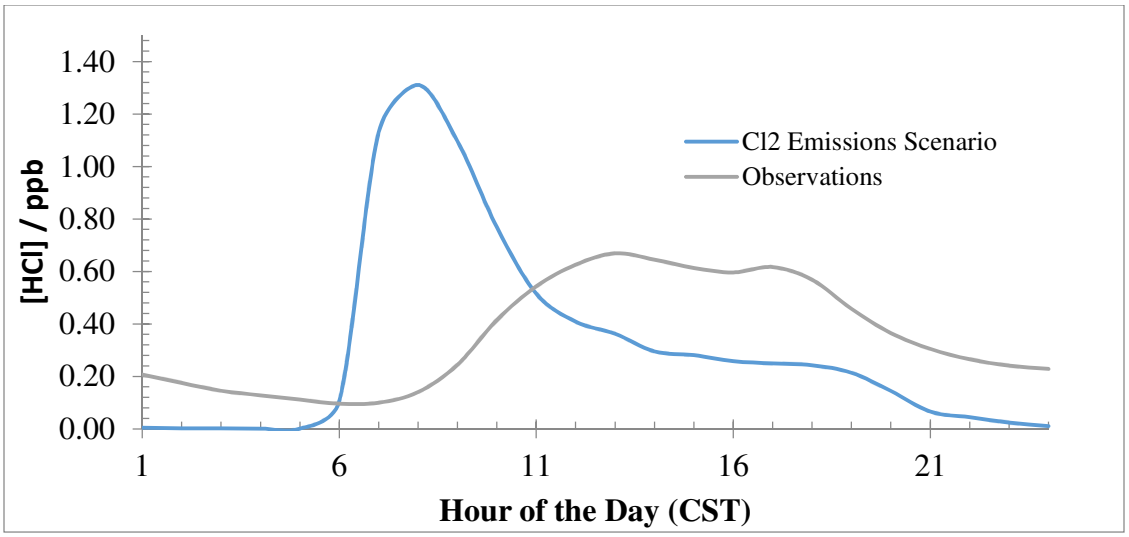

Figure 6-10: Hourly HCl concentrations averaged over the entire modeling episode compared to hourly average concentrations from observations (Griffin et al., 2011).

Due to the fact that resulting peak HCl concentrations in the EML grid cell peak very early in the morning (7:30 – 9:00 AM), a scenario where direct Cl_2 emissions produce the observed HCl is unlikely. The rapid rise in HCl concentrations in the early morning hours is due to the rapid photolysis of Cl_2 at sunrise. The rapid photolysis thus results in concentrations that are high enough in magnitude, on average, to explain observed HCl concentrations. However, the lack of a temporal match to the observations rules out this scenario as a likely possibility.

6.3.3. Modeling Results for Chlorinated Hydrocarbon Emissions Scenarios: CLV1

Emissions inputs with spatial and temporal patterns identical to those of CLTR, as represented in Figure 6-6, were developed for CLV1 and used in a modeling episode analogous to that described in the previous section. In addition to variations in scaling ratios for total emissions magnitudes, the rate of reaction 33 was varied between simulations as described in Section 6-2. It was determined that a rate of at least 10 times the base value (k_{33}^{S1}) was necessary for the reaction to produce $Cl^{\bullet}$ at the timing and magnitude necessary to produce HCl concentrations at EML similar to those that were observed. Figure 6-11 shows how the average daily pattern of HCl concentrations change as the value of k_{33} is increased. All scenarios shown in Figure 6-11 are from emissions inputs prepared with a scaling ratio of 11.2.

From this Figure, it appears that after the rate is increased past a certain value, the reaction proceeds too quickly, producing, on average, peak concentrations that occur too early in the day (9:00 – 9:30 AM).

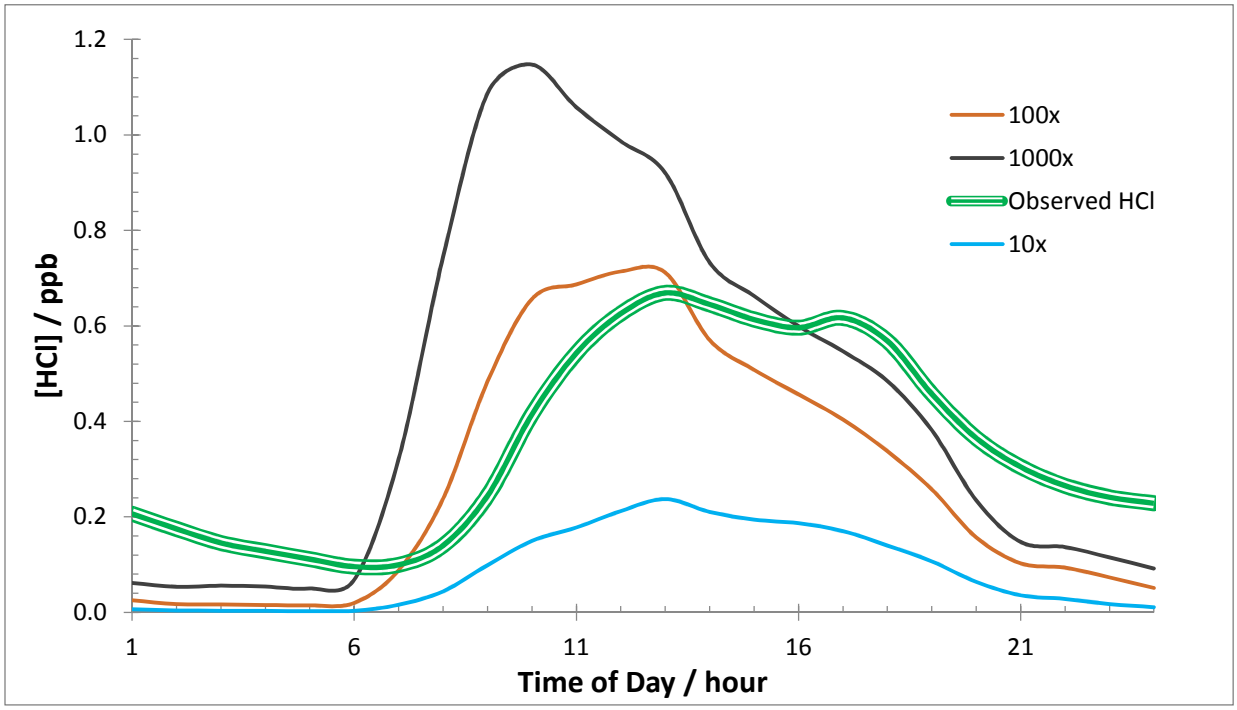

Figure 6-11. Comparison of observed HCl concentrations to episode average concentrations for modeling scenarios (scaling factor = 11.2) where k_{33} was varied from 3.39 x (10^{-12} – 10^{-10}) cm^3 $molecule^{-1}$ s^{-1} (i.e., 10x – 1000 times the rate of the OH + DCB reaction).

Model simulations were carried out for scenarios with emissions scaling factors of 0.7, 1.4, 2.8, 5.6, 8.4, 11.2, 22.4 and 44.8. Each emissions scenario was examined with reaction rates k_{33}^{base}, k_{33}^{S1}, k_{33}^{S2} and k_{33}^{S3}. As can be seen in Figure 6-11, k_{33}^{S1} resulted in the best average temporal pattern match with respect to observed HCl levels, and scenarios with the higher rates of reaction lead to peak concentrations earlier in the morning which did not match as well. However, the amount of chlorine released via reaction 33 at this rate was significantly lower than from k_{33}^{S2} and k_{33}^{S3} scenarios. Figure 6-12 shows additional representative time series (6/1 – 6/8) for several simulations using different emissions scaling factors. The point of these comparisons is to illustrate day-to-day variability, rather than to match specific days, since the modeling and observations are from different years. A representative scenario with each value of the rate constant was chosen to facilitate comparison of how

the CLV1 + $OH^{\bullet}$ reaction rate affected temporal patterns of HCl on a day-to-day basis during the simulations. Observed HCl concentrations are also included in the plot to serve as a point of reference. Note that the temporal lag between peaks in scenarios with lower rates of reaction is more pronounced on some days. This may be due day-to-day differences in local meteorology that caused peak concentrations to result more from transport from other grid cells rather than reaction within or near the Eagle Mountain Lake grid cell itself.

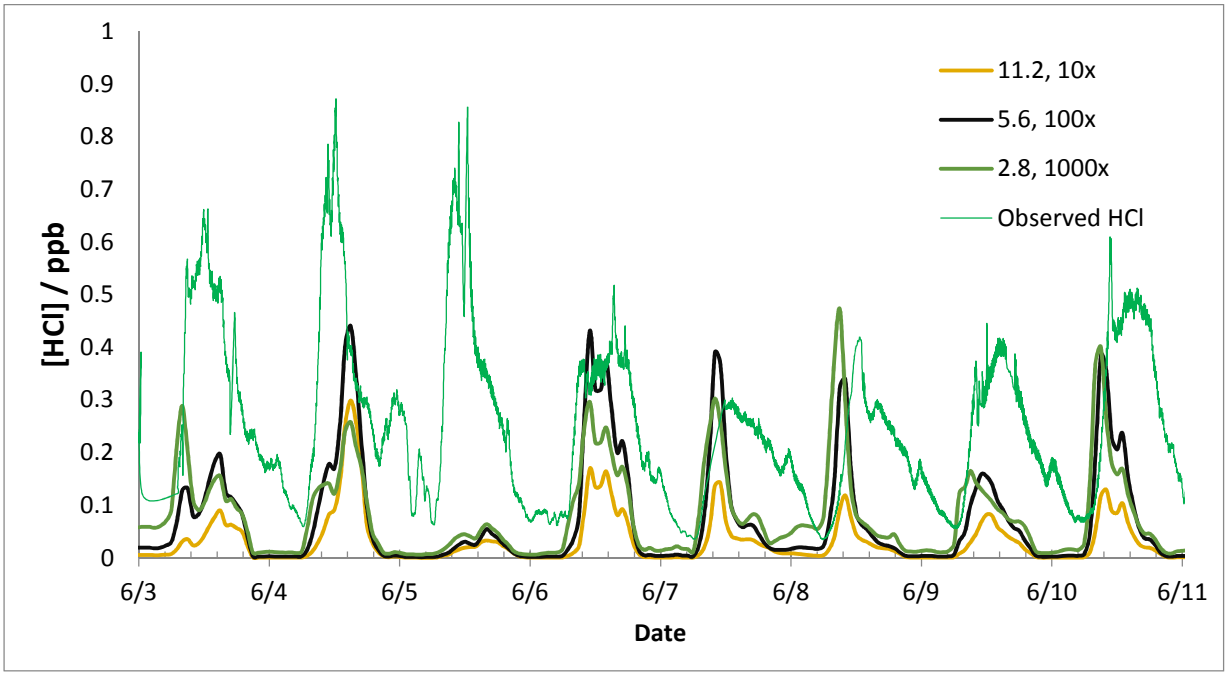

Figure 6-12. Representative time series comparing 3 scenarios using various emissions scaling factors and values for k_{33} was varied from 3.39 x (10^{-12} – 10^{-10}) cm^3 $molecule^{-1}$ s^{-1}.

In order to compensate for lower chlorine production resulting from the lower reaction rate, k_{33}^{S1}, higher emissions scaling factors had to be used. As can be seen in Figure 6-13, when elevated emissions scaling factors were tested, a scaling factor of 44.8 was found to be the threshold at which the episode hourly average concentrations closely matched those of the observed concentrations.

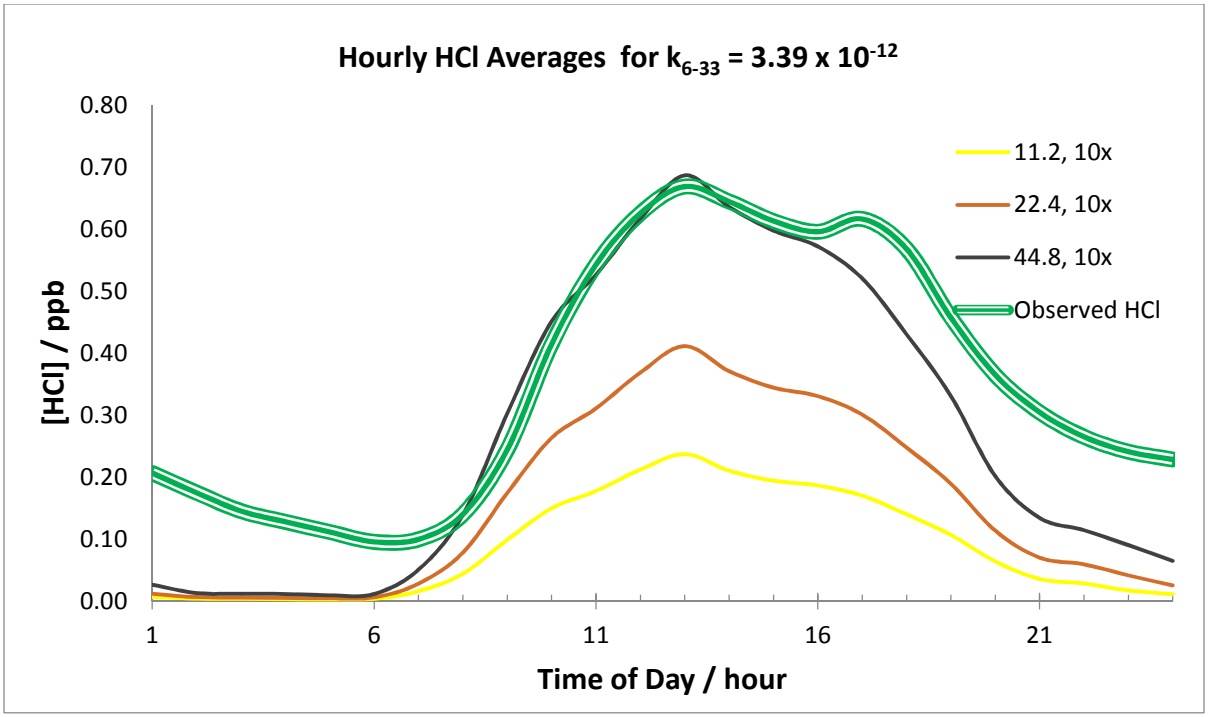

Figure 6-13. Episode hourly averages for 10x scenarios most closely matching the average daily pattern of observed HCl concentrations.

6.3.4. Modeling results for CLV1 Emissions: Alternate Emissions Patterns

A second set of scenarios was modeled using chlorinated organic emissions inventories with temporal patterns partially modeled after condensate tank breathing losses. The results were similar to those from the previous section but with several differences. One notable difference is observable in the fact that the scenarios with higher values of k_{33} (e.g., k_{33}^{S2} and k_{33}^{S3}) produce temporal concentration patterns that are more consistent with the observed patterns. This is likely because 50% of the emissions occur later in the day and thus do not react to produce HCl too early. Figure 6-14 demonstrates the resulting episode 1-hour averages for several scenarios when the breathing loss emissions pattern is used. These results can be compared to Figures 6-11 and 6-12 for insight on how the two different emissions patterns affect average HCl concentrations on an hour by hour basis.

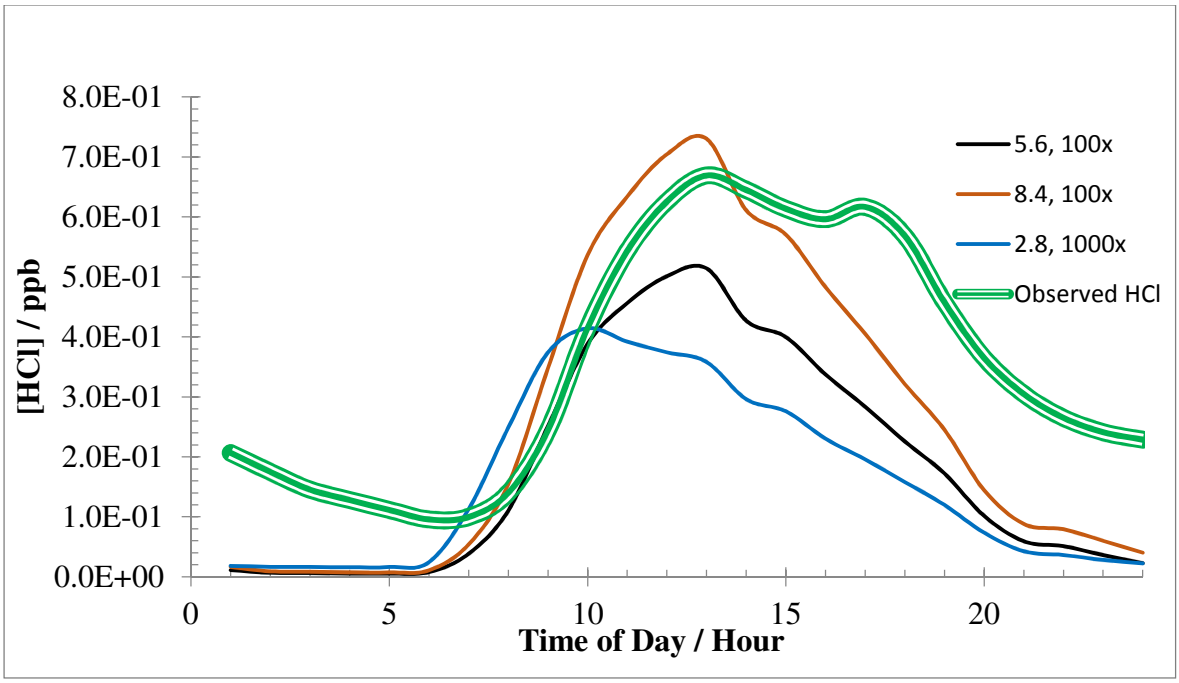

Figure 6-14. Comparison of the observed episode average HCl pattern to modeled average concentrations using the breathing loss emissions pattern for scaling ratios of 2.8, 5.6 and 8.4.

It should be noted from Figure 6-14 that the 1000x (k_{33}^{S3}) scenario still peaks slightly early on average. Additionally, the average peak shape is more pronounced due to the fact that emissions are released more rapidly towards the middle of the day. Concerning day-to-day time series, relatively consistent correlation of modeled HCl concentrations to the observations were found for scenarios using an emissions scaling factor of 5.6 with the k_{33}^{S2} rate constant. Peak concentrations were under predicted on some days, but the timing of the peaks was generally consistent with those observed. A representative time series demonstrating this is shown in Figure 6-15.

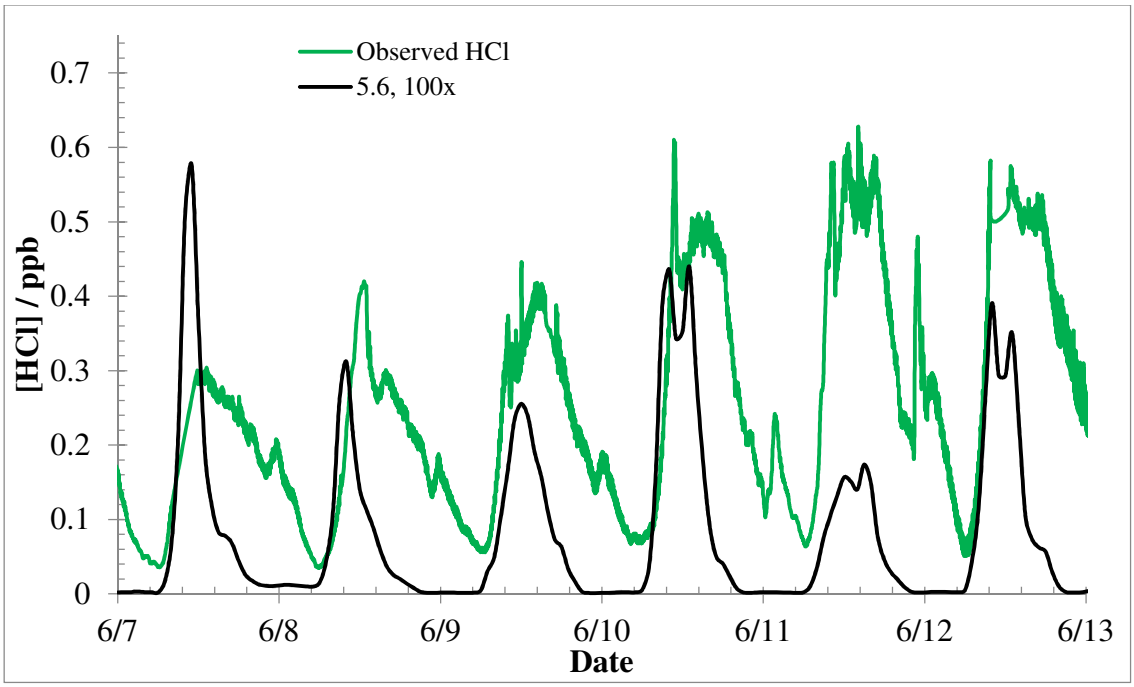

Figure 6-15. Observed HCl concentrations compared to a six day time series for a scenario with a scaling factor of 5.6 and a k_{33} value of 3.39 x 10^{-11} cm^3 $molecule^{-1}$ s^{-1}.

Slightly higher concentrations were obtained from an analogous scenario using an emissions scaling factor of 8.4. A factor of 5.6 is equivalent to emissions of approximately 80 metric tons of chlorine as dichlorinated hydrocarbons, an emission rate which is nearly an order of magnitude larger than the next largest anthropogenic chlorine source in the region (Table 3-1). This indicates a large un-inventoried source of chlorinated organics, and the plausibility of such a large chlorine source will be discussed in Section 6-4.

6.3.6. Long-Range Sea Salt Transport into the Dallas-Ft. Worth Region as a Source of Atomic Chlorine Precursors.

The results of simulations with the base PM inventory indicate that transport of particulate chloride from sea salt and subsequent volatilization of the chloride into gas phase HCl is insignificant with respect to concentrations in the EML grid cell. In these modeling scenarios, only loss mechanism for particulate chloride was deposition (wet and dry). Additionally, gas-particle partitioning of particulate species, including chloride, was treated using the ISORROPIA thermodynamic module (Nenes, Pandis, & Pilinis, 1998; Nenes, 1998). The largest concentration of HCl resulting at EML was

0.2 ppb. However, concentration peaks on most days were at or below 0.1 ppb, with most days having peak HCl concentrations below 2.5 x 10^{-2} ppb. Daily peak concentrations of particulate chloride were typically on the order of 1 x 10^{-3} ppb. Figure 6-16 shows the entire time series of particulate Cl^- and gas phase HCl concentrations at EML resulting from the CAMx simulations.

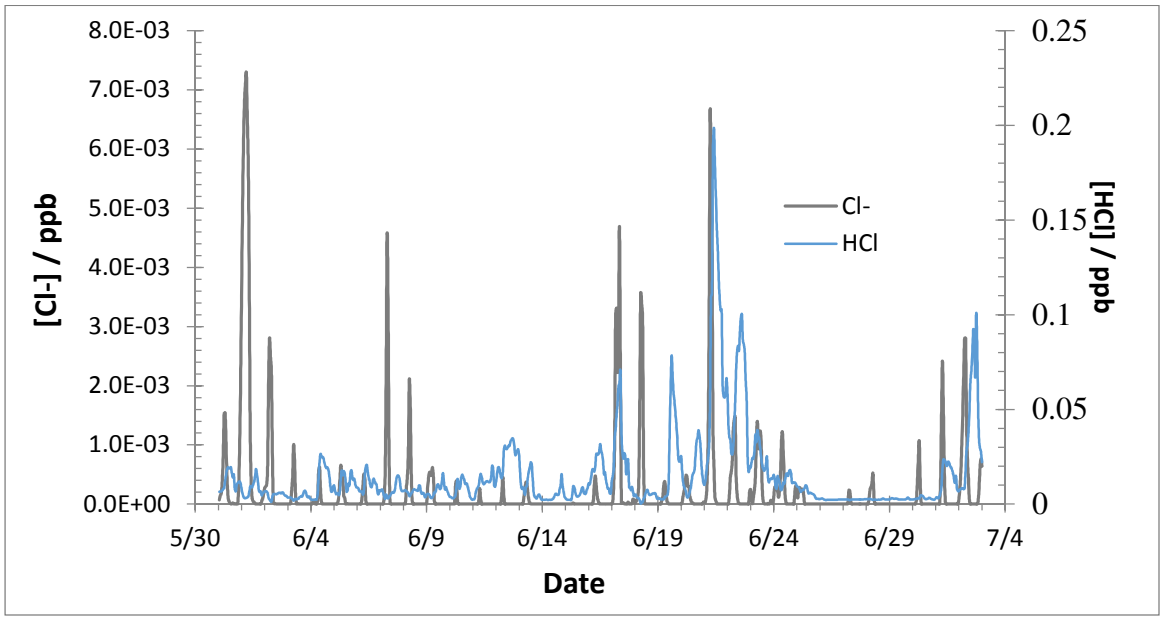

Figure 6-16: Time series of particulate chloride and HCl average concentrations in the 4km grid cell containing the location of the Eagle Mountain Lake measurement site.

A doubling of the sea salt inventory did not result in a doubling of either particulate chloride or HCl concentrations in the Eagle Mountain Lake grid cell. The increases from these extra emissions were most pronounced on days that had the largest concentrations in the base case scenario (6/21 and 7/2). Figure 6-17 shows a comparison of HCl concentrations between the base case scenario and a scenario in which particulate chloride emissions from sea salt were doubled. Figure 6-18 shows the same comparison for particulate chloride.

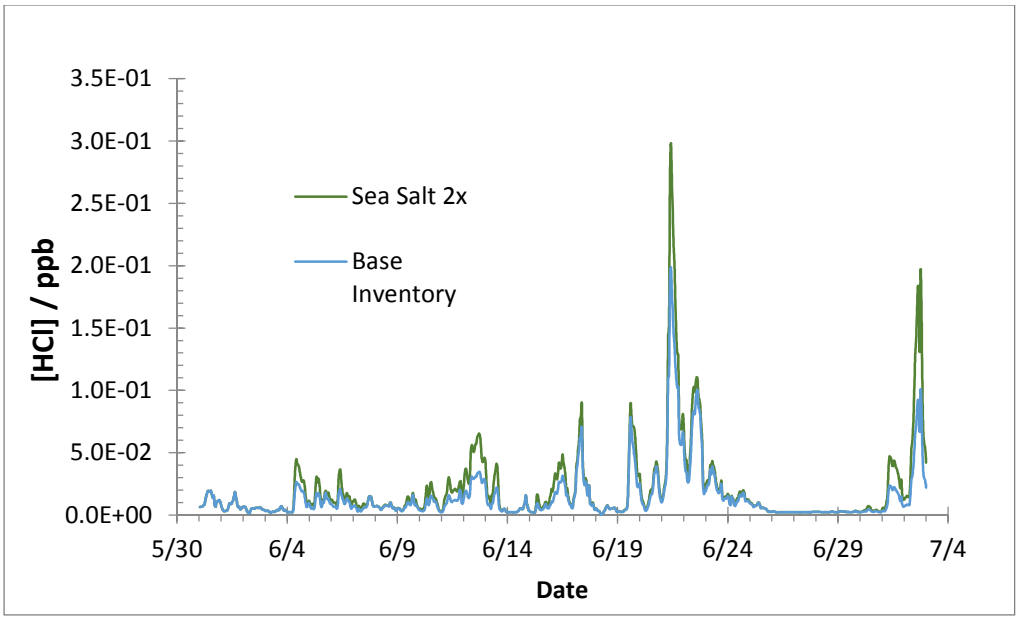

Figure 6-17: Time series of average HCl concentrations in the Eagle Mountain Lake Grid cell for the base PM inventory and a scenario wherein sea salt emissions in the Gulf of Mexico were doubled.

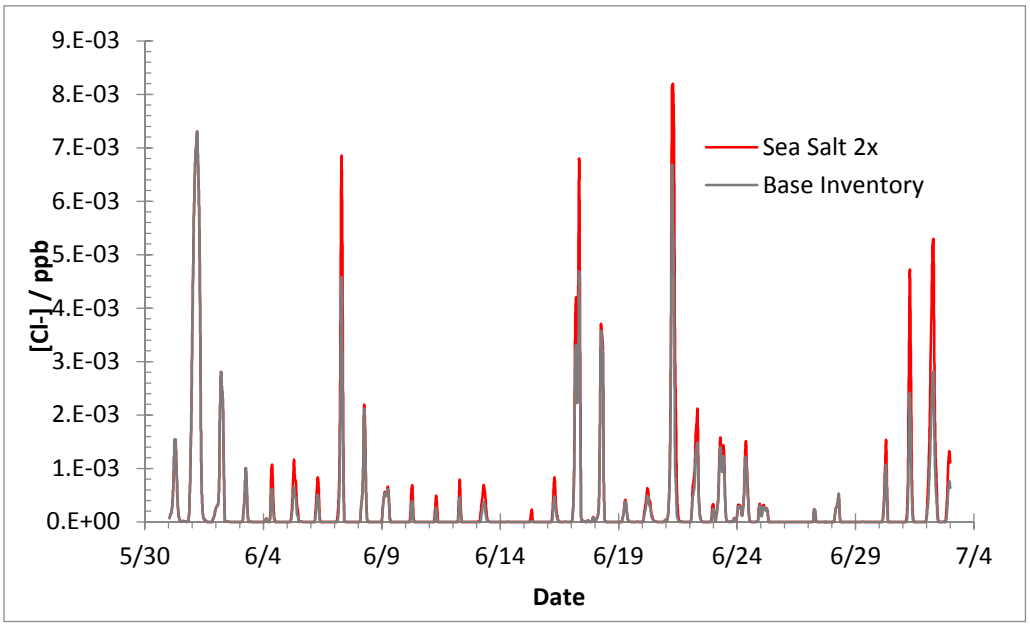

Figure 6-18: Time series of average particulate chloride concentrations in the Eagle Mountain Lake Grid cell for the base PM inventory and a scenario wherein sea salt emissions in the Gulf of Mexico were doubled.

6.4. Discussion

Results from modeling of the base case anthropogenic inventory (Chapter 3, Section 3.1) indicate that the combined emissions of industrial point sources, swimming pool chlorination, tap water usage, and wastewater treatment are insufficient to account for the observed HCl concentrations at EML.

However, it cannot be ruled out that some of the HCl comes from these sources, and a comparison of the diurnal patterns of modeled concentrations and observations reveals that the timing of daily peak HCl concentrations from the anthropogenic sources correlates well with the observations, albeit at a much lower magnitude.

Results also indicate that the emissions scenarios involving chlorinated organics which have been presented here are capable of providing HCl concentration patterns that match observations with respect to both magnitude and timing. However, the magnitudes of emissions necessary to create such patterns of HCl are large, ranging from 2-3 orders of magnitude higher than the next largest anthropogenic chlorine source in the region (Faxon & Allen, 2014b). Shale gas production operations are not typical of most urban areas and could possibly lead to increases in anthropogenic emissions of these species into the atmosphere.

However, one complicating factor is that it is difficult to imply such large sources of chlorinated organics as the source of the observed HCl in the absence of further direct observational evidence of elevated emissions of these compounds and identification of a source. Estimates (Faxon & Allen, 2014b) indicate that enough chloride can potentially be present in hydraulic fracturing fluid and flowback waters, and conservative calculations estimate that a Cl^- reservoir on the order of 10^2 metric tons could be created from the flow back water of a single well. However, there is also the issue of the absence of a known mechanism for the volatilization of this chloride necessary to account for the timing and order of magnitude of observed HCl concentrations from this source. Additionally, information about an exact gas phase chlorinated organic species and reaction mechanism are necessary if such a source is able to explain the observations.

In the absence of knowledge of the specific mechanism for organic chloride formation and volatilization, the current work serves as an exercise in bounding the values of necessary source strengths and chlorocarbon reactivity required for chlorinated hydrocarbon emissions to be the source of

the observed HCl. The largest scaling ratio used for chlorocarbon emissions (44.8) is equivalent to emissions on the order of 630 metric tons day^{-1} of chlorine as dichlorinated hydrocarbons, a magnitude which is nearly two orders of magnitude larger than the next largest anthropogenic source (Faxon & Allen, 2014b). Modeling of this emissions ratio in a constant, 24-hour emissions pattern resulted in HCl concentrations at EML that most matched the observations (Figure 6-13). However, if the alternate emissions scenario, which peaks during mid-day, is used, lower scaling ratios and emissions are necessary to achieve similar results. If indeed the source of $Cl^{\bullet}$ and subsequently, HCl, is linked to the photochemical cycle and a reaction of $OH^{\bullet}$, the overall rate of reactions such as those represented by the reaction surrogate CLV1 (reaction 33) will play a crucial role in the timing of resulting HCl concentrations. The observed timing of HCl concentration peaks occurring at the EML site in 2011 (Griffin et al., 2011) indicate that the mechanism is likely linked to the photochemical cycle. It is likely that an actual source of chlorinated hydrocarbons would consist of multiple species, each with separate volatilization rates and reactivities. In this case, a more complex suite of mechanism could be at play. However, as a first approximation, the modeling of reaction 33 in this work indicates that for such a scenario, the average reactivity of the chlorinated hydrocarbons with $OH^{\bullet}$ (k_{33}) likely lies in the range of $3.9 \times 10^{-12} – 3.9 \times 10^{-11}$ cm^3 $molecules^{-1}$ s^{-1}.

Regarding long range sea salt transport, CAMx modeling results indicate that particulate chloride emissions in the region from sea salt and other sources were found to be capable, in some instances, of contributing peak HCl concentrations reaching up to 0.1 ppb in the 4 km grid cell containing Eagle Mountain Lake. However, peak concentrations of this magnitude only occurred three times during the modeling episode and peak concentrations on the vast majority of the remaining days were on the order of 10^{-2} ppb (Figure 6-16). Thus, the results also suggest that sea salt is an unlikely source for explaining observed ppb-level HCl concentrations that occur on a daily basis. The lack of a doubling in either particulate chloride or HCl concentrations from a doubling of the particulate chloride

emissions inventory in the Gulf of Mexico indicates that long range sea salt transport from the Gulf is not the predominant source of either species in the Dallas-Ft. Worth region.

6.5. Conclusions

Overall, the results of this work indicate that well-known sources of reactive chlorine such as typical anthropogenic emissions sources or long range sea salt transport are unable to explain the HCl observations that were made at the EML site. The modeled average temporal pattern in HCl concentrations resulting from standard anthropogenic sources (industrial point sources, swimming pool chlorination, etc.) corresponds well to observations. Though it is possible that such sources contributed to the observed HCl, they are not capable of explaining a major proportion of the observed magnitude.

HCl resulting from the reactions of chlorinated hydrocarbons emitted in the region remains a possible scenario that could explain the observations. For this scenario to be possible, an average reactivity of emitted chlorocarbons with the hydroxyl radical must lie in the range of $3.9 \times 10^{-12} - 3.9 \times 10^{-11}$ cm^3 $molecules^{-1}$ s^{-1}. Additionally, a region-wide source of 150 metric tons chlorocarbon day^{-1} (as modeled by dichlorobenzene), is required to account for the magnitude of HCl observed at the EML site. However, further evidence is needed to support this hypothesis. Two areas of further study would be particularly useful. First, additional observations of any chlorinated hydrocarbons in the region would be helpful and are recommended as goals for future field studies. Additional measurements of gas phase chlorine species, including HCl, would also aid in providing an explanation and expanding the observations made at EML into a region-wide context. Second, the study of possible mechanisms leading to the formation and volatilization of chlorinated hydrocarbons from the processes involved in natural gas production would likely be fruitful. Such work would allow for a more accurate formulation of a route to gas phase $Cl^{\bullet}$ production and reinforce the possible explanations put forward in this work.

Chapter 7: Summary of Conclusions and Recommendations for Future Work

The work contained in this dissertation utilized modeling and experiments to investigate gaps in the understanding of the links between field observations of chlorine species, known emissions sources, and condensed chlorine reaction mechanisms that are used in models. Major findings and recommendations for future work are listed below.

Key Findings

- Maximum overnight $ClNO_2$ formation from the heterogeneous reaction of N_2O_5 on chloride aerosols is approximately 4.0 ppb, peaking in the early morning hours and dropping rapidly after sunrise. This calculation was made for conditions similar to southeast Texas during the summer.
- The maximum impact of heterogeneous $ClNO_2$ chemistry on peak O_3 concentrations ranges - 10.5% - 27%, relative to a base case scenario with no heterogeneous chemistry occurring. This range of impact is applicable when considering the chemistry alone and neglecting factors such as mass transport or dilution.
- Decreases in maximum O_3 concentrations due to $ClNO_2$ chemistry result when Y_{ClNO2} is low. This is due to the fact that the reactive uptake of N_2O_5 with a low yield of $ClNO_2$ serves as a NO_x sink, thus reducing the amount of gas phase NO_x that can participate in the O_3 production cycle.
- The presence of significant concentrations of VOCs in an air mass where heterogeneous $ClNO_2$ production is occurring can enhance O_3 production rates and maximum O_3 concentrations. However, in the presence of VOCs that are highly reactive towards NO_3, such as *t*-2-butene, little enhancement in O_3 production is expected.
- When modeled under similar meteorological conditions, inventoried gas phase atomic chlorine precursor emissions from known anthropogenic sources in the 19-county Dallas-Ft. Worth region are not capable of explaining elevated concentrations of HCl that were detected at the Eagle

Mountain Lake Monitoring Site in June, 2011. The average daily gap between observed and inventoried chlorine at the location of the observations is approximately 0.5 ppb.

- Chlorinated VOC emissions from natural gas production activities are capable of reproducing both the average diurnal pattern and magnitude of HCl concentrations that were observed at Eagle Mountain Lake. However, the magnitude of emissions required is on the order of 10^2 metric tons Cl day^{-1}, larger than other inventoried anthropogenic sources in the region.
- The rate of chlorinated VOC emissions necessary to explain the observations at Eagle Mountain Lake is highly sensitive to the rate of reaction between hydroxyl radicals and the chlorinated VOC. The best matches to observed diurnal patterns of HCl were obtained from simulations in which this rate of reaction was on the order of $10^{-12} – 10^{-11}$ cm^3 $molecule^{-1}$ s^{-1}
- Heterogeneous Cl_2 production in the presence of O_3 and particulate chloride was found in this work to occur on NH_4Cl particles in addition to its occurrence on NaCl particles as cited in previous studies.
- Heterogeneous Cl_2 production from particulate chloride was observed to occur in dry, low relative humidity conditions. Previous studies had suggested that Cl_2 production would only proceed in high RH conditions, where the particles are deliquesced.
- The observed range of the reactive uptake coefficient for the heterogeneous reaction of O_3 on NH_4Cl particles was $(0.01 – 2.67) \times 10^{-3}$.
- The observed rate of the heterogeneous reactive uptake for O_3 on NH_4Cl particles was observed to have a 2.5-fold increase in the presence of elevated relative humidity (75-80%).
- The addition of SOA to NH_4Cl particles reduces the observed reactive uptake coefficient for the heterogeneous OH mechanism by over an order of magnitude relative to a base case scenario involving dry, pure NH_4Cl particles. The suppressing effect of SOA is observed even in the

presence of elevated relative humidity, which otherwise leads to an increase in the observed reactive uptake.

- The production of Cl_2 was also observed for non-chloride particles ($(NH_4)_2SO_4$) when gas phase HCl, O_3 and HOOH were present. This was observed for both high NO_x and low NO_x conditions. If it is assumed that the mechanism of production is the same as the hydroxyl-radical mediated heterogeneous mechanism proposed for chloride particles, these scenarios resulted in the largest observed values of the reactive uptake.

Contributions from this Work

- The experimental work described here was the first to investigate heterogeneous Cl_2 production on NH_4Cl aerosols.
- The experimental work described here was the first to observe heterogeneous Cl_2 production from particulate chloride in dry (~5% RH) conditions.
- The experimental work described in this thesis was the first to investigate the impact of organic aerosol components on the efficacy of heterogeneous Cl_2 production from particulate chloride.
- Work done within this dissertation identified the major emissions sources of atomic chlorine precursors in the Dallas-Ft. Worth area and elucidated the gap between observed concentrations of HCl and inventory source strengths.
- This work was the first to bound values for the absolute potential impacts of $ClNO_2$ on O_3 production resulting from changes in the heterogeneous rate parameters for $ClNO_2$ production.
- A range of reactive uptake values for the heterogeneous production of Cl_2 from particulate chloride in the presence of O_3 was determined for the first time in this work.
- A comprehensive review of the literature pertaining to urban atmospheric chlorine chemistry was completed. This review compiled information on the following:
    - Impacts on tropospheric O_3 production from atmospheric Cl chemistry

- Homogeneous and heterogeneous reaction kinetics of chlorine radicals and related species
- Emissions inventories of atmospheric chlorine species, both organic and inorganic
- Observational evidence of inorganic atomic chlorine precursors
- Identification of areas where further work is still needed.

Recommendations for Future Work

- Additional observations of gas phase HCl, specifically within the region in and surrounding Dallas-Ft. Worth, would provide a larger context for previous observations and the modeling studies performed in this work.
- Further investigation of pathways for the production of chlorinated VOCs from the conditions present during hydraulic fracturing activities would be useful in extending and refining the hypothesis of chlorinated VOC emissions from natural gas production as an explanation for elevated HCl concentrations in the DFW region.
- Determination of products resulting from the reaction of OH and chlorinated VOCs produced from the conditions used during hydraulic fracturing activities would strengthen the results presented in this work. Additionally, measurement of rate constants for these same reactions would be useful.
- Experimental investigation of the heterogeneous chlorine production mechanism on NaCl in the conditions tested here would be useful for a comparison of the efficiency of the mechanism on differing chloride salts. In particular, scenarios with low relative humidity and those involving the addition of SOA to the particle phase would fill in gaps left by previous studies.

Appendix A – Supporting Materials for "Chlorine Chemistry in Urban Atmospheres: A Review"

C. B. Faxon[A,B], *D. T. Allen*[A]
[A]Center for Energy and Environmental Resources, University of Texas, M/C 27100, 10100, Burnet Road, Austin, TX 78758
[B]Corresponding author. Email: cfax@utexas.edu

A.1 Sensitivity of predicted ozone and $ClNO_2$ concentrations to rate parameter estimates for the heterogeneous $ClNO_2$ production mechanism

Simulation Methods

The SAPRC software developed by Dr. William Carter at UC Riverside was used in the box modeling for the parameter analysis. The CB05 condensed photochemical mechanism (G Z Whitten et al., 1980) was modified to include the parameterizations of the heterogeneous mechanism. Simulations were run from sunset to sunset for a 24-hour period. Initial conditions included ozone and NO_x concentrations of 50 and 20 ppbv, respectively. The heterogeneous mechanism was modeled as a pseudo first order reactions by the expressions shown below.

$$-\frac{d[N_2O_5]}{dt} = \frac{1}{4}\gamma\omega A[N_2O_5] \qquad \text{(Reaction A-1)}$$

$$\frac{d[ClNO_2]}{dt} = \frac{1}{4}\gamma\omega Y_{ClNO_2} A[N_2O_5] \qquad \text{(Reaction A-2)}$$

VOC Surrogate Mixture

The mixture of VOCs was a surrogate mixture formulated to represent an average urban VOC mixture. The formulation was based on EPA data collected from 1985 to1988 in 66 U.S. cities and has been used extensively since in both measurement and modeling studies. The 182 species represented in this dataset were condensed to the nine representative reactive species present in the surrogate mixture. The condensed mixture represents the same overall reactivity, per ppmv carbon (ppmC), as the original

mixture. An "Inert/Lost Carbon" category is included to represent the compounds that were removed due to low reactivities or condensed into smaller representative species. Table A-1 shows the constituents of the mixture (J. Stutz et al., 1998).

Table A-1. Surrogate VOC Mixture Composition

Species	CB05 Species	ppb $ppmC^{-1}$
n-Butane	4 PAR	70.7
n-Octane	7 PAR, 1 NR	22.3
Ethylene	ETH	13.4
Propene	1 PAR, 1 OLE	10.4
t-2-Butene	IOLE	10.4
Toluene	TOL	13.3
m-Xylene	XYL	16.3
Formaldehyde	FORM	7.9
Acetaldehyde	ALD2	7.6
Inert/Lost Carbon	NR	193.1

Parameter Value Ranges

The reactive uptake was varied between 0 and 0.038, an upper limit determined from the literature (Aldener et al., 2006; Griffin et al., 2011; Schweitzer et al., 1998; Thornton & Abbatt, 2005) Particle surface area was approximated by assuming a trimodal particle distribution, with 30%, 50%, and 20% (by mass) having average diameters of 0.1, 0.5 and 1.0 μm, respectively. In the simulations presented here, an aerosol concentration of 15 μg m^{-3} was used. $ClNO_2$ yield was varied between zero and one to correspond with the wide range of yield values reported in the literature (Brown et al., 2009; Frenzel et al., 1998; Griffin et al., 2011; E. M. Knipping, 2000b; Schweitzer et al., 1998; Thornton & Abbatt, 2005). VOC levels were varied between 0 – 1000 ppbC with a value of 300 ppbC considered to be a level representing a moderate urban concentration of VOCs.

Results and Discussion

The heterogeneous N_2O_5-$ClNO_2$ mechanism is able to reproduce $ClNO_2$ concentrations that have been observed in the environment within parameter ranges used in this study. Depending on the

combination of heterogeneous parameters, VOCs, and NO_x, the mechanism contributed to both peak ozone reduction as well as peak ozone increases. The range was a -10.5% to 27% change in peak O_3 concentrations relative to the base case scenario containing no heterogeneous chemistry. The decreases in ozone typically resulted from low values of $ClNO_2$ yield (0-15%) depending on the amount and types of VOCs present). This was likely due to a higher conversion rate of NO_x into nitric acid at lower $ClNO_2$ yield values, which simultaneously reduced the amount of $ClNO_2$ produced. Combinations of yields above 25% and reactive uptake coefficients greater than zero resulted in increases in peak ozone levels.

The effect of changing base VOC concentrations was also examined. Four scenarios with differing initial VOC concentrations were used: (1) 0 ppbC VOCs; (2) 300 ppbC VOCs; (3) 1000 ppbC VOCs; (4) 300 ppbC t-2-butene. The reason for isolating the impacts of t-2-butene within a single scenario is that it rapidly reacts with $NO_3^{\bullet}$, thus producing HNO_3 instead of N_2O_5 through the reaction of $NO_3^{\bullet}$ with NO_2. For all values of γ examined, the effect of increasing the value of the yield parameter from 0 – 100% at a fixed γ was a linear increase in peak ozone concentrations. This is summarized in Figure A-1.

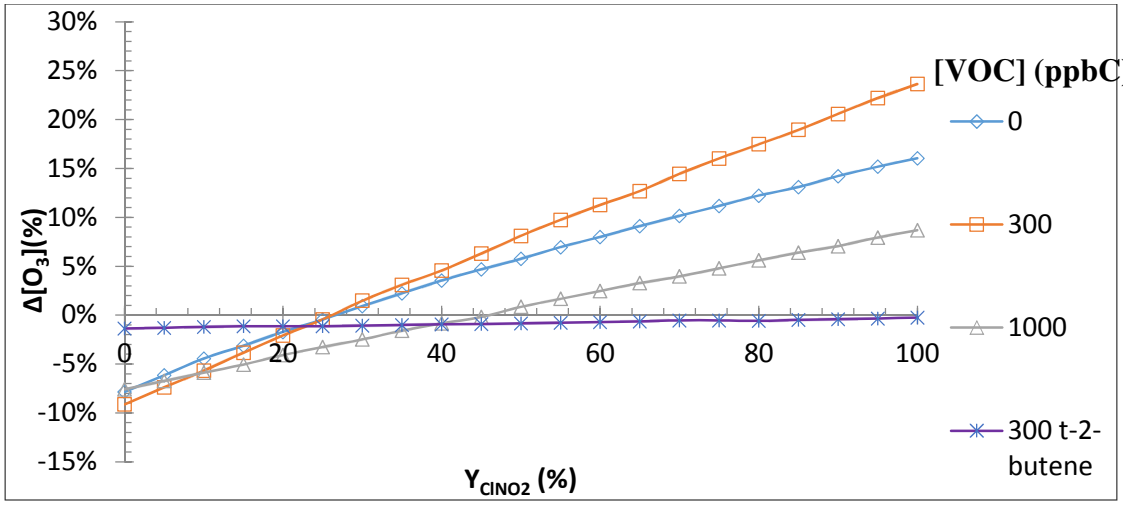

Figure A-1: Differences in peak O_3 concentrations (as %) compared to base case scenarios where the base case scenario assumes no heterogeneous reaction of N_2O_5. Surface area equivalent to PM = 15 µg m^{-3} as described in the methods section.

Figure A-2 shows the corresponding peak $ClNO_2$ concentrations during the yield variation scenarios.

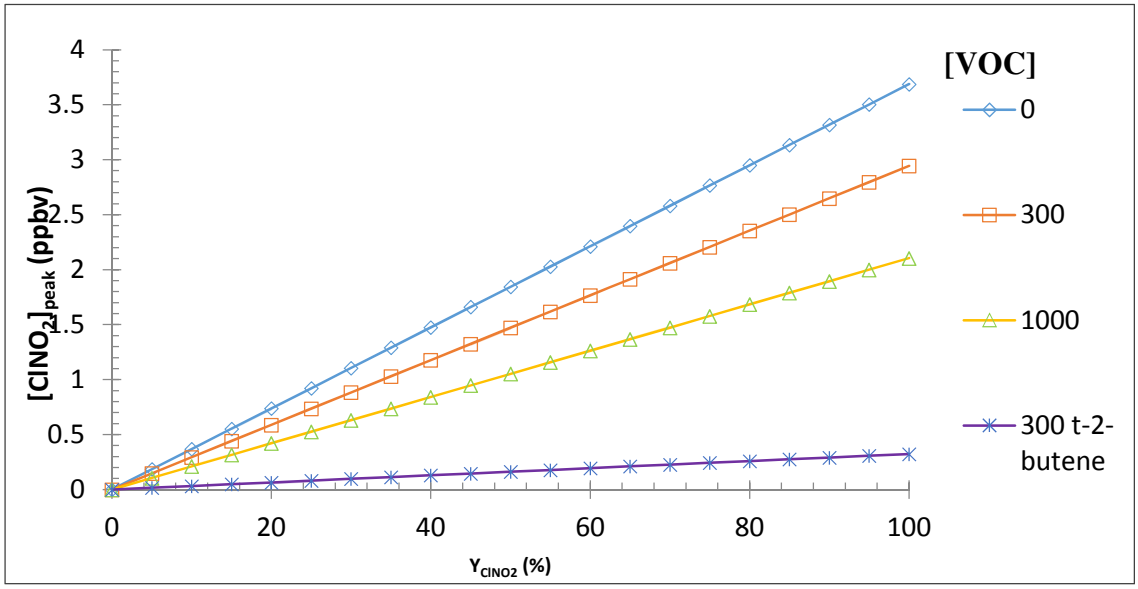

Figure A-2: Peak $ClNO_2$ concentrations from box modeling simulations.

For variations in the reactive uptake coefficient, $ClNO_2$ yield values were held constant at values ranging between 0 and 100 percent while the reactive uptake was varied between its lower and upper limits in sequential simulations. The effect of increases in the reactive uptake at a fixed yield value was an intensification of the impact on peak ozone concentrations elicited by the yield value. Figure S3 summarizes the impacts of these variations on peak ozone formation in simulations where surface area was set to correspond to a particle concentration of 15µg m^{-3} and the VOC concentration was 300 ppbC. Figure S4 shows the peak $ClNO_2$ production from the same set of simulations.

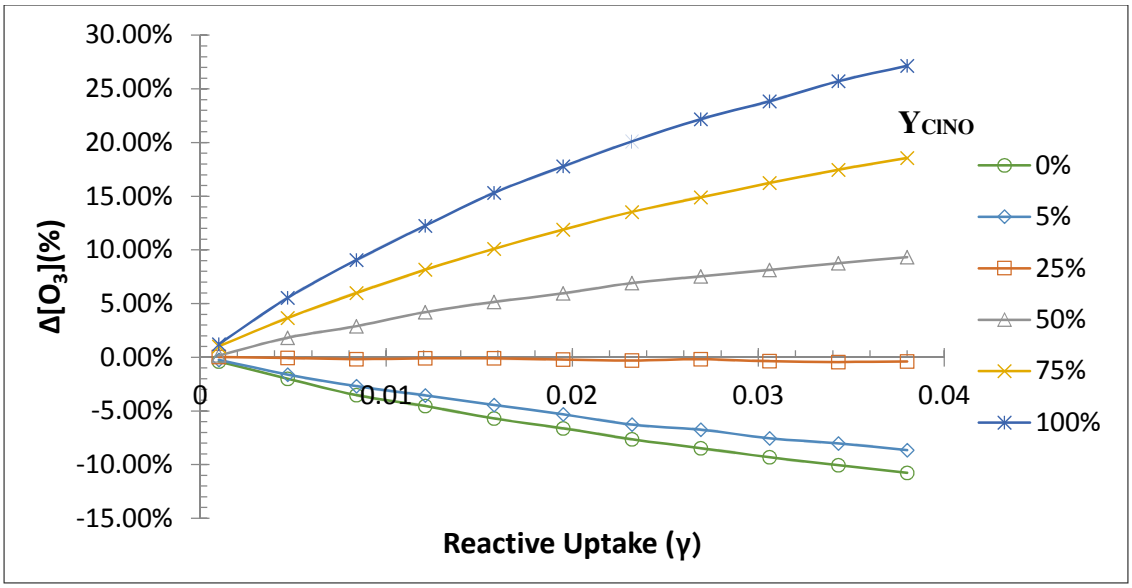

Figure A-3: Resulting peak O_3 increases over base case scenario (no heterogeneous reaction) from reactive uptake variation.

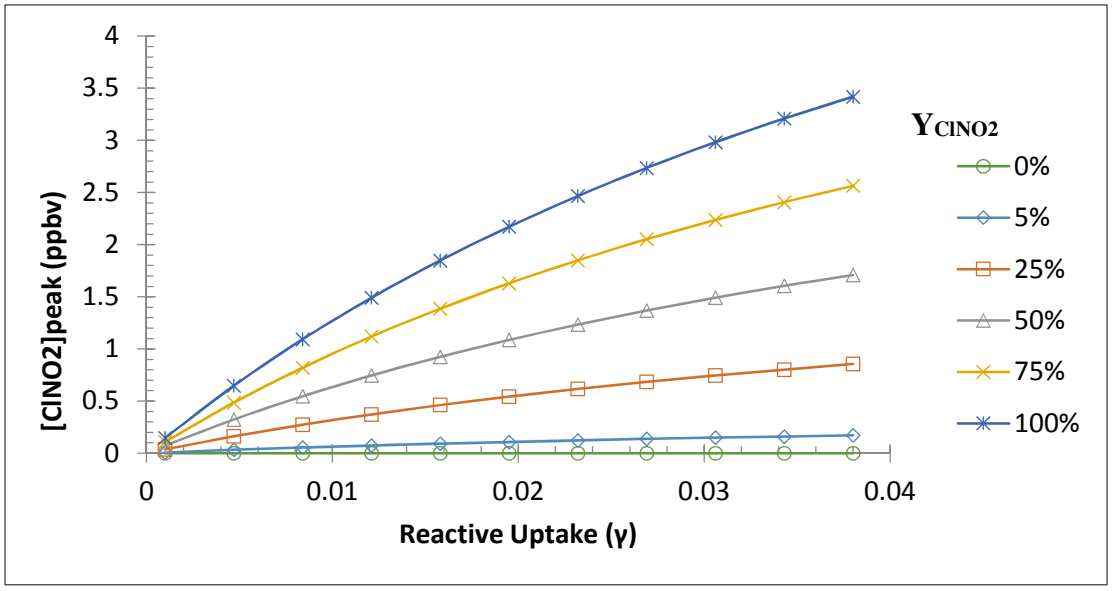

Figure A-4: Resulting peak $ClNO_2$ concentrations from reactive uptake variation.

Effects of Multi-Parameter Variation

The combined effects of the variation of multiple parameters can also be examined. As the contour plots in Figures S5 and S6 below show, higher combinations of parameter values lead to higher peak concentrations of $ClNO_2$ in the morning as well as larger increases in peak O_3 concentrations over the base case simulation in which no heterogeneous chlorine chemistry was included. However, the

variation of different parameters results in different effects. For example, a 10.8 ppbv increase in peak ozone over the base case peak concentration (74.8 ppb) results from initial conditions of 300 ppbC of VOC surrogate, a reactive uptake coefficient of 0.03 and a yield value of 0.75. By fixing reactive uptake at a value of 0.03 and increase yield from 0 to 0.75, the resulting increase in peak ozone concentration is 18.82 ppbv. However, fixing the yield parameter at a value of 0.75 and increasing the reactive uptake from 0 to 0.03 results in maximum ozone increase of 12.14 ppbv. These results illustrate the range of ozone impacts that can be achieved using rate parameters within accepted ranges. In the results discussed here, a particle surface area equivalent to a population of 15 µg m^{-3} was used.

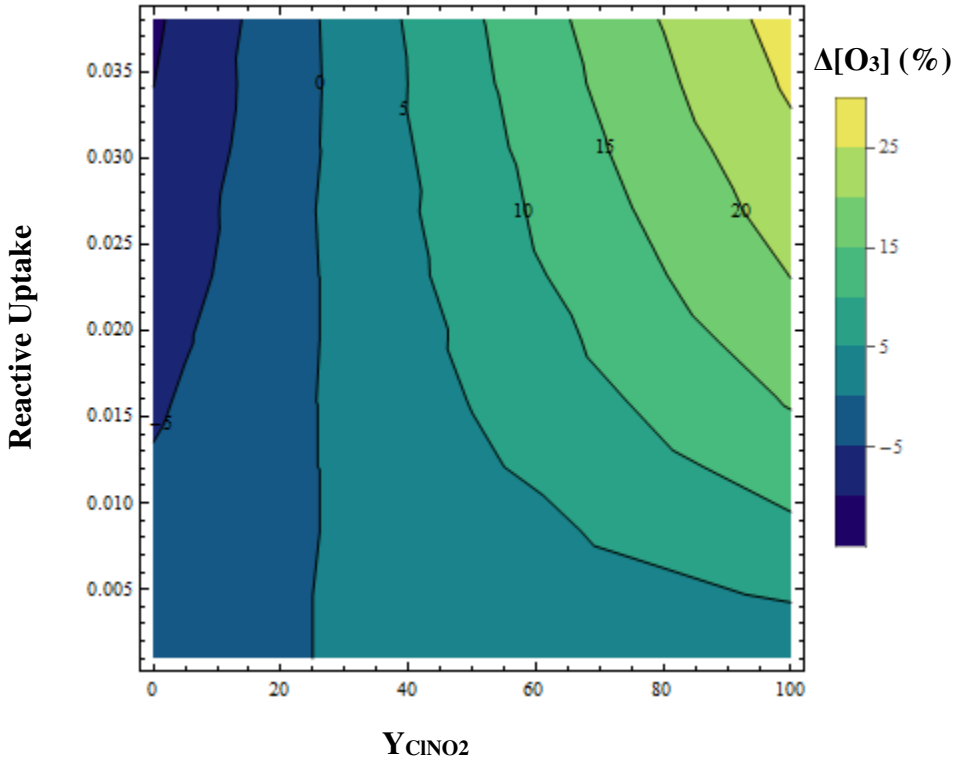

Figure A-5: Percentage peak O_3 increases in over the base case scenario (no heterogeneous reactions) for various combinations of the $ClNO_2$ yield and reactive uptake parameter values.

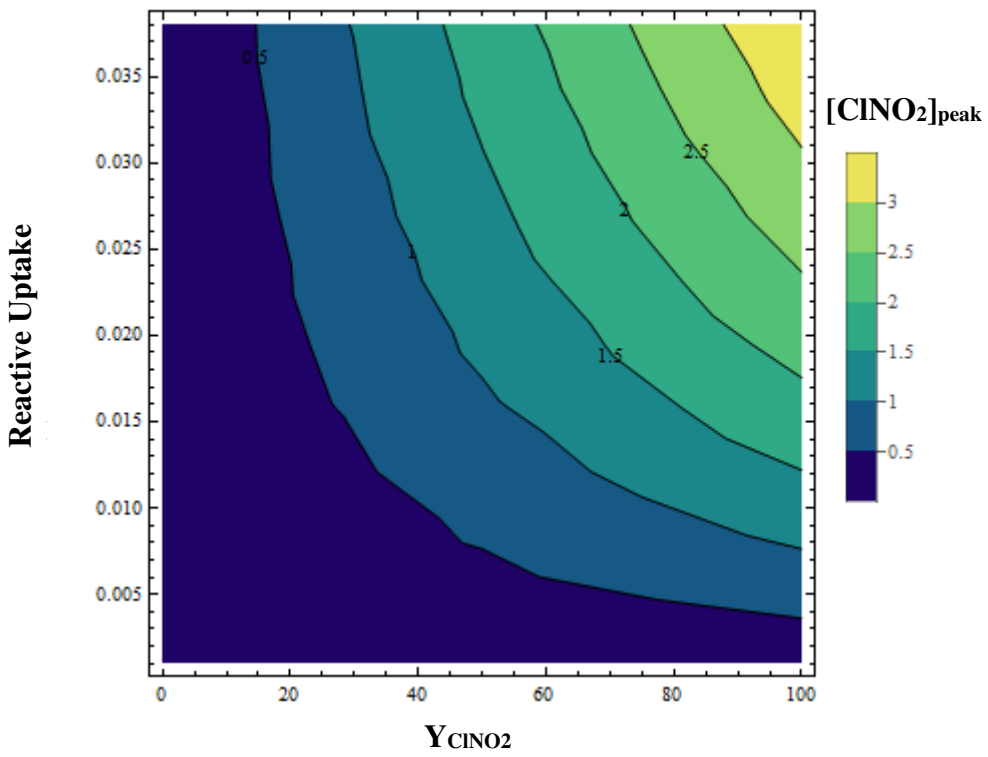

Figure A-6: Peak $ClNO_2$ concentrations (ppb) for various combinations of the $ClNO_2$ yield and reactive uptake parameter values.

Appendix B – Additional Review of the Literature Pertaining to Chlorine Chemistry in Urban Atmospheres

B.1 Background on Atmospheric Chemistry Mechanisms and the Development of Condensed Photochemical Mechanisms

Air quality simulation models (AQSMs) have proven to be useful tools in understanding atmospheric chemical and physical processes. A key component in the use of these models is the photochemical reaction mechanism that is contained within the model. A photochemical reaction mechanism is comprised of a set of chemical reactions that represent the complex interactions of naturally occurring and anthropogenic chemical species. Both organic and inorganic chemistries are represented in this manner, and traditionally the focus has been primarily on gas-phase chemistry. Recently, studies have indicated the need to include heterogeneous chemistry in order to construct a more complete picture of the chemical processes taking place in the atmosphere. This topic will be reviewed later in this chapter. Regardless of whether heterogeneous reactions are included, due to the distinctly non-linear characteristic of the behavior of atmospheric chemical interactions, the development of gas-phase photochemical mechanisms has proven to be indispensable in the study of atmospheric processes.

The development of photochemical mechanisms for use within AQSMs is not as straightforward as including all known reactions and rate constants. While this would certainly work well for detailed small scale chamber studies with only a few component species where a study of the exact mechanism is desired, the complexity of a reaction mechanism that would include the full mechanisms of each constituent species is infeasible for simulating ambient atmospheres. This infeasibility is due to limitations in the understanding of the elementary reactions of atmospheric photochemistry and to limitations imposed by available computing resources. Use of AQSMs is essential in the work described

in this thesis because the mechanisms are being tested using ambient observations, and proposed mechanisms must be able to predict the spatial and temporal variations in observations.

In order to effectively design a reaction mechanism for simulation, techniques to simplify mechanisms and minimize mechanism size while maximizing accuracy must be implemented. Such techniques are commonly referred to as grouping, lumping, or surrogate approximations. The three primary classes of species represented in lumped photochemical mechanisms are inorganic compounds, radicals and organic compounds. Typical inorganic species that are represented include oxides of nitrogen (NO, NO_2, NO_3 and N_2O_5), various forms of oxygen ($O^3(P)$, $O^1(D)$, O_2 and O_3), CO_2, H_2O, H_2O_2 and atmospherically relevant acids (HNO_3, H_2SO_4 and HCl) (Yarwood & Rao, 2005). Reactions between inorganic species are handled with explicitly represented products and reactants. This includes photolysis reactions, where the photolysis rate is calculated by taking into account the intensity of light over the relevant spectrum, the molecule's quantum yield and the absorption cross section of the molecule undergoing photolysis. Some examples of the reactions of inorganic species related to ozone chemistry, excerpted from the Carbon Bond and SAPRC-07 mechanisms, are shown below(William P L Carter, 2010a; Yarwood & Rao, 2005):

$NO_2 + O_3 \rightarrow NO_3$ (Reaction B-1)

$NO_3 + NO \rightarrow 2NO_2$ (Reaction B-2)

$N_2O_5 + H_2O \rightarrow 2HNO_3$ (Reaction B-3)

$O_3 + h\nu \rightarrow O^1(D) + O_2$ (Reaction B-4)

One of the most prevalent and varied classes of species found in lumped mechanisms is hydrocarbons, which has been repeatedly targeted for accurate abstraction. Abstraction of hydrocarbon chemistry has typically followed one of two paths to achieve the desired level of consolidation: the molecular approach or the structural approach. The molecular approach implements approximations by grouping the reactions of molecular groups. Alternatively, the structural approach employs

simplification via a lumping of species with the nature of the bonds between carbon atoms being the primary criterion. For example, the latter approach can be used to form separate surrogate groups for olefinic bonds and paraffinic bonds within hydrocarbon molecules, thus simplifying the chemistry while retaining a reasonable amount of accuracy. The benefits of this approach over the molecular grouping approach are that each type of bond in a molecule is accounted for and less surrogate groups are required (Adelman, Zachariah, 1999).

Examples of the molecular grouping of organic compounds can be taken from the SAPRC-07 mechanism and one of its condensed versions, CS07A. SAPRC-07 was produced as a comprehensive overhaul to the SAPRC-99 chemical mechanism, and updates included the addition of chlorine chemistry and a restructuring of the representation of peroxy chemistry. Some examples of the molecular grouping approach within SAPRC-07 are in table B-1. Note that differences in reactivities for similar molecules are accounted for by the creation of multiple molecular surrogates for large classes such as is done for alkanes (William P L Carter, 2010a).

Table B-1: Lumped Species in the SAPRC-07 Mechanism

Model Species	Species Included
ALK1	Alkanes and non-aromatics reacting only with OH with k_{OH} between 1.36-3.41x10^{-13} $cm^3molecules^{-1}s^{-1}$
ALK2	As above with k_{OH} between 3.41x10^{-13}-1.70x10^{-12} $cm^3molecules^{-1}s^{-1}$
ALK3	As above with k_{OH} between 1.70-3.41x10^{-12} $cm^3molecules^{-1}s^{-1}$
ALK4	As above with KOH between 3.41-6.81x10^{-12} $cm^3molecules^{-1}s^{-1}$
ALK5	As above with k_{OH} > 6.81x10^{-11} $cm^3molecules^{-1}s^{-1}$
ARO1	Aromatics with k_{OH} < 1.36x10^{-11} $cm^3molecules^{-1}s^{-1}$
ARO2	Aromatics with k_{OH} > 1.36x10^{-11} $cm^3molecules^{-1}s^{-1}$
RCHO	Saturated aldehydes with 3 or more carbons
RCOOH	Organic acids with 3 or more carbons
RNO3	Organic nitrates
MVK	Unsaturated ketones

Certain organic species with unique chemistry or chemistry that is very important to pollutant formation are represented explicitly. These species include methane, isoprene, ethylene and acetylene (Carter, 2010a). The creation of the condensed version CS07A included further consolidation of alkanes through the removal of model surrogate species ALK1, ALK2 and ALK5. The existing lumping scheme for alkanes was changed as shown below, condensing all alkenes into only two of the pre-existing classes, ALK3 and ALK4 (William P L Carter, 2010b):

SAPRC-07 ALK1 = 0.132 CS07 ALK3

SAPRC-07 ALK2 = 0.334 CS07 ALK3

SAPRC-07 ALK3 = CS07 ALK3

SAPRC-07 ALK4 = CS07 ALK4

SAPRC-07 ALK5 = CS07 ALK4

The above are examples of a molecular lumping strategy. Examples of the structural grouping approach can be taken from the lumping scheme contained within the Carbon Bond mechanism. In addition to molecular lumping for certain classes of molecules, many organic compounds within the Carbon Bond mechanism are lumped according to the character of the bonds between the carbon atoms in the species present. A surrogate species is created for each type of bond, and individual molecular species can be split between two surrogate species. Three primary structural surrogate species are OLE, which represents carbon-carbon double bonds and contains two carbon atoms, PAR, which represents single carbon bonds and contains one carbon atom, and ALD2, which contains two carbon atoms and represents a –CHO group and its adjacent carbon atom such as in the case of acetaldehyde and higher aldehydes (Gery et al., 1989). Examples of the assignment of molecular species into model species are shown in the Table B-2 (Gery, Whitten, Killus, & Dodge, 1989; Yarwood & Rao, 2005):

Table B-2: Organic Species Representation in the Carbon Bond Mechanism

Organic Species	Model Species
n-Butane	4 PAR
2,25-Trimethylpentane	8 PAR
Propene	1 OLE + 1 PAR
Acetaldehyde	1 ALD2
Caryophyllene	9 PAR + 3 OLE
2,4-dimethylhexane	8 PAR

As in SAPRC-07, some species are treated explicitly. In the Carbon Bond mechanism, this initially included (as of version CB05) methane, ethane, ethylene, isoprene, formaldehyde and acetaldehyde. Certain extensions have also been provided that can accommodate the explicit representation of 1,3-butadiene, acrolein, toluene, xylene isomers, and α- and β-pinene. Additionally, further detailing of carbon bond characterization has taken place, such as the differentiation between internal and terminal olefin carbon bonds by the introduction of the surrogate species IOLE (Yarwood & Rao, 2005).

The representation of radical chemistry includes both organic and inorganic species. Examples of common inorganic radicals include the hydroxyl radical (OH), the hydroperoxy radical (HO_2), halogen radicals such as the chlorine radical (Cl), and the nitrate radical (NO_3). Organic radicals include the methyl peroxy radical (CH_3O_2), the acetyl peroxy radical ($CH_3C(O)O_2$) and higher organic peroxy radicals. Each radical is either represented explicitly, as is the case with the hydroperoxy, hydroxyl and chlorine radicals, or it is represented in a lumped surrogate species, which typically contains radicals that are generated from similar pathways. With surrogate species, radicals are lumped in the sense that they may contain radical products produced from various precursors. A comparison of some of the most common explicit and lumped radical species in SAPRC-07 and Carbon Bond mechanisms is shown in table B-3 (William P L Carter, 2010a; Yarwood & Rao, 2005):

Table B-3: Radical Species in the SAPRC-07 and Carbon Bond Mechanisms

Mechanism	Class	Species	Details
SAPRC-07	Lumped	RCO3	Peroxy propionyl and higher peroxyacyl radicals
		MACO3	Peroxyacyl radicals formed from methacrolein and other acroleins
		RO2C	Peroxy radical operator that accounts for NO-->NO2, NO3-->NO2 and effects of peroxy radical reactions on peroxy radicals
		RO2XC	Peroxy radical operator that accounts for NO consumption, effects of peroxy radical reactions on NO3, acyl peroxy radicals and other peroxy radicals
	Explicit	OH	Hydroxyl radicals
		HO2	Hydroperoxide radicals
		MEO2	Methylperoxy radicals
		O1D	Excited Oxygen atom
Carbon Bond 5	Lumped	CXO3	Acylperoxy radicals with 3 or more carbon atoms
		ROR	Secondary alkoxy radicals
		XO2	Peroxy operator for NO-->NO2 from alkylperoxy (RO2) radicals
		XO2N	NO-->organic nitrate conversion from alkylperoxy radicals
	Explicit	OH	Hydroxyl radicals
		HO2	Hydroperoxy radical
		MEO2	Methylperoxy radical
		C2O3	Acetylperoxy radical

As can be seen in table B-3, the major inorganic radical species such as OH, HO_2 and CH_3O_2 are handled explicitly in both SAPRC-07 and Carbon Bond 5. Additionally, both models have developed peroxy operators to handle the effects of peroxy radical reactions on the oxides of nitrogen and organic nitrate formation. Specifics of radical production and termination pathways and details of how the peroxy operators work will be discussed further below.

The ability of a chemical mechanism to accurately represent the interactions of inorganic, organic and radical species has to be evaluated before it can be used for predicting pollutant concentrations or otherwise studying atmospheric chemical processes. This is typically done by comparing environmental chamber experiments, in which known amounts of chemical species are mixed and exposed to environmental conditions including a known temperature, relative humidity and amount of light, to simulations of the same conditions using the chemical mechanism under

investigation. The evolution of reactions and species concentration profiles can then be compared between the model simulation and the measurements made during the chamber study. In order for this evaluation process to be as effective as possible, comparison should be made to multiple chambers and chamber-specific parameters including lighting conditions and wall effects must be provided for the simulation. Through comparison to hundreds, and in some cases thousands, of environmental chamber experiments, it can be determined whether or not a given chemical mechanism is accurate enough for use in either scientific or regulatory settings. This method has been used to validate many chemical mechanisms, including versions of both the SAPRC and Carbon Bond mechanisms (Adelman, Zachariah, 1999; William P L Carter, 2010a, 2010b; Gery et al., 1989; Heo et al., 2010; Yarwood et al., 2010).

B.1.a The Carbon Bond Mechanism: An Example of Successful Photochemical Model Abstraction and Condensation

To date, one of the most successful applications of the structural lumping approach has been the ongoing development of the photochemical mechanism known as the Carbon Bond mechanism. The initial implementation of the Carbon Bond mechanism was intended for use in simulating the effect of NO_x and volatile organic compounds on urban ozone formation. Carbon Bond was first introduced by System Applications International, Inc. (SAI) in 1980, and was subsequently updated through the 80's. The original mechanism consisted of combination of explicit hydrocarbon chemistry as well as structurally lumped surrogate species. In total, there were 35 reactions, with 14 reactions contained in the inorganic set, and four lumped species and one explicit species comprising the organic set (G Z Whitten et al., 1980). Throughout the decade after its initial release, the Carbon Bond mechanism was updated to include a total of 170 reactions. This version, known as CBM-X, contained a mix of explicit inorganic chemistry, explicit organic chemistry for species that were environmentally important,

molecular-lumped surrogate organic species, and structurally lumped surrogate organic species(Adelman, Zachariah, 1999).

Further condensation of CBM-X, which already contained a degree of condensation, was done using several modeling approaches. This was determined to be necessary in order to create a highly compressed version of the Carbon Bond mechanism that could be more easily implemented in AQSMs while still retaining the ability to simulate chamber experiments accurately relative to explicit versions of the Carbon Bond mechanism. These approaches included the lumping of secondary reaction products, the reduction of species through the use of mathematical manipulation, and the inclusion of the surrogate species XO2 and XO2N, which serve as universal peroxy operators(Adelman, Zachariah, 1999).

Additionally, reactions deemed unnecessary for simulation at the urban scale were eliminated. For example, the oxidation of formaldehyde by the HO_2 radical was eliminated. The reason for this was that once formaldehyde is oxidized by HO_2, the newly formed hydroxymethylperoxy radical can rapidly undergo the reverse reaction, which takes place at a rate that is more than 10 orders of magnitude faster than either the reaction of formaldehyde and HO_2 or alternate reactions of the formaldehyde radical. With this in mind, the following reactions were eliminated from the mechanism (where FACD, FORM, FROX, and PROX are model species for formic acid, formaldehyde, the hydroxymethylperoxy radical and organic peroxide, respectively) (Gery et al., 1989):

$FORM + HO_2^{\bullet} \rightarrow FROX$ (Reaction B-5)

$FROX \rightarrow HO_2^{\bullet} + FORM$ (Reaction B-6)

$FROX + HO_2^{\bullet} \rightarrow PROX$ (Reaction B-7)

$FROX + NO \rightarrow NO_2 + HO_2^{\bullet} + FACD$ (Reaction B-8)

Additionally, the methoxy radical (represented as MEO) and its reactions were eliminated (where MNIT and MEN3 are isomers of methyl nitrate):

$$MEO + NO \rightarrow MNIT \quad \text{(Reaction B-9)}$$

$$MEO + NO \xrightarrow{O_2} FORM + HO_2^{\bullet} + NO \quad \text{(Reaction B-10)}$$

$$MEO + NO_2 \rightarrow MEN3 \quad \text{(Reaction B-11)}$$

$$MEO \xrightarrow{O_2} FORM + HO_2^{\bullet} \quad \text{(Reaction B-12)}$$

Elimination of the MEO reactions was deemed appropriate because the end result of the reactions of MEO is the production of FORM and HO_2. Products of reactions B-5 and B-7 either end up forming formaldehyde or undergo reaction to regenerate MEO. Therefore, these reactions were removed and the model species MEO was replaced by FORM + HO_2. To further reduce the number of species that needed to be represented, reaction products that did not appear as reactants in any reaction within the mechanism were discarded. This included model species such as PROX, ACAC (acetic acid) and EPOX (isoprene epoxide product) (Gery et al., 1989). Together with the aforementioned condensations and changes, this resulted in a newer version of Carbon Bond known as Carbon Bond IV (CB-IV) (Adelman, Zachariah, 1999).

The inclusion of the universal peroxy operator serves as an ideal example of species and reaction condensation. The XO2 operator was formulated to represent organic chemistry involving the production of alkylperoxy radicals. Alkylperoxy radicals participate in the oxidation of NO to NO_2, especially under high NO_x conditions, and thus serve as an important link in ozone formation chemistry. The explicit set of reactions is as follows (where $^{\bullet}$ indicates a radical species):

$$R_nH + OH^{\bullet} \rightarrow R_n^{\bullet}(H_2O) \quad \text{(Reaction B-13)}$$

$$R_n^{\bullet} + O_2 \rightarrow R_nO_2^{\bullet} \quad \text{(Reaction B-14)}$$

$$R_nO_2^{\bullet} + NO \rightarrow NO_2 + \text{other products} \quad \text{(Reaction B-15)}$$

In order to condense this chemistry, XO2 was made to represent the entire class of organic peroxy radicals that, upon reaction with NO, do not form an organic nitrate. Instead of explicitly representing

numerous organic peroxy radicals (represented as $R_nO_2^\bullet$ above), reaction B-16 is used as a condensed version of all reactions of the type represented in reaction B-15 (Adelman, Zachariah, 1999).

$$XO2 + NO \rightarrow NO_2 \qquad \text{(Reaction B-16)}$$

Similarly, the operator XO2N was used to collapse the following reaction scheme (here, PAR is the surrogate species in Carbon Bond that represents paraffinic bonds):

$$PAR + OH^\bullet \rightarrow R_nO_2R_m^\bullet + H_2O \qquad \text{(Reaction B-17)}$$

$$R_nO_2R_m^\bullet + NO \rightarrow NTR \qquad \text{(Reaction B-18)}$$

The above chemistry was compacted into the following reaction (where NTR is the surrogate species for organic nitrates):

$$XO2N + NO \rightarrow NTR \qquad \text{(Reaction B-19)}$$

When this approach was introduced, it was termed the 'prompt product' technique. It allowed for the accounting of important impacts of the reaction while eliminating the need for explicitly represented organic peroxy radicals (Adelman, Zachariah, 1999).

However, for appropriate representation of the chemistry in low-NO_x conditions, a self-reaction pathway was introduced into the mechanism that would be competitive with the NO oxidation pathway in NO_x limited situations. These additional XO2/XO2N reactions were done to prevent an overproduction of H_2O_2 and buildup of XO2N, which serves as a NO_x sink (reaction B-18). In the end, a set of five reactions was to represent the self-reactions of organic peroxy radicals as well as their reactions with $HO_2^\bullet$ (Adelman, Zachariah, 1999; Yarwood & Rao, 2005).

$$XO2 + HO_2^\bullet \rightarrow ROOH + O_2 \qquad \text{(Reaction B-20)}$$

$$XO2N + HO_2^\bullet \rightarrow ROOH + O_2 \qquad \text{(Reaction B-21)}$$

$$XO2 + XO2 \rightarrow \qquad \text{(Reaction B-22)}$$

$$XO2N + XO2N \rightarrow \qquad \text{(Reaction B-23)}$$

XO2N + XO2 → (Reaction B-24)

Concerning the kinetic rate parameters of these reactions, it was assumed that XO2 and XO2N react with $HO_2^{\bullet}$ at the same rate. Also, it was assumed that XO2 reacted with itself at the same rate as XO2N reacted with itself. The equating of these parameters served as a bit of further condensation by reducing the calculations for reaction rates. Overall, the addition of the universal peroxy operators XO2 and XO2N made the Carbon Bond mechanism more reactive with respect to ozone formation. Subsequent testing showed that the additional reactions involving the peroxy radical operators caused general increase in NO_x lifetimes, leading to an increase in ozone levels specifically in situations where NO_x concentrations were the limiting factor (Adelman, Zachariah, 1999).

The addition of the universal peroxy operators shown above is useful in handling the effects of radical chemistry on NO_x and hydrocarbon oxidations, but it does not handle the origin of the radicals. In the example above, the initiating radical in reactions B-13 and B-17 is the hydroxyl radical, OH, which is one of the most ubiquitous and important reactive species in the atmosphere. Despite its high reactivity, OH concentrations during day time are typically maintained on the order of 10^6 molecules cm^{-3}. The reason for the maintaining of relatively constant levels is that when the OH radical reacts with trace gases in the atmosphere, it is continually regenerated in a self-perpetuating reaction cycle. The examination of the cycle can begin with the photolysis of O_3 (Seinfeld & Pandis, 2006):

$O_3 + h\nu \rightarrow O(^3P) + O_2$ (Reaction B-25a)

$\rightarrow O(^1D) + O_2$ (Reaction B-25b)

Here, $O(^3P)$ is the ground state oxygen and $O(^1D)$ is an electronically excited oxygen molecule. Most $O(^1D)$ is stabilized back to ground state by the presence of N_2 and O_2 molecules in the atmosphere. However, a small percentage of $O(^1D)$ ends up producing OH radicals through reaction with water vapor (Seinfeld and Pandis, 2006):

$O(^1D) + H_2O \rightarrow 2OH^\bullet$ (Reaction B-26)

Additional sources of hydroxyl radicals include the photolysis of compounds containing an OH group (Seinfeld & Pandis, 2006; Yarwood & Rao, 2005):

$H_2O_2 + h\nu \rightarrow 2OH^\bullet$ (Reaction B-27)

$HONO + h\nu \rightarrow NO + OH^\bullet$ (Reaction B-28)

$HNO_3 + h\nu \rightarrow NO_2 + OH^\bullet$ (Reaction B-29)

Removal of the hydroxyl radical primarily takes place through reaction with NO_2 to form HNO_3, which is then removed from the atmosphere through rain or heterogeneous removal (Seinfeld and Pandis, 2006):

$OH + NO_2 + M \rightarrow HNO_3 + M$ (Reaction B-30)

Hydroxyl radicals are also removed from the atmosphere through reactions with trace gases, such as HCHO, H_2, O_3, SO_2, CO and CH_4. Through these reactions and reactions of the products, the hydroxyl radical is transformed into the hydroperoxy radical, HO_2. One of the most direct routes is through reaction with CO (Seinfeld and Pandis, 2006):

$CO + OH^\bullet \xrightarrow{O_2} CO_2 + HO_2^\bullet$ (Reaction B-31)

The hydroperoxy radical can also be formed from the reaction between hydrogen peroxide and the hydroxyl radical (Seinfeld and Pandis, 2006):

$H_2O_2 + OH^\bullet \rightarrow H_2O + HO_2^\bullet$ (Reaction B-32)

The hydroxyl cycle is closed primarily by the reaction of the hydroperoxy radical with NO or O_3 to regenerate a hydroxyl radical (Seinfeld & Pandis, 2006; Yarwood & Rao, 2005):

$HO_2^\bullet + NO \rightarrow NO_2 + OH^\bullet$ (Reaction B-33)

$HO_2^\bullet + O_3 \rightarrow 2O_2 + OH^\bullet$ (Reaction B-34)

Alternatively, a self-reaction of the hydroperoxy radical, followed by reaction B-27, can lead to regeneration of the hydroxyl radical, and it is worth noting that this reaction is a mechanism of hydroperoxy radical removal in the case of the low NO_x regime (Seinfeld and Pandis, 2006):

$HO_2^\bullet + HO_2^\bullet \rightarrow H_2O_2 + O_2$ (Reaction B-35)

Additional removal pathways for hydroxyl and hydroperoxy radicals from the atmosphere include the reaction between the two to produce molecular oxygen and water vapor (Seinfeld & Pandis, 2006; Yarwood & Rao, 2005):

$OH^\bullet + HO_2^\bullet \rightarrow O_2 + H_2O$ (Reaction B-36)

Aside from the hydroxyl and hydroperoxy radicals, another common radical in the atmosphere is the nitrate radical. Two sources of NO_3 are oxidation of NO_2 by O_3 and the breakdown of N_2O_5. Once formed, NO_3 oxidizes NO so rapidly that above a few parts per trillion, NO and NO_3 typically do not coexist. Additionally, NO_3 readily undergoes photolysis in one of two ways (Seinfeld and Pandis, 2006):

$NO_2 + O_3 \rightarrow NO_3^\bullet + O_2$ (Reaction B-37)

$N_2O_5 \overset{M}{\leftrightarrow} NO_2 + NO_3^\bullet$ (Reaction B-38)

$NO_3 + NO \rightarrow 2NO_2$ (Reaction B-39)

$NO_3 + h\nu \rightarrow NO + O_2$ (Reaction B-40a)

$\rightarrow NO_2 + O(^3P)$ (Reaction B-40b)

Another class of atmospheric radicals, and one whose importance has become more apparent over the past few decades, is that of halogen radicals. Details of the atmospheric importance of

production and reaction pathways of halogen radicals as well as the mechanism by which radicals in general propagate chain reactions that can lead to O_3 formation is discussed in full detail in Chapter 2.

Another class of mechanism condensation is that of the isoprene mechanism. Within the lower troposphere, isoprene is one of the most important biogenic volatile organic compounds (VOCs) present. In 1995, the EPA released BEIS2, which estimated that isoprene, among other VOCs, were being emitted in quantities much higher than previously thought. Therefore, proper determination of isoprene's reactivity and dominant reaction products is important to modeling scenarios where isoprene is present in significant amounts. Initially, an isoprene mechanism for the CB-IV mechanism was developed by Killus and Whitten in 1984, which only took into account 2 of 12 known pathways of isoprene's addition reaction with OH (Adelman, Zachariah, 1999). However, in 1996 Carter and Atkinson found highly reactive products from the 10 pathways that had previously been ignored (William P. L. Carter & Atkinson, 1996).

To address this issue, Dr. Carter of URC-Riverside created a 1-product isoprene mechanism which took into account the most reactive products of isoprene chemistry. Upon testing and evaluation, Dr. Carter's 1-product mechanism was proven to be more accurate when compared to the existing 2-product mechanism within the Carbon Bond mechanism. The 1-product mechanism also proved to be accurate relative to explicit isoprene mechanisms. The 1-product mechanism was officially adopted into the Carbon Bond mechanism for reasons including the minimization of required computer resources to simulate the chemistry and its higher rates of PAN production, which were being under predicted by the previous model (Adelman, 1999). The isoprene mechanism that was finally implemented into the Carbon Bond mechanism was an adaptation from the one developed by Carter for the SAPRC mechanism (Yarwood & Rao, 2005). Although the one product mechanism is able to accurately replicate the results of isoprene-NO_x chamber studies, the understanding of the complex chemistry in which isoprene is involved is still advancing (Adelman, 1999). Changes in the understanding of the

basic chemistry will undoubtedly be reflected in improvements and modifications of future versions of the isoprene chemistry. In fact, the most recent version of the Carbon Bond mechanism, CB6, includes updates to the reactions for isoprene (Yarwood et al., 2010).

Since the release of CB-IV, the Carbon Bond mechanism has undergone further improvements to increase its usability and versatility in modeling the chemistry related to regional air quality. In 2005, a comprehensive overhaul of CB-IV was done with the intention of improving its performance in predicting photochemical ozone formation, as well as refining other areas of the mechanism's chemistry. The inorganic reaction set was expanded to increase relevance for use in simulating urban and remote tropospheric settings. Other improvements to improve accuracy included a chlorine chemistry mechanism extension, explicit representation of ethane, methyl hydroperoxide, methyl peroxy radicals, and formic acid, and improved representation of NO_x cycling to track the fate of NO_x over periods of several days. Increased NO_x cycling was implemented by the inclusion of the following reactions, where PNA, NTR, ALD2 and ALDX are the CB05 model species for peroxynitric acid (HNO_4), organic nitrates, acetaldehyde and higher aldehydes (including propionaldehyde), respectively (Yarwood & Rao, 2005):

$$PNA + h\nu \rightarrow 0.610HO_2 + 0.610NO_2 + 0.390OH + 0.390NO_3 \quad \text{(Reaction B-41)}$$

$$HNO_3 + h\nu \rightarrow OH + NO_2 \quad \text{(Reaction B-42)}$$

$$N_2O_5 + h\nu \rightarrow NO_2 + NO_3 \quad \text{(Reaction B-43)}$$

$$NTR + OH \rightarrow HNO_3 + HO_2 + 0.330FORM + 0.330ALD2 + 0.330ALDX - 0.660PAR \quad \text{(Reaction B-44)}$$

$$NTR + h\nu \rightarrow HNO_3 + HO_2 + 0.330FORM + 0.330ALD2 + 0.330ALDX - 0.660PAR \quad \text{(Reaction B-45)}$$

The above reactions enhanced NO_x cycling by allowing the reaction of compounds that, in previous versions of the model, served as NO_x reservoirs, effectively trapping NO_x in these compounds once the transformation had taken place. The overall result of the NO_x being trapped was that the reactivity of the entire system was lowered. Organic nitrates in particular can serve as vehicles for long range NO_x transport due to their relatively long life spans, and thus the addition of reactions B-44 and B-45 are of particular importance with respect to long-range or long-term oxidant and O_3 chemistry in the troposphere (Zaveri & Peters, 1999).

Changes that were focused on further condensation consisted of the addition of new surrogate species including IOLE to represent internal olefinic bonds, TERP to represent all terpenes, and ALDX for the lumping of higher aldehydes. Additionally, a general revamping of kinetic rate constants was performed in order to coincide with NASA and IUPAC kinetic assessments which were published from 2003-2005 (Yarwood & Rao, 2005). This version of the mechanism has come to be known as CB05. More recently, in 2010, an optional expanded version of the CB05 toluene mechanism was released as CB05-TU. The extended toluene mechanism adds 16 new reactions and eight new species to the base CB05 toluene mechanism. Although the update adds to the existing amount of reactions and species, it is still represented in a highly condensed form relative to explicit toluene mechanisms, which could conceivably include thousands of reactions. These changes were considered necessary to more fully account for radical sources and NO_x sinks that are part of toluene degradation. The result of this is a mechanism that is more accurate in predicting ozone formation rates and levels in low NO_x conditions when toluene is present (Gary Z. Whitten et al., 2010).

As recently as 2010, the Carbon Bond mechanism has undergone further refinement with the release of CB6. Explicit representation of certain long-lived VOCs including propane, benzene, acetone and ethyne (acetylene) was added due to their effect on regional oxidant and O_3 chemistry. Other major updates include the inclusion of newly published chemical data by NASA and IUPAC panels, explicit

reactions for acetylene and benzene that can lead to organic aerosol formation and explicit representation for the VOC degradation products glyoxal, glycolaldehyde and methylglyoxal that can potentially participate in aqueous-phase reactions that lead to organic aerosol production. CB6 showed improvement in what had been a maximum O_3 under prediction bias in CB05 for simulation of aromatics. The new version is completely compatible with CB-IV and CB05, but the developers recommend the use of updated emissions inventories and other model inputs in order to fully utilize new features (Yarwood et al., 2010).

B.2 Impacts of Gas Phase Chlorine on Atmospheric Chemistry and Enhanced Ozone Formation

B.2.a Impacts of Reactive Chlorine Chemistry

The importance of chlorine radicals, relative to hydroxyl radical, in the atmospheric oxidation of hydrocarbons, has been studied by Finlayson-Pitts (1993). The rates of removal of hydrocarbons by each radical species can be written:

$$d[RH_i]^{Cl}/dt=k_p[ClX]\{ k_{Cl}^i[RH_i]/(\sum_i k_{Cl}^i[RH_i])\} \quad \text{(Equation B.2-1)}$$

$$d[RH_i]^{OH}/dt=k_p[OHX]\{ k_{OH}^i[RH_i]/(\sum_i k_{OH}^i[RH_i])\} \quad \text{(Equation B.2-2)}$$

In this analysis, k_{Cl}^i and k_{OH}^i are the rates of reaction of organic species i with the chlorine and hydroxyl radicals, respectively, and k_p is the rate of photolysis for each radical precursor. RH_i represents the current hydrocarbon under consideration. CLX represents the photolytic sources of atomic chlorine from reactions B-10 and B-12. Using this method, Finlayson-Pitts (1993) estimated that $Cl^\bullet$ concentrations that were two orders of magnitude less than $OH^\bullet$ concentrations would yield similar oxidation rates for organics (Barbara J Finlayson-Pitts, 1993).

Additional quantification of the difference in reaction rates between chlorine and hydroxyl radicals can be done by comparing the rates of alkylperoxy radical formation by each. This approach was taken

by Stutz et al. (2009), who found that for hydrocarbon mixtures representative of natural gas emissions, a gas phase concentration ratio of [Cl]/[OH] = 0.012 resulted in equal rates of hydrocarbon oxidation by chlorine atoms and hydroxyl radicals. For a mixture of alkanes, alkenes and aromatics, typical of emissions along a highway, the ratio increased to 0.069 (Jochen Stutz et al., 2009). These calculations indicate that chlorine atom concentrations that are 20-100 times lower than hydroxyl radical concentrations can cause equivalent levels of hydrocarbon oxidation. As a comparison, [Cl]/[OH] peak morning time concentration ratios in Houston, TX have been predicted to be within the range of 0.0012 – 0.0024 when taking $ClNO_2$ chemistry into account (Simon, 2008). Another study in Houston, TX an analysis of the products of isoprene reaction with chlorine, relative to the reaction products with hydroxyl radical, in an industrial source region, suggested a [Cl]/[OH] ratio of 0.041 (Riemer & Apel, 2002). These analyses suggest that, for Houston, chlorine radicals may account for 10% to 50% or more of the hydrocarbon reactivity.

B.3 Aqueous Phase Chlorine Chemistry

In addition to homogeneous gas phase reactions and heterogeneous gas-particle reactions, chlorine chemistry also occurs in aqueous droplets in the atmosphere. The ensemble of reactions within the aqueous phase is more appropriately termed multiphase chemistry than heterogeneous chemistry. However, for the purpose of modeling the uptake of gases into sea salt aerosols, which readily absorb water and can vary in constituent concentrations and phase with changes in relative humidity, the distinction between heterogeneous and multiphase chemistry becomes less definite. At 75% relative humidity, pure NaCl particles begin to take up water to form a concentrated solution which is diluted as the humidity increases further (B J Finlayson-Pitts, 2003). For example, chamber studies have shown that particulate chloride concentrations decrease from 6 M at 77.3% relative humidity down to 2 M at 93.9% relative humidity (Wolfgang Behnke et al., 1997).

Within the aqueous phase, chlorine species readily undergo reaction with common constituents of the particles. The chloride ion itself can undergo an initial reaction with hydroxide that sets off a chain of reactions leading to formation of molecular chlorine, which can subsequently volatilize into the gas phase (B J Finlayson-Pitts, 2003; William C Keene et al., 1990; E. M. Knipping, 2000b; Eladio M. Knipping & Dabdub, 2002; Oum et al., 1998; M J Rossi, 1996; Michel J Rossi, 2003; Jochen Stutz et al., 2009):

$OH_{(g)} \rightarrow OH_{(aq)}$ (Reaction B.2-46)

$OH + Cl^- \leftrightarrow HOCl^-$ (Reaction B.2-47)

$HOCl^- + Cl^- \leftrightarrow Cl_2^- + OH^-$ (Reaction B.2-48)

$HOCl^- + H^+ \leftrightarrow (HOClH^\bullet) \leftrightarrow Cl + H_2O$ (Reaction B.2-49)

$2Cl \rightarrow Cl_2$ (Reaction B.2-50)

$Cl + Cl^- \leftrightarrow Cl_2^-$ (Reaction B.2-51)

$2Cl_2^- \rightarrow Cl_2 + 2Cl^-$ (Reaction B.2-52)

$Cl + Cl_2^- \rightarrow Cl^- + Cl_2$ (Reaction B.2-53)

$Cl_{2(aq)} \rightarrow Cl_{2(g)}$ (Reaction B.2-54)

$Cl_2^- + H_2O_2 \rightarrow HO_2 + H^+ + 2Cl^-$ (Reaction B.2-55)

$Cl + H_2O_2 \rightarrow HO_2 + H^+ + Cl^-$ (Reaction B.2-56)

The reactions above provide a pathway for the release of molecular chlorine from the aqueous phase. It should be noted that the following reaction is also possible and dominates those above under most atmospheric conditions, allowing for more direct production of Cl_2 (E. M. Knipping, 2000b; Eladio M. Knipping, 2002; Oum et al., 1998; M J Rossi, 1996; Michel J Rossi, 2003):

$HOCl + Cl^- + H^+ \rightarrow Cl_2 + H_2O$ (Reaction B.2-57)

Additionally, the chloride ion can be oxidized by ozone that has dissolved into the aqueous phase (Finlayson-Pitts, 2003):

$O_3 + Cl^- \rightarrow ClO^- + O_2$ (Reaction B.2-58)

As seen in reactions B-46 and B-47, hypochlorous acid is formed in the presence of OH and can play an important role in aqueous chlorine chemistry. It can also directly react with the chloride ion itself and can account for up to 40% of the total oxidation of S(IV) ($k_{ox.}$= 7.6 x 10^8 $M^{-1}s^{-1}$) inside particles in certain situations, which reduces cloud condensation nuclei (B J Finlayson-Pitts, 2003):

$HOCl + Cl^- + H^+ \rightarrow Cl_2 + H_2O$ (Reaction B.2-59)

$SO_3^{2-} + HOCl \rightarrow HSO_4^- + Cl^-$ (Reaction B.2-60)

References

Adelman, Zachariah, E. (1999). *A Reevaluation of hte Carbon Bond-IV Photochemical Mechanism*. University of North Carolina at Chapel Hill.

Aldener, M., Brown, S. S., Stark, H., Williams, E. J., Lerner, B. M., Kuster, W. C., … Ravishankara, a. R. (2006). Reactivity and loss mechanisms of NO 3 and N 2 O 5 in a polluted marine environment: Results from in situ measurements during New England Air Quality Study 2002. *Journal of Geophysical Research*, *111*(D23), D23S73. doi:10.1029/2006JD007252

Aljawhary, D., Lee, A. K. Y., & Abbatt, J. P. D. (2013). High-resolution chemical ionization mass spectrometry (ToF-CIMS): application to study SOA composition and processing. *Atmospheric Measurement Techniques*, *6*(11), 3211–3224. doi:10.5194/amt-6-3211-2013

Allen, D. T. (2013). *Personal Correspondence*.

Appel, B. R., Tokiwa, Y., Povard, V., & Kothny, E. L. (1991). The Measurement of Atmospheric Hydrochloric Acid in Southern California. *Atmos. Environ.*, *25*(2), 525–527.

Aschmann, S. M., & Atkinson, R. (1995). Rate Constants for the Gas-Phase Reactions of alkanes with Cl atoms at 296. *International Journal of Chemical Kinetics*, *27*, 613–622.

Atkinson, R., Baulch, D. L., Cox, R. a., Crowley, J. N., Hampson, R. F., Hynes, R. G., … Troe, J. (2007). Evaluated kinetic and photochemical data for atmospheric chemistry: Volume III – gas phase reactions of inorganic halogens. *Atmospheric Chemistry and Physics*, *7*(4), 981–1191. doi:10.5194/acp-7-981-2007

Atkinson, R., Baulch, D. L., Cox, R. a., Crowley, J. N., Hampson, R. F., Hynes, R. G., … Wallington, T. J. (2008). Evaluated kinetic and photochemical data for atmospheric chemistry: Volume IV – gas phase reactions of organic halogen species. *Atmospheric Chemistry and Physics*, *8*(15), 4141–4496. doi:10.5194/acp-8-4141-2008

Ayres, R. U., & Ayres, L. W. (1997). The Life Cycle of Chlorine , Part II: Conversion Processes and Use in the European Chemical Industry. *Journal of Industrial Ecology*, *1*(2), 65–89. doi:10.1162/jiec.1997.1.2.65

Behnke, W., Elend, M., Krüger, U., & Zetzsch, C. (1999). The Influence of NaBr/NaCl Ratio on the Br-Catalysed Production of Halogenated Radicals. *Journal of Atmospheric Chemistry*, *34*, 87–99.

Behnke, W., George, C., Scheer, V., & Zetzsch, C. (1997). Production and decay of ClNO2 from the reaction of gaseous N2O5 with NaCl solution: Bulk and aerosol experiments. *J. Geophys. Res.*, *102*(D3), 3795–3804.

Behnke, W., Krüger, H.-U., Scheer, V., & Zetzsch, C. (1991). Formation of Atomic Cl from Sea Spray via Photolysis of Nitryl Chloride: Determination of the Sticking Coefficient of N2O5 on NaCl Aerosol. *J. Aerosol Sci.*, *22*(1), S609–S612.

Behnke, W., & Zetzsch, C. (1989). Heterogeneous Formation of Chlorine Atoms from Various Aerosols in the Presence of O3 and HCl. *J. Aerosol Sci.*, *20*(8), 1167–1170.

Behnke, W., & Zetzsch, C. (1990). Heterogeneous Photochemical Formation of Cl Atoms from NaCl Aerosol, NOx and Ozone. *J. Aerosol Sci.*, *21*, S229–S232.

Bertram, T. H., Kimmel, J. R., Crisp, T. a., Ryder, O. S., Yatavelli, R. L. N., Thornton, J. a., … Worsnop, D. R. (2011a). A field-deployable, chemical ionization time-of-flight mass spectrometer. *Atmospheric Measurement Techniques*, *4*(7), 1471–1479. doi:10.5194/amt-4-1471-2011

Bertram, T. H., Kimmel, J. R., Crisp, T. a., Ryder, O. S., Yatavelli, R. L. N., Thornton, J. a., … Worsnop, D. R. (2011b). A field-deployable, chemical ionization time-of-flight mass spectrometer: application to the measurement of gas-phase organic and inorganic acids. *Atmospheric Measurement Techniques Discussions*, *4*(2), 1963–1987. doi:10.5194/amtd-4-1963-2011

Bertram, T. H., & Thornton, J. A. (2009). Toward a general parameterization of N2O5 reactivity on aqueous particles: the competing effects of particle liquid water, nitrate and chloride. *Atmospheric Chemistry and Physics Discussions*, *9*(4), 15181–15214. doi:10.5194/acpd-9-15181-2009

Bielski, B. H. J. (1978). Reevaluation of the spectral and kinetic properties of HO2 and O2- free radicals. *Photochemistry and Photobiology*, *28*, 645–649.

Bjergbakke, E., Navaratnam, S., Parsons, B. J., & Swallow, A. J. (1981). Reaction between HO2* and Chlorine in Aqueous Solution. *J. Am. Chem. Soc.*, *103*, 5926–5928.

Brimblecombe, P., & Clegg, S. L. (1988). The solubility and behaviour of acid gases in the marine aerosol. *Journal of Atmospheric Chemistry*, *7*(1), 1–18. doi:10.1007/BF00048251

Brown, S. S., Dubé, W. P., Fuchs, H., Ryerson, T. B., Wollny, A. G., Brock, C. a., … Ravishankara, a. R. (2009). Reactive uptake coefficients for N 2 O 5 determined from aircraft measurements during the Second Texas Air Quality Study: Comparison to current model parameterizations. *Journal of Geophysical Research*, *114*, 1–16. doi:10.1029/2008JD011679

Buxton, G. V., Greenstock, C. L., Helman, W. P., & Ross, A. B. (1988). Critical Review of rate constants for reactions of hydrated electrons, hydrogen atoms and hydroxyl radicals (OH/O in Aqueous Solution). *Journal of Physical and Chemical Reference Data*, *17*(2), 513. doi:10.1063/1.555805

Cai, X., & Griffin, R. J. (2006). Secondary aerosol formation from the oxidation of biogenic hydrocarbons by chlorine atoms. *Journal of Geophysical Research*, *111*(D14), 1–14. doi:10.1029/2005JD006857

Cai, X., Ziemba, L. D., & Griffin, R. J. (2008). Secondary aerosol formation from the oxidation of toluene by chlorine atoms. *Atmospheric Environ*, *42*(32), 7348–7359. doi:10.1016/j.atmosenv.2008.07.014

Canosa-Mas, C. E., Hutton-Squire, H. R., King, M. D., Stewart, D. J., Thompson, K. C., & Wayne, R. P. (1999). Laboratory Kinetic Studies of the Reactions of Cl Atoms with Species of Biogenic Origin: Δ3-Carene, Methacrolein and Methyl Vinyl Ketone. *Journal of Atmospheric Chemistry*, *34*, 163–170.

Carter, W. P. L. (2010a). Development of a Condensed SAPRC-07 Chemical Mechanisms. *Report to the California Air Resources Board, Contract No. 05-750*, 1–94.

Carter, W. P. L. (2010b). Development of the SAPRC-07 Chemical Mechanism and Updated Ozone Reactivity Scales. *Report to the California Air Resources Board, Contracts No. 03-318, 06-408, and 07-730*, 1–381.

Carter, W. P. L., & Atkinson, R. (1996). Development and evaluation of a detailed mechanism for the atmospheric reactions of isoprene and NOx. *International Journal of Chemical Kinetics*, *28*(7), 497–530. doi:10.1002/(SICI)1097-4601(1996)28:7<497::AID-KIN4>3.0.CO;2-Q

Carter, W. P. L., Dongmin, L., & Malkina, I. L. (1997). *Investigation of the Atmospheric Ozone Formation Potential of Trichloroethylene* (pp. 1–71).

Carter, W. P. L., Luo, D., Malkina, I. L., & Pierce, J. A. (1995). *Environmental Chamber Studies of Atmospheric Reactivities of Volatile Organic Compounds. Effects of Varying Chamber and Light Source* (pp. 1–104). Retrieved from http://www.cert.ucr.edu/~carter/pubs/explrept.pdf

Carter, W. P. L., Luo, D., & Malkina, L. (1997). Investigation of the Atmospheric Reactions of Chlorociprin. *Atmospheric Environment*, *31*(10), 1425–1439.

Chang, S., & Allen, D. T. (2006a). Atmospheric chlorine chemistry in southeast Texas: impacts on ozone formation and control. *Environmental Science & Technology*, *40*(1), 251–62. Retrieved from http://www.ncbi.nlm.nih.gov/pubmed/16433359

Chang, S., & Allen, D. T. (2006b). Chlorine chemistry in urban atmospheres: Aerosol formation associated with anthropogenic chlorine emissions in southeast Texas. *Atmospheric Environment*, *40*, 512–523. doi:10.1016/j.atmosenv.2006.04.070

Chang, S., McDonald-Buller, E., Kimura, Y., Yarwood, G., Neece, J., Russell, M., … Allen, D. (2002). Sensitivity of urban ozone formation to chlorine emission estimates. *Atmospheric Environment*, *36*(32), 4991–5003. doi:10.1016/S1352-2310(02)00573-3

Chang, S., Tanaka, P., Mcdonald-buller, E., & Allen, D. T. (2001). Emission inventory for atomic chlorine precursors in Southeast Texas. *Report on Contract 9880077600-18 between The University of Texas and the Texas Natural Resource Conservation Commission*, 1–27.

Charlson, R. J., Schwartz, S. E., Hales, J. M., Cess, R. D., Coakley, J. a, Hansen, J. E., & Hofmann, D. J. (1992). Climate forcing by anthropogenic aerosols. *Science*, *255*(5043), 423–30. doi:10.1126/science.255.5043.423

Cohan, a, Chang, W., Carrerassospedra, M., & Dabdub, D. (2008). Influence of sea-salt activated chlorine and surface-mediated renoxification on the weekend effect in the South Coast Air Basin of California. *Atmospheric Environment*, *42*(13), 3115–3129. doi:10.1016/j.atmosenv.2007.11.046

Connick, R. E. (1947). The Interaction of Hydrogen Peroxide and Hypochlorous Acid in Acidic Solutions Containing Chloride Ion. *J. Am. Chem. Soc.*, *69*, 1509–1514.

Crowley, J. N., Ammann, M., Cox, R. a., Hynes, R. G., Jenkin, M. E., Mellouki, a., … Wallington, T. J. (2010). Evaluated kinetic and photochemical data for atmospheric chemistry: Volume V – heterogeneous reactions on solid substrates. *Atmospheric Chemistry and Physics*, *10*(18), 9059–9223. doi:10.5194/acp-10-9059-2010

Crump, J. G., & Seinfeld, J. H. (1981). Turbulent deposition and gravitational sedimentation of an aerosol in a vessel of arbitrary shape. *Journal of Aerosol Science*, *12*(5), 405–415. doi:10.1016/0021-8502(81)90036-7

Davidson, C. I., Phalen, R. F., & Solomon, P. a. (2005). Airborne Particulate Matter and Human Health: A Review. *Aerosol Science and Technology*, *39*(8), 737–749. doi:10.1080/02786820500191348

Davis, R. A., Ruiz-Ibanez, G., & Sandall, O. C. (1992). Nonisothermal Analysis of the Reaction Kinetics for Chlorine in Basic Hydrogen Peroxide. *Ind. Eng. Chem. Res.*, *31*, 1461–1465.

De Haan, D. O., & Finlayson-Pitts, B. J. (1997). Knudsen Cell Studies of the Reaction of Gaseous Nitric Acid with Synthetic Sea Salt at 298 K. *The Journal of Physical Chemistry A*, *101*(51), 9993–9999. doi:10.1021/jp972450s

Draxler, R. R. (1999). *HYSPLIT_4 User's Guide*. Retrieved from http://www.arl.noaa.gov/documents/reports/arl-230.pdf

Draxler, R. R., & Hess, G. (2010). *Description of the HYSPLIT_4 Modeling System*. Retrieved from http://www.arl.noaa.gov/documents/reports/arl-224.pdf

Draxler, R. R., & Hess, G. D. (1998). *An Overview of the HYSPLIT_4 Modelling System for Trajectories, Dispersion, and Deposition* (Vol. 47, pp. 295–308). Retrieved from http://www.arl.noaa.gov/documents/reports/MetMag.pdf

Eastern Research Group, I., & Sage Environmental Consulting. (2011). *City of Fort Worth Natural Gas Air Quality Study* (pp. 1–320). Retrieved from http://fortworthtexas.gov/uploadedFiles/Gas_Wells/AirQualityStudy_final.pdf

Elliot, A. J., & Buxtont, G. V. (1992). Temperature Dependence of the Reactions OH + O2- and OH + HO2 in Water up to 200 C. *J. Chem. Soc. Faraday Trans.*, *88*(17), 2465–2470.

Erickson, D. J. I., Suezaret, C., Keene, W. C., & Gong, S. L. (1999). A general circulation model based calculation of HCI and CINO2 production from sea salt dechlorination : Reactive Chlorine Emissions Inventory annual production of sea distributions of via direct scavenging or chemical production from The generation of se. *J. Geophys. Res.*, *104*(D7), 8347–8372.

Eriksson, E. (1959). The Yearly Circulation of Chloride and Sulfur in Nature; Meteorological, Geochemical and Pedological Implications. Part I. *Tellus*, *11*(4), 375–403.

Faraji, M., Kimura, Y., McDonald-Buller, E., & Allen, D. (2008). Comparison of the carbon bond and SAPRC photochemical mechanisms under conditions relevant to southeast Texas. *Atmospheric Environment*, *42*(23), 5821–5836. doi:10.1016/j.atmosenv.2007.07.048

Faxon, C. B., & Allen, D. T. (2013). Chlorine chemistry in urban atmospheres: a review. *Environmental Chemistry*, *10*(3), 221. doi:10.1071/EN13026

Faxon, C. B., & Allen, D. T. (2014a). Modeling reactive chlorine chemistry in a shale gas production region, *unpublished - manuscript in preparation*.

Faxon, C. B., & Allen, D. T. (2014b). Development of a Reactive Chlorine Emissions Inventory for the Dallas-Fort Worth Region, *unpiblished - manuscript in preparation*.

Finlayson-Pitts, B. J. (1993). Chlorine Atoms as a Potential Tropospheric Oxidant in the MArine Boundary Layer. *Research on Chemical Intermediates*, *19*(3), 235–249.

Finlayson-Pitts, B. J. (2003). The tropospheric chemistry of sea salt: a molecular-level view of the chemistry of NaCl and NaBr. *Chemical Reviews*, *103*(12), 4801–22. doi:10.1021/cr020653t

Finlayson-Pitts, B. J., Ezell, M. J., & Pitts, J. N. J. (1989). Finlayson-Pitts, et al. - Formation of chemically active chlorine compounds by reactions of atmospheric NaCl particles. *Nature*, *337*(19), 241–244.

Finley, B. D., & Saltzman, E. S. (2006). Measurement of Cl 2 in coastal urban air. *Geophysical Research Letters*, *33*(11), L11809. doi:10.1029/2006GL025799

Finley, B. D., & Saltzman, E. S. (2008). Observations of Cl2 , Br2 , and I2 in coastal marine air. *Journal of Geophysical Research*, *113*(D21), 1–14. doi:10.1029/2008JD010269

FracFocus. (2013). FracFocus Chemical Disclosure Registry. Retrieved January 05, 2013, from http://fracfocus.org/

Frenzel, A., Scheer, V., Sikorski, R., George, C., Behnke, W., & Zetzsch, C. (1998). Heterogeneous Interconversion Reactions of BrNO 2 , ClNO 2 , Br 2 , and Cl 2, *5*(97), 1329–1337.

Gard, E. E. (1998). Direct Observation of Heterogeneous Chemistry in the Atmosphere. *Science*, *279*(5354), 1184–1187. doi:10.1126/science.279.5354.1184

George, C., Ponche, J. L., Mirabel, P., Behnke, W., Scheer, V., & Zetzsch, C. (1994). Study of the Uptake of N2O5 by Water and NaCl Solutions. *J. Phys. Chem.*, *98*, 8780–8784.

George, I. J., & Abbatt, J. P. D. (2010). Heterogeneous oxidation of atmospheric aerosol particles by gas-phase radicals. *Nature Chemistry*, *2*(9), 713–22. doi:10.1038/nchem.806

Gery, M. W., Whitten, G. Z., Killus, J. P., & Dodge, M. C. (1989). A Photochemical Kinetics Mechanism for Urban and Regional Scale Computer Modeling. *J. Geophys. Res.*, *94*(D10), 12,925–12,956.

Graedel, T. E., & Keene, W. C. (1995). Tropospheric budget of reactive chlorine The nine species , to be HOCI and / or vigorous chlorine cycling appears to occur among seasalt aerosol , and CId . The principal of the annual stratospheric chlorine, *9*(1), 47–77.

Graedel, T. E., & Keene, W. C. (1996). The budget and cycle of Earth's natural chlorine. *Pure & Appl. Chem.*, *68*(9), 1689–1697.

Griffin, R., Dibb, J., Lefer, B., & Steiner, A. (2011). *Final Report: Surface Measurements and One-Dimensional Modeling Related to Ozone Formation in the Suburban Dallas-Fort Worth Area* (pp. 1–45).

GWPC, G. W. P. C., & ALL, A. C. (2009). *Modern Shale Gas Development in the United States: A Primer*. Retrieved from http://www.all-llc.com/publicdownloads/ShaleGasPrimer2009.pdf

Hall, D. C. (2012). *Dallas City Hall Website*. Retrieved from http://www.dallascityhall.com

Harrison, R. M., & Allen, A. G. (1990). Measurements of Atmospheric HNO3, HCl and Associated Species on a Small Network in Eastern England. *Atmos. Environ.*, *24A*(2), 369–376.

Held, A. M., Halko, D. J., & Hurst, J. K. (1978). Mechanisms of Chlorine Oxidation of Hydrogen Peroxide. *J. Am. Chem. Soc.*, *100*(18), 5732–5740.

Heo, G., Kimura, Y., McDonald-Buller, E., Carter, W. P. L., Yarwood, G., & Allen, D. T. (2010). Modeling alkene chemistry using condensed mechanisms for conditions relevant to southeast Texas, USA. *Atmospheric Environment*, *44*(40), 5365–5374. doi:10.1016/j.atmosenv.2009.10.001

Herrmann, H., Majdik, Z., Ervens, B., & Weise, D. (2003). Halogen production from aqueous tropospheric particles. *Chemosphere*, *52*(2), 485–502. doi:10.1016/S0045-6535(03)00202-9

Hildebrandt, L., Donahue, N. M., & Pandis, S. N. (2009). and Physics High formation of secondary organic aerosol from the photo-oxidation of toluene, (1996), 2973–2986.

Hildebrandt, L., Henry, K. M., Kroll, J. H., Worsnop, D. R., Pandis, S. N., & Donahue, N. M. (2011). Evaluating the mixing of organic aerosol components using high-resolution aerosol mass spectrometry. *Environmental Science & Technology*, *45*(15), 6329–35. doi:10.1021/es200825g

Holzwarth, G., Balmer, G., & Soni, L. (1984a). The fate of chlorine and chloramines in cooling towers: Henry's Law Constants for Flashoff. *Water Res.*, *18*(11), 1421–1427.

Holzwarth, G., Balmer, R. G., & Soni, L. (1984b). The fate of chlorine in recirculating cooling towers: Field Results. *Water Res.*, *18*(11), 1429–1435.

Hov, Φ. (1985). The Effect of Chlorine on the Formation of Photochemical Oxidants in Southern Telemark, Norway. *Atmospheric Environment*, *19*(3), 471–485.

Hu, D., Chen, J., Ye, X., Li, L., & Yang, X. (2011). Hygroscopicity and evaporation of ammonium chloride and ammonium nitrate: Relative humidity and size effects on the growth factor. *Atmospheric Environment*, *45*(14), 2349–2355. doi:10.1016/j.atmosenv.2011.02.024

Hu, J. H., & Abbatt, J. P. D. (1997). Reaction Probabilities for N 2 O 5 Hydrolysis on Sulfuric Acid and Ammonium Sulfate Aerosols at Room Temperature. *J. Phys. Chem.*, *101*, 871–878.

Hunt, S. W., Robertson, W. H., Roeselová, M., Vieceli, J., Wang, W., Wingen, L. M., … Jungwirth, P. (2004). *Reactions of Ozone and Hydroxyl Radical With Sea Salt Aerosol: Implications Aqueous Sea Salt Particles in the Atmosphere*. Retrieved from http://marge.uochb.cas.cz/~roesel/present/CRC_talk.pdf

Impey, G. A., Shepson, P. B., Hastie, D. R., & Barrie, L. A. (1997). Measurements of photolyzable chlorine and bromine during the Polar Sunrise Experiment 1995. *J. Geophys. Res.*, *102*(D13), 16,005–16,010.

Impey, G. A., Shepson, P. B., Hastie, D. R., Bartie, L. A., & Lafayette, W. (1997). Measurement technique for the determination of photolyzable chlorine and bromine in the atmosphere, *102*.

Jacob, D. J. (2000). Heterogeneous chemistry and tropospheric ozone, *34*(April 1998).

Jobson, B. T., Niki, H., Bottenheim, J., Hopper, F., & Leaitch, R. (1994). Measurements of C2-C6 hydrocarbons during the Polar Sunrise 1992 Experiment ' Evidence for Cl atom and Br atom chemistry, *99*(May 1989).

John, W., Wall, S. M., & Ondo, J. L. (1988). A New Method for Nitric Acid and Nitrate Aerosol Measurement Using the Dichotomous Sampler. *Atmos. Environ.*, *22*(8), 1627–1635.

Kanakidou, M., Seinfeld, J. H., Pandis, S. N., Barnes, I., Dentener, F. J., Facchini, M. C., … Wilson, J. (2005). Organic aerosol and global climate modelling: a review. *Atmospheric Chemistry and Physics1. Kanakidou M, Seinfeld JH, Pandis SN, Barnes I, Dentener FJ, Facchini MC, et Al. Organic Aerosol and Global Climate Modelling: A Review. Atmos Chem Phys [Internet]. 2005 Mar 30;5(4):1053–123. Available from: Http://www.a*, *5*(4), 1053–1123. doi:10.5194/acp-5-1053-2005

Karlsson, R. S., Szente, J. J., Ball, J. C., & Maricq, M. M. (2001). Homogeneous Aerosol Formation by the Chlorine Atom Initiated Oxidation of Toluene. *The Journal of Physical Chemistry A*, *105*(1), 82–96. doi:10.1021/jp001831u

Keene, C., Aslam, M., Khalil, K., Erickson, J., Archie, I. I. I., Graedel, E., … Li, Y. F. (1999). Composite global emissions of reactive chlorine from anthropogenic and natural sources : Reactive Chlorine Emissions Inventory. *Journal of Geophysical Research*, *104*(1998), 8429–8440.

Keene, W. C., Pszenny, A. A. P., Gallowayt, J. N., Division, O. C., & Causeway, R. (1993). Measurement Technique for Inorganic Chlorine Gases in the Marine Boundary Layer, (18), 866–874.

Keene, W. C., Pszenny, A. A. P., Jacob, D. J., Duce, R. A., Galloway, J. N., Schultz-Tokos, J. J., … Boatman, J. F. (1990). The Geochemical Cycling of Reactive Chlorine Through the Marine Troposphere. *Global Biogeochemical Cycles*, *4*(4), 407–430.

Keene, W. C., Sander, R., Pszenny, A. A. P., Vogt, T. R., Crutzen, P. J., Galloway, J. N., … Hall, C. (1998). AEROSOL pH IN THE MARINE BOUNDARY LAYER : A REVIEW AND MODEL EVALUATION, *29*(3).

Kercher, J. P., Riedel, T. P., & Thornton, J. A. (2009). Chlorine activation by N2O5: simultaneous, in situ detection of ClNO2 and N2O5 by chemical ionization mass spectrometry. *Atmos. Measu. Tech.*, *2*, 193–204.

Khalil, M. A. K., Moore, R. M., Harper, D. B., Lobert, J. M., Erickson, D. J., Koropalov, V., … Keene, W. C. (1999). Natural emissions of chlorine-containing gases: Reactive Chlorine Emissions Inventory. *Journal of Geophysical Research*, *104*(D7), 8333–8346.

Kılıç, M., & Çınar, Z. (2008). Hydroxyl radical reactions with 4-chlorophenol as a model for heterogeneous photocatalysis. *Journal of Molecular Structure: THEOCHEM*, *851*(1-3), 263–270. doi:10.1016/j.theochem.2007.11.022

Kiliç, M., Koçtürk, G., San, N., & Cinar, Z. (2007). A model for prediction of product distributions for the reactions of phenol derivatives with hydroxyl radicals. *Chemosphere*, *69*(9), 1396–408. doi:10.1016/j.chemosphere.2007.05.002

Knipping, E. M. (2000a). Experiments and Simulations of Ion-Enhanced Interfacial Chemistry on Aqueous NaCl Aerosols. *Science*, *288*(5464), 301–306. doi:10.1126/science.288.5464.301

Knipping, E. M. (2000b). Experiments and Simulations of Ion-Enhanced Interfacial Chemistry on Aqueous NaCl Aerosols. *Science*, *288*(5464), 301–306. doi:10.1126/science.288.5464.301

Knipping, E. M. (2002). Modeling Cl 2 formation from aqueous NaCl particles: Evidence for interfacial reactions and importance of Cl 2 decomposition in alkaline solution. *Journal of Geophysical Research*, *107*(D18). doi:10.1029/2001JD000867

Knipping, E. M., & Dabdub, D. (2002). Modeling Cl 2 formation from aqueous NaCl particles: Evidence for interfacial reactions and importance of Cl 2 decomposition in alkaline solution. *Journal of Geophysical Research*, *107*(D18), 4360. doi:10.1029/2001JD000867

Knipping, E. M., & Dabdub, D. (2003). Impact of chlorine emissions from sea-salt aerosol on coastal urban ozone. *Environmental Science & Technology*, *37*(2), 275–84. Retrieved from http://www.ncbi.nlm.nih.gov/pubmed/12564898

Kosak-Channing, L. F., & Helz, G. R. (1983). Solubility of Ozone in Aqueous Solutions of 0-0.6 M Ionic Strength at 5-30 C. *Environmental Science & Technology*, *17*(3), 145–9. doi:10.1021/es00109a005

Laux, J. M., Hemminger, J. C., & Finlayson-Pitts, B. J. (1994). X-ray photoelectron spectroscopic studies of the heterogeneous reaction of gaseous nitric acid with sodium chloride: Kientics and contribution to the chemistry of the marine troposphere. *Geopys. Res. Lett.*, *21*(15), 1623–1626.

Lin, C.-J., & Pehkonen, S. O. (1999). The chemistry of atmospheric mercury: a review. *Atmospheric Environment*, *33*, 2067–2079.

Lind, J. A., Kok, G. L., Lind, A., & Journal, L. K. (1994). Correction to "Henry's law determinations for aqueous solutions of hydrogen peroxide, methylhydroperoxide, and peroxyacetic acid" by John A. Lind and Gregory L. Kok. *J. Geophys. Res.*, *99*(D10), 21,119.

Liu, B. Y. H., & Agarwal, J. K. (1974). Experimental Observation of Aerosol Deposition in Turbulent Flow. *Aerosol Science*, *5*, 145–155.

Livingston, F. E., & Finlayson-Pitts, B. J. (1991). The Reaction of Gaseous N2O5 with Solid NaCl at 298K: Estimated Lower Limit to the Reaction Probability and Its Potential Role in Tropospheric and Stratospheric Chemistry. *Geopys. Res. Lett.*, *18*(1), 17–20.

Lobert, J. M., Keene, W. C., Logan, J. A., & Yevich, R. (1999). Global chlorine emissions from biomass burning : Reactive Chlorine Emissions Inventory. *Journal of Geophysical Research*, *104*(D7), 8373–8389.

Maben, J. R., Keene, C., Pszenny, A. A. P., Galloway, J. N., & C, C. (1995). Volatile inorganic CI in surface air over eastern of, *22*(24), 3513–3516.

Makower, B., & Bray, W. C. (1933). The Rate of Oxidation of Hydrogen Peroxide by Chlorine in the Presence of Hydrochloric Acid. *J. Am. Chem. Soc.*, *55*(12), 4765–4776.

Marsh, A. R. W., & McElroy, W. J. (1985). The Dissociation Constant and Henry's Law Constant of HCl in Aqueous Solution. *Atmos. Environ.*, *19*(7), 1075–1080.

Matusca, P., Schwarz, B., & Bachmann, K. (1984). Measurements of Diurnal Concentration Variations of Gaseous HCl in Air in the Sub-nanogram Range. *Atmos. Environ.*, *18*(8), 1667–1675.

Mazurek, M., Masonjones, M. C., Masonjones, H. D., Salmon, L. G., Cass, G. R., Hallock, K. A., & Leach, M. (1997). Visibility-reducing organic aerosols in the vicinity of Grand Canyon National Park: Properties observed by high resolution gas chromatography National. *Journal of Geophysical Research*, *102*(D3), 3779–3793.

McCulloch, A., Aucott, M. L., Benkovitz, C. M., Graedel, T. E., Kleiman, G., Midgley, P. M., & Li, Y.-F. (1999). Global emissions of hydrogen chloride and chloromethane from coal combustion, incineration and industrial activities: Reactive Chlorine Emissions Inventory. *Journal of Geophysical Research*, *104*(D7), 8391. doi:10.1029/1999JD900025

McMurry, P. H., & Rader, D. J. (1985). Aerosol Wall Losses in Electrically Charged Chambers. *Aerosol Science and Technology*, *4*(3), 249–268. doi:10.1080/02786828508959054

Mielke, L. H., Furgeson, A., & Osthoff, H. D. (2011). Observation of $ClNO_2$ in a mid-continental urban environment. *Environmental Science & Technology*, *45*(20), 8889–96. doi:10.1021/es201955u

Mulder, P., & Louw, R. (1986). Vapour-phase chemistry of arenes. Part XII. Reaction of chlorobenzene and derivatives with hydroxyl radicals at approx. 290C. Hydroxy-dechlorination., *224*, 220–224.

Nelson, L., Rattigan, O., Neavyn, R., & Sidebottom, H. (1990). Absolute and Relative Rate Constants for Reactions of Hydroxyl Radicals and Chlorine Atoms with Series of Aliphatic Alcohols and Ethers at 298K. *International Journal of Chemical Kinetics*, *22*, 1111–1126.

Nenes, A. (1998). ISORROPIA : A New Thermodynamic Equilibrium Model for Multiphase Multicomponent Inorganic Aerosols, 123–152.

Nenes, A., Pandis, S. N., & Pilinis, C. (1998). ISORROPIA : A New Thermodynamic Equilibrium Model for Multiphase Multicomponent Inorganic Aerosols. *Aquatic Geochemistry*, *4*, 123–152.

Neta, P., Huie, R. E., & Ross, A. B. (1988). Rate Constants for Reactions of Inorganic Radicals in Aqueous Solution. *Journal of Physical and Chemical Reference Data*, *17*(3), 1027. doi:10.1063/1.555808

Ng, N. L., Herndon, S. C., Trimborn, a., Canagaratna, M. R., Croteau, P. L., Onasch, T. B., … Jayne, J. T. (2011). An Aerosol Chemical Speciation Monitor (ACSM) for Routine Monitoring of the Composition and Mass Concentrations of Ambient Aerosol. *Aerosol Science and Technology*, *45*(7), 780–794. doi:10.1080/02786826.2011.560211

Nissenson, P., Thomas, J. L., Finlayson-Pitts, B. J., & Dabdub, D. (2008). Sensitivity and uncertainty analysis of the mechanism of gas-phase chlorine production from NaCl aerosols in the MAGIC model. *Atmospheric Environment*, *42*(29), 6934–6941. doi:10.1016/j.atmosenv.2008.04.041

Nordmeyer, T., Wang, W., Ragains, M. L., Finlayson-Pitts, B. J., Spicer, C. W., & Plastridge, R. A. (1997). Unique products of the reaction of isoprene with atomic chlorine: Potential markers of chlorine atom chemistry. *Geopys. Res. Lett.*, *24*(13), 1615–1618.

NSPF, N. S. P. F. (2012). *CDC Fact Sheet for Pool Staff: Your Disinfection Team - Chlorine & pH*. Retrieved from http://nspf.org/Files/cdcfnlphcl.pdf

Osthoff, H. D., Roberts, J. M., Ravishankara, a. R., Williams, E. J., Lerner, B. M., Sommariva, R., … Brown, S. S. (2008). High levels of nitryl chloride in the polluted subtropical marine boundary layer. *Nature Geoscience*, *1*(5), 324–328. doi:10.1038/ngeo177

Oum, K. W., Lakin, M. J., DeHaan, D. O., Brauers, T., & Finlayson-Pitts, B. J. (1998). Formation of Molecular Chlorine from the Photolysis of Ozone and Aqueous Sea-Salt Particles. *Science*, *279*(5347), 74–76. doi:10.1126/science.279.5347.74

Parrish, D. D., Allen, D. T., Bates, T. S., Estes, M., Fehsenfeld, F. C., Feingold, G., … Williams, E. J. (2009). Overview of the Second Texas Air Quality Study (TexAQS II) and the Gulf of Mexico Atmospheric Composition and Climate Study (GoMACCS). *Journal of Geophysical Research*, *114*, D00F13. doi:10.1029/2009JD011842

Paulson, S. E., Chung, M., Sen, A. D., & Orzechowska, G. (1998). Measurement of OH radical formation from the reaction of ozone with several biogenic alkenes. *J. Geophys. Res.*, *103*(D19), 25,533–25,539.

Pechtl, S., & von Glasow, R. (2007). Reactive chlorine in the marine boundary layer in the outflow of polluted continental air: A model study. *Geophysical Research Letters*, *34*(11), L11813. doi:10.1029/2007GL029761

Pierce, J. R., Engelhart, G. J., Hildebrandt, L., Weitkamp, E. a., Pathak, R. K., Donahue, N. M., … Pandis, S. N. (2008). Constraining Particle Evolution from Wall Losses, Coagulation, and Condensation-Evaporation in Smog-Chamber Experiments: Optimal Estimation Based on Size Distribution Measurements. *Aerosol Science and Technology*, *42*(12), 1001–1015. doi:10.1080/02786820802389251

Pior, R. (2012). *Personal Correspondence* (p. 1). Fort Worth, TX.

Pszenny, A. a. P., Fischer, E. V., Russo, R. S., Sive, B. C., & Varner, R. K. (2007). Estimates of Cl atom concentrations and hydrocarbon kinetic reactivity in surface air at Appledore Island, Maine (USA), during International Consortium for Atmospheric Research on Transport and Transformation/Chemistry of Halogens at the Isles of Shoals. *Journal of Geophysical Research*, *112*(D10), D10S13. doi:10.1029/2006JD007725

Pszenny, A. A. P., Keene, W. C., Jacob, D. J., Fan, S., Maben, J. R., & Zetwo, M. P. (1993). Evidence of Inorganic Chlorine Gases Other than Hydrogen Chloride in Marine Surface Air. *Geopys. Res. Lett.*, *20*(8), 699–702.

Pszenny, A. A. P., Moldanov, J., Keene, W. C., Sander, R., Maben, J. R., Martinez, M., … Prinn, R. G. (2004). Halogen cycling and aerosol pH in the Hawaiian marine boundary layer. *Atmos. Chem. Phys.*, *4*, 147–168.

Raff, J. D., Njegic, B., Chang, W. L., Gordon, M. S., Dabdub, D., Gerber, R. B., & Finlayson-pitts, B. J. (2009). Chlorine activation indoors and outdoors via surface-mediated reactions of nitrogen, *106*(33).

Ragains, M. L., & Finlayson-Pitts, B. J. (1997). Kinetics and Mechanism of the Reaction of Cl Atoms with 2-Methyl-1,3-butadiene (Isoprene) at 298 K. *J. Phys. Chem. A*, *5639*(96), 1509–1517.

Ravishankara, A. R. (1997). Heterogeneous and Multiphase Chemistry in the Troposphere. *Science*, *276*, 1058–1065.

Reff, A., Bhave, P. V, Simon, H., Pace, T. G., Pouliot, G. a, Mobley, J. D., & Houyoux, M. (2009). Emissions inventory of PM2.5 trace elements across the United States. *Environmental Science & Technology*, *43*(15), 5790–6. Retrieved from http://www.ncbi.nlm.nih.gov/pubmed/19731678

Riedel, T. P., Bertram, T. H., Crisp, T. A., Williams, E. J., Lerner, B. M., Vlasenko, A., … Thornton, J. a. (2012). Nitryl chloride and molecular chlorine in the coastal marine boundary layer. *Environmental Science & Technology*, *46*(19), 10463–70. doi:10.1021/es204632r

Riemer, D., & Apel, E. (2002). *Final Report to: Texas Natural Resource Conservation Commission, Contract 58203473* (pp. 1–15). Retrieved from http://tceq.info/assets/public/implementation/air/am/contracts/reports/oth/ConfirmingPresenceandExtentOfOxidationByCI.pdf

Roberts, J. M., Osthoff, H. D., Brown, S. S., & Ravishankara, a R. (2008a). N2O5 oxidizes chloride to Cl2 in acidic atmospheric aerosol. *Science (New York, N.Y.)*, *321*(5892), 1059. doi:10.1126/science.1158777

Roberts, J. M., Osthoff, H. D., Brown, S. S., & Ravishankara, a R. (2008b). N2O5 oxidizes chloride to Cl2 in acidic atmospheric aerosol. *Science (New York, N.Y.)*, *321*(5892), 1059. doi:10.1126/science.1158777

Roberts, J. M., Osthoff, H. D., Brown, S. S., Ravishankara, A. R., Coffman, D., Quinn, P., & Bates, T. (2009). Laboratory studies of products of N 2 O 5 uptake on Cl − containing substrates. *Geophysical Research Letters*, *36*(20), L20808. doi:10.1029/2009GL040448

Rogozen, M. B., Rich, H. E., Guttman, M. A., Corporation, S. A. I., Grosjean, D., & Williams, E. L. (1988). *Sources and Cocnentrtions of Chloroform Emissions in the South Coast Air Basin: Executive Summary* (pp. 1–44).

Rolph, G. D. (2014). Real-time Environmental Applications and Display sYstem (READY) Website. *NOAA Air Resources Laboratory*. Retrieved January 07, 2012, from http://ready.arl.noaa.gov

Rossi, M. J. (1996). Atmospheric Pollution: The Role of Heterogeneous Chemical Reactions. *Chimia*, *50*, 199–208.

Rossi, M. J. (2003). Heterogeneous reactions on salts. *Chemical Reviews*, *103*(12), 4823–82. doi:10.1021/cr020507n

Ruiz-ibanez, G., & Sandall, O. C. (1991). Kinetics for the Reaction between Chlorine and Basic Hydrogen Peroxide. *Ind. Eng. Chem. Res.*, *30*(2), 1105–1110.

Sander, S. P., Friedl, R. R., Barker, J. R., Golden, D. M., Kurylo, M. J., Sciences, G. E., … Orkin, V. L. (2011). Chemical Kinetics and Photochemical Data for Use in Atmospheric Studies: Evaluation Number 17. *JPL Publication 10-6*, (17).

Sarwar, G., & Bhave, P. V. (2007). Modeling the Effect of Chlorine Emissions on Ozone Levels over the Eastern United States. *Journal of Applied Meteorology and Climatology*, *46*(7), 1009–1019. doi:10.1175/JAM2519.1

Sarwar, G., Simon, H., Bhave, P., & Yarwood, G. (2012). Examining the impact of heterogeneous nitryl chloride production on air quality across the United States. *Atmospheric Chemistry and Physics*, *12*(14), 6455–6473. doi:10.5194/acp-12-6455-2012

Sauer, M. C., Brown, W. G., & Hard, E. J. (1984). O(3P) Atom Formation by the Photolysis of Hydrogen Peroxide in Alkaline Aqueous Solutions. *J. Phys. Chem.*, *88*, 1398–1400.

Saul, T. D., Tolocka, M. P., & Johnston, M. V. (2006). Reactive uptake of nitric acid onto sodium chloride aerosols across a wide range of relative humidities. *The Journal of Physical Chemistry. A*, *110*(24), 7614–20. doi:10.1021/jp060639a

SBI. (2007). *U.S. Market for Swimming Pool Equipment and Maintenance Products. Market research report SKU: SB1461666*. Retrieved from http://www.marketresearch.com/SBI-v775/Swimming-Pool-Equipment-Maintenance-Products-1461666/view-toc/

Schütze, M., & Herrmann, H. (2002). Determination of phase transfer parameters for the uptake of HNO3, N2O5 and O3 on single aqueous drops. *Physical Chemistry Chemical Physics*, *4*(1), 60–67. doi:10.1039/b106078n

Schwartz, S. E. (1984). Gas- and Aqueous-Phase Chemistry of HO2 in Liquid Water Clouds. *J. Geophys. Res.*, *89*(4), 11,589–11,598.

Schweitzer, F., Mirabel, P., & George, C. (1998). Multiphase Chemistry of N2O5 , ClNO2 , and BrNO2, *2*(3), 3942–3952.

Seinfeld, J. H., & Pandis, S. N. (2006). *Atmospheric Chemistry and Physics: From Air Pollution to Climate Change*. Hoboken, New Jersey: John Wiley & Sons.

Simon, H. (2006). *Comprehensive assessment of fine particulate matter emissions inventories and development of improved allocation profiles*. The University of Texas at Austin.

Simon, H. A. (2008a). Heterogeneous N 2 O 5 Chemistry in the Houston Atmosphere.

Simon, H. A. (2008b). *Heterogeneous N2O5 Chemistry in the Houston Atmosphere*. The Universoty of Texas at Austin.

Simon, H., Kimura, Y., McGaughey, G., Allen, D. T., Brown, S. S., Coffman, D., Roberts, J. M. (2010). Modeling heterogeneous ClNO2 formation, chloride availability, and chlorine cycling in Southeast Texas. *Atmospheric Environment*, *44*(40), 5476–5488. doi:10.1016/j.atmosenv.2009.09.006

Simon, H., Kimura, Y., McGaughey, G., Allen, D. T., Brown, S. S., Osthoff, H. D., Lee, D. (2009). Modeling the impact of ClNO 2 on ozone formation in the Houston area. *Journal of Geophysical Research*, *114*, D00F03. doi:10.1029/2008JD010732

Singh, H. B., Gregory, G. L., Anderson, B., Browell, E., Sachse, G. W., Davis, D. D., Merrill, J. (1996). Low ozone in the marine boundary layer of the tropical Pacific Ocean: Photochemical loss, chlorine atoms, and entrainment. *Journal of Geophysical Research*, *101*(D1), 1907. doi:10.1029/95JD01028

Singh, H. B., & Kasting, J. F. (1988). Chlorine-Hydrocarbon Photochemistry in the Marine Troposphere and Lower Stratosphere. *Journal of Atmospheric Chemistry*, *7*, 261–285.

Sokolov, O., Hurley, M. D., Wallington, T. J., Kaiser, E. W., Platz, J., Nielsen, O. J., … Lesclaux, R. (1998). Kinetics and Mechanism of the Gas-Phase Reaction of Cl Atoms with Benzene. *The Journal of Physical Chemistry A*, *102*(52), 10671–10681. doi:10.1021/jp9828080

Spicer, C., Chapman, E., Finlayson-Pitts, B., Plastrige, R., Hubbe, J., Fast, J., & Berkowitz, C. (1998). Unexpectedly high concentrations of molecular chlorine in coastal air. *Nature*, *394*(July 1998), 353–356. Retrieved from http://www.nature.com/nature/journal/v394/n6691/abs/394353a0.html

Sturges, W. T., & Barrie, L. A. (1988). Chlorine, Bromine and Iodine in Arctic Aerosols. *Atmos. Env.*, *22*(6), 1179–1194.

Stutz, J., Ackermann, R., Fast, J. D., & Barrie, L. (2002). Atmospheric reactive chlorine and bromine at the Great Salt Lake, Utah. *Geophysical Research Letters*, *29*(10), 18–21.

Stutz, J., Ezell, M. J., Ezell, a. a., & Finlayson-Pitts, B. J. (1998). Rate Constants and Kinetic Isotope Effects in the Reactions of Atomic Chlorine with n -Butane and Simple Alkenes at Room Temperature. *The Journal of Physical Chemistry A*, *102*(44), 8510–8519. doi:10.1021/jp981659i

Stutz, J., Jobson, B. T., & Sumner, A. L. (2009). Impact of Reactive Halogen Species on the Air Quality in California Coastal Areas. *Final Report to the Coordinating Research Council, Inc. and the California Air Resources Board in Fulfillment of Contracts A-62-1 and A-62-2 and Agreement #05-307*, 1–125.

Sullivan, R. C., Guazzotti, S. a., Sodeman, D. a., Tang, Y., Carmichael, G. R., & Prather, K. a. (2007). Mineral dust is a sink for chlorine in the marine boundary layer. *Atmospheric Environment*, *41*(34), 7166–7179. doi:10.1016/j.atmosenv.2007.05.047

Tanaka, P. L. (2003a). An environmental chamber investigation of chlorine-enhanced ozone formation in Houston, Texas. *Journal of Geophysical Research*, *108*(D18), 4576. doi:10.1029/2002JD003314

Tanaka, P. L. (2003b). Development of a chlorine mechanism for use in the carbon bond IV chemistry model. *Journal of Geophysical Research*, *108*(D4), 4145. doi:10.1029/2002JD002432

Tanaka, P. L., Riemer, D. D., Chang, S., Yarwood, G., McDonald-Buller, E. C., Apel, E. C., … Allen, D. T. (2003a). Direct evidence for chlorine-enhanced urban ozone formation in Houston, Texas. *Atmospheric Environment*, *37*(9-10), 1393–1400. doi:10.1016/S1352-2310(02)01007-5

Tanaka, P. L., Riemer, D. D., Chang, S., Yarwood, G., McDonald-Buller, E. C., Apel, E. C., … Allen, D. T. (2003b). Direct evidence for chlorine-enhanced urban ozone formation in Houston, Texas. *Atmospheric Environment*, *37*(9-10), 1393–1400. doi:10.1016/S1352-2310(02)01007-5

Thomas, J. L., Jimenez-Aranda, A., Finlayson-Pitts, B. J., & Dabdub, D. (2006). Gas-phase molecular halogen formation from NaCl and NaBr aerosols: when are interface reactions important? *The Journal of Physical Chemistry. A*, *110*(5), 1859–67. doi:10.1021/jp054911c

Thornton, J. A., & Abbatt, J. P. D. (2005). N(2)O(5) reaction on submicron sea salt aerosol: kinetics, products, and the effect of surface active organics. *The Journal of Physical Chemistry. A*, *109*(44), 10004–12. doi:10.1021/jp054183t

Thornton, J. A., Kercher, J. P., Riedel, T. P., Wagner, N. L., Cozic, J., Holloway, J. S., … Brown, S. S. (2010). A large atomic chlorine source inferred from mid-continental reactive nitrogen chemistry. *Nature*, *464*(March), 271–274. doi:10.1038/nature08905

Thornton, J. A., Kercher, J. P., Riedel, T. P., Wagner, N. L., Cozic, J., Holloway, J. S., … Brown, S. S. (2010). A large atomic chlorine source inferred from mid-continental reactive nitrogen chemistry. *Nature*, *464*(7286), 271–4. doi:10.1038/nature08905

U.S. Dept. of Commerce: U.S. Census Bureau. (2013). *State and County QuickFacts*. Retrieved from http://quickfacts.census.gov/qfd/

USEPA, O. of R. and D. (2011a). *Plan to Study the Potential Impacts of Hydraulic Fracturing on Drinking Water Resources* (pp. 1–190). Retrieved from http://water.epa.gov/type/groundwater/uic/class2/hydraulicfracturing/upload/hf_study_plan_110211_final_508.pdf

USEPA, O. of R. and D. (2011b). *Proceedings of the Technical Workshops for the Hydraulic Fracturing Study : Chemical & Analytical Methods* (pp. 1–122). Retrieved from http://water.epa.gov/type/groundwater/uic/class2/hydraulicfracturing/upload/proceedingsofhfchemanalmethodsfinalmay2011.pdf

USEPA, U. S. E. P. A. (2012). *WaterSense: An EPA Partnership Program*. Retrieved from http://epa.gov/watersense/our_water/water_use_today.html

Volpe, C., Wahlen, M., Pszenny, A. A. P., & Spivack, A. J. (1998). Chlorine isotopic composition of marine aerosols : Implications for the release of reactive chlorine and 1tCl cycling rates Relative They through experiments that this 2- Nss NI-I4 Note : Nss-SO42-. *Geophysical Research Letters*, *25*(20), 3831–3834.

Wahner, A., & Zetzsch, C. (1983). Rate Constants for the Addition of OH to Aromatics (Benzene, p-Chloroaniline, and o-, m-, and p-Dichlorobenzene) and the Unimolecular Decay of the Adduct. Kinetics into a Quasi-Equilibrium. *J. Phys. Chem.*, *87*(24), 4945–4951.

Wang, L., Arey, J., & Atkinson, R. (2005). Reactions of chlorine atoms with a series of aromatic hydrocarbons. *Environmental Science & Technology*, *39*(14), 5302–10. Retrieved from http://www.ncbi.nlm.nih.gov/pubmed/16082960

Wang, L., Thompson, T., McDonald-Buller, E. C., & Allen, D. T. (2007). Photochemical modeling of emissions trading of highly reactive volatile organic compounds in Houston, Texas. 2. Incorporation of chlorine emissions. *Environmental Science & Technology*, *41*(7), 2103–7. Retrieved from http://www.ncbi.nlm.nih.gov/pubmed/17438749

Wang, L., Thompson, T., Mcdonald-buller, E. C., Webb, A., & Allen, D. T. (2007). Policy Analysis Photochemical Modeling of Emissions Trading of Highly Reactive Volatile Organic Reactivity Based Trading and Potential for Ozone Hot Spot Formation. *Environ. Sci. Technol.*, *41*(7), 2095–2102.

Wang, W., & Finlayson-Pitts, B. J. (2001). Unique markers of chlorine atom chemistry in coastal urban areas: The reaction with 1,3-butadiene in air at room temperature. *Journal of Geophysical Research*, *106*(D5), 4939. doi:10.1029/2000JD900683

Watson, R. T. (1977). Rate Constants for Reactions of ClOx of Atmospheric Interest. *J. Phys. Chem. Ref. Data*, *6*(3), 871–917.

Whitten, G. Z., Heo, G., Kimura, Y., McDonald-Buller, E., Allen, D. T., Carter, W. P. L., & Yarwood, G. (2010). A new condensed toluene mechanism for Carbon Bond: CB05-TU☆. *Atmospheric Environment*, *44*(40), 5346–5355. doi:10.1016/j.atmosenv.2009.12.029

Whitten, G. Z., Hogo, H., & Killus, J. P. (1980). The Carbon-Bond Mechanism: A Condensed Kinetic Mechanism for Photochemical Smog. *Environmental Science & Technology*, *14*(6), 690–700.

Wiedinmyer, C., Akagi, S. K., Yokelson, R. J., Emmons, L. K., Al-Saadi, J. a., Orlando, J. J., & Soja, a. J. (2011). The Fire INventory from NCAR (FINN): a high resolution global model to estimate the emissions from open burning. *Geoscientific Model Development*, *4*(3), 625–641. doi:10.5194/gmd-4-625-2011

Wilhelm, E., Battino, R., & Wilcock, R. J. (1977). Low-Pressure Solubility of Gases in Liquid Water. *Chemical Reviews*, *77*(2), 219–262.

Wingenter, O. W., Blake, D. R., Blake, N. J., Sive, B. C., Rowland, F. S., Atlas, E., & Flocke, F. (1999). Tropospheric hydroxyl and atomic chlorine concentrations, and mixing timescales determined from hydrocarbon and halocarbon measurements made over the Southern Ocean. *Journal of Geophysical Research*, *104*(D17), 21,819–21,828.

Wingenter, O. W., Kubo, M. K., Blake, N. J., Smith, T. W., Blake, D. R., & Rowland, F. S. (1996). Hydrocarbon and halocarbon measurements as photochemical and dynamical indicators of atmospheric hydroxyl, atomic chlorine, and vertical mixing obtained during Lagrangian flights. *Journal of Geophysical Research*, *101*(D2), 4331. doi:10.1029/95JD02457

Xu, F., Wang, H., Zhang, Q., Zhang, R., Qu, X., & Wang, W. (2010). Kinetic properties for the complete series reactions of chlorophenols with OH radicals-relevance for dioxin formation. *Environmental Science & Technology*, *44*(4), 1399–1404. doi:10.1021/es9031776

Yarwood, G., Jung, J., Whitten, G. Z., Heo, G., Mellberg, J., & Estes, M. (2010). Updates to the Carbon Bond Mechanism for Version 6 (CB6). In *Presented at the 9th Annual CMAS Conference, Chapel Hill, NC, October 11-13* (Vol. 6, pp. 1–4).

Yarwood, G., & Rao, S. (2005). Updates to the Carbon Bond Chemical Mechanism: CB05. *Report RT-04-00675*.

Yatavelli, R. L. N., Lopez-Hilfiker, F., Wargo, J. D., Kimmel, J. R., Cubison, M. J., Bertram, T. H., … Thornton, J. a. (2012). A Chemical Ionization High-Resolution Time-of-Flight Mass Spectrometer Coupled to a Micro Orifice Volatilization Impactor (MOVI-HRToF-CIMS) for Analysis of Gas and Particle-Phase Organic Species. *Aerosol Science and Technology*, *46*(12), 1313–1327. doi:10.1080/02786826.2012.712236

Zaveri, R. a., & Peters, L. K. (1999). A new lumped structure photochemical mechanism for large-scale applications. *Journal of Geophysical Research*, *104*(D23), 30387. doi:10.1029/1999JD900876

Zetzsch, C., & Behnke, W. (1992). Heterogeneous Photochemical Sources of Atomic Cl in the Tropospehre.pdf. *Ber. Bunsenges. Phys. Chem.1*, *96*(3), 488–493.

Zetzsch, C., Pfahler, G., & Behnke, W. (1988). Heterogeneous Formation of Chlorine Atoms from NaCl in a Photosmog System. *J. Aerosol Sci.*, *19*(7), 1203–1206.